

Department of Petroleum Engineering

**Gas Hydrates Investigations of Natural Gas with High Methane
Content and Regenerated Mono-Ethylene Glycol**

Khalifa Mohamed Ali Al Harooni

**This thesis is presented for the Degree of
Doctor of Philosophy
of
Curtin University**

July 2017

DECLARATION OF ACADEMIC INTEGRITY

To the best of my knowledge and belief this thesis contains no material previously published by any other person except where due acknowledgment has been made.

This thesis contains no material which has been accepted for the award of any other degree or diploma in any university.

Signature:



(Khalifa Al Harooni)

Date: 10 of July 2017

COPYRIGHT

I warrant that I have obtained, where necessary, permission from the copyright owners to use any third-party copyright material reproduced in the thesis (e.g. questionnaires, artwork, unpublished letters), or to use any of my own published work (e.g. journal articles) in which the copyright is held by another party (e.g. publisher, co-author).

Signature:



(Khalifa Al Harooni)

Date: 10 of July 2017

DEDICATION

*I would like to dedicate my thesis to my dear mother, for her prayers and wishes to
see me as an educated person*

To the memory of my father (Peace be upon him)

To my divine wife and my son for their greatest support and patience

To my brothers, sisters, family, and friends for their prayers and encouragement

ACKNOWLEDGMENT

In The Name of Allah, The Most Gracious, The Most Merciful

‘My Lord, Grant me the power and ability to be grateful for Your favours which You have bestowed upon me and upon my parents, and to do righteousness in a manner that would please You. And admit me by Your mercy among Your righteous servants’ (Holy Quran - 27:19)

The first and foremost acknowledgement for this work goes to the almighty Allah, without whom all inspiration is relative, empty, and incoherent. He endowed me with an erudite supervisor, Associate Professor Ahmed Barifcani. This work would not have come to light without Professor Barifcani’s technical guidance, professional support and continuous encouragement. His networking with other departments established a flexible and creative research environment, which has fostered my own academic maturity. Equally, I owe sincere gratitude to my co-supervisor, Associate Professor Stefan Iglauer, and my associate supervisor, Dr David Pack, for the inspiration and warm encouragement. I would not have these great publications without their continuous input, copy editing, and guidance in addressing the reviewers’ critical comments during my PhD study. I am lucky and proud to be their student. I am also very thankful to my panel committee chairperson, Professor Brian Evans, especially for leading the supervisory PhD panel meetings and ensuring my research progress is going well with the plan.

I would like to convey special thanks and appreciation to Mr Varun Ghodkay for preparing MEG degradation samples and in reviewing my manuscripts.

I would like to thank Professor Rolf Gubner and Chevron Australia Pty. Ltd for providing me with the opportunity to work with such a scientifically interesting and challenging project of the MEG pilot plant in the Curtin Corrosion Engineering Industry Centre (CCEIC).

I would like to thank all the technicians at the Department of Petroleum Engineering and Corrosion Engineering Industry Centre, especially Mr Saif Ghadban, Dr Guanliang Zhou, Mr Bob Webb, and Mr Leigh Bermingham, for all the time they dedicated to ensuring my set-up was operational.

I would like to thank the government of the Sultanate of Oman (Ministry of Higher Education) for sponsoring my study and for my employer Petroleum Development Oman LLC, the Consulate General of the Sultanate of Oman, and the Omani Students Society of Western Australia for their moral and financial support during the study period.

Further, I would like to thank Marwa Al-Hadhrami for her great contribution to chapter three of this work. I'm especially grateful to Petroleum Development Oman LLC and the Ministry of Oil and Gas Sultanate of Oman for permission to publish the work in chapter three.

In addition, I would like to thank the other research and administrative staff in the Petroleum Department for their support, as well as my colleagues and office-mates (previous and current PhDs students) who have offered their friendship, advice, and support.

Ultimately, I am thankful to Almighty Allah for all opportunities that I have had. In addition, my sincere thanks and gratitude go to my family, especially my mother for her encouragement, prayers, and love that helped me throughout the project. I would also like to thank my brothers, sisters, family and friends for their cheer throughout this long process. My final and most significant acknowledgement must be given to my wife, Zeyana Al Maskari, and my son, Mohammed, for their patience while I was working on this project. Without their help, love, and forbearance, this project would not have been done.

BRIEF BIOGRAPHY OF THE AUTHOR

Khalifa Al Harooni joined the Petroleum Development Oman LLC (PDO) in 1994 as production trainee where he was awarded ONC (BTEC) certificate in production operation in September 1998 and worked as a production technician in various fields. In 2000, he received a full scholarship from PDO for HNC and BEng study. In June 2001, he was awarded HNC certificate in Electrical and Electronic Engineering, from Wigan and Leigh College, UK, and in June 2004 he was awarded a degree in BEng Instrumentation and Control Engineering, a first class bachelor's degree with honours from TEESIDE University, UK.

Between 2004 and 2013, Khalifa worked as development instrument supervisor, production engineer, lead production engineer, and production supervisor at different fields. Khalifa is skilled in the oil and gas operation and process, maximising hydrocarbon production from subsurface/well production assets through well activity management, identifying and following up on unrealised production potential, analysing sub-surface/well-related activities for the Integrated Production Plan in liaison with petroleum engineering, well services, operations services, etc.,. During this period, Khalifa also enrolled in distance learning study at Curtin University, Western Australia (joint program with Shell Open University) where he was successfully awarded a master's degree in Petroleum Technology in August 2011.

In 2013, Khalifa received a full scholarship from the government of the Sultanate of Oman to conduct his PhD study. He has been doing his PhD studies in Petroleum Engineering since September 2013 at Curtin University of Technology, Western Australia, conducting research on gas hydrates of natural gas with high methane content and regenerated mono-ethylene glycol. So far, the PhD project has three published journal articles, one conference presentation (OTC Malaysia), two submitted articles, and three others articles on-going manuscripts for publication.

ABSTRACT

Mono-ethylene Glycol (MEG) is used as a hydrate inhibitor. Due to its high cost, large consumption rate, and its environmental impact, MEG is regenerated for reuse. During the regeneration process, rich MEG undergoes thermal exposure by distillation/ reclamation to remove the water and salts, in which thermal degradation process may occur. The contents of this thesis constitute seven experimental and computational extensive studies, on methane and natural gas ($\text{CO}_2/\text{C}_2\text{--C}_5$) hydrates with regenerated MEG and other ingredients after thermally exposed to high temperatures, utilising the stirred cryogenic sapphire cell, autoclave and MEG benchtop facility. The primary focus lies with investigating the effect of thermally degraded pure MEG, thermally degraded MEG with corrosion inhibitors, and regenerated MEG on gas hydrate kinetics. Hydrate equilibrium experimental data obtained from each study was used to calculate hydrate depression value and provide new hydrate regression functions profiles. The MEG degradation samples were prepared using an autoclave, and the degradation products were then analysed. Results showed that MEG was degraded when exposed to above 135 °C, also conclude that thermally exposed MEG causes a drop in hydrate inhibition performance due to thermal degradation effects. The study of thermally degraded MEG with Methyl Di-Ethanolamine (MDEA) and film forming corrosion inhibitor (FFCI) established that they also cause hydrate inhibition drop but less than that of pure thermally degraded MEG, which is caused by the additional inhibition effects of MDEA and FFCI. In addition, hydrate phase boundaries and regression functions were developed to provide a deep insight into the operating envelope of the thermally degraded MEG solutions. Advance study was conducted to evaluate six analytical techniques for analysing the degradation level of various MEG solutions. The analytical techniques evaluated were pH measurement, electrical conductivity, change in physical characteristics, ion chromatography, high performance liquid chromatography–mass spectroscopy, and gas hydrate inhibition performance. Detailed analyses were performed to evaluate the performance of the six analytical techniques in terms of their capability in identifying, monitoring, and quantifying the MEG degradation level. Furthermore, a novel MEG degradation levels scale was developed for the first time. A MEG regeneration/reclamation pilot plant at Curtin University was used to investigate the influence of regenerated MEG of clean-up

phase of a typical gas field on natural gas hydrate kinetics. The study solution contains MEG, condensate, drilling muds with high concentrations of divalent cations, particulates and various production chemicals. Intensive investigations, conclusions and recommendations are provided for operation optimisation, analytical techniques and effect on gas hydrate kinetics. In summary, these studies have brought a new focus on the effect of thermally degraded MEG with corrosion inhibitors and of regenerated MEG on gas hydrate kinetics.

PUBLICATIONS

Published and Accepted Papers:

1. **AlHarooni, Khalifa**, Ahmed Barifcani, David Pack, Rolf Gubner, and Varun Ghodkay. "Inhibition effects of thermally degraded MEG on hydrate formation for gas systems." *Journal of Petroleum Science and Engineering*, 2015, 135, pp 608–617.(<https://doi.org/10.1016/j.petrol.2015.10.001>)
2. **AlHarooni, Khalifa**, David Pack, Stefan Iglauer, Rolf Gubner, Varun Ghodkay, and Ahmed Barifcani. "Analytical Techniques for Analyzing Thermally Degraded Monoethylene Glycol with Methyl Diethanolamine and Film Formation Corrosion Inhibitor." *Energy & Fuels*, 2016, 30 (12), pp 10937–10949. (**DOI:** [10.1021/acs.energyfuels.6b02116](https://doi.org/10.1021/acs.energyfuels.6b02116))
3. **AlHarooni, Khalifa**, David Pack, Stefan Iglauer, Rolf Gubner, Varun Ghodkay, and Ahmed Barifcani. "Effects of Thermally Degraded Monoethylene Glycol with Methyl Diethanolamine and Film-Forming Corrosion Inhibitor on Gas Hydrate Kinetics." *Energy & Fuels*, 2017, 31 (6), pp 6397–6412 (**DOI:** [10.1021/acs.energyfuels.7b00733](https://doi.org/10.1021/acs.energyfuels.7b00733))
4. **AlHarooni, Khalifa**, Rolf Gubner, Stefan Iglauer, David Pack, and Ahmed Barifcani. "Influence of Regenerated Monoethylene Glycol on Natural Gas Hydrate Formation." *Energy & Fuels*, 2017, 31 (11), pp 12914–12931 (**DOI:** [10.1021/acs.energyfuels.7b01539](https://doi.org/10.1021/acs.energyfuels.7b01539))

Conference Paper

1. **AlHarooni, K. M.**, A. Barifcani, D. Pack, and S. Iglauer. "Evaluation of Different Hydrate Prediction Software and Impact of Different MEG Products on Gas Hydrate Formation and Inhibition." *In Offshore Technology Conference Asia*. Offshore Technology Conference, 2016.

Manuscripts Submitted or in Preparation:

1. **AlHarooni, Khalifa**, Stefan Iglauer, David Pack, and Ahmed Barifcani. "Hydrate Plug Mitigation Techniques and Application for Gas Lift System." (**To be Submit**)
2. Khalid Alef, **Khalifa AlHarooni**, Stefan Iglauer, Rolf Gubner, Ahmed Barifcani. "Cycling effect of regenerated MEG during switchover of corrosion prevention strategies (pH stabilization to film forming corrosion inhibitor)." (**Submitted**)

TABLE OF CONTENTS

DECLARATION OF ACADEMIC INTEGRITY	I
COPYRIGHT	II
DEDICATION	III
ACKNOWLEDGMENT	IV
BRIEF BIOGRAPHY OF THE AUTHOR	VI
ABSTRACT	VII
PUBLICATIONS	IX
TABLE OF CONTENTS	XI
LIST OF FIGURES	XIX
LIST OF TABLES	XXXII
Chapter 1 Introduction	1
1.1 Background	1
1.2 Research Objectives	4
1.3 Thesis Outline and Organisation	5
Chapter 2 Literature Review	9
2.1 Introduction	9
2.2 Gas hydrate Structure and Formation Mechanism	9
2.2.1 Cubic structure I	10
2.2.2 Cubic structure II	11
2.2.3 Hexagonal structure H	12

2.3	Gas Hydrate Nucleation	17
2.3.1	Local structuring nucleation hypothesis	17
2.3.2	Labile Cluster Nucleation Hypothesis	19
2.3.3	Nucleation at the interface hypothesis	22
2.3.4	Morphology of gas hydrate nucleation	24
2.3.5	Gas Hydrate Memory Effect Phenomenon	26
2.4	Hydrate Growth	32
2.5	Hydrate Growth Correlations	33
2.5.1	Hydrate Growth Kinetics	34
2.6	Hydrate Dissociation	36
2.7	Thermodynamic Inhibitors	44
2.8	Low-Dosage Hydrate Inhibitors	48
2.8.1	Kinetic Inhibitor	48
2.8.2	Anti-Agglomerants	49
2.9	Hydrates in Natural Gas Production and Transport Systems	51
2.10	Mono-Ethylene Glycol	53
2.10.1	Hydration of Ethylene Oxide to Produce Ethylene Glycol	55
2.11	MEG Regeneration and Reclamation Systems	58
2.11.1	Convention Recovery Model	60
2.11.2	Full-stream Reclamation Model	61
2.11.3	Slip-stream Reclamation Model	63
2.12	MEG Degradation	64

2.12.1	Types of degradation	65
2.13	Gaps in Literature	70
Chapter 3	Case study: Various Gas Hydrate Mitigation Techniques Applied to a Gas Lift System in a South Field of Oman	72
3.1	Introduction	72
3.2	Problem Description	75
3.3	Hydrate Formation History	80
3.4	Symptoms and Troubleshooting to Determine Hydrate Formation at XS Field Facility	83
3.4.1	Gas Hydrate at Fuel Supply Line	83
3.4.2	Flaring As a Result of Gas Hydrate	84
3.4.3	Analysing Gas Lift Well Trends Using Nibras (in-house) Monitoring Portal and PI ProcessBook	85
3.5	Thermodynamic Hydrate Inhibition and Dissociating Techniques:	91
3.5.1	Installation of Rockwool Insulators	91
3.5.2	Installation of Electrical Heat Tracing	97
3.5.3	Hot Gas Bypass across Third Stage Discharge Coolers of Reciprocating Compressor K-XS05	101
3.5.4	After-Coolers Discharge Temperature Adjustment of the New GL Compressor K-XS35	102
3.5.5	Maintaining External Compressors K-XS33A/B/C/D Discharge Gas Temperature	102

3.5.6 Decreasing the system pressure below hydrate stability point	103
3.6 Conclusion and recommendations	104
Abbreviations	106
Chapter 4 Evaluation of Different Hydrate Prediction Software and Impact of Different MEG Products on Gas Hydrate Formation and Inhibition	107
4.1 Abstract	107
4.2 Introduction	108
4.3 Description of Equipment and Processes	109
4.3.1 Materials, Equipment and Testing Process	109
4.3.2 Experimental procedure	110
4.4 Results and Discussion	112
4.4.1 Comparison of computational results	113
4.4.2 Influence of MEG product (MEG supplier) on methane hydrate formation	115
4.5 Conclusions	116
Chapter 5 Inhibition Effects of Thermally Degraded MEG on Hydrate Formation for Gas Systems	118
5.1 Abstract	118
5.2 Introduction	118
5.3 Methodology	122
5.3.1 Materials and Equipment	122
5.3.2 General experiment procedure	123

5.3.3	Testing methods	125
5.3.4	Thermally degraded MEG samples preparation	125
5.3.5	MEG degradation Identification Techniques	126
5.4	Results and discussions	127
5.4.1	Hydrate formation/dissociation behaviour of binary CH ₄ –H ₂ O system	
		127
5.4.2	MEG degradation products identification	130
5.4.3	Effect of thermally degraded MEG on hydrate inhibition performance	
		133
5.5	Conclusion	136
Chapter 6	Effects of Thermally Degraded Monoethylene Glycol with Methyl Diethanolamine and Film-Forming Corrosion Inhibitor on Gas Hydrate Kinetics	138
6.1	Abstract (Figure 6-1)	138
6.2	Introduction	139
6.3	Experimental Methodology	144
6.3.1	Equipment and Materials	144
6.3.2	Preparation of Thermally Exposed (Degraded) MEG Samples	145
6.3.3	Experiment Procedure	148
6.3.4	Consistency of Results and Phase Boundary	149
6.4	Results and Discussions	151
6.4.1	Effect of Thermally Degraded MEG on Hydrate Inhibition Performance	152

6.4.2	Effects of Pure MDEA on Gas Hydrate Formation	158
6.4.3	Effects of Pure FFCI on Gas Hydrate Formation	159
6.4.4	Hydrate Phase Boundary	162
6.5	Conclusions	165
Chapter 7 Analytical Techniques for Analyzing Thermally Degraded Monoethylene Glycol with Methyl Diethanolamine and Film Formation Corrosion Inhibitor		169
7.1	Abstract (Figure 7-1)	169
7.2	Introduction	170
7.3	Experimental Methodology	174
7.3.1	Materials	174
7.3.2	Experimental Procedure	175
7.4	Results and Discussion	181
7.4.1	pH Measurements	181
7.4.2	Electrical Conductivity Measurements	182
7.4.3	Physical Observations	183
7.4.4	Identification of MEG Degradation Products	185
7.4.5	Hydrate Inhibition Performance Test	188
7.5	Conclusions	192
Chapter 8 Influence of Regenerated Mono-ethylene Glycol on Natural Gas Hydrate Formation		196
8.1	Abstract (Figure 8-1)	196

8.2	Introduction	197
8.3	Methodology	204
8.3.1	MEG Pilot Plant	204
8.3.2	Gas Hydrate Experiment	205
8.3.3	Scenarios	206
8.3.4	MEG pilot plant operating philosophy	206
8.3.5	Gas Hydrate Experiment	210
8.4	Results and Discussion	214
8.4.1	MEG Pilot Plant	214
8.4.2	Gas Hydrate Inhibition Test	226
8.5	Conclusions	230
Chapter 9	Conclusions and Recommendations	234
9.1	Conclusions	234
9.1.1	<i>Investigation of gas hydrate problems and mitigation techniques applied in the gas-lift system at one of the oil fields in the Sultanate of Oman</i>	235
9.1.2	<i>Evaluation of Different Hydrate Prediction Software and Impact of Different MEG Products on Gas Hydrate Formation and Inhibition</i>	235
9.1.3	<i>Inhibition effects of thermally degraded MEG on hydrate formation for gas systems</i>	236
9.1.4	<i>Effects of Thermally Degraded Monoethylene Glycol with Methyl Diethanolamine and Film-Forming Corrosion Inhibitor on Gas Hydrate Kinetics</i>	236

9.1.5 <i>Analytical Techniques for Analysing Thermally Degraded Monoethylene Glycol with Methyl Diethanolamine and Film Formation Corrosion Inhibitor</i>	237
9.1.6 <i>Influence of Regenerated Mono-ethylene Glycol on Natural Gas Hydrate Formation</i>	238
9.2 Recommendations	239
APPENDIX A: Official Permissions and Copyrights	243
Reference	248

LIST OF FIGURES

Figure 1-1 Examples of naturally-occurring gas hydrates: (a) massive; (b) laminae; after Worthington (2010)	1
Figure 1-2 Number of publications on gas hydrates between 1997 to 2016 (Curtin University library catalogue database)	2
Figure 1-3 Natural gas hydrate plug in a transport pipeline (normally under high pressure and low temperature)	3
Figure 1-4 Diagrammatic representation of the thesis' organisation	8
Figure 2-1 Crystal structures sI hydrate; four unit cells viewed along a cubic crystallographic axis. All cavities are assumed to be filled; adapted after Koh (2002)	10
Figure 2-2 A 5^{12} pentagonal dodecahedral cavity enclosing methane (left) and a $5^{12}6^2$ tetrakaidecahedral cavity enclosing ethane (right); adapted after Koh (2002)	10
Figure 2-3 Crystal structures sII hydrate; two unit cells observed along a face diagonal. All cavities are supposed to be filled; adapted after Koh (2002)	11
Figure 2-4 Propane inside a hexakaidecahedral $5^{12}6^4$ cavity; adapted after Koh (2002)	12
Figure 2-5 Crystal structures of sH hydrate. The positions of the hydrogen atoms have not been encompassed; four unit cells were aligned along the six-fold crystallographic axis. $5^{12}6^8$ has been highlighted by the blue guests and all cavities assumed to be filled; adapted after Koh (2002).	13
Figure 2-6 Gas hydrates crystal structures; adapted after (Giavarini et al., 2011, Timothy S. Collett et al., 2009)	13
Figure 2-7 Reddish methane hydrate flame (Flammable ice); after (Suess et al., 1999, Giavarini et al., 2011)	16

Figure 2-8 Comparison of guest size, hydrate type, and cavities occupied for various hydrate formers; after Giavarini et al. (2011)	17
Figure 2-9 Growth of local structure nucleation lines (with time shown in nanoseconds) indicate the hydrogen-bond network; after (Moon et al., 2003c)	19
Figure 2-10 Stable sharing of faces in a 5^{12} cavity with methane gas, formed by 6 ns; after (Moon et al., 2003c)	19
Figure 2-11 Labile cluster nucleation; adapted after Aman et al. (2016)	20
Figure 2-12 Schematic of hydrate formation/dissociation on an isochoric method; adapted after Christiansen et al. (1994)	21
Figure 2-13: Determination of the hydrate dissociation point (equilibrium) from the Pressure-Temperature trend by the intersection point of the cooling and heating cycles (our work).	22
Figure 2-14 Methane hydrate start formation at interface of a PVT cell; after AlHarooni,Pack, et al. (2016)	23
Figure 2-15 Gas hydrate nucleation at gas-water interface; after Sloan et al. (2008b)	23
Figure 2-16 Massive methane hydrate crystals; after Wu et al. (2010)	24
Figure 2-17 Massive methane hydrate crystals (our work).	24
Figure 2-18 Whiskery methane hydrate crystals; after Wu et al. (2010)	25
Figure 2-19 Whiskery methane hydrate crystals (side view and top view) (our work).	25
Figure 2-20 Jelly methane hydrate crystals; after Wu et al. (2010)	25
Figure 2-21 Jelly methane hydrate crystals (our work).	25
Figure 2-22 Consecutive hydrate formation cooling curves for several runs; adapter after Schroeter et al. (1983)	26

Figure 2-23 Hydrate formation repetition of same fluid after dissociation; adapted after Wu et al. (2010)	27
Figure 2-24 Macroscopic crystal morphology of carbon dioxide hydrate formation from water droplets; adapted after Servio et al. (2003).	28
Figure 2-25 Structure screenshots of the residual clathrate (a) and ice (b) in the hydrate melt; after Rodger (2000).	30
Figure 2-26 Single Crystal Growth; adapted after Sloan et al. (2008b)	33
Figure 2-27 Schematic of hydrate dissociation mechanism; after (Bishnoi et al., 1996, Clarke et al., 2000)	37
Figure 2-28 Driving forces for hydrate decomposition modified; adapted after (Hong, 2003)	38
Figure 2-29 Old axial one sided dissociation of a hydrate in a pipeline; adapted after Davies et al. (2006).	39
Figure 2-30 Radial dissociation of a hydrate in a pipeline; adapted after Peters et al. (2000)	39
Figure 2-31 Time sequence of radial dissociation of laboratory hydrate plugs in a pipeline; lower part dissociate faster due to effect of gravity; adapted after Peters et al. (2000)	40
Figure 2-32 Incorrect and sudden depressurisation of hydrate plug in high pressure pipeline causing the hydrate plug to being launched like a projectile; adapted after (Carroll, 2014, Giavarini et al., 2011)	41
Figure 2-33 Hydrate plug dissociation incident happened due to incorrect single sided depressurization procedure; after (Koh et al., 2010)	42
Figure 2-34 Incorrect thermal remediation of hydrate plug in high pressure pipeline causing pipeline rupture; adapted after (Carroll, 2014, Giavarini et al., 2011)	44

Figure 2-35 Effect of addition of different concentration of MEG on shifting hydrate equilibrium curve of natural gas (Methane 79.1%, CO₂ 2.5%, iso-Pentane 1.7%, n-Pentane 1.7%, iso-Butane 2%, n-Butane 2%, propane 4%, Ethane 7%) , plotted by Multiflash prediction software (PR equation of state). 45

Figure 2-36 Effect of addition of 25 wt% of different thermodynamic inhibitors on shifting hydrate equilibrium curve of system of natural gas (Methane 79.1%, CO₂ 2.5%, iso-Pentane 1.7%, n-Pentane 1.7%, iso-Butane 2%, n-Butane 2%, propane 4%, Ethane 7%), plotted by Multiflash prediction software (PR equation of state). 46

Figure 2-37 Chemical structure of Luvicap® EG (a) and Gaffix® VC-713 (b); after (Rojas et al., 2010, Ding et al., 2009) 49

Figure 2-38 Case history of Deepwater Gulf of Mexico where injection of LDHI (AA) permits extra gas production in Methanol limited system; after Frostman et al. (2003) 50

Figure 2-39 Gas hydrate plug in a pipeline; after (Boschee, 2012, Irmann-Jacobsen, 2012) 51

Figure 2-40 Probable locations of hydrate formation in an offshore system; after (Giavarini et al., 2011) 52

Figure 2-41: Hydrate formation during winter season at Gas lift manifold caused by drop in ambient temperature and high differential pressure across the control valve (Joule –Thompson effect); (Courtesy of Petroleum Development Oman) 52

Figure 2-42 Hydrate plug formations in "s" shapes; adapted after Joachim (2013) 53

Figure 2-43 Flow scheme of conventional ethylene oxide (EO) to MEG process; adapted after Kawabe (2010) 56

Figure 2-44 Schematic diagram of reaction mechanisms of acid and base catalysed hydration of ethylene oxide (C_2H_4O) to ethylene glycols; after van Hal et al. (2007).	57
Figure 2-45 Fields location of MEG regeneration plants around the world; adapted after Craig Dugan (2009).	58
A) Feed blending	B) Pre-treatment Figure 2-46 CCEIC
MEG pilot plant operation areas; (1) Condensate tank, (2) Brine tank, (3) Feed blender, (4) three-phase separator, (5) Pre-treatment vessel, (6) Recycle pump, (7) Recycle heater.	59
Figure 2-47 CCEIC MEG pilot plant operation areas; (1) Distillation column, (2) Reboiler, (3) Reflux condenser, (4) Rotary flash separator, (5) overhead condenser, (6) condensed MEG collector.	60
Figure 2-48 Full-stream Reclamation; adapted after Joosten et al. (2007)	62
Figure 2-49 Full-stream MEG reclaimer in the Gulf of Mexico; adapted after Van Son (2000)	62
Figure 2-50 Slip-stream MEG reclamation model; adapted after Lehmann et al. (2014)	63
Figure 2-51 Possible pathway for MEG degradation by mineralisation in the UV/ H_2O_2 system. The results have presented stepwise oxidation of ethylene glycol by reaction with OH; adapted after McGinnis et al. (2000).	66
Figure 3-1: Sultanate of Oman field location map. The red arrow indicates north and the blue arrow indicates south (Sanchez et al., 2011, Al Salhi et al., 2001).	73
Figure 3-2: Artificial lift systems distribution in PDO (Al-Bimani et al., 2008)	74
Figure 3-3: XS Field Production Station Overview	74

Figure 3-4: XS production station common gas lift compressors discharge temperature (Aug. 2013 to Oct. 2015)	76
Figure 3-5: Gas hydrate blockage inside pipeline; after (Fraser, 2013)	76
Figure 3-6: Hydrate formation at low point of flowline; adapted after (Jamaluddin et al., 1991)	77
Figure 3-7: Hydrate Formation Phase Envelope for XS Field using Multiflash software P-R EOS. The coloured region is the operating envelope of pressure up to 70 bar; the red region is where hydrate can exist, and the green is where hydrate cannot exist.	78
Figure 3-8: Hydrate formation phase envelope for XS field using Multiflash software P-R EOS with different methanol injection percentages, gas composition input extracted from Figure 3-9	79
Figure 3-9: XS Field gas analysis report (courtesy of PDO)	80
Figure 3-10: Total deferment of all PDO fields due to hydrate formation (during the winter season). Note: CN field shows high hydrate deferment in 2017 as a result of sending rich gas caused by a process upset (PDO deferment report-March-2017).	82
Figure 3-11: XS Field total deferment because of hydrate formation (where ➔ for total reconciled deferment number) (PDO deferment report-March-2017)	83
Figure 3-12: Hydrate formation monitoring at fuel supply line using PI ProcessBook (courtesy of PDO)	84
Figure 3-13: Flaring because of gas hydrate formation using PI ProcessBook (courtesy of PDO)	85
Figure 3-14: Gas Hydrate at W102 using Nibras tool (courtesy of PDO)	86
Figure 3-15: Gas Hydrate at W082 using Nibras tool (courtesy of PDO)	86

Figure 3-16: Gas Hydrate at W102 from 09/12/15-13/12/15 using PI ProcessBook (courtesy of PDO)	87
Figure 3-17: W101 well parameters using Nibras tool (courtesy of PDO)	88
Figure 3-18 W071 using Nibras tool (courtesy of PDO)	89
Figure 3-19 W084. This well shows that although there is hydrate, the well is still self-flowing as THP did not drop using Nibras tool (courtesy of PDO).	89
Figure 3-20: W102 is a very sensitive well. THP drops fast as gas lift flow drops because of hydrate formation using Nibras tool (courtesy of PDO).	90
Figure 3-21: W099 is a sensitive well. THP drops fast as gas lift flow drops because of hydrate formation using Nibras tool (courtesy of PDO).	90
Figure 3-22: Rockwool Insulator	92
Figure 3-23: Methanol Injection Point (courtesy of PDO)	93
Figure 3-24: UNISIM Simulation Screenshot - Case 3 (process continued in Figure 3-25)	94
Figure 3-25: UNISIM Simulation Screenshot - Case 3 (process continued from Figure 3-24)	95
Figure 3-26: A-XS64 gas lift manifold main header/flow control valves side before EHT implementation (courtesy of PDO)	98
Figure 3-27: A-XS64 gas lift manifold main header/flow control valves side after EHT implementation (courtesy of PDO)	98
Figure 3-28: A-XS64 gas lift manifold after flow control valves side before EHT implementation (courtesy of PDO)	99
Figure 3-29: A-XS64 gas lift manifold after flow control valves side after EHT implementation (courtesy of PDO)	99

Figure 3-30: Heat-tracing coil with covered insulation across FCVs (courtesy of PDO)	100
Figure 3-31 Heat tracing panel (courtesy of PDO)	100
Figure 3-32 Rockwool insulation and EHT locations	101
Figure 3-33: Proposed hot gas bypass across 3 rd stage cooler E-XS14	102
Figure 3-34: Temperature profile during winter using PI ProcessBook (courtesy of PDO)	103
Figure 3-35: Trial of pressure reduction on W102 at RGS3 using PI ProcessBook (courtesy of PDO)	104
Figure 4-1 PVT sapphire cell layout.	111
Figure 4-2 PVT Cryogenic sapphire cell unit.	111
Figure 4-3 Hydrate formation stages.	112
Figure 4-4 Hydrate formation / dissociation start points and literature data for binary CH ₄ -H ₂ O systems.	113
Figure 4-5 Hydrate Formation /Start Dissociation curves for binary CH ₄ -H ₂ O systems.	114
Figure 4-6 Hydrate formation curves for CH ₄ – (10 wt% MEG solutions) of the three supplied MEG (X-MEG, Y-MEG, Z-MEG) and CH ₄ -water.	116
Figure 5-1 The PVT sapphire cell layout.	124
Figure 5-2 Hydrate locus of start formation /start dissociation and literature for binary CH ₄ –H ₂ O system.	128
Figure 5-3 Hydrate locus curve for binary CH ₄ –H ₂ O system of hydrate formation /start dissociation/end dissociation.	129

Figure 5-4 Hydrate formation pattern captured by the mounted camera (estimate driven from hydrate start nucleation till all water completely converted to hydrate). 130

Figure 5-5 Degradation products identification using HPLC-MS technique for samples of thermally degraded MEG to 48 h. 131

Figure 5-6 Degradation products identification using IC technique for samples of thermally degraded MEG to 48 h. 132

Figure 5-7 Various Sample bottles of thermally degraded lean MEG for 48 h. 132

Figure 5-8 Hydrate locus of Methane with 25 wt% thermally degraded MEG to different exposure time. Hammerschmidt temperature shift prediction equation obtained from Bai et al. (2005). 134

Figure 5-9 Hydrate locus of Methane with 25 wt% thermally degraded MEG to 48 h for different temperatures. Hammerschmidt temperature shift prediction equation obtained from Bai et al. (2005). 135

Figure 5-10 Captured images of hydrates formation of methane with 25 wt% of thermally degraded MEG to 180 °C at 125 bar. 136

Figure 6-1 Abstract Graphics 139

Figure 6-2 Methane gas hydrate phase boundaries of solution A exposed to 135 °C. 140

Figure 6-3 Overview of the MEG closed loop system. 142

Figure 6-4 Schematic of the PVT unit. 145

Figure 6-5. Schematic of the autoclave. 147

Figure 6-6. Start hydrates formation. 149

Figure 6-7. Hydrates full blockage. 149

Figure 6-8 Hydrate formation locus of methane gas with solution A and literature data [with data of thermally degraded pure MEG (without MDEA or FFCI)], plotted using a semilogarithmic scale, as the logarithm of the hydrate formation locus has almost linear behavior.(Mohammadi et al., 2009) Literature data for pure MEG (without additives) is added to the figure for comparison (Windmeier et al., 2014a, Sloan et al., 2008a, Maekawa, 2001, Jager et al., 2001, Carroll, 2014, AlHarooni et al., 2015). The Hammerschmidt temperature shift prediction equation was obtained from Bai et al. (2005).

150

Figure 6-9 Hydrate formation locus of methane gas with solution A and regression functions of fitted data.

153

Figure 6-10 Hydrate formation at liquid–gas interface.

155

Figure 6-11 Hydrate formation locus of methane gas with solution B and regression functions of fitted data.

156

Figure 6-12 Hydrate formation locus of methane gas with solution C and regression functions of fitted data.

158

Figure 6-13 Hydrate formation locus of methane gas with pure MDEA at different concentrations and regression functions of fitted data.

159

Figure 6-14 Hydrate formation locus of methane gas with pure FFCI at different concentration.

160

Figure 6-15 Methane gas hydrate phase boundaries of solution A exposed to 165 °C.

162

Figure 6-16 Methane gas hydrate phase boundaries of solution A exposed to 185 °C.

163

Figure 6-17 Methane gas hydrate phase boundaries of solution A exposed to 200 °C.

163

Figure 6-18 Methane gas hydrate phase boundaries of solution B exposed to 185 °C.	164
Figure 6-19 Methane gas hydrate phase boundaries of solution C exposed to 185 °C.	164
Figure 7-1 Abstract Graphics	170
Figure 7-2 Overview of the MEG closed loop system.	174
Figure 7-3 Autoclave sketch	175
Figure 7-4 Cryogenic sapphire cell schematic.	176
Figure 7-5 (A) Hydrate formation. (B) Hydrate fully converted	180
Figure 7-6 pH values as a function of exposure temperature for Table 7-2 solutions.	182
Figure 7-7 Electrical conductivity as a function of exposure temperature for solutions I–III (Table 7-2)	183
Figure 7-8 MEG solutions after heat treatment. Higher temperatures lead to more degradation (= darker color).	184
Figure 7-9 Foam formation in solution “I” thermally exposed to 200 °C.	185
Figure 7-10 Degradation product concentrations in thermally exposed MEG solutions measured via IC.	186
Figure 7-11 Degradation product concentrations in thermally exposed MEG solutions measured via HPLC–MS.	187
Figure 7-12 Hydrate dissociation curves of methane–MEG solutions for different thermal exposure temperatures; solid curves represent fitted data ($R^2 > 0.98$).	189
Figure 7-13 Methane-solution “I” hydrate dissociation curve with literature (Sloan et al., 2008a, Carroll, 2002, Maekawa, 2001, Jager et al., 2001, Windmeier et al.,	

2014a, Peng et al., 1976, Hemmingsen et al., 2011, AlHarooni et al., 2015, AlHarooni,Barifcani, et al., 2016).	190
Figure 7-14 Degradation level scale of MEG solutions (to be used in conjunction with Table 7-5)	195
Figure 8-1 Abstract Graphics	197
Figure 8-2 MEG pilot plant schematic.	199
Figure 8-3. MPV viewing strip.	207
Figure 8-4. Hydrate Formation.	210
Figure 8-5 An example of an isochoric temperature search method used for identifying the equilibrium point of reclaimed solution of scenario C2.	212
Figure 8-6. Equilibrium curve of natural gas with 20 wt % solution of scenario B1 (salt-laden rich MEG + drilling mud (no condensate)), literature data added for comparison. (Hemmingsen et al., 2011, Chapoy,Mazloum, et al., 2012, Haghghi et al., 2009, Lee et al., 2011, Smith et al., 2016)	213
Figure 8-7. Brine Tank divalent-monovalent cation concentrations (ppm). Note: Na ⁺ , K ⁺ and Ca ²⁺ follow right-hand axis.	215
Figure 8-8. Three phase separator divalent-monovalent cation concentrations (ppm). Note: Na ⁺ , K ⁺ and Ca ²⁺ follow right-hand axis.	215
Figure 8-9. MEG Pre-treatment Vessel divalent-monovalent cation concentrations (ppm) at MEG outlet. Note: Na ⁺ , K ⁺ , and Ca ²⁺ follow right-hand axis.	216
Figure 8-10 TPS: Base scenario: clean fluid.	217
Figure 8-11 TPS: with drilling mud.	217
Figure 8-12 Reboiler vessel during and after operation of scenario E.	218
Figure 8-13 Rich Glycol Tank divalent-monovalent cation concentrations (ppm). Note: Na ⁺ , K ⁺ , and Ca ²⁺ follow right-hand axis.	219

Figure 8-14 Lean Glycol Tank divalent-monovalent cation concentrations (ppm).	
Note: Na ⁺ , K ⁺ , and Ca ²⁺ follow right-hand axis.	220
Figure 8-15 Salts precipitated in the reclaimer.	221
Figure 8-16. Reclaimer condensed side divalent-monovalent cation concentrations (ppm). Note: Na ⁺ , K ⁺ , and Ca ²⁺ follow right-hand axis.	222
Figure 8-17. Reclaimer (RC) condensed/slurry sides total divalent-monovalent cation concentrations (ppm) corresponding with electrical conductivities (μ S/cm) of reclaimer condensed outlet, reclaimer slurry outlet, and reboiler outlet. Note: total cation concentrations follow right-hand axis.	223
Figure 8-18 MEG wt % concentration.	224
Figure 8-19. Experimental data and operating conditions of scenario “F2”. Total operation time: 12.92 hours.	225
Figure 8-20. Experimental equilibrium points of natural gas hydrates in the presence of different Reboiler (RB) and Reclaimer (RC) MEG solutions for different scenarios (section 8.3.3); solid curves represent best fit; ● represent equilibrium conditions of 20 wt % fresh MEG; ■ represent equilibrium conditions of 100% deionized water.	227
Figure 9-1 Memory effect experiment of 20 wt% MEG with natural gas.	241
Figure 9-2 Various hydrate crystal morphology and agglomerants behaviour with current video recording facility.	242

LIST OF TABLES

Table 2-1 Properties of the three common unit crystals; adapted after Sloan (2003)	14
Table 2-2 Researcher's findings on memory effect vanishment.	31
Table 2-3 Hydrate depression temperature “ ΔTd ” of Brustad et al. (2005) and of Figure 2-36, and the regression functions (sorted from highest to poorest inhibitor), where P is pressure and T is the temperature.	47
Table 2-4 Physical properties of MEG and Methanol; adapted after Akers (2009)	54
Table 2-5 The disadvantages and advantages of the three MRU operating models	64
Table 2-6 literature review of MEG degradations Impacts	67
Table 3-1: Gas lift wells distribution	81
Table 3-2: Study Cases	96
Table 3-3: Methanol Injection Connections	106
Table 4-1 MEG properties.	110
Table 5-1 Mono-ethylene glycol properties characteristics at atmospheric pressure (Aylward et al., 2008, Braun et al., 2001).	126
Table 5-2 Hydrate formation temperature deviation towards the right side of the hydrate curve.	134
Table 6-1 Solution Matrix for Thermally Exposed Samples (AlHarooni,Pack, et al., 2016).	146
Table 6-2 Solution Matrix for Gas Hydrate Inhibition Performance Test (AlHarooni,Pack, et al., 2016).	147
Table 6-3. Solution A: Hydrate Depression Temperature ^a Due to Thermal Degradation	154
Table 6-4. Solution B: Hydrate Depression Temperature Due to Thermal Degradation ^a	156

Table 6-5. Methane Gas Hydrate Depression Temperature (given in ΔT_d versus deionized water) of Various Solutions at Different Pressures (sorted from poorest to highest inhibitor) ^a	161
Table 6-6. Phase Boundary Region Areas (Figure 6-2 and Figure 6-15 to Figure 6-19)	165
Table 7-1 MEG and MDEA Properties at Atmospheric Pressure (Aylward et al., 2008, Braun et al., 2001).	175
Table 7-2 Solutions Tested and Thermal Exposure Conditions ^a	177
Table 7-3 Hydrate Performance Test Solutions	178
Table 7-4 Gas Hydrate Dissociation Temperature Shift of Methane–MEG Solutions Versus Baseline of Methane-Deionized water ($\Delta ^\circ\text{C}$) and the Regression Functions of the Fitted Data ^a	191
Table 7-5 Evaluation of Analytical Techniques for Measurement of Thermal Degradation of MEG Solutions.	194
Table 8-1 Salt-laden rich MEG composition ^a	205
Table 8-2. Composition of the synthetic natural gas for the gas hydrate test	206
Table 8-3. Ca^{2+} concentration and % precipitated before and after reboiler	218
Table 8-4. Reclaimer divalent-monovalent cations partition.	221
Table 8-5 Experimental hydrate depression temperature for natural gas with 20 wt % of various MEG solutions from the reboiler outlet, and the regression functions (sorted from poorest to highest inhibitor) ^a	229
Table 8-6. Experimental hydrate depression temperature for natural gas with 20 wt % of various MEG solutions collected from the reclaimer outlet, and the fitted regression functions (sorted from poorest to highest inhibitor) ^b	230

Table 9-1 Experimental equilibrium condition of natural gas with various MEG/condensate mixture	240
--	-----

Chapter 1 Introduction

1.1 Background

Gas hydrates, also known as clathrate hydrates, are ice-like crystalline compounds consisting of water/ice molecules (host) and gas molecules (guest) (Figure 1-1). They usually form when guest molecules are trapped in the host cavities that are composed of hydrogen-bonded of water molecules under conditions of high pressure and low temperatures. The temperatures at which gas hydrates form are usually higher than the ice formation temperature of water (0 °C), making it a unique phenomenon.



Figure 1-1 Examples of naturally-occurring gas hydrates: (a) massive; (b) laminae; after Worthington (2010)

Gas hydrates compress gas volume and raise energy density. That is, one m³ of methane hydrate comprises around 164 m³ of gas at standard temperature and pressure conditions (Giavarini et al., 2011).

Gas hydrates were first accidentally encountered by Joseph Priestley in 1790 but were formally discovered by Sir Humphrey Davy in 1810, when he cooled a solution saturated with chlorine gas to a temperature below 9 °C to form some crystals of an ice-like material (Makogon, 2015). From this discovery, succeeding research was conducted focusing on identifying other gases that can form hydrates. Villard and others in the year 1888 found that light hydrocarbon gases (such as ethane, methane, and propane) can also form gas hydrates (Holder et al., 1976, Demirbas, 2010). E. G. Hammerschmidt was the first to observe gas hydrate blockage in transport lines above ice formation temperatures in 1934. This discovery triggered the critical importance of gas hydrates by the oil and gas industry and accelerated the hydrate research rate on finding the conditions at which hydrate crystals grow, calculating when they would form, and prevention techniques (Hammerschmidt, 1939). Large

deposits of methane hydrates were first discovered in 1967 by the Russians in the Siberian permafrost (Falenty et al., 2009). Further, a large methane hydrate deposit was found in the Messoyakha gas field, in which this decomposition of gas hydrate contributed to the total gas production (more than five billion m³) from this field since its discovery (Giavarini et al., 2011).

Since the discovery of gas hydrates, it has become a subject of interest in areas such as thermodynamic modelling and simulation, flow assurance, drilling and well operations, exploration geology, chemistry, energy resource, storage and transport, H₂S and CO₂ capture, water desalination, environmental sciences, and other new technological applications (Sloan et al., 2008b, Sloan et al., 2010, Sloan, 2003, 2005, Koh et al., 2007, Zerpa et al., 2010, Makogon, 2010, Eslamimanesh et al., 2012, Aaron et al., 2005). There is no doubt in the immense benefits associated with a clearer understanding of hydrate-related issues on the different levels mentioned. The key to such understanding lies in the excellent knowledge base on the microscopic and macroscopic interactions that defines gas hydrate formation kinetics.

Figure 1-2 displays the accelerating number of publications in the past 20 years with a total of 8,561 publications (Curtin University library catalogue database), supporting the importance of gas hydrate studies and management.

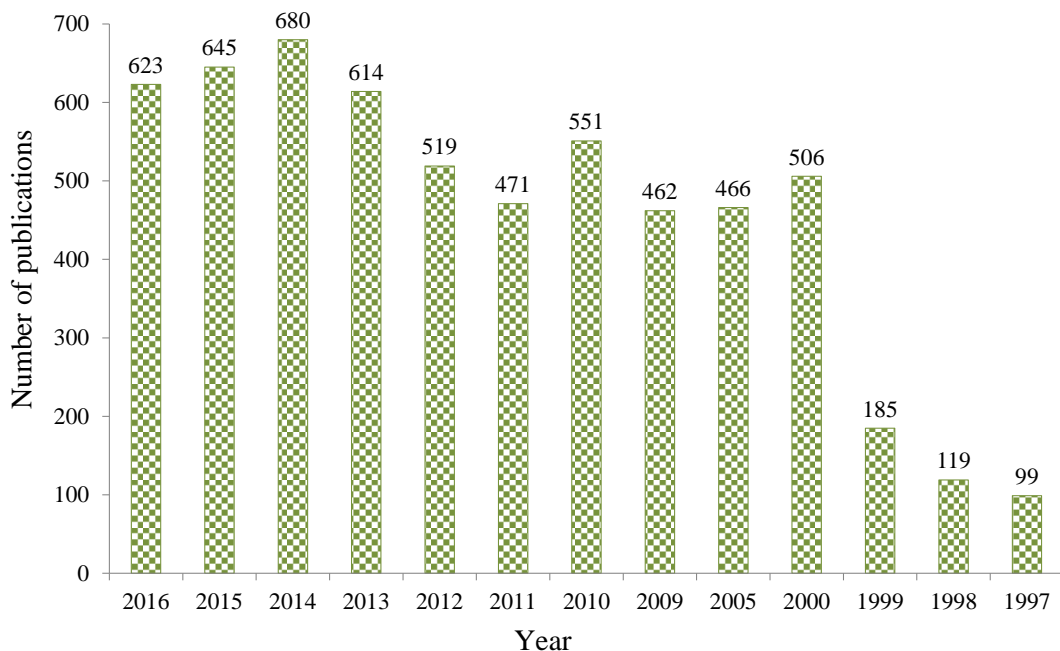


Figure 1-2 Number of publications on gas hydrates between 1997 to 2016 (Curtin University library catalogue database)

Gas hydrates plug formation in natural gas transport pipelines (Figure 1-3) cause high economic loss and safety risks. The global annual cost of using thermodynamic inhibitors in 2006 was estimated at \$500 million USD (Uchida et al., 2007). Hydrate plugs can occur in extremely low-temperature and high-pressure conditions in cases of wet gas production (dehydration unit failure or formation water production), inhibition system failure, during start up and because of significant Joule-Thomson cooling effects (Koh et al., 2007, Sloan et al., 2008b).

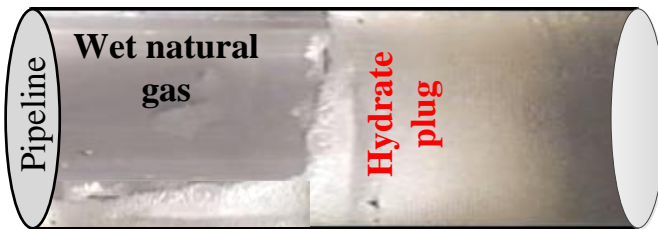


Figure 1-3 Natural gas hydrate plug in a transport pipeline (normally under high pressure and low temperature)

Hydrate formation can be prevented thermodynamically by altering the temperature and pressure region at which hydrates are stable. Thermodynamic prevention can be implemented by various methods, such as injecting thermodynamic inhibitors [mostly methanol and mono-ethylene glycol (MEG) that work by establishing hydrogen bonds among alcohol chains and the water, which reduces the activity of water in the forming hydrates], heating the system to above hydrate formation temperature, insulating the flow lines, separating the free water and gas dehydration, and reducing the operating pressure. In colder environments and high operating pressure systems, the percentage of thermodynamic inhibitor injection varies between 10 and 65 wt%. While methanol is the most efficient thermodynamic inhibitor, MEG is preferred over methanol because of low losses in the vapour phase, low toxicity, and ease of recovery and recycling. MEG recycling and reuse are implemented by MEG regeneration and reclamation plant. The design of such plants is complex, involving collaboration with multi-engineering disciplines and evaluating many design factors, such as the life expectancy of the field, corrosion risks, precipitation, water formation breakthrough, and thermal-oxidative degradation. The Curtin Corrosion Engineering Industries Centre (CCEIC) has constructed a full MEG pilot plant, including feed blending, pre-treatment, regeneration (distillation), and reclamation stages with storage tanks to replicate a real MEG recovery process. Regenerated and reclaimed MEG samples (20 wt%)

were experimentally analysed for natural gas hydrate inhibition performance by a PVT sapphire cell rig.

MEG can undergo thermal-oxidative degradation once exposed to high temperatures and oxygen and produces organic acids such as glycolic and acetic acids. These degradation products affect both the corrosion rate and the hydrate inhibition performance. Detailed studies were conducted in this thesis about the effect of regenerated MEG and degraded MEG on the gas hydrate inhibition performance of pure MEG and once mixed with corrosion inhibitors [Methyldiethanolamine (MDEA) and Film Forming Corrosion Inhibitor (FFCI)]. Furthermore, the thermodynamic functions of MDEA and FFCI on hydrate formation were analysed. It was found that they function as thermodynamic hydrate inhibitor. On the other hand, six MEG degradation analytical techniques were investigated, and a MEG degradation severity scale was developed. MEG is injected at a high rate to maintain a safe operating margin based on worst case scenarios of high pressure, low temperature, water cuts, and gas composition change. Before this study, the scenario of a fall in hydrate inhibition efficiency because of MEG degradation was not evaluated. Imposing MEG degradation factors on MEG injection calculation will maintain the safe operating margin. In this thesis, state-of-the-art knowledge of MEG regeneration and degradation effect on gas hydrate inhibition is investigated and presented.

1.2 Research Objectives

The main aim of this work is to investigate the feasibility of the thermodynamic relationship between the regenerated and the thermally degraded MEG on gas hydrate inhibition performance among natural gas with high methane content systems.

Consequently, the objectives of the project are:

1. To investigate the hydrate inhibition performance of thermally degraded MEG that's exposed to 165, 180 and 200 °C on methane gas hydrate.
2. To investigate the hydrate inhibition efficiency of thermally degraded MEG with corrosion inhibitors (MDEA and FFCI) that are exposed to 135, 165, 185 and 200 °C on a methane gas system, develop a hydrate phase boundary, and calculate the metastable region.

3. To investigate and develop novel data on the thermodynamic functions of MDEA and FFCI as gas hydrate inhibitors.
4. To investigate various analytical techniques for analysing severity levels of thermally degraded MEG and develop a novel MEG degradation scale.
5. To investigate the influence of regenerated and reclaimed MEG in the presence of complex fluids of condensates, corrosion inhibitors, drilling mud and other contaminants on hydrate inhibition of natural gas with high methane content.
6. To evaluate different hydrate prediction software with PVT cell experimental data and develop a prediction correlation function.
7. To analyse various gas hydrate mitigation techniques applied to a gas lift system.

1.3 Thesis Outline and Organisation

Mono-ethylene glycol is used widely as a thermodynamic hydrate inhibitor in various natural gas pipelines and gas processing plants. As a result of the large consumption rate of MEG, the high capital cost, and the disposal environmental impact, MEG regeneration is considered as the best solution to overcoming these impacts. During the regeneration, rich MEG undergoes thermal exposure by distillation and reclamation to remove water and salts, in which the thermal degradation process may occur.

This thesis presents extensive experimental and computational studies on natural gas hydrates (with high methane content) in presece of regenerated and thermally degraded MEGs by utilising a PVT sapphire cell, autoclave, and MEG benchtop facility at Curtin Corrosion Engineering Industries Centre (CCEIC).

This thesis consists of nine chapters, including the introduction, literature review, results and discussion (six chapters), conclusion and recommendation for future research works. Figure 1-4 provides a diagrammatic representation of the thesis organisation.

Chapter 1 — Introduction — gives a brief introduction of the background, general issues encountered, and solutions regarding natural gas hydrate formation and inhibition. This chapter also includes the research objectives and the thesis' structural organisation.

Chapter 2 — Literature review — a comprehensive review and summary of the various aspects of natural gas hydrates: structure and formation mechanisms,

nucleation, morphology, memory effect, growth, dissociation, thermodynamic inhibitors, low-dosage hydrate inhibitors, hydrates in natural gas production and transport systems, mono-ethylene glycol, MEG regeneration and reclamation systems, MEG degradation and gaps in literature

Chapter 3 — Investigation of gas hydrate problems and mitigation techniques applied in the gas-lift system at one of the oil fields in the Sultanate of Oman— this chapter gives an introduction, problem description, hydrate formation history, symptoms, and troubleshooting for determining hydrate formation and evaluating the implemented thermodynamic mitigation techniques.

Chapter 4 — Evaluation of Different Hydrate Prediction Software and Impact of Different MEG Products on Gas Hydrate Formation and Inhibition. OTC-26768-MS.2016 — evaluates different hydrate prediction software and MEG products with PVT cell experimental data and develops a prediction correlation function.

Chapter 5 — Inhibition effects of thermally degraded MEG on hydrate formation for gas systems. J. Pet. Sci. Eng. 2015; 135C: pp 608-617— investigates inhibition effects of thermally degraded MEG on methane hydrate formation and analyses MEG exposed to temperatures of 135 to 200 °C for the duration of 4 and 48 hours and pressure ranges of 50–300 bar.

Chapter 6 — Effects of Thermally Degraded Monoethylene Glycol with Methyl Diethanolamine and Film-Forming Corrosion Inhibitor on Gas Hydrate Kinetics. Energy Fuels. 2017; 31 (6): pp 6397–6412—investigates the effects of thermally degraded MEG exposed to temperatures of 135, 165, 185 and 200 °C with Methyl Di-Ethanolamine and Film Forming Corrosion Inhibitor on gas hydrate kinetics, analyses the hydrate inhibition performance of three different solutions at selected concentrations and pressures (50 to 300 bar).

Chapter 7 — Analytical Techniques for Analyzing Thermally Degraded Monoethylene Glycol with Methyl Diethanolamine and Film Formation Corrosion Inhibitor. Energy Fuels. 2016; 30 (12): pp 10937–10949 — evaluates different analytical techniques for analyzing thermally degraded MEG with MDEA and FFCI, focusing on evaluating six analytical techniques (pH, electrical conductivity, physical characteristics, IC/HPLC-MS, and gas hydrate inhibition performance) for analysing

the degradation level of various MEG solutions that were thermally exposed (135 °C to 200 °C) for 240 hours.

Chapter 8 — Influence of Regenerated Mono-ethylene Glycol on Natural Gas Hydrate Formation—investigates the influence of regenerated and reclaimed MEG solutions on natural gas hydrates (with high methane content). The MEG solutions were collected from a MEG pilot plant, simulating six scenarios of typical initial start-up and clean-up stages of a gas field. The clean-up stage contains complex fluids of condensate, drilling mud with high concentrations of mineral salts, particulates, and various production chemicals.

Chapter 9 — Conclusions and recommendations — concludes with significant findings from this study and provides recommendations for future research.

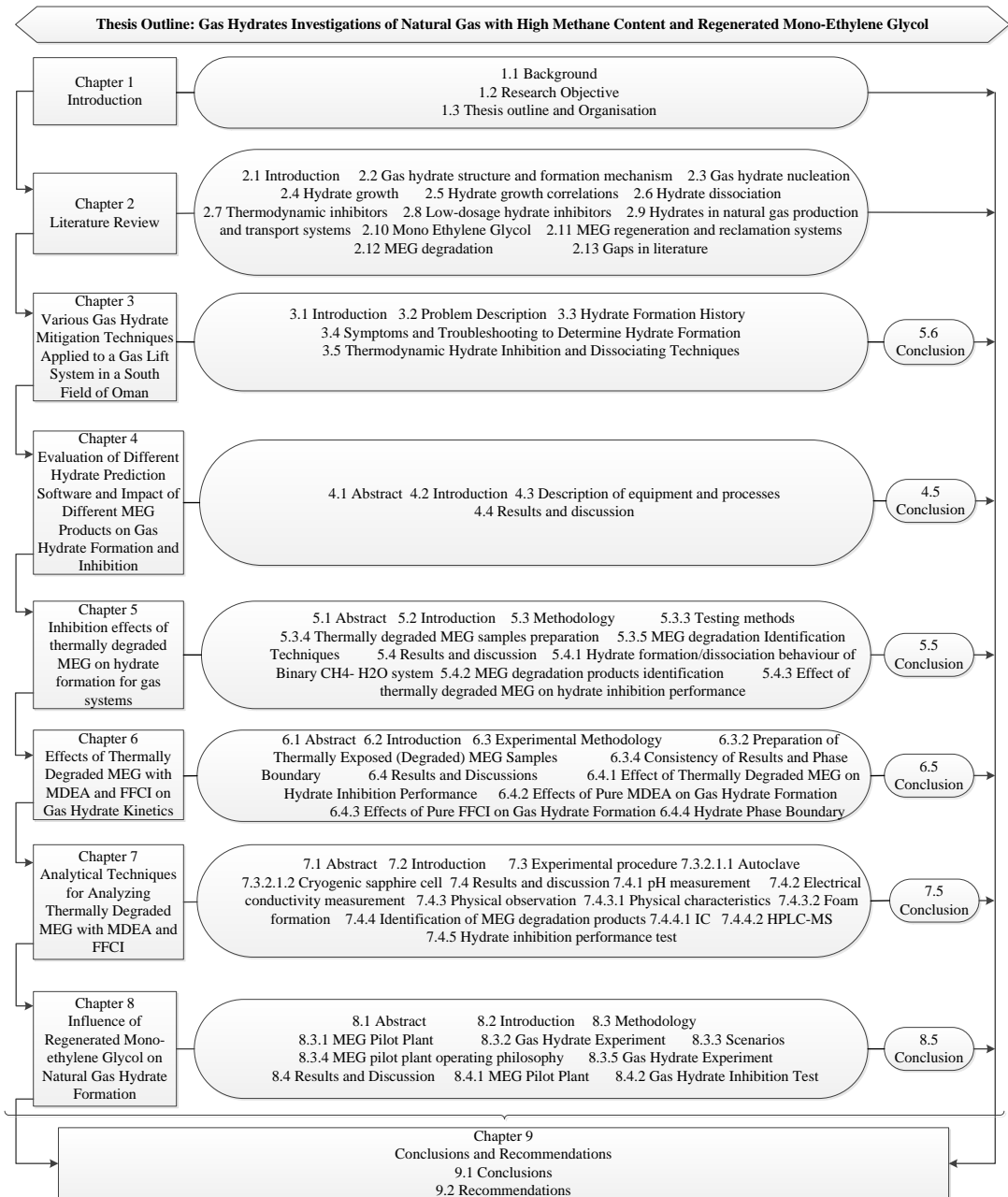


Figure 1-4 Diagrammatic representation of the thesis' organisation

Chapter 2 Literature Review

2.1 Introduction

The literature review chapter provides a core explanation on gas hydrates and regenerated Mono Ethylene Glycol. The initial section has presented the overview of gas hydrate structures and nucleation mechanisms. An extensive review on the kinetics of hydrate formation and growth has been discussed following the first section of this chapter. This review highlights essential hydrate formation mechanisms in gas and liquid systems. Additionally, thermodynamic hydrate inhibitors (Methanol, Mono-ethylene glycol, Diethylene glycol and Triethylene glycol, etc.,) along with the low-dosage hydrate inhibitors (Kinetic Inhibitor and Anti-Agglomerants) and others hydrate inhibitor methods have also been discussed. Hydrates formation in natural gas production and transport systems are presented together with safety impact consequences while dissociating hydrate plugs in pipelines. Following on is an overview of mono-ethylene glycol, the property, production of MEG, different models of MEG regeneration and reclamation systems and MEG degradation. Finally, the gap in literature is discussed. The contextual background is endowed in this chapter to emphasise the overall chapters of the thesis.

2.2 Gas hydrate Structure and Formation Mechanism

Gas hydrates are ice like solid components, often emphasised as crystalline compounds when compared to other molecules as determined by appropriate shapes and sizes in hydrogen-bonded water molecules cages. Clathrate hydrates is a Latin root word where clatratus means barred or latticed. Gas hydrate structures form once molecules of water form a cage, comprising of small gas molecules (< 0.9 nm) such as ethane, methane or carbon dioxide, at adequate pressures and low-temperature conditions (typically < 27 °C and > 6 bar). It is important to note that the gas molecules and the water cage are not bonded chemically; however, the formation of the water cage is generated by hydrogen bonding of adjacent water molecules. The repulsion force of the trapped gas in the water cage is what restricts it from collapsing. The concentration value of gas molecules in the hydrate structure can be up to 170 times, that's is, 170 m^3 of gas molecules can be stored in just 1 m^3 of hydrate. (Sloan et al., 2010). It is important to note that formation of gas hydrates

are not welcomed by all gas molecules as guests molecules are constrained by molecules with low water solubility attributes, and particular molecular size (Martín et al., 2009, Jacobson et al., 2010). The size of the gas molecule is the reliant variable in distinctive hydrate crystal structures and are classified as cubic structures I, II and H (Sloan et al., 2008b).

2.2.1 Cubic structure I

Cubic structure I (Figure 2-1) are outweighed in the natural environment of the earth, comprising small guests molecules of 0.4 to 0.55 nm such as; C₁ (methane), C₂ (ethane) (Figure 2-2), and CO₂.

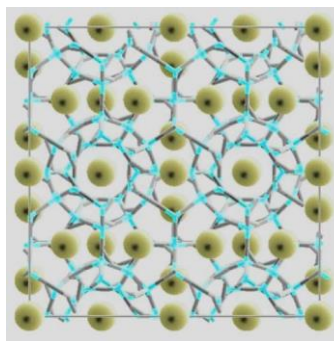


Figure 2-1 Crystal structures sI hydrate; four unit cells viewed along a cubic crystallographic axis. All cavities are assumed to be filled; adapted after Koh (2002)

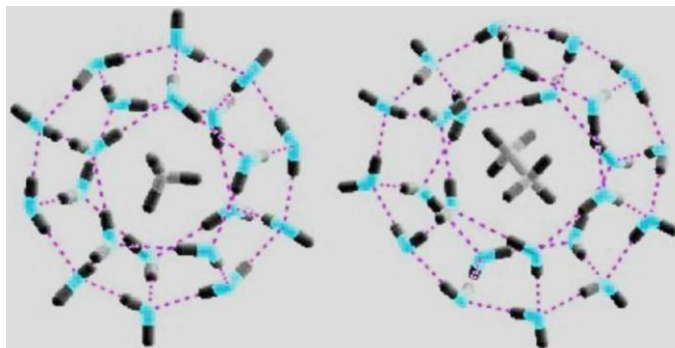


Figure 2-2 A 5¹² pentagonal dodecahedral cavity enclosing methane (left) and a 5¹²6² tetracaidecahedral cavity enclosing ethane (right); adapted after Koh (2002)

Structure I are comprised of 46 water molecules and are determined as body-centered structures. The tetracaidecahedral 5¹²6² cavities and the pentagonal dodecahedral 5¹² cavities are the two types of cavities of structure I (Table 2-1). 12 pentagonal faces and two hexagonal faces are included in the tetracaidecahedral 5¹²6² cavity and is comparatively larger than the building block of pentagonal dodecahedral 5¹². To relieve the hydrogen bond strain, the formation of structure I is linked with additional

water molecules with the vertexes of the pentagonal dodecahedral 5^{12} cavities (Sloan et al., 2010) (Figure 2-6). Thereby, guest molecules identity significantly influences the kinetics and the stability of hydrate formation as structure I hydrate comprises of two 5^{12} cavities for every six $5^{12}6^2$ cavity (Christiansen et al., 1994).

The cavities of structure I hydrates can only enclose smaller diameter gas molecules, such as methane having 4.36 Å and ethane 5.50 Å (Sloan et al., 2010). Conversely, the 5^{12} cavity can trap the methane molecules as it has a smaller diameter, while the $5^{12}6^2$ cavity can trap ethane gas with a larger diameter which is too large to fit the 5^{12} cavity (Figure 2-2). The hydration reaction of methane (CH_4) is given in Eq 2-1:



Where N_{hyd} is the molar ratio of water reacting with methane, normally this number is 6 (Worthington, 2010), however this value can range from 5.75 to 17 (Lonero, 2008).

2.2.2 Cubic structure II

Cubic structure II (Figure 2-3) comprises of larger guests molecules of 0.6 to 0.7 nm in process systems, which include; C_2 , C_3 (propane) (Figure 2-4) and iC_4 (isobutane).

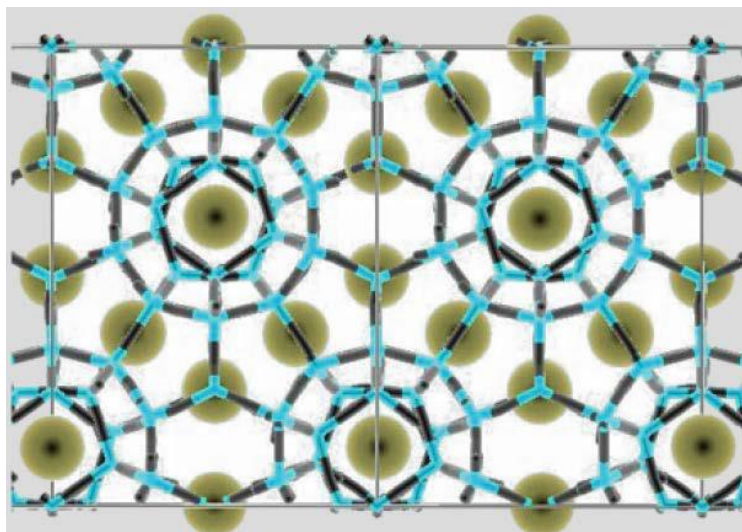


Figure 2-3 Crystal structures sII hydrate; two unit cells observed along a face diagonal. All cavities are supposed to be filled; adapted after Koh (2002)

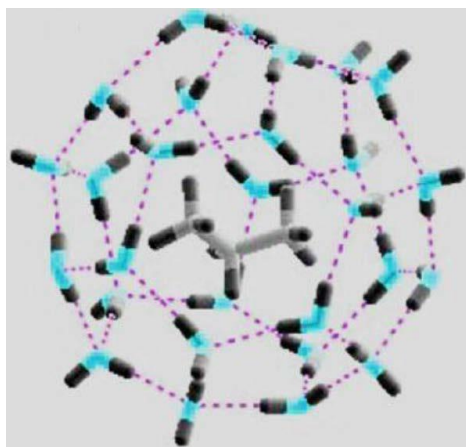


Figure 2-4 Propane inside a hexakaidecahedral $5^{12}6^4$ cavity; adapted after Koh (2002)

A cubic framework is entailed in structure II hydrates in which the formation of a diamond lattice takes place, containing 136 water molecules (Table 2-1). The pentagonal dodecahedral 5^{12} building block and a hexakaidecahedral cavity $5^{12}6^4$ are the two types of cavity present in structure II hydrates comprising of four hexagonal and 12 pentagonal faces. A larger free diameter of 6.66 Å is mostly seen in the $5^{12}6^4$ cavity, which consequently forms into a larger cavity for enclosing guest molecules (Sloan et al., 2010). Figure 2-4, demonstrates a propane molecule containing a diameter of 6.50 Å, placed within larger cavity. The formation of structure II hydrate crystal unit requires eight larger $5^{12}6^4$ cavities and 16 small 5^{12} cavities. It is evident from the experimental observation that structure II hydrates can enclose propane, isobutane, krypton, nitrogen and argon (Christiansen et al., 1994).

2.2.3 Hexagonal structure H

The observance of structure H hydrates (Figure 2-5) is not commonly perceived in natural gas environments when comparing with structure I and structure II hydrates. In particular, it combines with the two types of guest molecules, small and large guest's molecules (0.8 to 0.9 nm) such as C₅-C₆ (pentanes-hexanes). On the contrary, structure H hydrates possess significant attention in the oil industry.

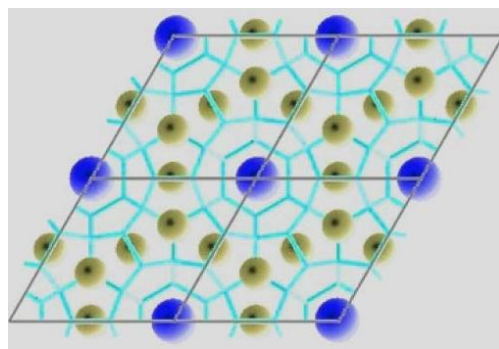


Figure 2-5 Crystal structures of sH hydrate. The positions of the hydrogen atoms have not been encompassed; four unit cells were aligned along the six-fold crystallographic axis. $5^{12}6^8$ has been highlighted by the blue guests and all cavities assumed to be filled; adapted after Koh (2002).

The formation of the hexagonal crystal structure with a large cavity is made through 34 water molecules of structure H hydrates (Figure 2-6). Ripmeester et al. (1987) have stated that additional three square faces are contained in the sH cavities. Additionally, the formation of structure H hydrate crystal unit contains one large icosahedral $5^{12}6^8$ cavity, two small irregular dodecahedral $4^35^66^3$ cavities and three small pentagonal dodecahedral 5^{12} cavities (Timmis et al., 2010). Large guest molecules are required within the formation of structure H hydrates by occupying $5^{12}6^8$ cavities and with the presence of small molecules; for example methane. Therefore, the presence of structure H hydrates is emerged in denser hydrocarbon mixtures such as condensates and oil.

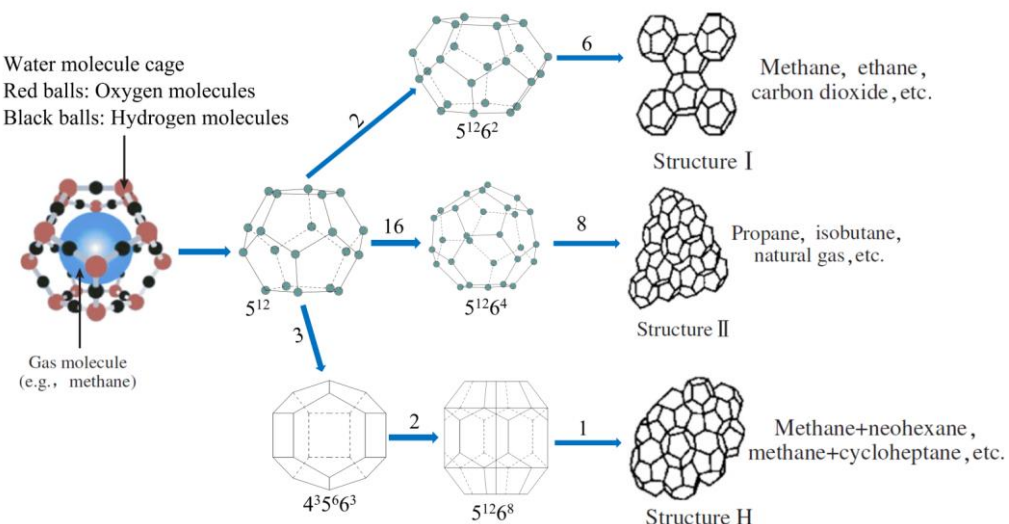


Figure 2-6 Gas hydrates crystal structures; adapted after (Giavarini et al., 2011, Timothy S. Collett et al., 2009)

The properties of the three common unit crystals are demonstrated in Table 2-1. Sloan (2003) has indicated that smaller cages are not able to trap big single guest molecules and thus, obliged to be filled in the larger cages even though both small and large cages exist in the crystal structure. Conversely, both cages can be filled with smaller molecules.

Table 2-1 Properties of the three common unit crystals; adapted after Sloan (2003)

Hydrate crystal structure	I		II		H		
Cavity	Small	Large	Small	Large	Small	Medium	Large
Description	5^{12}	$5^{12}6^2$	5^{12}	$5^{12}6^4$	5^{12}	$4^35^66^3$	$5^{12}6^8$
No of cavity per unit cell	2	6	16	8	3	2	1
Average cavity radius (\AA)	3.95	4.33	3.91	4.73	3.91 [§]	4.06 [§]	5.71 [§]
Coordination number*	20	24	20	28	20	20	36
Number of water/unit cell	46		136		34		

* Number of oxygen at the periphery of each cavity.

[§] Estimates of structure H cavities form geometric models.

The production of hydrate cavities takes place when there is a reduction in the water temperature and becomes stable when filled with the gas molecules (Pedersen et al., 2014). According to the experiments, approximately 0.9 is the required ratio of the size of the guest molecule to the cavity to become stable (Gabitto et al., 2010), whereas the optimal range of 0.86-0.98 stable ratios was identified by Sloan et al. (2010).

Only one normal guest molecule is present inside each cage of all hydrate structures. Conversely, it is probable that multiple small guest molecules including noble gases or hydrogen occupy a single cage at such conditions of high pressures. It has been suggested by Mao et al. (2002) that hydrogen atoms can form with four occupants in the large cage and two occupants in the small cage of hydrate structure II at a high pressure conditions. Hydrates are crystalline in nature but non-stoichiometric as some cavities are left unoccupied and as there is a clear pattern between the diameters of the cavity and the ratio of the guest molecule (Sloan et al., 2008b). Moreover, same

composition of 15 mole% guests and 85 mole% water is found in the three hydrate types when all cavities are occupied (Sloan et al., 2010).

When the cavities in the crystal structure are occupied with only one type of gas molecule, this is called a simple hydrate. Methane (CH_4), hydrogen sulphide (H_2S), carbon dioxide (CO_2) and ethane (C_2H_6) are examples of simple structure I natural gas hydrates. In addition, nitrogen, propane and iso-butane are examples of simple structure II natural gas hydrates. Moreover, the formation of binary hydrates can be formed by the clathrate of two gases such as CO_2 and CH_4 and C_2H_6 and CH_4 . Binary CH_4-CO_2 mixture forms only structure I hydrate. However, for the situation of the binary $\text{CH}_4-\text{C}_2\text{H}_6$ mixture (both forms sI individually) the formation of structure I or structure II might take place, based on the temperature and pressure conditions (Sloan et al., 2008b). Gases do not occupy all the cavities when forming hydrates. As stated by Sloan (1998), typical hydrate occupancies of large cavities is 50% while the small cavity is 95%. Detailed gas hydrates morphological structures are given elsewhere (Makogon, 1981, Sloan, 1998, Ribeiro et al., 2008).

Hydrate formation usually takes place between the interface of guest molecule and the aqueous phases because of the availability of the high concentrations of both guest gases and host cavities which exceed the mutual fluid solubilities. This solid interface layer prevents further hydrate formation causing an interaction barrier between the gas-liquid phases, unless fluid surface renewal is activated such as by agitation or turbulent flow (Makogon et al., 2000, Mostowfi et al., 2014).

According to experimental observation of hydrate and ice, there are assorted different distinctive physical and chemical properties even though they have almost apparently similar. However, the most significant properties is that hydrate can clathrate at 0 °C or higher temperature, and sinks in water due to higher density whereas ice floats on the water surface (Giavarini et al., 2011). Moreover, the trapped gases of a gas hydrate can undergo combustion when exposed to extreme heat (Figure 2-7) while this property cannot be revealed for ice (Suess et al., 1999).



Figure 2-7 Reddish methane hydrate flame (Flammable ice); after (Suess et al., 1999, Giavarini et al., 2011)

Von Stackelberg (1949) has introduced the correlation between the type of hydrate formed and the size of the molecule. The chart produced by Von Stackelberg (1949) [redrawn by Giavarini et al. (2011) and Carroll (2014)] is shown in Figure 2-8, which indicates that the gas hydrate nature relies on the guest molecule size. It is revealed from the chart (Figure 2-8) that hydrates are not formed with molecules containing diameters less than 3.8 \AA ($1 \text{ \AA} = 1 \times 10^{-10} \text{ m}$). From the chart, it is clear that initial hydrate formers commence with molecules diameters of 4 \AA such as nitrogen and krypton. The formation of type I or type II hydrate is limited with molecule sizes larger than 7 \AA . Type H hydrates can be formed through slightly larger molecules however, the formation of hydrate is limited by 9 \AA . Thereby, molecules with greater molecules diameters than 9 \AA are non-formers, such as hexane, larger paraffin hydrocarbons and pentane.

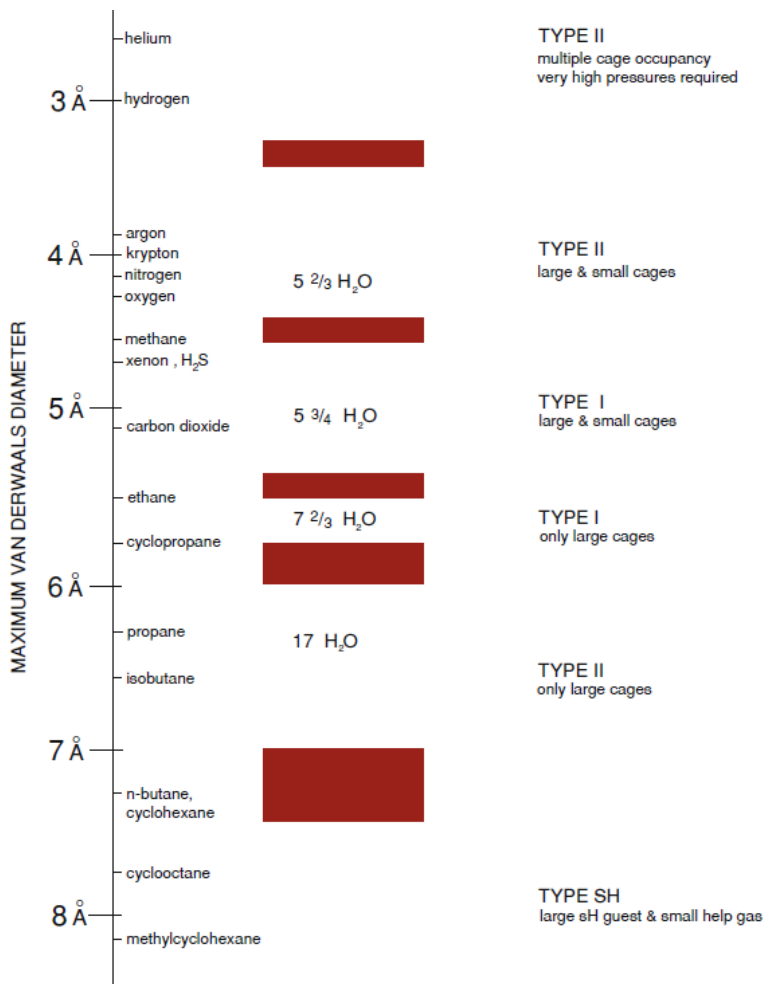


Figure 2-8 Comparison of guest size, hydrate type, and cavities occupied for various hydrate formers; after Giavarini et al. (2011)

2.3 Gas Hydrate Nucleation

Hydrate nucleation is considered as a process of expansion and dispersion of small water and gas clusters that accomplish appropriate crystal size for continued growth. According to Mullin (2001), restricted hydrate nucleation experimental verification is revealed from the involvement of tens to thousands of molecules in the stochastic and microscopic process. Labile cluster nucleation and local structuring nucleation are two major hypotheses that exist in the current experiments and modelling (Sloan et al., 2008b).

2.3.1 Local structuring nucleation hypothesis

Radhakrishnan et al. (2002) suggested that local structuring nucleation hypothesis is supported by the formation of carbon dioxide hydrate, indicating that a local structuring model can be used to replace the labile cluster nucleation hypothesis. The arrangement of guest molecules is caused by thermal functions in a similar manner to

that of the hydrate phase in the local structuring model. Conversely, the disruption of water molecules structure throughout the guest molecules is evident, compared with rest of the water phase. The arrangement of the gas and water phases is structured closely to the hydrate phase heading towards the formation of critical size hydrate nucleus and subsequently growth.

The computation of Landau-Ginzburg free energy for carbon dioxide hydrate nucleation and Monte Carlo simulations have been performed through isobaric and isothermal experimental method (Radhakrishnan et al., 2002). These experiments allowed advance analysis of the nucleation mechanism at the interface level, which concluded within the study of Christiansen et al. (1994) on agglomeration of labile clusters might not be favoured thermodynamically. The free energy required to form clusters is much higher than the energy required for collapsing, thus requiring higher energy to overcome the free energy barrier. Radhakrishnan et al. (2002) have indicated that it is almost impossible to form nuclei by labile clusters for carbon dioxide hydrates due to the free energy barrier. They also proposed two major mechanisms of nucleation to initiate the clathrate phase nucleation based on local structuring hypothesis. The first mechanism states that a selection of guest molecules is derived by a thermal fluctuation to restructure in a clathrate configuration. The disturbance in the bulk structures is also seen among the surrounded guest molecules of the water molecule structures, which indicate a stochastic nature. The second mechanism states that, if the number of the critical nucleus has been surpassed by the entire extent of guest molecules in the locally ordered arrangement, this will result in local stability caused by the relaxation of the surrounding water molecules. The critical nuclei formation is the resultant from the clusters parameters of host-host and guest-guest that is similar to a clathrate hydrate. Another similar model was simulated by Moon et al. (2003a) using MD simulations of methane hydrate nucleation. These researchers demonstrated that formation of methane hydrates eventually took place at the water interface, as revealed from a steady growth of clathrate clusters of the simulated system. Evidence for long-range structures is provided in accordance with the local structuring nucleation hypothesis, observed in the changes in the structures over the entire simulation. The indication of hydrogen bonds forming hydrate structures is illustrated from the snapshots of ‘hydrate-like’ water lines connecting with methane molecules (Figure 2-9), demonstrating the

restructure over a longer range of water molecules instead of creating independent molecules.

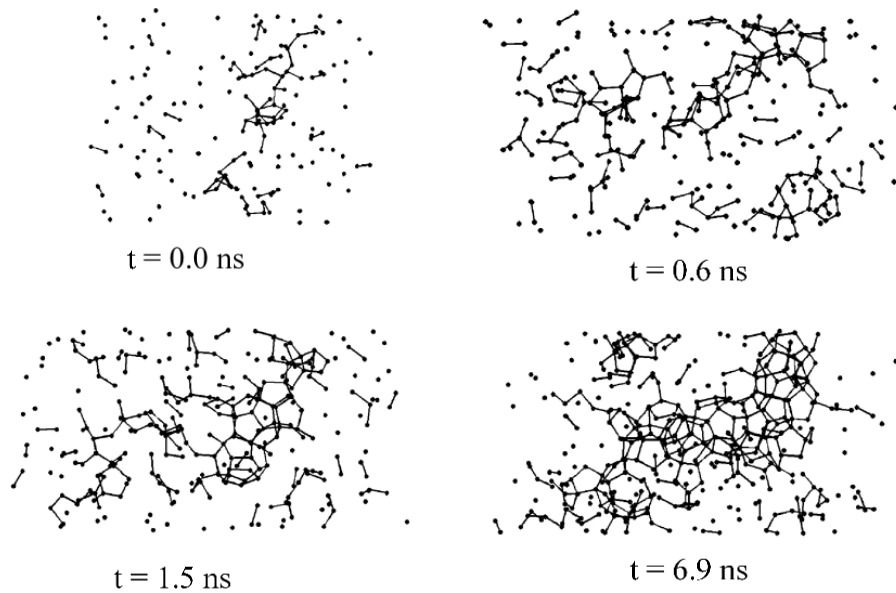


Figure 2-9 Growth of local structure nucleation lines (with time shown in nanoseconds) indicate the hydrogen-bond network; after (Moon et al., 2003c)

The investigation of Moon et al. (2003c) for the water molecule cluster formation, demonstrating that the faces shared generated stable cages. This supports the hypothesis of the labile cluster nucleation. The model of a 5^{12} cavity is illustrated in Figure 2-10, in which it shows the sharing face to develop a stable cluster. It has been concluded that although the methane-water simulations show similarity to the labile cluster hypothesis, it is consistent with the local order model of nucleation.

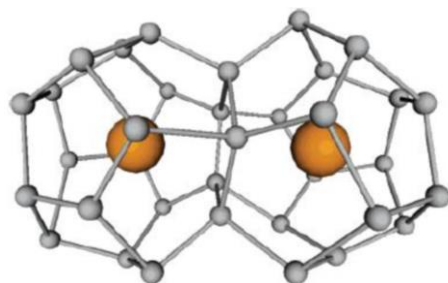


Figure 2-10 Stable sharing of faces in a 5^{12} cavity with methane gas, formed by 6 ns; after (Moon et al., 2003c)

2.3.2 Labile Cluster Nucleation Hypothesis

Initial conditions of labile cluster nucleation hypothesis is the stage when temperature and pressure are in the hydrate region while there is no possibility of

observations of the dissolved gas molecules. Point A in Figure 2-11 illustrates the initial condition where the labile cluster nucleation hypothesis relies on the presumption that hexamer and pentamer labile ring structures are organized by pure liquid water molecules (Schicks, 2010). Stillinger (1980) has evaluated that the water network structures are mostly caused by hydrogen bonds. The formation of labile clusters is immediately reflected at point B, and combined with agglomerate clusters until the formation of hydrate unit cells (point C) with respect to the guest molecule dissolution in water. A critical size was extended to point D, where unit cells were combined and agglomerate from which growth begins. Labile clusters formation size (or coordination number) is augmented with the guest molecule size in each cluster shell. For instance, natural gas components' coordination numbers for carbon dioxide, ethane, propane, I-butane and methane are 24, 24, 28, 28 and 20 respectively (Sloan et al., 2008b).

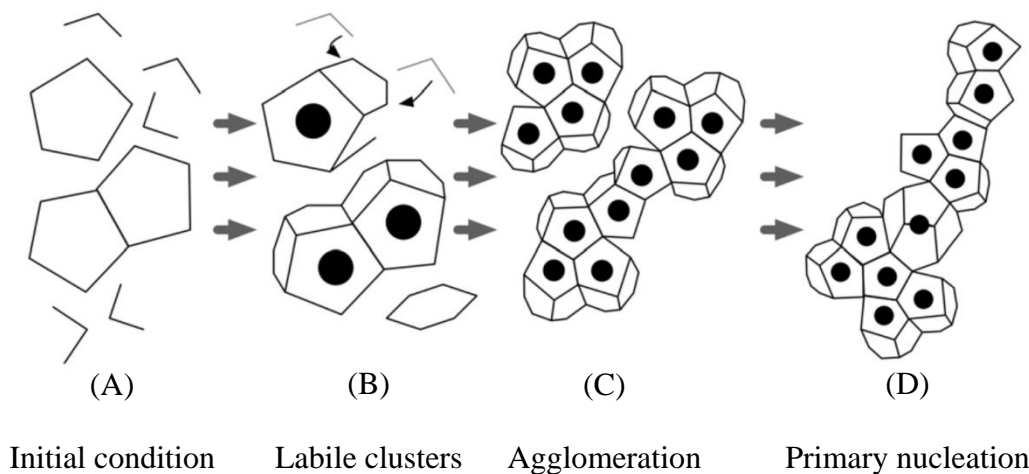


Figure 2-11 Labile cluster nucleation; adapted after Aman et al. (2016)

It is assumed that guest molecules are dissolved in a single cage in contrast to the local structuring hypothesis where local structuring nucleation cannot be observed with long range arrangement. The labile cluster nucleation process (Figure 2-11) can be linked to the physical hydrate formation/dissociation process at a PVT cell using isochoric method (constant volume) as shown in Figure 2-12. Before point 1 the gas is not dissolved in water. As pressure increases (point 1), the guest molecules start to dissolve within the water resulting in the formation of labile clusters around the polar guest molecules. It is evident that labile clusters are bounded to different clusters for producing the hydrate unit cells in the metastable phase of the cooling period due to

the existence of labile clusters in subcritical size between points 1 and 2. The joining of labile clusters at point 2 becomes evident in which to achieve the critical size of nucleation. Although the completion of primary nucleation has been succeeded at point 2 and quick hydrate growth is achieved, fast pressure drop is encompasses (between points 2 and 3) due to the encapsulation of gas molecules in the hydrate crystals. Point 3 is the end of the hydrate growth process, where hydrate formation stops. By moving the structure from point 3 to point 4 and by heating the system on a higher temperature commences the hydrate dissociation process. It decomposes the hydrate agglomerates into the liquid and vapour phases. However, quasi-crystalline metastable cluster structures remain in the liquid form at a certain degree of superheating (Christiansen et al., 1994).

The hydrate formation/dissociation process in a PVT cell using isochoric method is also shown in Figure 2-13 and chapter 8.

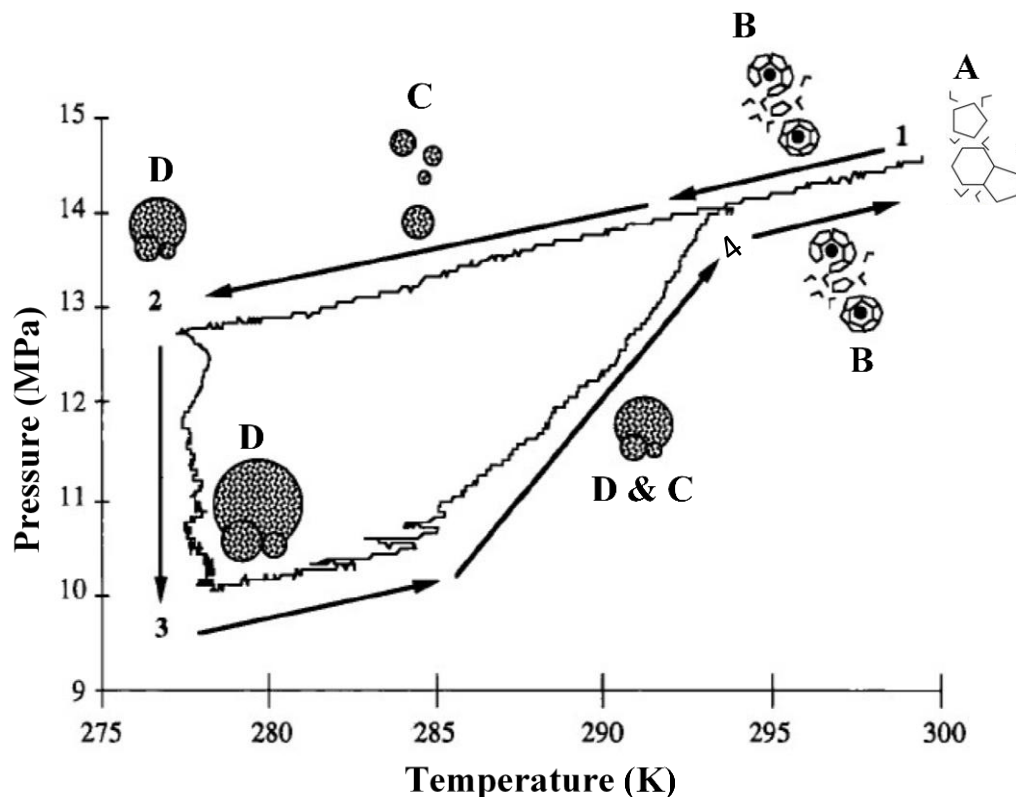


Figure 2-12 Schematic of hydrate formation/dissociation on an isochoric method; adapted after Christiansen et al. (1994)

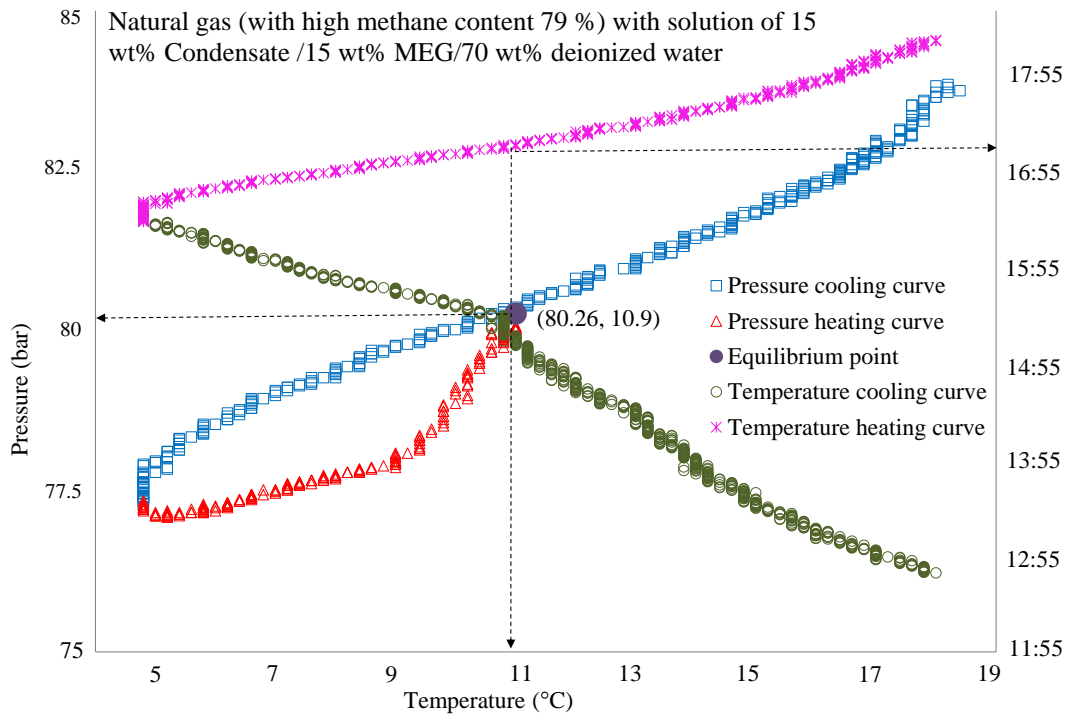


Figure 2-13: Determination of the hydrate dissociation point (equilibrium) from the Pressure-Temperature trend by the intersection point of the cooling and heating cycles (our work).

The rate of hydrate nucleation is another core focus for labile cluster nucleation. Christiansen et al. (1994) have asserted that formation of structure II hydrates ultimately results by hydrate nucleation kinetics. On the contrary, the excessive contradictions on this assertion and existence of newer experimental evidence demonstrate the energy restriction for the labile clusters agglomeration in larger form as compared to the requirement of disintegrated clusters (Radhakrishnan et al., 2002).

2.3.3 Nucleation at the interface hypothesis

As discussed by Kvamme (2000), the occurrence of the nucleation is emerged on the vapour side of the interface rather than on the liquid side. Rodger (1990) conducted a simulation for molecular dynamics and indicated that gas molecules cause through attractive dispersion forces captivate the surface of the water interface. The disruption of water molecule structures occur at the interface when the molecules are formed into a layer, and results into a hydrogen bonding network formation in gas hydrates.

The location of hydrate nucleation was experimentally investigated by Long et al. (1996), in which they found that nucleation for carbon dioxide hydrates that occurred on the vapour side of the gas/water interface. Moon et al. (2003c) have studied the molecular dynamics of hydrate formation in which they specified that the formation of methane hydrates favourably take place at the gas/water interface. This has also been observed by AlHarooni,Pack, et al. (2016) (Figure 2-14).



Figure 2-14 Methane hydrate start formation at interface of a PVT cell; after AlHarooni,Pack, et al. (2016)

Figure 2-15 show the adsorption and clustering of gas hydrate nucleation at the interface on the gas side. It is assumed that movement of the gas molecules at the vapour phase travel towards the vapour-liquid interface, indicating the preferred placement for hydrate nucleation. The aqueous surface then adsorbs the gas molecule and form cages across the gas molecule (guest). The labile clusters agglomeration accomplish a critical size in which the occurrence of growth is seen on the gas side of the interface. This results in quicker hydrate growth, doubles the time compared to the water side (Sloan et al., 2008b).

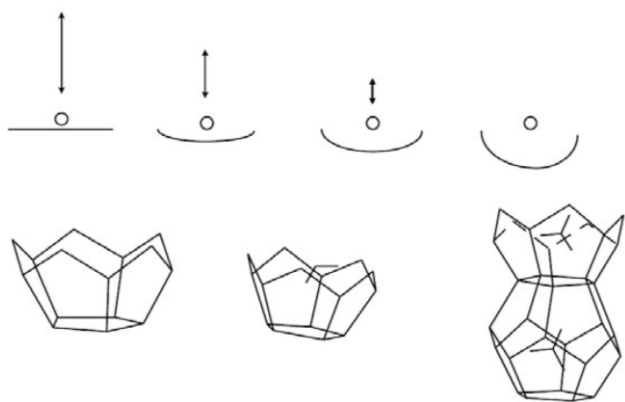


Figure 2-15 Gas hydrate nucleation at gas-water interface; after Sloan et al. (2008b)

2.3.4 Morphology of gas hydrate nucleation

Makogon (1997) and Wu et al. (2010) have conducted experiments that have shown different types of crystallisation. They identified three morphology types for hydrate crystals namely: massive, whiskery, and jelly. Wu et al. (2010) observed, by the naked eye, that massive, whiskery, and jelly crystals for methane gas hydrates appeared at 4~8 °C and 50~70 bar.

Figure 2-16 (a-c) and Figure 2-17 present the morphology of massive gas hydrate nucleation formed above the gas-liquid interface. Figure 2-18 (a-c) and Figure 2-19 show the morphology of whiskery gas hydrate nucleation which appears after complete hydrate formation, which grows upward in the gas phase.

The morphology jelly gas hydrate nucleation is illustrated in Figure 2-20 and Figure 2-21. The formation of jelly crystals is observed in the second hydrate process, which has followed hydrate dissociation process. Generally, jelly crystals are produced under particular circumstances in bulk water. Whiskery crystals augment in a liquid and volume of gas, and massive crystals augment regularly in a volume of gas (Makogon, 1997, Wu et al., 2010).

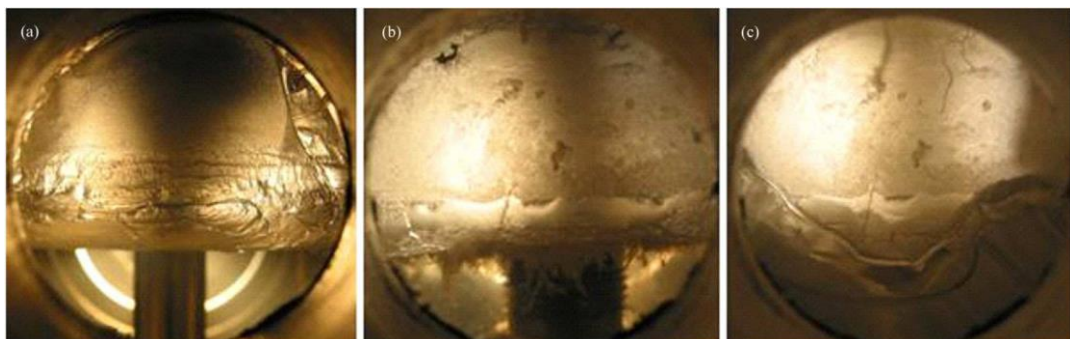


Figure 2-16 Massive methane hydrate crystals; after Wu et al. (2010)



Figure 2-17 Massive methane hydrate crystals (our work).



Figure 2-18 Whiskery methane hydrate crystals; after Wu et al. (2010)



Figure 2-19 Whiskery methane hydrate crystals (side view and top view) (our work).

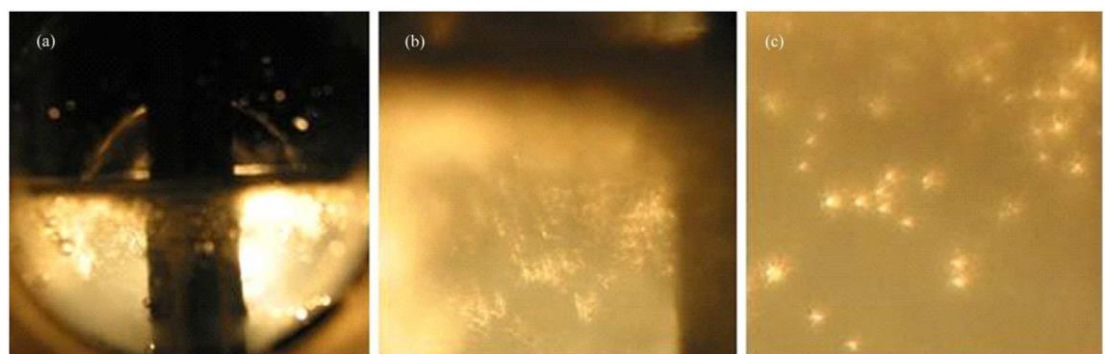


Figure 2-20 Jelly methane hydrate crystals; after Wu et al. (2010)



Figure 2-21 Jelly methane hydrate crystals (our work).

2.3.5 Gas Hydrate Memory Effect Phenomenon

Gas hydrate memory phenomenon is the ability of gas hydrate, when melted at moderate temperatures, for retaining a memory of their structure (Parent et al., 1996, Takeya et al., 2000). Therefore, the melted hydrate obtains formation of hydrate at shorter induction time and relaxation condition compared to with no previous hydrate history (fresh water) (Vysniauskas et al., 1983).

Makogon (1974) has published an examination of memory effect, in which the formation of hydrates rapidly emerges from the melted hydrate when compared to no previous hydrate history. Memory effect surveillance has been considered in the previous forty years, such as through the work of Schroeter et al. (1983). These researchers demonstrate that successive cooling cycles with same dissociated liquid results in a decreased formation point as seen in Figure 2-22. The Figure shows how hydrate formation becomes more relaxed at each repeated experiment, cycle C3 formed more easily than C2 and C1, and cycle C2 formed more easily than C1.

The gas hydrate memory effect study has attracted researchers' interest, with the mechanism analysed from different aspects (Makogon, 1981, Lederhos et al., 1996, Parent et al., 1996, Takeya et al., 2000, Ohmura et al., 2003, Arjmandi et al., 2005, Sloan et al., 2008b, Duchateau et al., 2009, Del Villano et al., 2011, Sefidroodi et al., 2013).

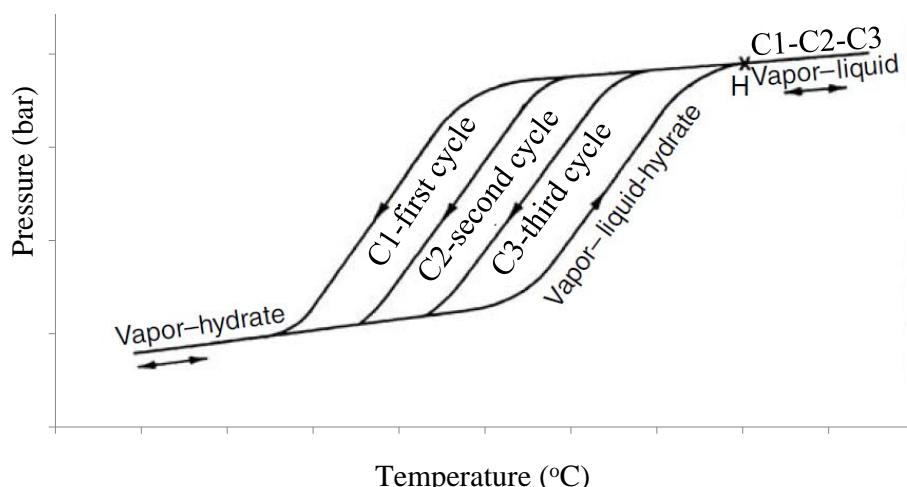


Figure 2-22 Consecutive hydrate formation cooling curves for several runs; adapter after Schroeter et al. (1983)

The study of Wu et al. (2010) represented the induction time for methane gas hydrate nucleation. Once gas hydrate is formed and is dissociates, the second formation happens at marginally greater temperatures when compared to the earlier formation (Figure 2-23). It also applies to the cycles C3 and C4 as the time of nucleation decline for each successive test. The increment of both dissociation and nucleation temperatures is determined with each successive cycle, which demonstrates the prompt hydrate formation caused by memory effect. Once the melted hydrate had been warmed to $> 25^{\circ}\text{C}$, memory effect is destroyed, as aligned with the findings of Link et al. (2003) and Takeya et al. (2000). Memory effect phenomena could be used as a hydrate promoter technique for hydrate development projects.

Lee,Susilo, et al. (2005) reported that the higher induction times are achieved from the longer dissociated hydrate left before reformation. The hydrate dissociation has shown higher induction time for dissociated hydrate left for 12 hours compared to 1 hour. The outcomes are aligned with the results of Vysniauskas et al. (1983) and Ohmura et al. (2003), in which they reported the influence of the thermal history of water on the hydrate induction times. The study has examined that induction time for dissociated hydrate is less than that of warm water.

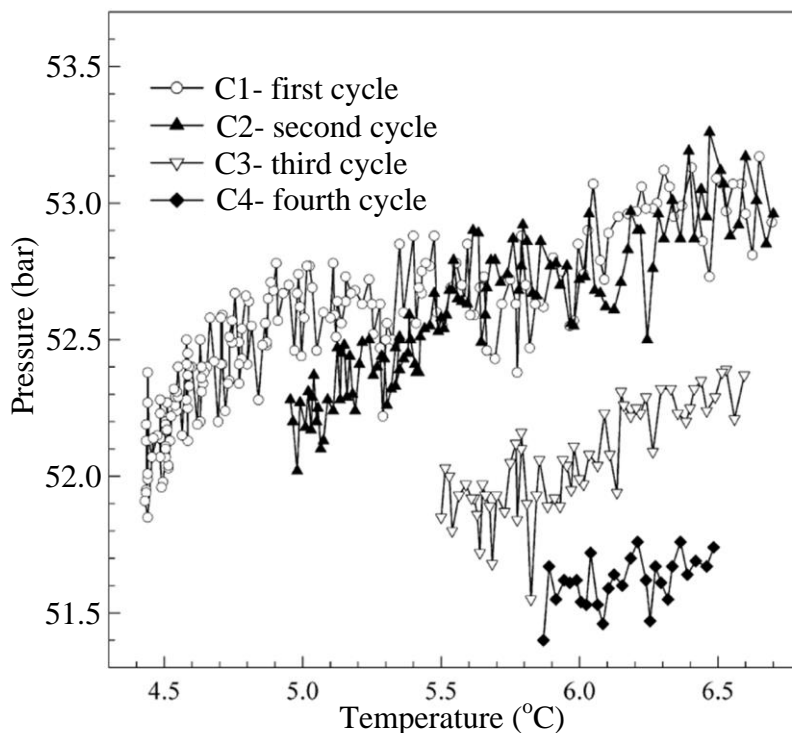


Figure 2-23 Hydrate formation repetition of same fluid after dissociation; adapted after Wu et al. (2010)

Servio et al. (2003) had focussed on analysing the effects of the macroscopic crystal morphology of carbon dioxide and methane hydrates made from water droplets. They showed that memory effect accelerated the hydrate growth. (Figure 2-24). Their analysis showed that after 30 minutes of hydrate full dissociation of a fresh water droplet with previous hydrate history, the size of a 10 minutes hydrate growth was equivalent to a 25 hours hydrate growth of a water droplet with no previous hydrate history [Figure 2-24 (a) and (b)]. Another distinction, made in their research, showed that hydrate surface before decomposition for 24 hours exhibited surface depressions due to water depletion [Figure 2-24 (a)]. For 10 minutes of hydrate growth on water droplet that experienced fully dissociated for 24 hours before reformation, resulted in irregular and jagged surface with numerous needle-like crystals encompassing outward away from the surface [Figure 2-24 (b)]. Alternatively, a 10 minutes of hydrate growth on a water droplet that has left for 30 minutes after fully dissociated, resulted in smooth and shiny surface [Figure 2-24 (c)].

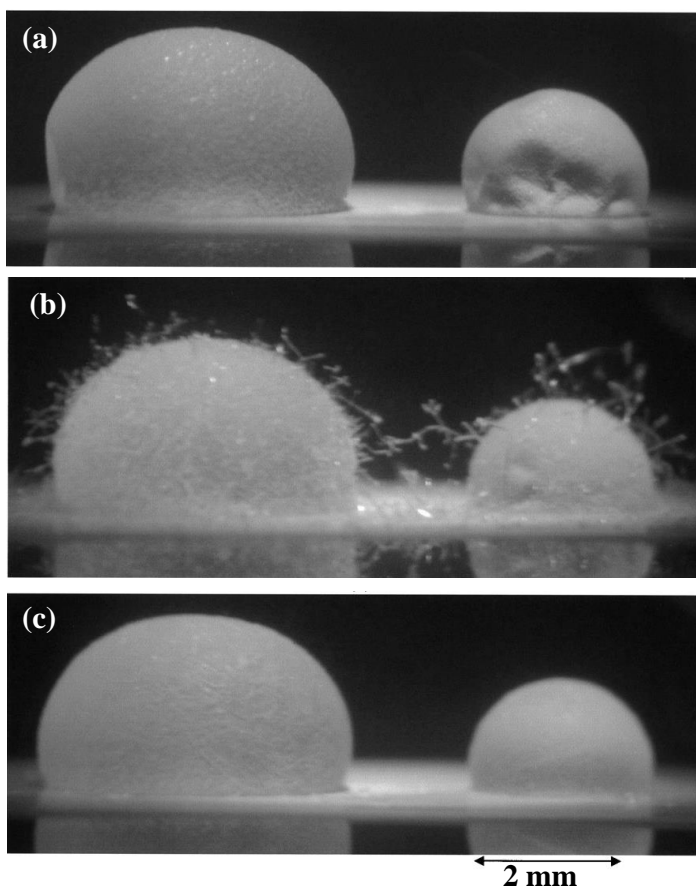


Figure 2-24 Macroscopic crystal morphology of carbon dioxide hydrate formation from water droplets; adapted after Servio et al. (2003).

The assertion was shown from the hypothesis indicating that after hydrate dissociation, residual clusters of water molecules originate the memory effect. While it is obviously not a thermodynamic effect, the exact cause of the memory effect is unclear. The examination of hydrate forming systems was completed several times to indicate the water clustering signs with respect to viscosity, interfacial, refractive index, and tension after hydrate dissociation (Ohmura et al., 2003). The experimental studies conducted by Ohmura et al. (2003) [using Hydrochlorofluorocarbon], by Takeya et al. (2000) (using CO₂ hydrates from CO₂ dissolved water) and by Sloan et al. (1998) (different gases) support the residual water clustering hypothesis. The consolidation of this hypothesis are further conducted through molecular-dynamics simulation studies in order to illustrate the memory effect mechanism (Báez et al., 1994, Rodger, 2000, Yasuoka et al., 2000). A distribution of ice-like water molecular structures has been reported by Rodger (2000), showing generation of liquid water by hydrate dissociation rather than in a hydrate-cage structures. It has been further concluded that decomposition of hydrate take place when dissolved gas remains in solution. Also the experimental studies of Bylov et al. (1997) and Ohmura et al. (2000) exhibited negative results. (Buchanan et al., 2005) were unable to find any sign of memory effect (continues hydrate crystals post dissociation) using neutron scattering. It has been further concluded that the existence of structural memory effects have not emerged in a comprehensive equilibrated system. These findings led to a negative view of the above hypothesis (Figure 2-25).

Buchanan et al. (2005) suggested that immediate observations after melting (less than 2 hours), and conducting experiments at lower temperatures and pressures, will result in longer duration and become difficult for differentiating the real attributes of memory effect and of poor equilibrium conditions. Conversely, a conclusive physical image of the memory effect should be derived for further simulation analyses.

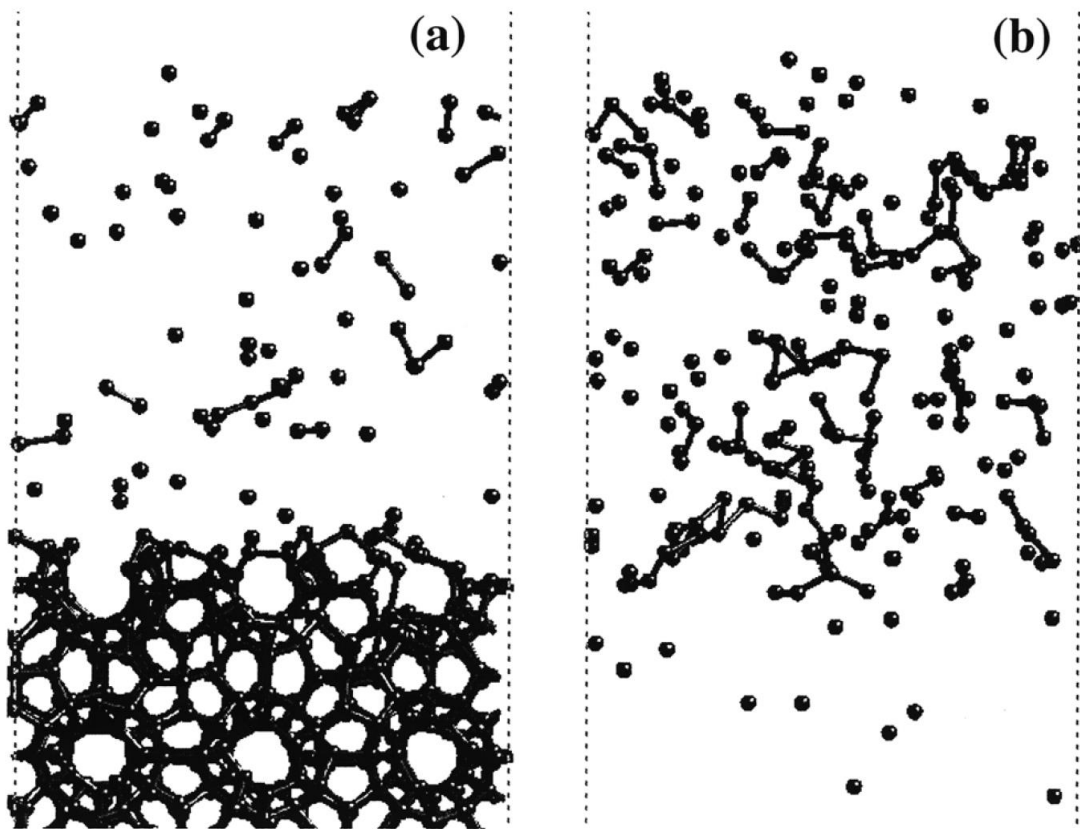


Figure 2-25 Structure screenshots of the residual clathrate (a) and ice (b) in the hydrate melt; after Rodger (2000).

Memory effect can be destroyed once the hydrate system is moved sufficiently far away from hydrate equilibrium point (formation region) (i.e., sufficiently heated) or enough time is given (Giavarini et al., 2011). For methane gas hydrate at 150 bar, the memory effect can disappear, when the solution is heated to approximately 5.5 °C to 8 °C above the equilibrium point (Uchida et al., 2000). Table 2-2 below represents the researcher's comments on memory effect vanishment.

Table 2-2 Researcher's findings on memory effect vanishment.

Authors	Findings
Sloan et al. (2008b)	Evaluated that memory effects are vanished when the melted water is heated above 24 °C.
Lederhos et al. (1996)	Considered that the residual structure was destroyed for natural gas (with 87.2% C1), after heating the liquid to 28 °C.
Takeya et al. (2000)	Found that the memory effect of CO ₂ /Water was destroyed when the melted water was heated to 25 °C.
Wu et al. (2010)	Found that promotion of memory effect is dependent on the dissociation temperature, and the memory effect of methane gas vanished when the heating of hydrate was higher than 25 °C.
(Makogon, 1997)	Established that there is no residual structure remains to promote hydrate once an upper temperature limit of about 30 °C is passed.
Becker et al. (2008)	Concluded that no memory effect exists for experiment conducted using mixtures of tetrahydrofuran and water.
Chen et al. (2013)	Conducted experiments using Methane/diesel oil/ sorbitan monolaurate and concluded that memory effect cannot be eliminated if it is maintained near the hydrate formation point even for a long time (more than 165 hours), while it will vanish when the system is raised 5 °C beyond the equilibrium temperature.
Sefidroodi et al. (2013)	The memory influence of cyclopentane hydrate formation does not always vanish with the superheating of 8.4 °C for the duration of 20 minutes. It has been suggested that the influence of the memory is in the bulk water phase and is possibly because of residual clathrate which cannot be detected by bare eyes.
Wilson et al. (2010)	Evaluated that the influence of gas hydrates memory effect is destroyed when it is heated to 4 °C beyond the equilibrium temperature. On the other hand, they reported that 'THF' hydrates do not hold memory effect.
Del Villano et al. (2011)	Reported that memory effect of natural gas with KHI is lost when heating to 8.4 °C above the equilibrium temperature.

While performing hydrate experiments in this study the hydrate equilibrium shift changes caused by memory effect was avoided by:

- (i) Starting the first test at the highest pressure and then lowering the pressure as proceeding.
- (ii) Shearing the liquid to the maximum shear stress (at ≈ 1500 RMP).
- (iii) Heating the liquid in sapphire cell to above 30 °C before succeeding the experiment.

The memory effect has significant implications for flow assurance and gas research. It is recommended that once hydrate is formed in a pipe or flow line, hydrate dissociation process must follow by water removal as this melted water having residual entity (i.e., dissolved gas, persistent crystallites and residual structure) will accelerate reformation of gas hydrate and so plug the transport lines. Equally, memory effect phenomena can be utilised as a hydrate promoter for hydrate technologies of storage, transportation and utilisation of natural gases in the hydrate form (Sloan et al., 2008b, Wu et al., 2010).

2.4 Hydrate Growth

After hydrate nucleation step, the second step of forming a solid hydrate mass is the hydrate growth and coalescence. For this phase, mass and heat transfer plays a significant role. The rate of hydrate growth depends on the kinetics of crystal growth (at the hydrate surface) and component mass transfer (of growing crystal surface). Moreover, the process of hydrate crystal growth is classified into four categories; single crystal growth (Figure 2-26), hydrate film/shell growth (at the interface), multiple crystal growths (in an agitated system), and growth of metastable phases. It is assumed that modelling and hydrate growth data are more acceptable when compared to nucleation phenomena Sloan et al. (2008b).

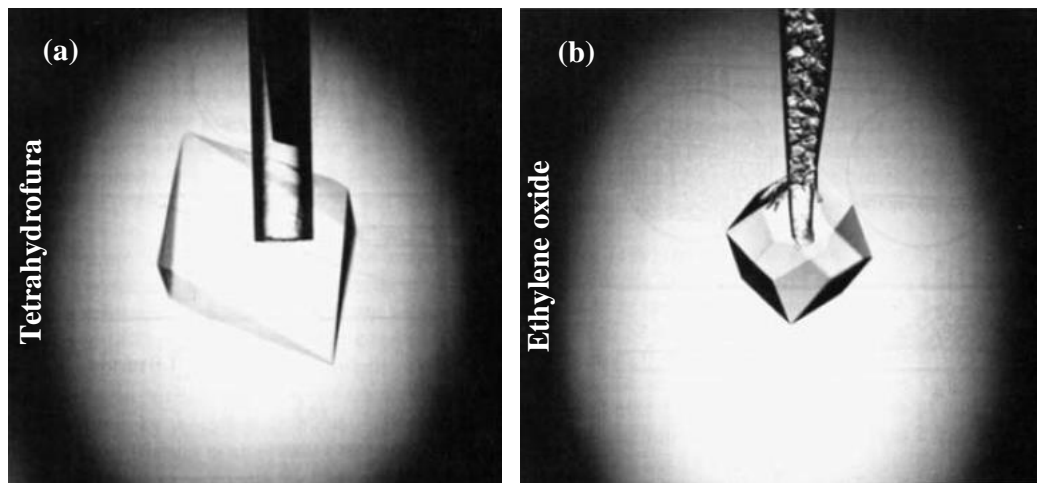


Figure 2-26 Single Crystal Growth; adapted after Sloan et al. (2008b)

Sloan et al. (2008b) summarised the hydrate growth state of the art with below statements:

- The placement of data can be fitted based on the parameters, which ultimately reveal the existence of growth model. The data were obtained mostly from the high-pressure reactor and therefore, formation rates cannot be implicated in a pipeline. Additionally, the accessibility of flow loop data is beneficial.
- The acceptance of modelling and hydrate growth data is evident as compared to the nucleation phenomena where the appearance of growth data is linear for approximately 100 min in Englezos' data (Englezos et al., 1987a).
- Structure I are reliant for mostly obtained data whereas structure II reflects number of pipeline hydrates on the basis of propane components of natural hydrocarbons.
- The formation of metastable phases do not account the models or the simulations during hydrate growth.
- The effects of heat and transfer can be highly determined in multiphase systems as compared to intrinsic kinetics.

2.5 Hydrate Growth Correlations

Assorted correlations were constructed for crystal process model as several extensive investigations have studied hydrate growth mechanisms. The determination of controlling the formation rate is essential by acknowledging and representing the formation process. The classification of key correlations relies on three existing growth aspects; heat transfer, growth kinetics and mass transfer.

There are further restrictions of each model to which actual hydrate growth is represented; however the validation of correlations was reflected among research groups. Hydrate growth is slightly affected through kinetics than the effect of mass and heat transfer. Therefore, greater application has been practically reflected among late models (Sloan et al., 2008b).

2.5.1 Hydrate Growth Kinetics

Englezos et al. (1987a) have proposed the hydrate formation in methane and ethane with the kinetic growth correlations. Crystallisation theory was used to produce the model along with mass transfer phenomena to demonstrate the kinetics formation at the hydrocarbon-water interface. There are three hydrate formation steps assumed to derive the work validation. The first step is the commencement of transport between phases. The second one is the diffusion through the boundary layer. The third step is the water adsorption process (Englezos et al., 1987a, Sloan et al., 2008b, Englezos et al., 1987b). The description of hydrate formation in mixtures of the gases is extended by focusing on the individual model of methane and ethane (Englezos et al., 1987b). The focus of the growth kinetics model is supposed to react to a boundary layer or interface and utilising the core aspect of diffusion. Particle size is considered as a particle diameter when a minor inconsistency is found from the model, the modification for carbon dioxide hydrates is removed with this error (Malegaonkar et al., 1997). According to past literature (Englezos et al., 1987a, Englezos et al., 1987b), there are two equations of gas hydrate growth with one adjustable parameter in the kinetic model. The representation of total consumed gas moles/second by the hydrate with respect to the extent of growth per particle $\left(\frac{dn_i}{dt}\right)_p$, is given by Eq 2-2:

$$\left(\frac{dn_i}{dt}\right)_p = K^* A_p (f_i^b - f_i^{eq}) \quad \text{Eq 2-2}$$

The surface area of each particle is represented by A_p while the fugacity of the component is represented by f_i^b and f_i^{eq} respectively in the bulk and at equilibrium. The rate constant of hydrate formation growth is represented by K^* (combining the rate constant for adsorption and transfer processes). The association of mass transfer coefficient and the reaction rate constant is shown with K^* in Eq 2-3.

$$\frac{1}{K^*} = \frac{1}{k_r} + \frac{1}{k_d} \quad \text{Eq 2-3}$$

It is evident that correlations endow an appropriate basis for future works whereas several limitations have been shown for the growth kinetics model. By using experimental data from compounds, the formation of structure I hydrate is revealed from the limitations of the fitting model. However, the accuracy of the model cannot be proven for structure II and structure H hydrates. The extrapolation of the model and the sensitivity of the model at the turbidity point are further considered as limitations (Sloan et al., 2008b).

The real gas equation (Eq 2-4) is also used to study and analyse growth experiments (Atkins et al., 2017).

$$PV = zn RT \quad \text{Eq 2-4}$$

where P is pressure, V is gas volume, z is compressibility factor, n is number of moles, R is universal gas constant, and T is temperature of the gas.

The pressure drop in the gas phase was the resultant through the principle of mass conservation for an isochoric system. In the liquid phase, the approximation of the amount of formed hydrates is determined by hydrate growth. Thus, Eq 2-4 yields:

$$\Delta n = \frac{V}{zRT} \Delta P \quad \text{Eq 2-5}$$

Where;

Δn = amount of gas consumed during hydrate formation or the amount of hydrates formed and ΔP = measured pressure drop resulted by hydrate formation.

The approximation of the term $\frac{V}{zRT}$ as the constant of proportionality cannot be modified considerably as $\Delta n \propto \Delta P$ indicated that the pressure drop in the gas phase and the amount of gas consumed in the liquid phase are directly associated with each other. The extent of formation of gas hydrates can be estimated from the employed concept in order to fill structure I and II systems cavities, when the appropriate systems of gas hydrate growth are met. Growth processes involve fast reactions of coupled mass and heat transfer especially during the early nucleation stage. Primarily it is limited by mass transfer of the reactants to the growing hydrate crystal and a simultaneous removal of heat away from the growing crystal. Such coupled heat and mass transfer is a complex process especially for a multicomponent system. Mass

and heat transfer models have been summarised and may be found in the literature (Kjelstrup et al., 2001, Abay, 2011, Taylor et al., 1993, Delgado et al., 2001).

2.6 Hydrate Dissociation

Hydrate dissociation enthalpy is a vital attribute for dissociation process and hydrate formation. The process of hydrates formation is structured like ice, which indicates the relaxation in the heat transfer process. On the contrary, the pre-requisite for hydrates dissociation is to overwhelm the activation energy and distribute the intermolecular and hydrogen bonds of the hydrate structures, as hydrates dissociation is further considered as an endothermic process (Giavarini et al., 2011)

In the past 40 years, the hydrate decomposition was proposed through numerous models. Analytical, theoretical and numerical models are included in the proposed models with modifying complex degrees (Clarke et al., 2000). In the earlier studies, the earliest model of hydrate dissociation was used with no restrictions of mass and heat transfer for the kinetics of hydrate dissociation (Kim et al., 1987). A two-step dissociation model indicates that the lattice of the particle is destroyed at the surface; subsequently, the surface absorbs the guest molecule. From the proposed model, it is indicated that the difference in fugacity of the guest molecule is correlated with the decomposition rate. This correlation was compared with the surface area of the hydrate particles under decomposition conditions at equilibrium. This correlation describes the rate of hydrate decomposition (Kim et al., 1987) as:

$$-\left(\frac{dn_H}{dt}\right) = k_d A_s (f_e - f) \quad \text{Eq 2-6}$$

Where

A_s = Surface area of the decomposing hydrates,

k_d = Decomposition rate constant,

f_e = Fugacity of the guest molecule at equilibrium,

f = Fugacity of the guest at the solid surface

It is evident from the model that methane hydrates decomposition relies on particle surface area, pressure and temperature. In general, it is important to notify that it is the first time that the model studied the kinetics of hydrate decomposition intrinsically regardless of the influence of mass and heat transfer (Bishnoi et al., 1996). Figure 2-27 shows the proposed process.

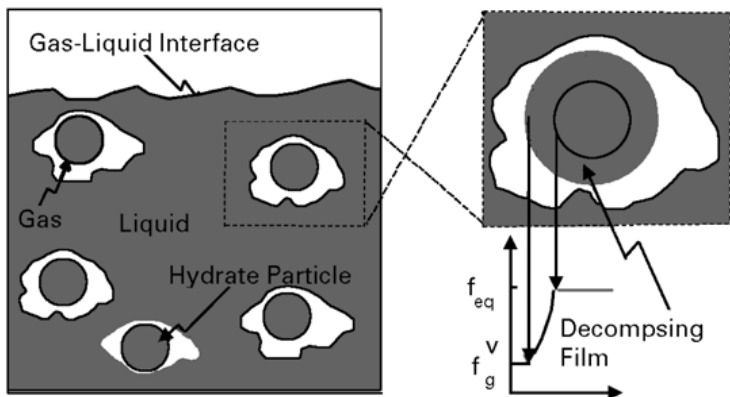


Figure 2-27 Schematic of hydrate dissociation mechanism; after (Bishnoi et al., 1996, Clarke et al., 2000)

With the existence of new models, the decomposition of hydrates is also investigated by current the model, which has the ability to provide a reason for the size of hydrate. Moreover, the hydrate decomposition could be reduced with particle size estimations, increasing the entire activation energy by 3 kJ/mol and up to 4 times (Clarke et al., 2001b). Kim et al. (1987) had proposed that size of the particles should remain constant whereas Clarke et al. (2001b) accepted the difference in the size of particles. The determination of decomposition rates for carbon dioxide hydrates are executed by Clarke et al. (2001a) and Clarke et al. (2005) showing the mixture of ethane and methane. Furthermore, the activation energy determination for structure II hydrates was found to be lower when compared to structure I hydrates. This emphasises that the dissociation can be faster in structure II hydrates when compared to structure I hydrates.

Assorted approaches have been attempted to separate hydrates. Depressurization is the most common method for hydrate dissociation. It is examined that dissociation is easily achieved using this method with the requirement of little energy input as the conditions of the hydrate will exceed the hydrate stability zone. Hydrates can be broken down at a particular pressure by increasing the temperature. The second method is mostly used, but the primary concern is that it is cost-expensive as a lot of energy is consumed by hydrates, when comparing with depressurisation. Injection of chemical inhibitors is the third method involved for the hydrate dissociation.

The contribution of heat transfer is very much more accepted for hydrate dissociation than intrinsic kinetics. The domination of initial stages of dissociation is revealed from the inherent kinetics in which the gradient temperature among the interface and

the hydrates is very small or non-existent. The increment is shown in the gradient temperature, and then dissociation is controlled by heat transfer as dissociation process continues after implication (Sloan et al., 2008b). Three disassociation methods influence the hydrate system and lead to an eventual breakdown and destabilisation of gas hydrates (Figure 2-28). The initial condition of the hydrate is assumed at a temperature of T_i and a pressure of P_i . Depressurisation method reduces the pressure below the equilibrium value to P_0 and brings in a decomposition driving force of $(P_{el} - P_0)$. Thermal stimulation method increases the hydrate temperature to T_2 to bring in a decomposition driving force of $(P_{e2} - P_i)$. Inhibitor injection shifts the hydrate phase equilibrium P-T condition to bring in a decomposition driving force of $(P_{e3} - P_i)$.

Where P_{el} and P_{e2} are the equilibrium pressure of the temperature T_i and T_2 respectively, P_{e3} is the equilibrium pressure of temperature T_i (Hong, 2003).

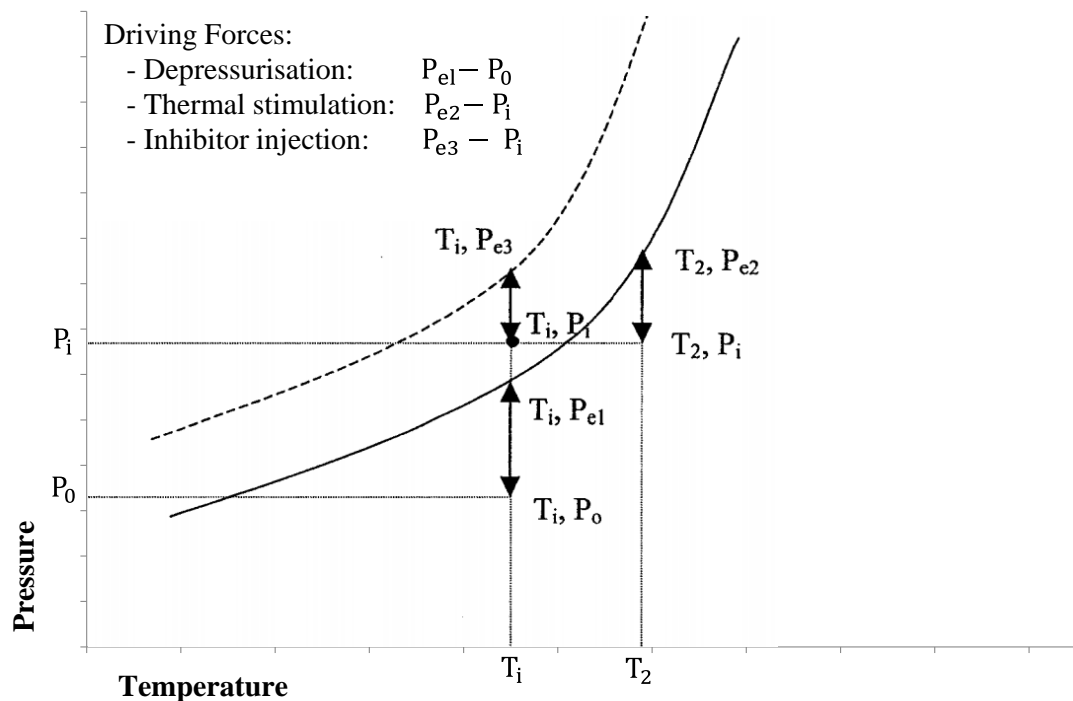


Figure 2-28 Driving forces for hydrate decomposition modified; adapted after (Hong, 2003)

The latest discovery of the radial model demonstrates more rapid dissociation with the larger surface area. However, an axial dissociation was the first established hydrate dissociation model, where it model slower plug dissociation as shown in

Figure 2-29. Hydrate dissociation is currently conceptualised by radial dissociation model, the hydrate plug start dissociate from the pipe wall into the centre of the pipe, surrounded by a water phase (with a hydrate plug centralised in a pipeline), as demonstrated in Figure 2-30 (Peters et al., 2000).



Figure 2-29 Old axial one sided dissociation of a hydrate in a pipeline; adapted after Davies et al. (2006).

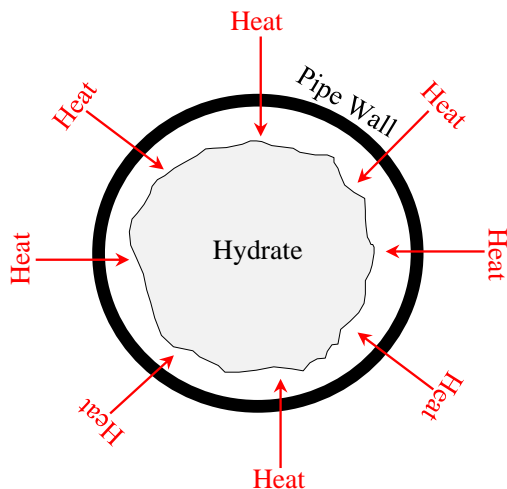


Figure 2-30 Radial dissociation of a hydrate in a pipeline; adapted after Peters et al. (2000)

Figure 2-31 shows 3 hours' time sequence of three hydrate plug dissociation. It demonstrates that the pipe radically evolves heat flow in which hydrate plug dissociate initially at the pipe wall, following the pattern of radial dissociation model which is based on the plug radius and irrelevant of plug length. Also in this model, it is assumed that during pipeline depressurization, the temperature of hydrate is reduced below the temperature of the surroundings causing heat to flow radially inward to melt the hydrate (Peters et al., 2000).

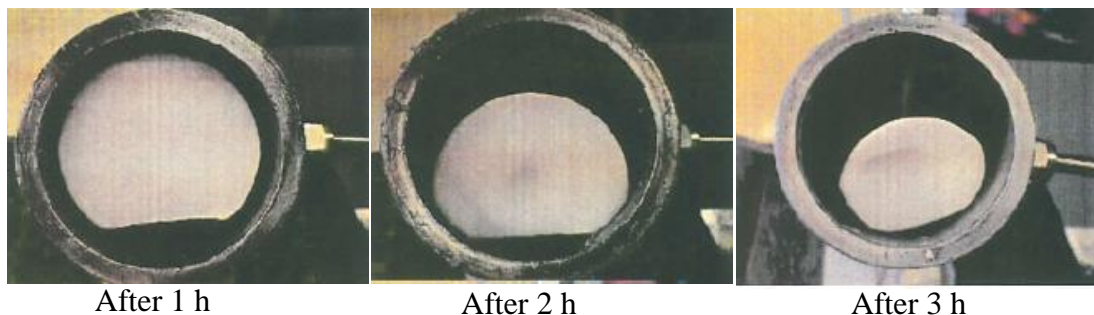
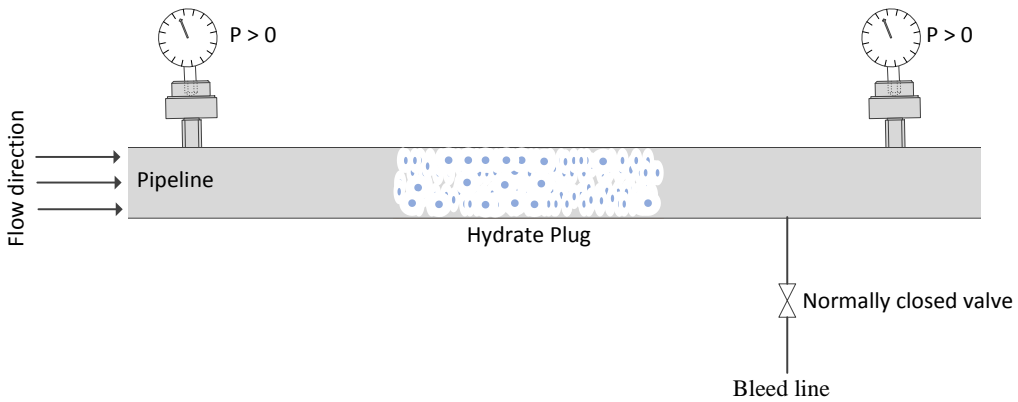


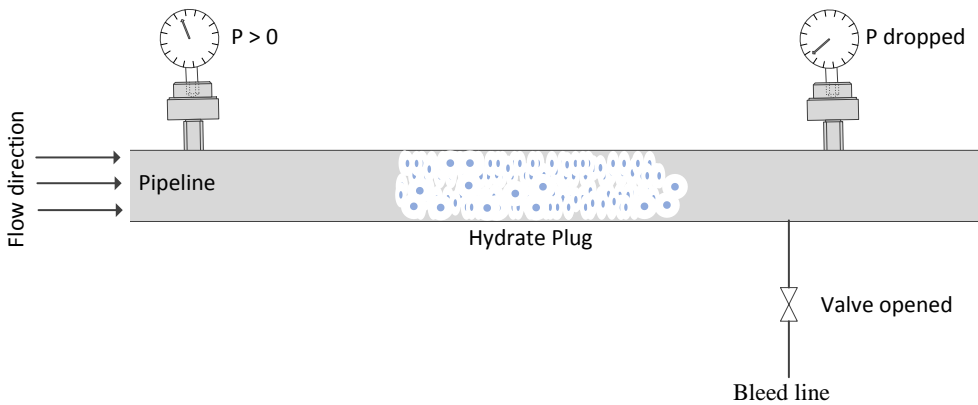
Figure 2-31 Time sequence of radial dissociation of laboratory hydrate plugs in a pipeline; lower part dissociate faster due to effect of gravity; adapted after Peters et al. (2000)

The completion of hydrate formation is experimentally examined to measure the thermodynamic equilibrium point because of the commencement of dissociation and formation of water drops. Thermodynamics attribute whether the system can potentially describe the hydrate dissociation along with the determined equilibrium conditions conducted by dissociation experiments (Schicks, 2010). The significant illustration of hydrate dissociation is radially understood with respect to the remediation of these issues in the pipeline (Davies et al., 2006). There are numerous mitigation techniques applied for hydrates dissociation, including depressurization, chemical inhibitor injection and thermal stimulation. (Carroll, 2014, Mokhatab et al., 2007, Haukalid et al., 2017).

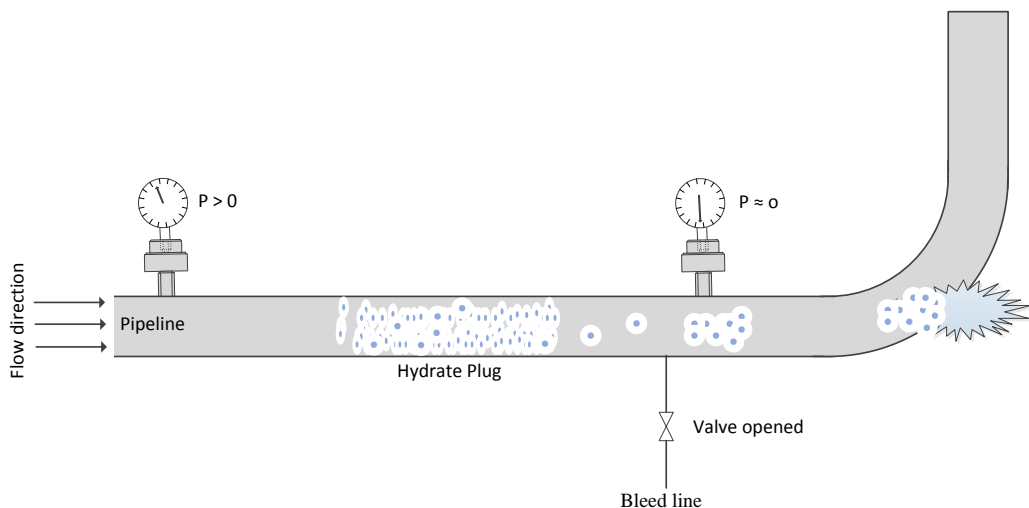
Hydrate depressurization technique can be potentially dangerous if appropriate procedures are not followed as shown in Figure 2-32 (a-c). Hydrate blockage is dissociated by bleeding the line downstream of the hydrate plug [Figure 2-32 (b)]. As pipeline is depressurized at one side, the plug can be loosened and would be projected like a bullet alongside the pipeline at very high velocity, as demonstrated by Figure 2-32 (c) and Figure 2-33 (Carroll, 2014). Xiao et al. (1998) have contributed to the study of simulating hydrate plug velocities by depressurization method with the help of a transient multiphase flow simulator OLGA. They found that a number of parameters influence plug movements during simulations, which include plug size, the existence of oil or condensate, plug location and size of the plug.



(a) Hydrate formed at high pressure result in plugging the pipeline



(b) Depressurisation technique is conducted by open the bleed valve at the downstream of the hydrate plug, to reduce the pressure and dissociate the hydrate plug.



(c) With sudden pressure drop, hydrate plug began to travel at high velocity

Figure 2-32 Incorrect and sudden depressurisation of hydrate plug in high pressure pipeline causing the hydrate plug to being launched like a projectile; adapted after (Carroll, 2014, Giavarini et al., 2011)



Figure 2-33 Hydrate plug dissociation incident happened due to incorrect single sided depressurization procedure; after (Koh et al., 2010)

To overcome this situation, the depressurization should be conducted on both sides of the hydrate plug and minimise the differential pressure (below 10%) across the hydrate plug. On the other hand, if it is not possible to depressurize both sides of the plug, then step depressurization of one side should be applied by step releasing and closing the bleeding line until full plug dissociation (Carroll, 2014).

The application of thermal remediation is another hydrate dissociation technique. Many techniques are used for thermal remediation such as: application of heat bundles (applied in Gulf of Mexico King subsea multiphase flowlines), spraying steam on the line, installation of electrical heat tracing (implemented in North American Arctic, Nakika's North, PDO south field), and installation of external insulators (such as Rockwool). On the contrary, individuals must be cautious while implicating such methods. Figure 2-34 shows a severe and dangerous situation of incorrect implementation of thermal remediation leading to a pipe burst. Incorrect implementation involves exceeding the pipe maximum allowable working pressure, heating medium not spanned homogeneously across the entire hydrate plug and if no bleed line is provided for the local high pressure to be released. It is examined from Figure 2-34 that liquid water will be produced and gas will be released through the dissociated plug. The volume of 1 m³ of dissociated hydrate discharges 170 Sm³ of

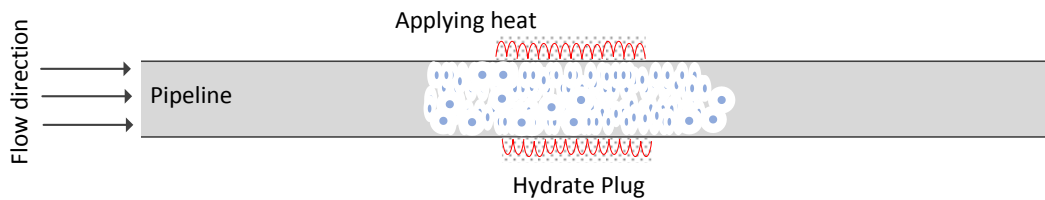
gas. The 1 m^3 dissociated hydrate also leads to a production of 51.45 kmol of water that occupies a liquid volume of 0.927 m^3 . This refers that if 1 m^3 of hydrate is dissociated in a limited space, there is merely 0.073 m^3 ($1\text{m}^3 - 0.927 \text{ m}^3$) available for the 170 Sm^3 of released gas.

According to (Loverude et al., 2002), the ideal gas law can be utilised crudely to estimate the pressure of the released gas. We can see from the ideal gas law that release pressure can be estimated as per Eq 2-7, which confirms the pressure is independent of the volume dissociated in a confined space conditions (Carroll, 2014).

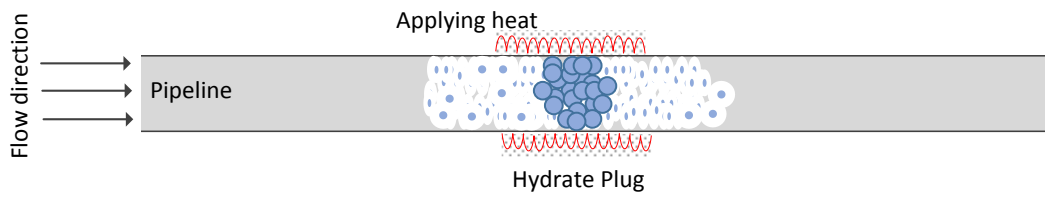
$$P_1 V_1 = P_2 V_2 \quad \text{or} \quad P_2 = \frac{P_1 V_1}{V_2} = \frac{170 \times 101.325}{0.073} = 236 \text{ MPa} \quad \text{Eq 2-7}$$

Although Eq 2-7 does not provide an accurate value, it gives some magnitude of the pressure build-up. As shown in the calculations, the released pressure is enormous and capable of bursting most of the pipelines (Carroll, 2014).

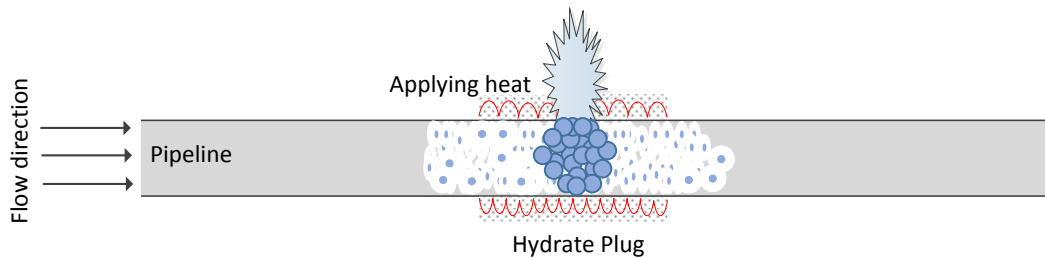
More dangerous scenario could occur with multiple plugs that form in series in a pipeline, as shown in Figure 2-34 (d). Multiple plugs can trap high intermediate pressure, so more precautions should be taken by decreasing slowly the pressure of both sides of the plugs to maintain thermal and hydraulic control of the clearing process. Instead, if there is movement in hydrate plug, the pressure build-up in the dissociated section can also result in a hydrate projectile, with a high potential for pipe rupture.



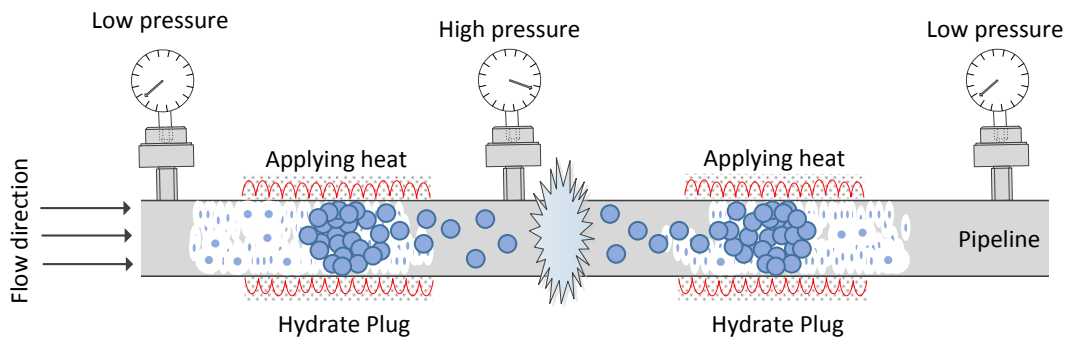
- (a) Thermal technique is placed near the centre of the hydrate plug, to increase the temperature and dissociate the plug.



- (b) With continues heating, hydrate plug began to dissociate causing rise in the pressure.



(c) With continues heating, pressure builds up due to thermal dissociation, the pipeline bursts.



(d) Multiple hydrate plug that traps intermediate pressure, causing pressure build up due to hydrate dissociation, resulting in pipeline bursts.

Figure 2-34 Incorrect thermal remediation of hydrate plug in high pressure pipeline causing pipeline rupture; adapted after (Carroll, 2014, Giavarini et al., 2011)

Following the above techniques, Chapter 3 will present a field case study of various gas hydrate dissociation/mitigation techniques applied in a gas lift system of a south field of Oman, which includes:

- Installation of rock-wool insulators.
- Installation of electrical heat tracing.
- Decreasing the system pressure.
- Methanol injection.
- Increasing gas lift temperature.

2.7 Thermodynamic Inhibitors

The addition of thermodynamic hydrate inhibitors (THI) such as MEG, effectively shifts hydrate equilibrium curve to the left region of the original curve towards higher pressures and lower temperatures. Clustering effects of a molecule of MEG is two hydroxyl groups that form hydrogen bonding with water molecules. The

formation of hydrogen bonds is comparatively similar to hydrate formation. Therefore, the MEG inhibition greatly relies on aqueous phase concentration for inhibiting water molecules that are participating in the clathrate (Cha et al., 2013). The consequent reduction in the water activity coefficient and the dilution of the water phase are the primary thermodynamic indicators of the mechanism, mitigating the impact of hydrate formation (Hemmingsen et al., 2011). Normally, THI is added at a relatively high concentration of about 10 wt% to 60 wt% in the aqueous phase (Olabisi et al., 2014). The hydrate equilibrium data in the presence of different concentrations of MEG (0 wt% to 50 wt%) are shown in Figure 2-35, this also shown by other researchers (Cha et al., 2013, Haghghi et al., 2009, Hemmingsen et al., 2011).

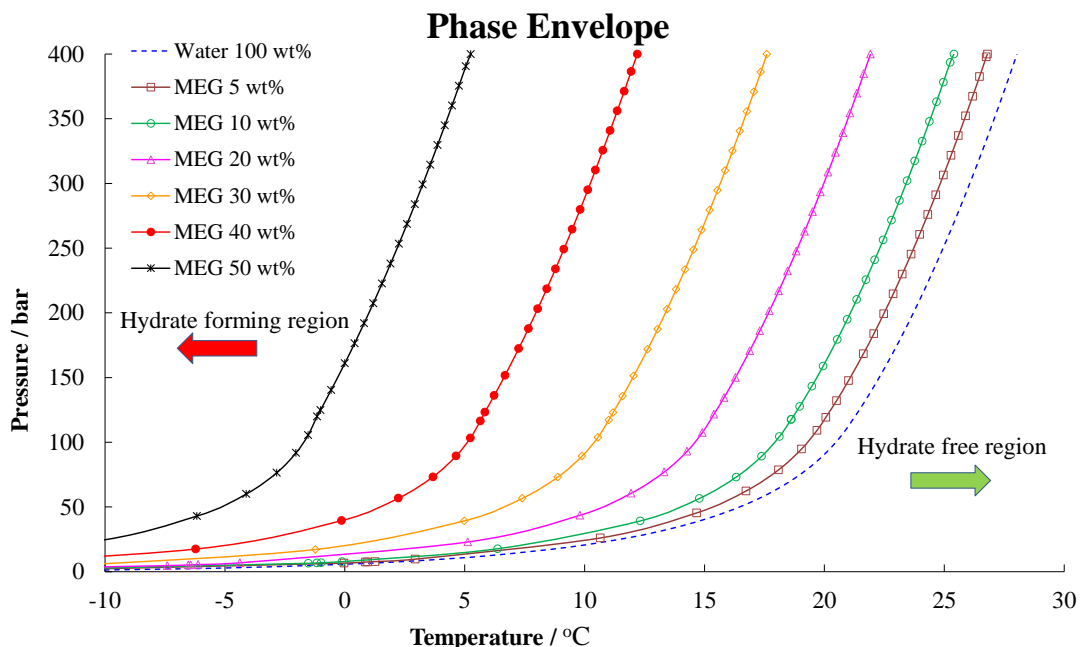


Figure 2-35 Effect of addition of different concentration of MEG on shifting hydrate equilibrium curve of natural gas (Methane 79.1%, CO₂ 2.5%, iso-Pentane 1.7%, n-Pentane 1.7%, iso-Butane 2%, n-Butane 2%, propane 4%, Ethane 7%) , plotted by Multiflash prediction software (PR equation of state).

Traditional thermodynamic inhibitors include methanol (molecular weight (MW) 62.07) and ethylene glycols [mono-ethylene glycol (MW 62.07), diethylene glycol (MW 106.12) and triethylene glycol (MW 150.17)]. The lower the molecular weight, the better the hydrate suppression performance (Brustad et al., 2005). Figure 2-36 represents the hydrate equilibrium data of natural gas with 25 wt% of different

thermodynamic inhibitors in the aqueous phase, compared to 100 wt% water. The hydrate depression temperature and the regression functions of the fitted data are reported in Table 2-3. For a given pressure, the hydrate depression value (ΔT_d) was determined as shown by Eq 2-8.

$$\Delta T_d = T_{equ}(100 \text{ wt\% water}) - T_{equ}(25 \text{ wt\% of THI}) \quad \text{Eq 2-8}$$

Where $T_{equ}(100 \text{ wt\% water})$ is the natural gas hydrate equilibrium temperature measured with 100 wt% water and $T_{equ}(25 \text{ wt\% of THI})$ is the natural gas hydrate equilibrium temperature measured with 25 wt% of different THI's. A higher " ΔT_d " value corresponds to a higher depression (better inhibition performance).

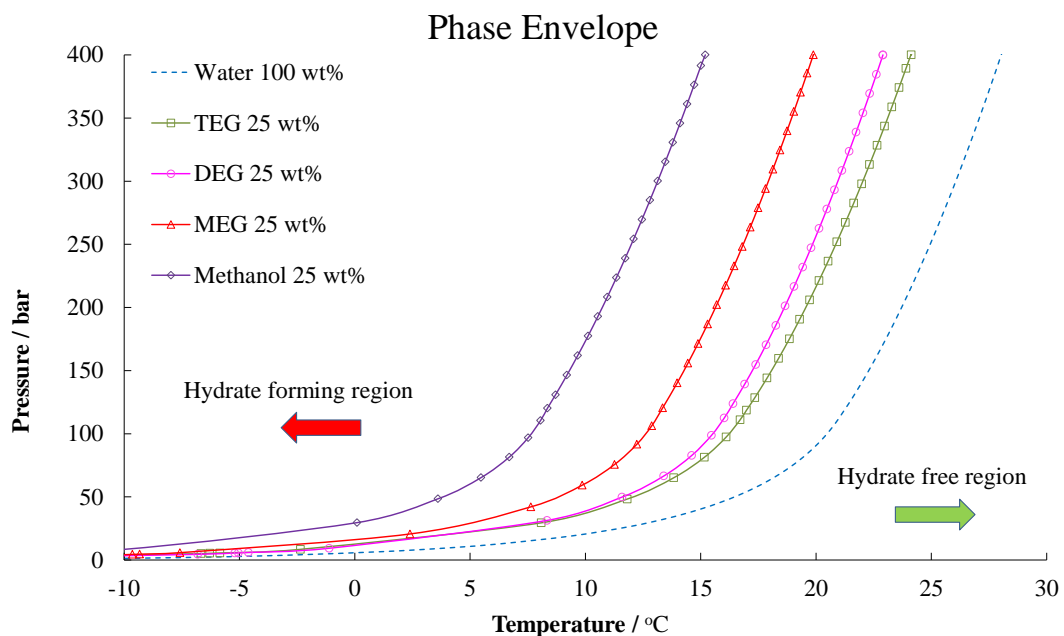


Figure 2-36 Effect of addition of 25 wt% of different thermodynamic inhibitors on shifting hydrate equilibrium curve of system of natural gas (Methane 79.1%, CO₂ 2.5%, iso-Pentane 1.7%, n-Pentane 1.7%, iso-Butane 2%, n-Butane 2%, propane 4%, Ethane 7%), plotted by Multiflash prediction software (PR equation of state).

Summarising the results from Figure 2-36 and Table 2-3, methanol shows superior hydrate inhibition performance in terms of shifting the hydrate curve mostly to the left side [with average depression value (ΔT_d) of 12.9 °C], followed by MEG, DEG (diethylene glycol) and TEG (triethylene glycol) respectively.

Table 2-3 Hydrate depression temperature “ ΔT_d ” of Brustad et al. (2005) and of Figure 2-36, and the regression functions (sorted from highest to poorest inhibitor), where P is pressure and T is the temperature.

Regression functions of different THI	Pressure (bar) versus ΔT_d ($^{\circ}\text{C}$)							Average ΔT_d ($^{\circ}\text{C}$)
	50	100	150	200	250	300	Multi- flash soft- ware	
Methanol: $P_{(\text{methanol})} = 0.0004 T^6$ $- 0.0167 T^5$ $+ 0.2683 T^4 - 1.7749 T^3$ $+ 5.4311 T^2 - 1.4058 T + 36.422$	12.8	12.8	12.9	13.0	13.0	12.9	12.9	12.3
MEG: $P_{(\text{MEG})} = - 0.0005 T^5$ $+ 0.0235 T^4 - 0.2596 T^3 + 0.9525 T^2 + 2.5605 T + 20.902$	7.6	8.0	7.9	8.1	8.1	6.1	7.6	7.1
DEG: $P_{(\text{DEG})} = - 0.0006 T^5$ $+ 0.0366 T^4 - 0.7226 T^3 + 6.347 T^2 - 22.058 T + 48.992$	5.0	4.9	5.0	5.1	5.1	5.0	5.0	4.6
TEG: $P_{(\text{TEG})} = - 0.0004 T^5$ $+ 0.0219 T^4 - 0.4192 T^3 + 3.4254 T^2 - 9.1563 T + 28.593$	4.6	4.2	4.1	4.1	4.1	4.0	4.2	3.9

Analysing Table 2-3, we can see that hydrate depression temperature “ ΔT_d ” of Brustad et al. (2005) followed the same pattern of the Multiflash prediction software (Figure 2-36) with an average deviation value of 7%.

Furthermore, ionic salts functions as thermodynamic inhibitors, such as sodium chloride that might exist in the water formation. Ionic salts can be utilised for ultra-deepwater projects or mixed with an organic inhibitor (e.g. MEG) to boost hydrate inhibition efficiency (Masoudi et al., 2005).

Obanijesu, Barifcani, et al. (2014) have reported that inert gases, including hydrogen and nitrogen functions as hydrate inhibitors. On the contrary, depression of hydrate formation are caused by dilution effect; therefore, more research is required to

establish the chemical nature of H₂ and N₂ that vitally contributes to hydrate depression.

Low-Dosage Hydrate Inhibitors (LDHI), such as Kinetic Hydrate Inhibitors (KHI) and Anti Agglomerants (AA) becoming popular in West Africa, UK fields, and the Gulf of Mexico (Frostman et al., 2001, Mehta et al., 2002). In contrast, many limitations occur specifically for long distance gas-condensate tie backs. In general, KHIs show limited hydrate formation suppression, and require a continuous oil or condensate phase for an efficient performance (Kim et al., 2014b, Brustad et al., 2005).

2.8 Low-Dosage Hydrate Inhibitors

A simple observation executes the concept of low-dosage hydrate inhibitors reveal that particular fish do not freeze in sub-zero temperature as microscopic ice crystals are bounded on the secretion of a protein, and consequently it prevents its subsequent growth. The discovery of kinetic hydrate inhibitors is driven by the evidence of anti-freeze proteins (Mehta et al., 2002, Franks et al., 1987).

The presence of low-dosage hydrate inhibitors (LDHI) is comparatively new in the oil and gas field. low-dosage hydrate inhibitor chemicals work by inhibiting hydrate growth and nucleation at very low concentrations in the aqueous phase compared to THI's (typically < 1 wt%) (Ding et al., 2010). Furthermore, LDHIs are classified by their inhibition mechanism into anti-agglomerants and kinetics.

2.8.1 Kinetic Inhibitor

Low-dosage hydrate kinetic inhibitor alter the hydrate formation kinetics by reacting and increasing the time of hydrate formation by delaying the initial hydrate nucleation. These inhibitors are generally water-soluble polymers, which work by prolonging the formation of hydrate crystals, such as Luvicap® EG and Gaffix® VC-713 (Figure 2-37) (Ding et al., 2010). Moreover, kinetic inhibitors can adsorb growing hydrate crystals at the hydrate/water interface, preventing small hydrate crystals to grow into larger crystals; therefore, it slows down the rate of growth and prolongs the duration before plug occurs. This delay in hydrate growth means that systems may operate within the hydrate stable area of the phase diagram for a given length of time without the appearance of hydrates (Anklam et al., 2008).

Kim et al. (2014b) evaluated the synergist function of adding 0.2 wt% of PVCap with 20 wt% MEG and confirmed that this results in 36% longer delay time, and the MEG concentration can be reduced by 20 wt%. Conversely, there are two major drawbacks of the kinetic hydrate inhibitors. The drawbacks of kinetic hydrate inhibitors is that it is only significant when the sub-cooling is slightly less than 14°C and the performance drop with the occurrence of other injected chemicals (corrosion inhibitors) (Kim et al., 2014b). Correspondingly, it is not evident that the effectiveness of kinetic inhibitors is valid at higher pressures (Brustad et al., 2005).

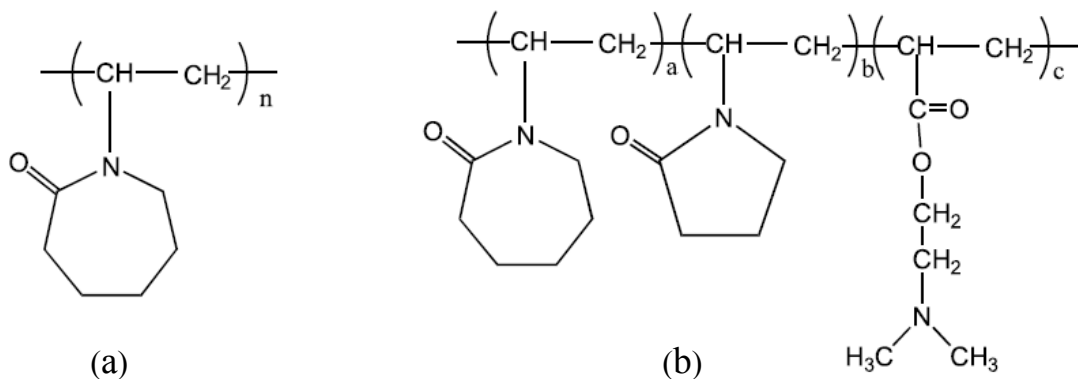


Figure 2-37 Chemical structure of Luvicap® EG (a) and Gaffix® VC-713 (b); after (Rojas et al., 2010, Ding et al., 2009)

2.8.2 Anti-Agglomerants

Low-dosage hydrate anti-agglomerant (AA) inhibitors work by preventing the hydrate crystals agglomeration (clustering) before reaching the stage of plug formation. This is achieved by adhering to the hydrate crystal surfaces, helping to form separate stabilised crystals as a slurry which does not block the pipeline ensuring continuous flow within the hydrocarbon phase (Ding et al., 2010).

The key to the AA effectiveness is their structures and surfactant properties. AA surfactants are thought to work by containing polar head groups that can interact with the lattice of hydrate water molecules, and a hydrophobic tail group that attracts the hydrocarbon phase (Huo et al., 2001, Bergflødt et al., 2004).

Shell described a successful LDHI trial in their Popeye subsea well (Mehta et al., 2002). The subsea well suffered high watering which required to inject 250 bpd of methanol which exceeded the current injection capability (175 bpd), led to partial hydrate blockage. As a quick solution, AA was executed at 0.35 gal/bbl water (0.8% of the water volume) giving a 95% reduction in chemical usage compared with

methanol. In this trial, AA implementation showed positive results and the well was opened up and resulted in additional of 20 mmscfd of gas production. Shell estimates a net present value of \$8 million improvement because of the implementation of the LDHI (AA) (Frostman et al., 2003). The AA trial results are illustrated in Figure 2-38. Kim et al. (2014b) reported that AA have a drawback in constraining performance with high water cut wells, while Popeye subsea well trial proves the positive results with high water cut wells.

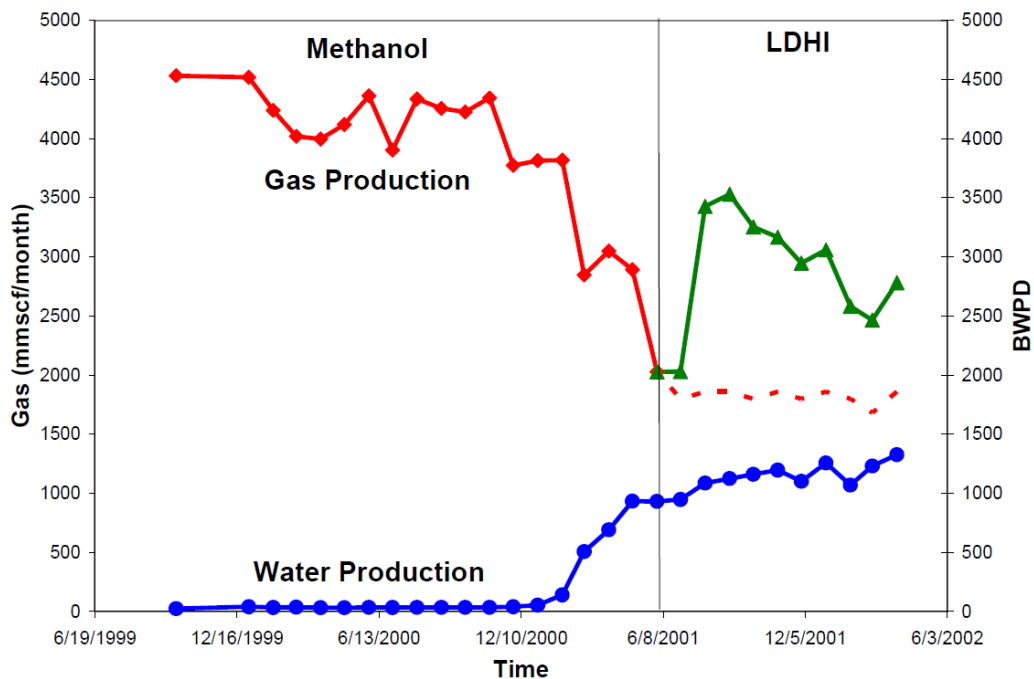


Figure 2-38 Case history of Deepwater Gulf of Mexico where injection of LDHI (AA) permits extra gas production in Methanol limited system; after Frostman et al. (2003)

Currently how LDHIs work at a molecular level is not yet fully understood or documented, even though they have now been applied in the field. Thus, LDHI's have a high application potential to replace the thermodynamic inhibitors (Anklam et al., 2008). However, the use of LDHI's is restricted on the Norwegian continental shelf due to their toxicity and low biodegradability. The work of developing new and more environmentally friendly LDHIs is currently ongoing (Lee et al., 2007, Del Villano et al., 2008, Kelland, 2006).

2.9 Hydrates in Natural Gas Production and Transport Systems

Hydrates formation in gas pipeline systems represents a severe concern in flow assurance in the oil and gas industry, especially because gas hydrates can cause flow blockages, which can arise safety and operational hazards (Kim, Lee, et al., 2017). The risk of hydrate formation increases with the production of formation water (Hemmingsen et al., 2011). If hydrate formation is not correctly inhibited, the chance of occurrence of entire cross-sectional area by hydrate blockage is increased due to the accumulation and growth of hydrate crystals (Figure 2-39).



Figure 2-39 Gas hydrate plug in a pipeline; after (Boschee, 2012, Irmann-Jacobsen, 2012)

Figure 2-40 shows the common locations for hydrates formation in a subsea petroleum production system and include the wellhead, flowline and riser. Hydrate formation is occurring also in the onshore fields where the gas system is operated at high pressure (above hydrate equilibrium point). Chapter 3 presents hydrate formation at onshore gas lift system. Hydrate formation can occur in different places in the oil and gas industry and can depend on many factors such as; the operating pressure and temperature, the nature of the hydrate forming component (i.e. type of gaseous guest molecule, single- or multiple component gas), and the composition of the water phase (pure water or water with condensate or dissolved salts/inhibitors) (Erstad, 2009).

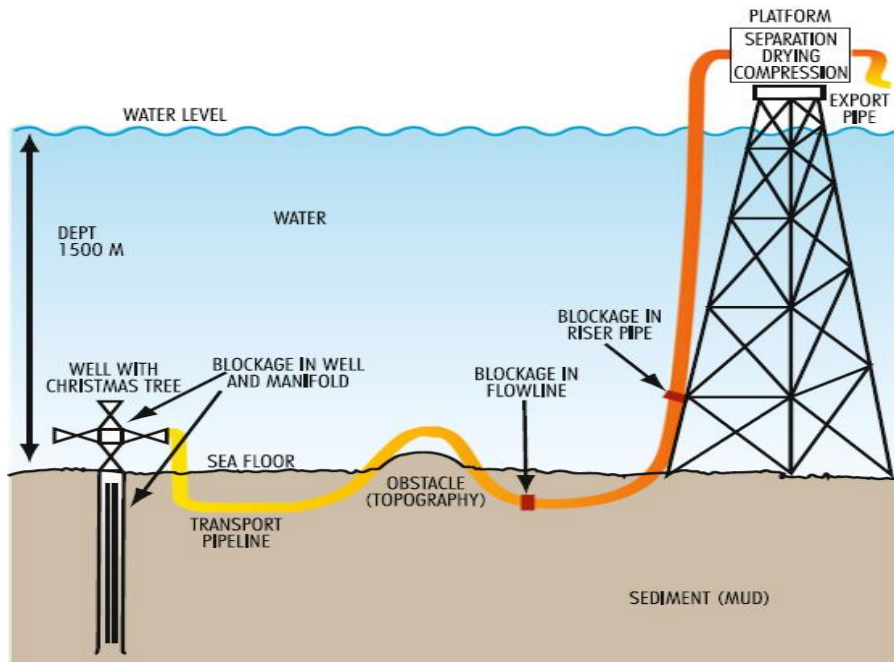


Figure 2-40 Probable locations of hydrate formation in an offshore system; after (Giavarini et al., 2011)



Figure 2-41: Hydrate formation during winter season at Gas lift manifold caused by drop in ambient temperature and high differential pressure across the control valve (Joule –Thompson effect); (Courtesy of Petroleum Development Oman)

The correlation of plug formation is revealed by the following events. These events should be prevented, or up front precautions should be implemented (Joachim, 2013):

- Start-ups following emergency shut-in
- An uninhibited water phase
- A sudden reduction in pressure is influenced from Joule-Thompson at orifices specifically include short radius elbows, open control valves, sudden enlargement in pipelines.

One of the greater hydrate blockage risks is in the long distance transmission pipelines raised from the high compression pressures (≈ 70 bar) to maintain optimum operating conditions for transmission (Mokhatab et al., 2012). Another location of greater hydrate blockage risks is where water is accumulating, such as in “S” shapes locations in flowlines (Figure 2-42). Pipeline topography which provokes water accumulations are particularly vulnerable and may require pigging or inhibitor injection to prevent hydrate formation. For many fields, it is practically unenforceable to design and operate hydrate-free systems. In many cases, this is due to seabed topography. If a flow line requires hydrate inhibition, it is very likely that hydrates will form during the operational lifetime. This emphasises the importance of identifying the high risk locations of hydrate formation so that hydrate prevention and dissociations can be addressed (Joachim, 2013).

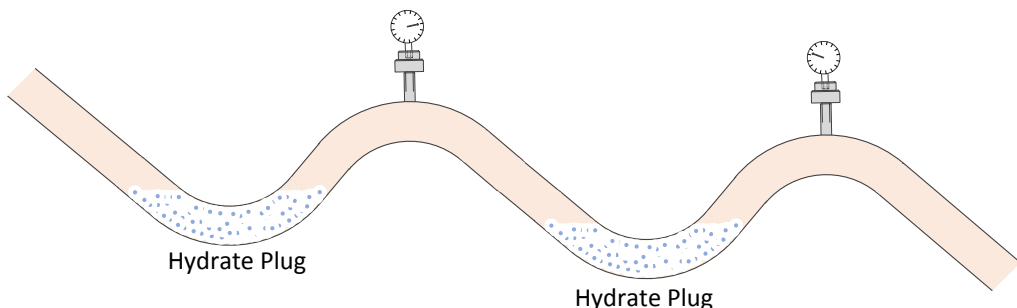


Figure 2-42 Hydrate plug formations in "S" shapes; adapted after Joachim (2013)

2.10 Mono-Ethylene Glycol

Ethylene glycol is a clear and colourless liquid, viscous, odourless, and toxic with sweet taste. First preparation of ethylene glycol goes back as early as 1856, but it was not produced commercially until the 1920s by the Union Carbide (U.S. firm). The direct oxidation of ethylene is the currently effective technology for producing ethylene glycol. At the start of the 1930s, the direct oxidation of ethylene was developed by a French firm and afterwards restructured by Union Carbide. New technologies have been elaborated by Shell and the engineering firm Scientific

Design in the 1940s using ethylene oxidation (Fosfuri, 2006). Ethylene glycol is widely used worldwide in various processes and applications such as inhibiting of gas hydrate, engines cooling system, antifreeze systems; mixed with hydraulic brake fluids, and emerged as a raw material and as a solvent. The worldwide call for MEG is high and evaluated as 17 million tons per year with an estimate of 7% yearly growth rate (Kawabe, 2010).

Table 2-4 Physical properties of MEG and Methanol; adapted after Akers (2009)

	Mono-ethylene Glycol	Methanol
Family	Glycol	Alcohol
Representation		
Chemical Formula	$C_2H_4(OH)_2$	CH_3OH
Appearance	Colourless liquid	Colourless liquid
Molecular Weight	68.068 g/mol	32.04 g/mol
Viscosity (cp) @ 20 °C	21 centipoise	0.55 centipoise
Density (g/cc) @ 20 °C	1.1135 g/cm ³	0.9715 g/cm ³
Freezing Point , °C	-12.9 °C	-97 °C
Boiling Point, °C	197.3 °C	64.7 °C
Flash Point	111 °C	11 °C
Solubility in Water	Fully miscible	Fully miscible
NFPA 704 rating and GHS pictograms		
Toxic when ingested		<ul style="list-style-type: none"> - Flammable - Toxic when ingested

Table 2-4 above compares some of the selected physical properties of the most commonly used thermodynamic inhibitors, MEG and methanol. Monoethylene glycol is a diol (alcohols that have two hydroxyl groups in each molecule) with the

chemical formula $C_2H_4(OH)_2$. MEG is a hygroscopic and entirely miscible in water, and is able to absorb double its weight in water at 100% relative humidity (Gomes et al., 2002).

2.10.1 Hydration of Ethylene Oxide to Produce Ethylene Glycol

MEG is produced from thermal or catalytic reaction of ethylene oxide (C_2H_4O). Liquid-phase hydration is the most common method of ethylene oxide hydrolysis (van Hal et al., 2007). The occurrence of ethylene oxide (EO) is determined through the multi-tubed catalytic reactor where high purity oxygen and ethylene (C_2H_4) are combined across a solid bed of silver catalyst. The multi-tubed catalytic reactor operate usually at a pressure range of 10-30 bar and temperature range of 210 °C to 285 °C depending what the design specifies (Nielsen et al., 1977). EO production selectivity is boosted by the use of a silver catalyst. The silver catalyst works by adsorbing oxygen on the silver ion surface in order to form an ionised superoxide which promotes reaction with ethylene (Verykios et al., 1980).

Non-Catalytic phase hydrolysis reaction with a presece of a high volume of water is the preferred method for commercial production of MEG (operates at a temperature range of 140 to 230 °C). The use of high volume (22:1 by mole basis) of water in this method is to cease further production of higher glycols, when combining ethylene glycol and ethylene oxide (Weisz et al., 1962). The produced glycols is then purified by routing the produced glycol through a series of distillation columns, each operating at higher pressure than the next column (Figure 2-43).

The energy generated from the conversion of EO to MEG is utilised in the heating process of the distillation columns. Vacuum distillation technique is used for each distillation column process to produce a different type of glycols (MEG, DEG and TEG) as shown in Figure 2-43 and Eq 2-9 to Eq 2-11(Kawabe, 2010).



Figure 2-43 is the flow scheme showing the statistical revelation of successive glycol reactions, which is identified through the feed ratio of water and EO. The selectivity

of MEG is increased with the dilution of EO and a large excess of water. For instance, 89 percent selectivity of MEG needs 20 mol of excess water to 1 mol of EO (Kawabe, 2010).

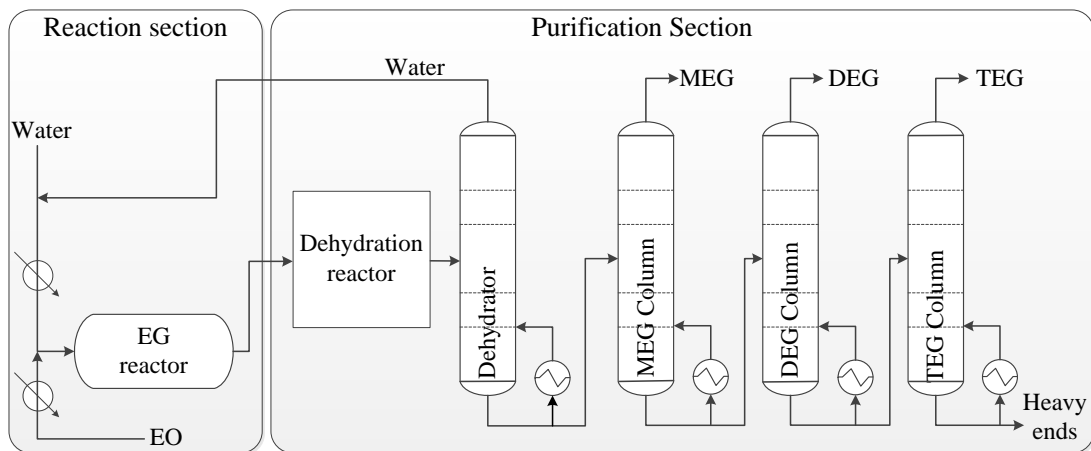


Figure 2-43 Flow scheme of conventional ethylene oxide (EO) to MEG process; adapted after Kawabe (2010)

Numerous patents have been filed for the production and obtaining a high selectivity of MEG such as by Broz (1975), Kawabe (2000), Bhise (1983), Robson et al. (1985), Foster et al. (1978), Van Kruchten (1999) and Strickler et al. (2000). (With few processes operational due to financial restraints and technological development challenges).

Appropriate catalysts are used to attain high MEG selectivity; therefore, it is considered as one of the simplest methods of technological developments. This concept has been based on considerable research. For instance, the catalyst concept was investigated using some metal complex anions (Robson et al., 1985). In addition, van Hal et al. (2007) aimed to explore different types of catalysts hydration of EO to MEG including salen compound catalysts, amine and bi-function catalysts. It has been determined that the consistency of acid or base catalysed reactions is dependent on the acidity and basicity of the preferred catalyst. The mechanism is described in the reaction schemes, as shown in Figure 2-44. A proton first attacks the nucleophilic oxygen of an ethylene oxide molecule to create an intermediate species, $CH_4(OH^+)CH_2$ to subsequently convert to a more stable $s, + CH_4(OH)CH_2$ for acid catalyzed reaction. Water molecules react with the second intermediate species to create a mono-ethylene glycol. The reaction rate is increased with both strongly

acidic and basic catalysts. Conversely, the selectivity of MEG formation is not increased using the same catalysts. The core intermediate species are distinctive due to the difference in basicity and acidity of the catalysts used. It releases a proton while maintains the reaction constant acidity. Another intermediate species could react with another EO in order to produce Diethylene glycol. Higher glycals and triethylene might be produced by the same mechanism based on the base catalysed, followed by the same reaction as shown in Figure 2-44.

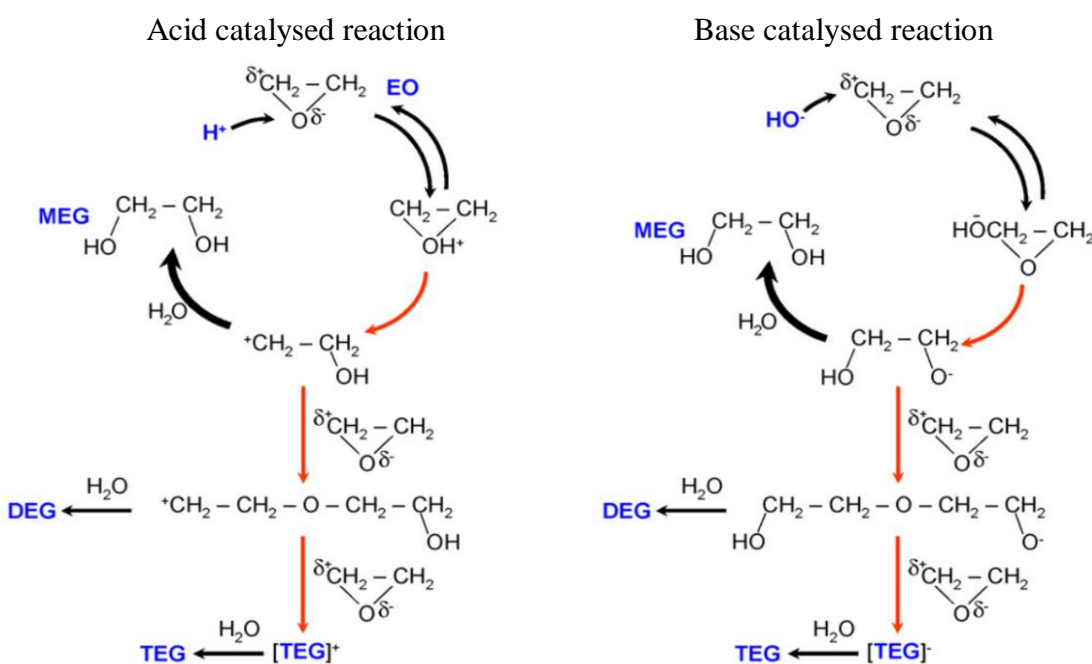


Figure 2-44 Schematic diagram of reaction mechanisms of acid and base catalysed hydration of ethylene oxide (C_2H_4O) to ethylene glycals; after van Hal et al. (2007).

The OMEGA (only MEG advantage) process was developed by Shell Global Solutions with the partnership of Mitsubishi Chemical and utilised catalysts of CRI Catalyst Company for catalysing the ethylene conversions to EO to MEG. 99% of EO were effectively converted into MEG with no other heavy glycals produced.

Shell has claimed that with additional MEG production of 14.7-27.5% per tonne of ethylene from the OMEGA processes, it utilises 30% less wastewater and 20% less steam, results in less greenhouse gas emissions in contrast with the traditional EO/MEG method (Shell Global Solutions, 2009). Ethylene carbonate is encompassed in OMEGA process as it is created with the existence of phosphorus halide catalyst and carbon dioxide. A small quantity of water is added to the hydrolysis–ethylene

carbonate reaction to produce MEG and carbon dioxide. The carbon dioxide is then recycled and added into the feed stream. Additionally to the enhanced process effectiveness of OMEGA plant, the cost is less both operational and capital expenditure (van Hal et al., 2007).

2.11 MEG Regeneration and Reclamation Systems

MEG is expensive and used in large amounts therefore, it is essential to recycle it (Bikkina et al., 2012). Maintaining a higher reliability of MEG supply is greatly reliant on good MEG regeneration and reclamation systems. If the sole issue of concern only about the MEG Regeneration Unit (MRU) is separating water from MEG, then the design would be simple. However, there is complexity involved in the design of the MRU production facility to mitigate the impact of these contaminants on operation due to their presence in the pipeline (Latta et al., 2016). MEG reclamation and regeneration systems may be described as closed loop systems. Where, ‘Rich MEG’ from the wellhead and pipeline is routed to MRU to purify it to ‘Lean MEG’ where it is injected again at the wellhead for hydrate inhibition (AlHarooni et al., 2017). MEG regeneration and reclamation is the preferred option for continuous injection at various gas fields around the world as shown in Figure 2-45.

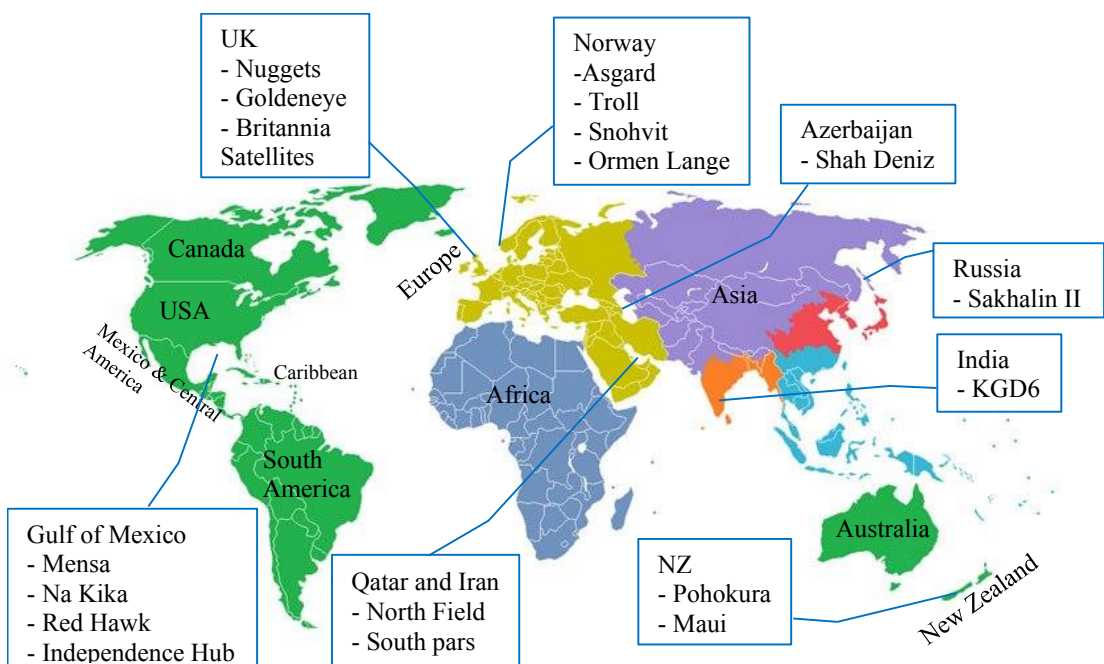
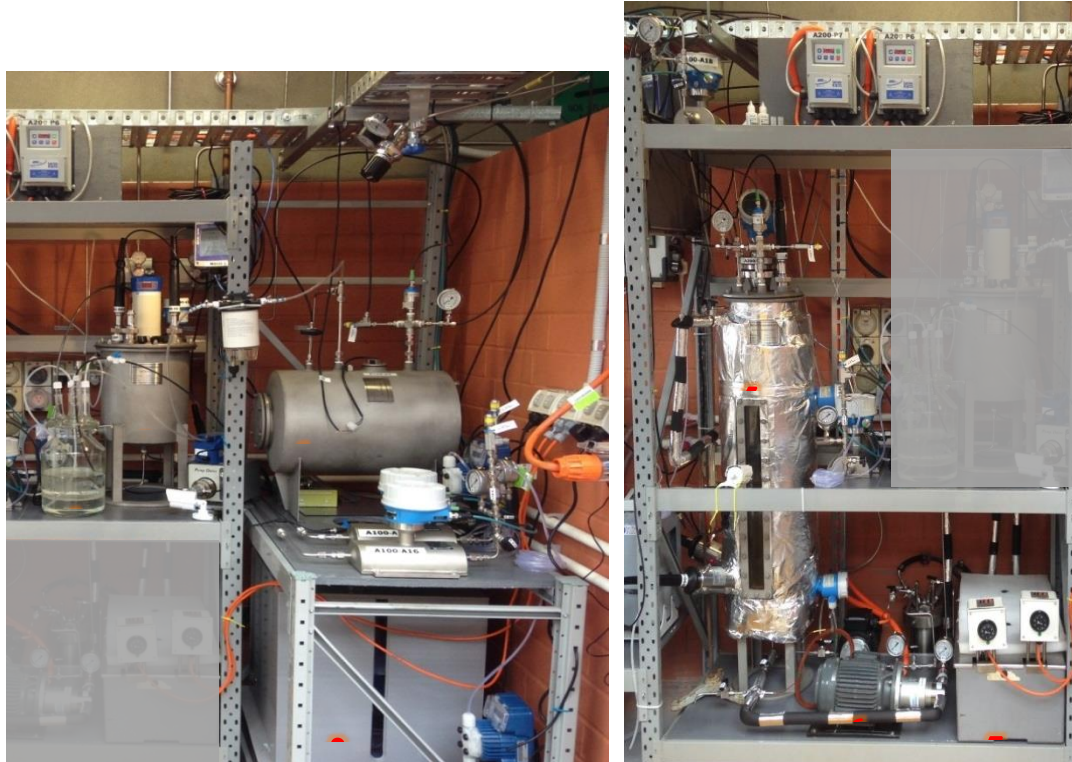


Figure 2-45 Fields location of MEG regeneration plants around the world; adapted after Craig Dugan (2009).

The closed loop MEG regeneration system comprises three operational areas; Feed blending, Pre-treatment and Regeneration/Reclamation (Baraka-Lokmane et al., 2013, Yong et al., 2015). These operational areas are illustrated in Figure 2-46 and Figure 2-47 for the recently constructed MEG pilot plant by the Curtin Corrosion Engineering Industry Centre (CCEIC) (Zaboon et al., 2017). This pilot plant will be discussed in Chapter 8 for the study of the efficiency of thermodynamic hydrate inhibition of both regenerated and reclaimed MEG solutions.



A) Feed blending

B) Pre-treatment

Figure 2-46 CCEIC MEG pilot plant operation areas; (1) Condensate tank, (2) Brine tank, (3) Feed blender, (4) three-phase separator, (5) Pre-treatment vessel, (6) Recycle pump, (7) Recycle heater.



C) Regeneration



D) Reclamation

Figure 2-47 CCEIC MEG pilot plant operation areas; (1) Distillation column, (2) Reboiler, (3) Reflux condenser, (4) Rotary flash separator, (5) overhead condenser, (6) condensed MEG collector.

There are three models available in the design of MEG regeneration and reclamation plants: slip-stream reclamation, full reclamation, and conventional regeneration (Lehmann et al., 2014, Brustad et al., 2005).

2.11.1 Convention Recovery Model

The process of convention regeneration is the least preferred and least employed approach due to high chance of causing MEG degradation and the requirement of water separation. Conventionally, many systems are not designed to tolerate the high volume of water formation, particularly from the wells. It will usually require a water separation process before re-injecting MEG (Latta et al., 2016). Convention regeneration is commonly applied in conditions where the MEG recovery stream is

having a low level of total dissolved solids (Nazzer et al., 2006). Convention regeneration principle works by distilling over the water, with controlling pressure to atmospheric conditions and the temperature to the specifications required for the lean MEG purity.

Another issue with the applicational of convention process of regeneration is the part of contaminants in the product stream of MEG. Within the distillation column, the water is boiled off, lean MEG will be contaminated with production chemicals and salts. Nevertheless, if the same MEG kept recycled, MEG degradations may take place in the system even if the MEG contamination is considered low. This will require MEG replacement or top up to maintain inhibition performance.

The Shell Mensa plant, which is situated in the Gulf of Mexico, has gained considerable interest. The system utilises the MEG for both dehydration and hydrates control. It has experienced operational issues linked with the MEG regeneration plants. As completion fluids and formation water feed in to the plant, the conventional regeneration process has caused a higher level of plugging and scaling within the system. Other issues were also suffered through the contamination of MEG product causing injection line blockages (Brustad et al., 2005).

2.11.2 Full-stream Reclamation Model

The full reclamation process is one of the most employed processes (Figure 2-48), which is used for MEG regeneration along with the option of slipstream method, if required. The procedure focuses on rich MEG monitored by boiling and distillation in a flash separator to gain appropriate lean MEG product. It discourses the major issue of the convention recovery procedure, due to this it can lodge higher rates of water formation and deal suitably with the dissolved solids (Nazzer et al., 2006).

A typical reclamation process commences with a stage of pre-treatment, where MEG is heated and depressurized within a three-phase separator to separate hydrocarbons from the mixture. The rich free hydrocarbon MEG is then routed to the vacuum operated flash separator (typically 0.10-0.15 bara) in order to increase the MEG purity and eliminate contaminants. It has been evaluated that the flash separator usually vaporises MEG by applying low temperature for preventing the process from decomposition and elimination of the contaminants. The contaminants removal may include non-volatile chemicals, particles, and salt. The rich MEG exits as vapours

from the flash separator. The outgoing flow of the product stream (vapourised MEG) will flow into a distillation column for separation. The liquid product stream flows into a centrifugal decanter for the contaminants filtration (Brustad et al., 2005).

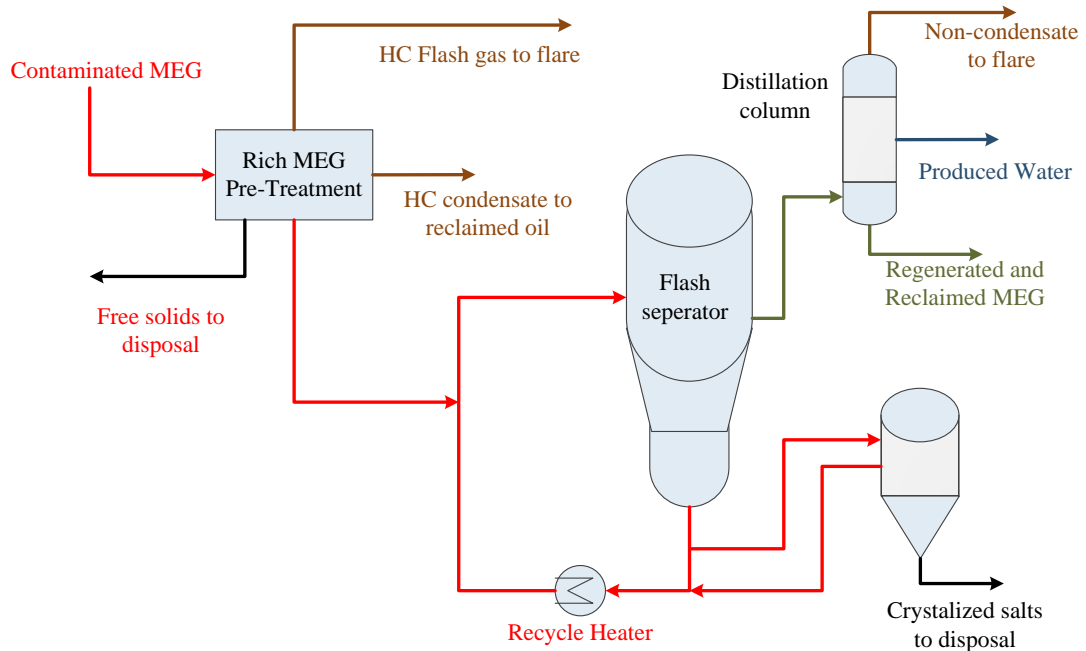


Figure 2-48 Full-stream Reclamation; adapted after Joosten et al. (2007)



Figure 2-49 Full-stream MEG reclaimer in the Gulf of Mexico; adapted after Van Son (2000)

2.11.3 Slip-stream Reclamation Model

The salt removal process of slipstream is an edition of the conventional regeneration method. It uses an ion exchanges (reclaimer) for treating part of the flow with highly salt content for re-use (Figure 2-50). pH inhibitors and stabilisers are also removed in the slipstream through a salt removal procedure. Whereas, a full regeneration stream has a reclaimer applied to the complete elimination of salts and non-volatile chemicals. When operators need the highest recovery of MEG, the systems of slipstream can usually be designed based on an operators request taking into consideration the endorsement of the higher operation price of the system in contrast with the full reclamation model.

The most important critical issues observed in the industry with the slipstream salt removal process is when the pH stabilising and chemical inhibitors are being re-used. These particles of re-used chemicals will exist over time and accumulate inside the loop system. It develops critical issues of scaling, equipment safety, and blockages of the injections points. A slip-stream model will be discussed in Chapter 8 to investigate the efficiency of thermodynamic hydrate inhibition of MEG solutions collected from a MEG pilot plant, simulating six scenarios of the start-up and clean-up phases of a typical gas field.

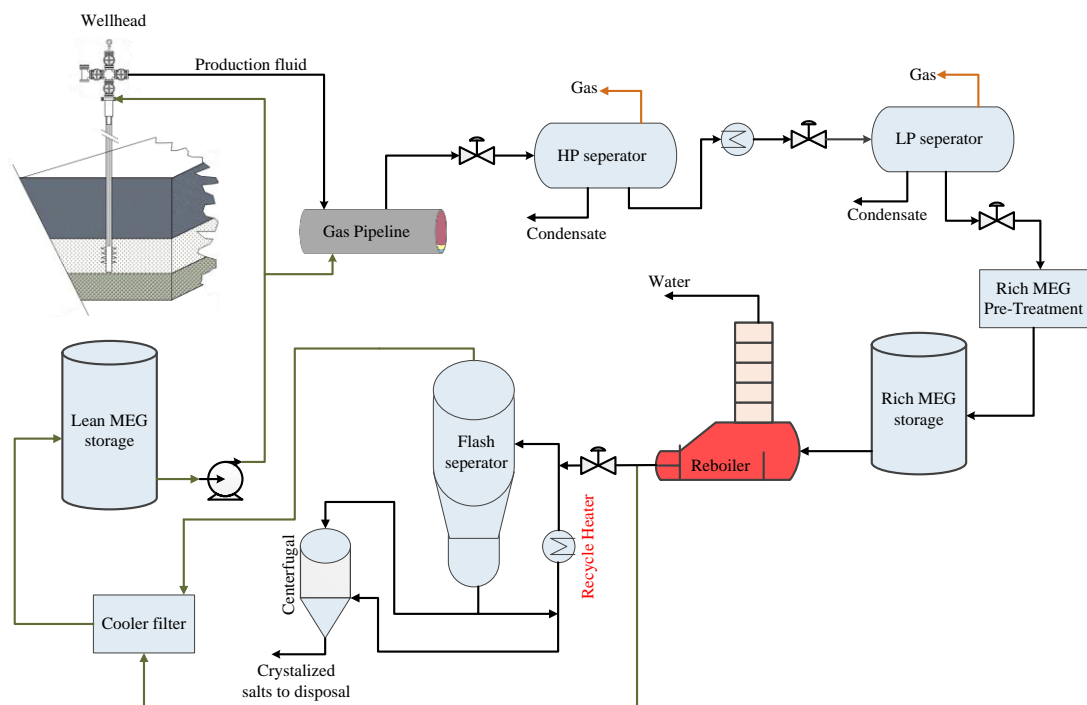


Figure 2-50 Slip-stream MEG reclamation model; adapted after Lehmann et al. (2014)

The disadvantages and advantages of the three MRU operating models are compared in Table 2-5.

Table 2-5 The disadvantages and advantages of the three MRU operating models

Operating model	Disadvantages	Advantages
Convention Recovery	Unable to handle MEG with continuous formation water production. Non-volatile chemicals and salts gather in the closed loop.	Least expensive option
Full-Stream reclamation	Higher capital expenditure & larger size	The non-volatile chemicals and salts are removed. It can withstand higher formation water rates.
Slip-Stream reclamation	MEG's viscosity and density influenced by impurities and salt. Higher chance of corrosion and plugging.	Reconcentration is not entirely relied on the MEG reclamer operation. Superior flexibility in operating MEG reclamer. Lower capital expenditure and plant size. pH stabilisers and chemical extracts may be reused and reserved. Lower cooling and heating operating envelope with less MEG vaporised.

2.12 MEG Degradation

The degradation of glycols under various conditions is a major factor, affecting its performance. All organic materials decompose when subjected to different factors; such as metal ions in solution, gaseous and liquid species, ultraviolet (UV) radiation, thermal energy or mechanical loading (De Rosa, 1986, P. M et al., 2015). MEG is used as a hydrate inhibitor in transportation pipelines and gas processing plants. Regenerating MEG is an environmental and economical solution due to its high cost and consumption rate and also its environmental influence. Thermal degradation of MEG may arise when heated at a high temperature, during the regenerating process at the reboiler. Generally, there are several factors that are used to determine the degradation efficiency including microbial population, nutrients supply, acclimation degree, organic structure and environment. The factor of the environment may comprise of the temperature, oxygen content, and pH level (Haritash et al., 2009).

2.12.1 Types of degradation

2.12.1.1 Oxidative Degradation

Oxidative degradation arises when a fluid is exposed to air at high temperatures. It is one of the most common types of degradation process as it produces some carboxylic acids and aldehydes that usually results in sludge formation (Rebsdat et al., 2000). While fluid chemistries are influenced at various temperatures and experience oxidation at high temperatures. Oxygen degrades polymers by reaction with polymer free radicals to form hydroperoxides (ROOH) and peroxy free radicals (ROO[•]) to lower molecular weight (MW). Free radicals can restore the molecule and atoms that have an unshared electron to form a stable structure. Many of the properties suffer due to the decline in molecular weight, and it often leads to chain scission. At least, 5-10% reduction in MW could cause failure. Using antioxidants and avoiding contact with oxygen are the ways to prevent oxidative degradation (Ezrin et al., 2001).

2.12.1.2 Thermal Degradation

The thermal degradation of a substance is formed when a substance chemically decomposes and starts to undergo detectable chemical and physical change by adding heat to more than the recommended maximum temperature. For MEG thermal degradation, Psarrou et al. (2011) suggested that the thermal degradation of MEG will take place above temperatures of 157°C, even in the absence of oxygen, and consequently, the MEG colour will change to yellow. In spite of MEG, which is not toxic, its degradation and decomposition includes the oxalic acid, formic acid and glycolic acid, which are dangerous for the environment and human health. Therefore, precautions must be taken not to decompose and degrade MEG during operations (Rossiter et al., 1983).

2.12.1.3 Biodegradation

Biodegradation (breakdown of an organic compound) is the predominant degradation pathway for ethylene glycol in water. The rate of biodegradation depends on many factors, such as type and number of microorganisms present, ambient temperature, acclimation and the concentration of ethylene glycol in the water body (Act, 2000). Biodegradation can also be caused by mineralisation, when exposing a solution to ultraviolet light (UV) and hydrogen peroxide (H₂O₂). Wang et al. (1993) suggested

that OH is a system that may degrade ethylene glycol, formed by UV absorbed by H_2O_2 , as shown in Figure 2-51.

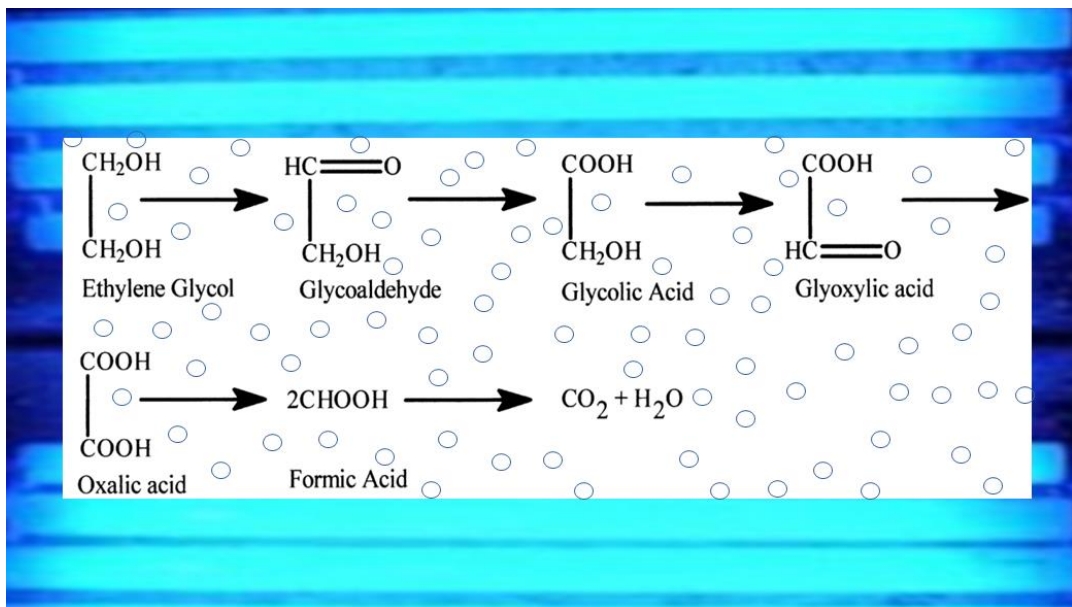


Figure 2-51 Possible pathway for MEG degradation by mineralisation in the UV/ H_2O_2 system. The results have presented stepwise oxidation of ethylene glycol by reaction with OH; adapted after McGinnis et al. (2000).

A proper understanding of thermal degradation is the primary factor in the performance for MEG to remain competitive. Many experiments and evaluations have been conducted by researchers to study various effects of MEG degradation and products identification techniques. It is highly likely that MEG degradation products will initiate internal corrosion and disturb the process. If this happens, the corrosion would grow with time to undermine the pipe's integrity by destroying its material, which results in the pipe failure. Additionally, when the process of degradation is commenced, hydrate inhibition performance will drop (AlHarooni et al., 2017). Operational cost is also expected to be increased as fresh MEG will require to be topped up into the system to ascertain the needed lean MEG purity. Based on this, development of adequate knowledge in hydrate-MEG degradation relationship would go a long way in solving many problems in the industry. Table 2-6 below is a literature review of some of the works done in the area of MEG degradations (oxidative, thermal and biodegradation), showing researchers concern and area of interest.

Table 2-6 literature review of MEG degradations Impacts

Reference	Findings	Impact of degradation
(Evans et al., 1974)	The biodegradation of MEG has been evaluated in river waters, found that MEG biodegrades based on the temperature of the river water and the bacterial state. It biodegrades completely within 3 days at temperatures of 20 °C and within 7 days at temperatures of < 8 °C.	Evaluating biodegradation level
(Dwyer et al., 1983)	Study rates of anaerobic biodegradation of ethylene glycols.	Product identification
(Rossiter et al., 1983)	The ion-chromatography liquid chromatographic method has been applied to the detection of acidic species (glycolic and formic acids) in thermo-oxidatively degraded MEG solutions. Heating the glycol solutions in the presence of metallic copper produced the greatest extent of degradation. Metallic aluminium increased the amount of formic acid produced.	Product identification
(Rossiter Jr et al., 1985, Clifton et al., 1985)	They investigated the thermal oxidative degradation of aqueous ethylene glycol solutions. The concentrations of acidic degradation products (glycolic and formic acids) were measured using the Ion Chromatography. Reactions were carried out with aeration at 75, 86 and 101°C in the presence of copper/ aluminium. Degradation level was higher when copper metal was present in heated, aerated solutions. Exclusion of oxygen from the system is an effective means of suppressing degradation since it is a thermal oxidative process.	pH measurement and product identification
(Brown et al., 1986)	The thermal oxidative degradation of ethylene glycol at temperatures as low as 100°C results in the evolution of CO ₂ as one of the degradation products. The rate of O ₂ consumption during this process appears to follow zero order kinetics. Both the rate of O ₂ consumption and the rate of CO ₂ evolution accelerated in the presence of copper.	Thermal oxidative stability
(Monticelli et al., 1988)	When aluminium alloy 6351 (used as oxidative degradation catalyst) gets in contact with MEG solutions (exposed to 108 °C), this caused MEG degradation and so formation of organic acids (formic, acetic, oxalic and glycolic acid). MEG degradation leads to an increase in the uniform corrosion rate and the occurrence of pitting corrosion.	Corrosion consideration
(Rudenko et al., 1997)	They studied the characteristics of ethylene glycols as a heat transfer agent. They confirmed that the thermal decomposition of ethylene glycols without oxidation is possible only above 157 °C.	Operation conditions

Table 2-6 literature review of MEG degradations Impacts (continued)

(McGinnis et al., 2000)	The results indicated that exposing MEG to ultraviolet light/H ₂ O ₂ system leads to MEG degradation by mineralisation (Figure 2-51).	Effect of UV/H ₂ O ₂
(Madera et al., 2003)	They reported that, when glycol is heated, it will slowly degrade and the pH of the glycol solution will decrease, leading to corrosion and foaming problems. They concluded that formic acid, acetic acid and glycolic acid could be identified as the main degradation products of EG using ion chromatographic methods.	Product identification
(Jordan et al., 2005)	Exposing MEG to high temperature will cause thermal degradation.	Scale consideration
(Brustad et al., 2005)	Minimising the oxygen level within the closed loop MEG system is very important to avoid transformation of iron carbonate to iron oxide(s), avoid an increased corrosion rate and avoid possible degradation of the MEG.	Design consideration
(Nazzer et al., 2006)	High skin temperatures of heat exchanger increase MEG degradation and losses.	Design technology
(Psarrou et al., 2011)	Present results of MEG degradation under regeneration/reclamation conditions and how the degradation products influence the determination of alkalinity and the total dissolved CO ₂ content. The main products of MEG degradation [oxidative/thermal (140 °C)] were glycolic and formic acid.	Operation conditions
(Ranjbar et al., 2013)	The results showed that corrosion rates are increasing with temperature due to the changes in pH of the solution as a result of thermal degradation of MEG and the formation of acetic and formic acids. Also present of oxygen in MEG solution will accelerate the organic acid formation.	Corrosion
(Teixeira et al., 2015)	Thermal degradation of MEG starts at 162 °C.	Exergy analysis
(Yong et al., 2015)	The salt produced during MEG regeneration dissociate to form scaling, degradation of the regenerated MEG and corrosion which can ultimately impact on the safety of the operation, personnel and environment. A Perkin Elmer Spectrum 100 FT-IR Spectrometer was used to identify degradation product. The corrosion would affect the system's shelf-life while the MEG degradation would impact on the operating cost.	Operation concerns

Table 2-6 literature review of MEG degradations Impacts (continued)

(AlHarooni et al., 2015)	Experiments were conducted to test hydrate inhibition performance of thermally degraded MEG exposed to high temperatures (165, 180, and 200 °C). Results conclude that thermally exposed MEG causes a drop in hydrate inhibition performance due to thermal degradation.	Gas hydrate consideration
(Latta et al., 2016)	Stopping air ingress into MEG system reduces MEG degradation.	Design consideration
(AlHarooni, Pack, et al., 2016)	This study evaluated six analytical techniques for analysing degradation levels of various MEG solutions (MEG/FFCI/MDEA) that were thermally exposed to 135, 165, 185, and 200 °C.	Analytical techniques / Gas hydrate
(AlHarooni et al., 2017)	This study focused on analysing the kinetics of methane gas hydrate with thermally exposed MEG solutions with corrosion inhibitors (MDEA and film forming) to 135–200 °C. Results established that thermally degraded solutions cause hydrate inhibition drop.	Gas hydrate consideration

Through the present research (Table 2-6 and others), the effects of MEG degradation in oil and gas systems have been evaluated, which has concluded that there are still many unidentified concerns, related to the impact on flow assurance. The effect of MEG degradation on gas hydrate is considered as entirely a new area for research and there was no literature available concerning this problem except from our work. Therefore, this study has contributed to investigate and develop the functionality and analytical techniques of degraded MEG, which may also serve as a new contribution to scientific knowledge.

2.13 Gaps in Literature

It is important to minimise the thermal exposure and the oxygen levels inside the MEG regeneration/reclamation systems to prevent its possible degradation (Teixeira et al., 2015, Nazzer et al., 2006, Madera et al., 2003, Montazaud, 2011, Brustad et al., 2005). Furthermore, the rate of MEG degradation is accelerated by high temperature and metal ions of solutions. The studies have suggested that formic acid and glycolic are the main products of MEG degradation (Clifton et al., 1985, Psarrou et al., 2011). Before this study, the available articles on MEG degradation were considered primarily on MEG's influence on the aspects of identification of MEG degradation products (Madera et al., 2003), and the influence on corrosion rate of metallic components. No research has been conducted on MEG degradation effect on hydrate inhibition performance. AlHarooni et al. (2015) (chapter 5) bridged this gap by identifying the influence of thermally degraded pure MEG on gas hydrate inhibition; while AlHarooni et al. (2017) (Chapter 6) studied the effects of thermally degraded MEG with film forming and methyl diethanolamine corrosion inhibitor on gas hydrate inhibition.

We further identified the analytical techniques that can be utilised to recognise the severity level of thermally degraded MEG and developed a novel MEG thermal degradation scale. Moreover, this scale also provided a quick evaluation of the regenerated MEG to adjust MEG doses and corrosion protection strategies (AlHarooni, Pack, et al., 2016) (chapter 7).

As there is a knowledge gap in evaluating hydrate inhibition performance of MEG once it undergoes regeneration and reclamation. Chapter 8 further investigates this.

This work opened a new area of research interest on thermal MEG degradation-hydrate relationship, and the association between the final products of regenerated and reclaimed MEG with gas hydrate inhibition performance.

In the following chapters, we will present the following topics:

- Gas Hydrate in Gas Lift system
- Inhibition effects of thermally degrade MEG on hydrate formation for gas systems
- Effects of thermally degraded MEG with Methyl Diethanolamine and Film-Forming Corrosion Inhibitor on gas hydrate kinetics

- Analytical techniques for analysing thermally degraded MEG with Methyl Diethanolamine and Film Forming Corrosion Inhibitor
- Influence of regenerated MEG on natural gas hydrate formation

Chapter 3 Case study: Various Gas Hydrate Mitigation Techniques Applied to a Gas Lift System in a South Field of Oman

3.1 Introduction

Petroleum Development Oman (PDO) is the largest petroleum exploration and production (E&P) company in the Sultanate of Oman. PDO currently operates more than 4000 wells scattered over 100 fields in over 113,550 km² of the concession area. PDO produces approximately 843,490 barrels of crude and 44 million Sm³ (standard cubic meter) of gas per day. The fields are assigned to south and north directorates (Figure 3-1) and have a variety of characteristics regarding reservoir types, development plans and production drive techniques (Al-Khodhori, 2003, Petroleum Development Oman, 2003). The production assets within the north directorate include Fahud, Lekhwair, Yibal and Qarn Alam, and those within the south directorate include Bahja, Nimr and Marmul.

The crude oil export facilities and the administrative headquarters are located on the coast in Mina Al Fahal (Petroleum Development Oman, 2003). PDO produces around 23% of its oil from gas lift wells (GL), 38% from electric submersible pumps (ESP), 27% from beam pumps, 10% from natural flow and 2% from screw pumps (Figure 3-2) (Al-Bimani et al., 2008). South Oman fields are mostly produced via beam pumps (with only XS field having GL wells), and North Oman fields are mostly produced via gas lift wells, with ESP scattered over all fields (Al-Khodhori, 2003).

XS Field Production Station (Figure 3-3) is located in the south of Oman. It receives gross fluids from its own field as well as from four other fields. These fields are producing through gas lift, ESP, and free flowing. Gas lift is widely used in mature oil fields as an artificial lift mechanism (Shao et al., 2016). Gas lift systems require injecting a specific amount of high-pressure gas through the tubing into gas lift valves to lower the hydrostatic pressure difference along the tube (Miresmaeli et al., 2015). The oil is exported via a 20-inch pipeline to the Main Oil Line via South Oman Booster Station. The produced water is used for water injection and deep water disposal (DWD).

The gas is used for gas lift wells of the XS field. The surplus gas is further treated in the gas conditioning unit (GCU) for exporting to the South Oman Gas Line (SOGL).

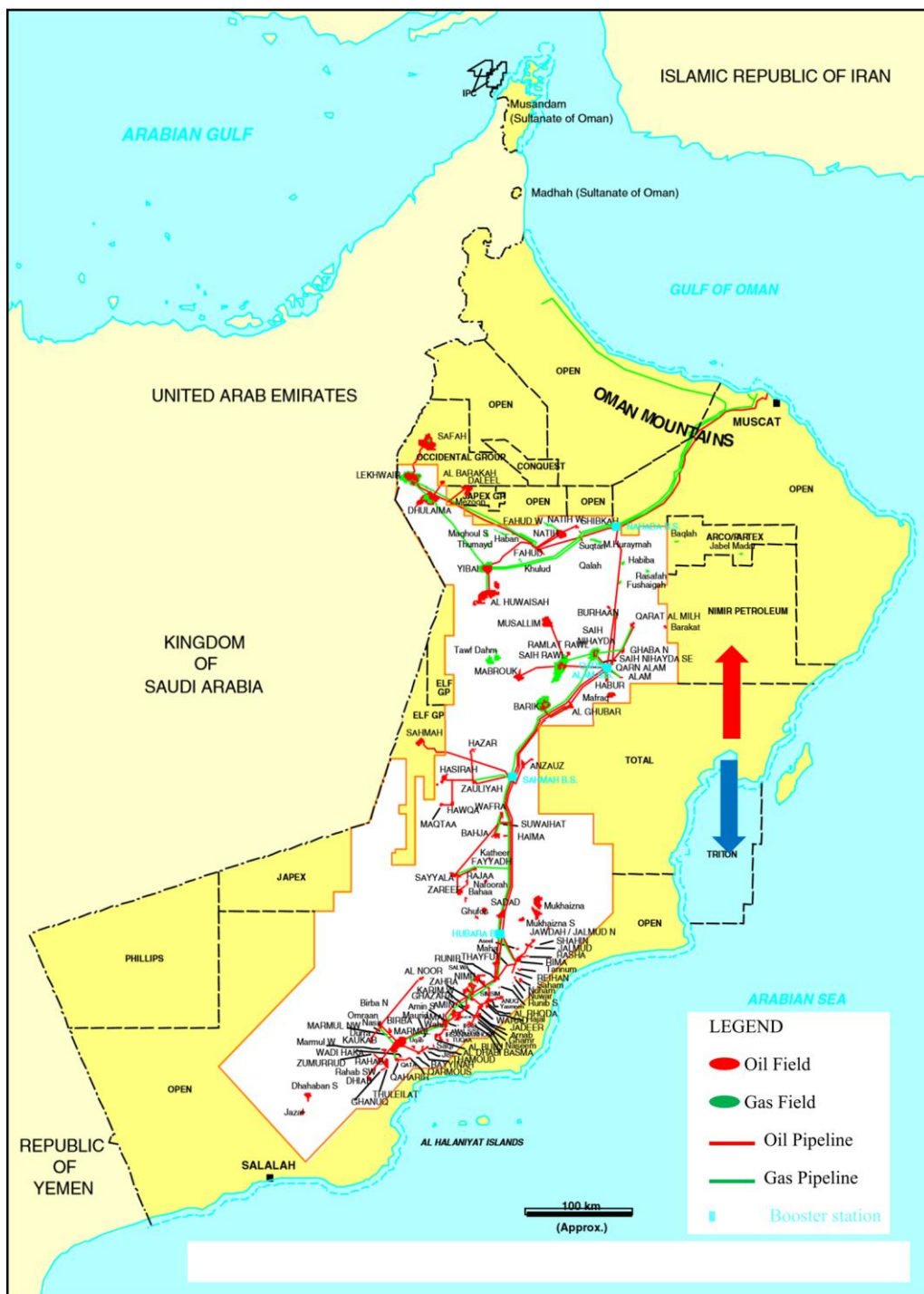


Figure 3-1: Sultanate of Oman field location map. The red arrow indicates north and the blue arrow indicates south (Sanchez et al., 2011, Al Salhi et al., 2001).

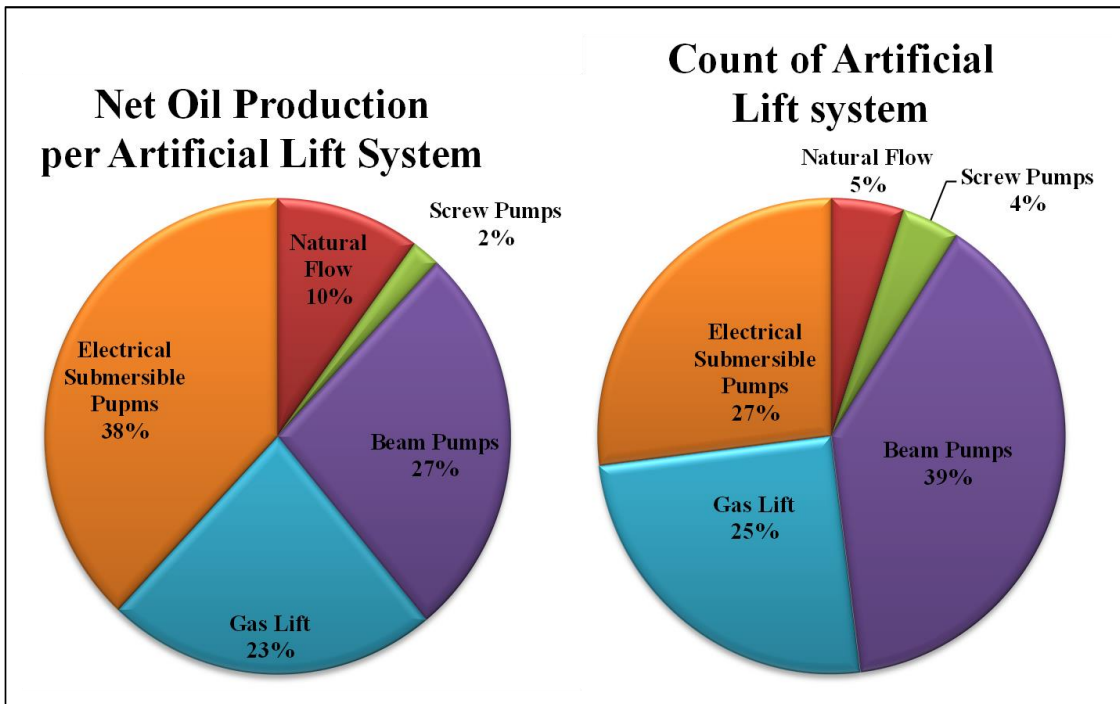


Figure 3-2: Artificial lift systems distribution in PDO (Al-Bimani et al., 2008)

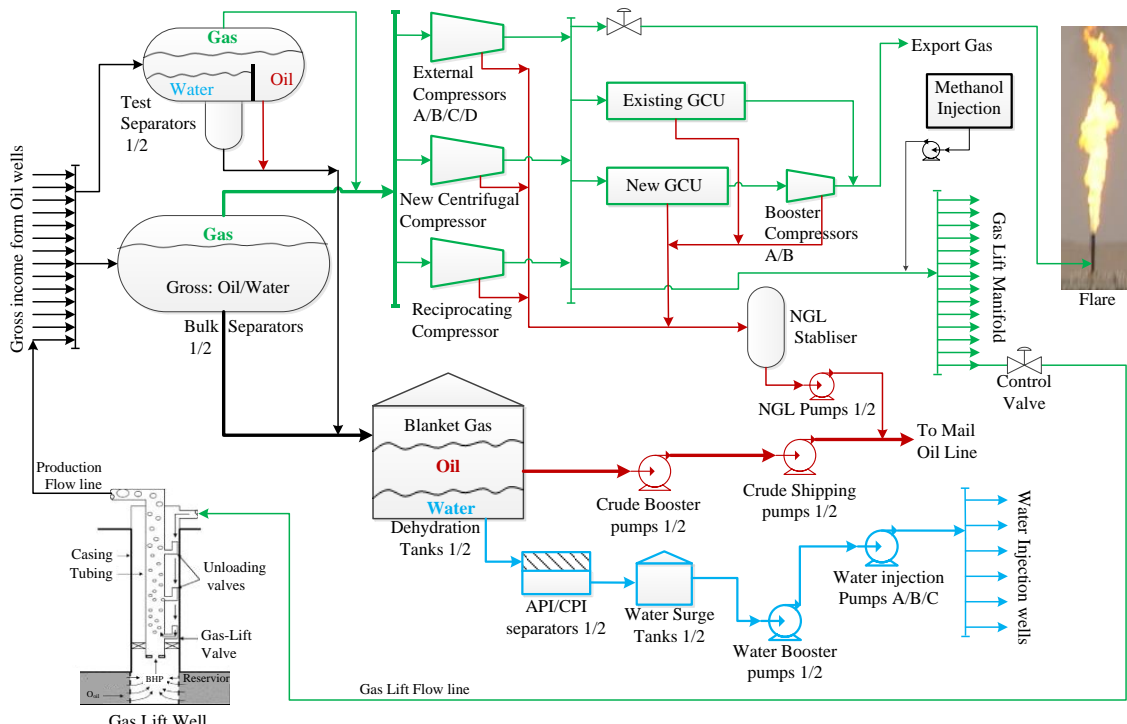


Figure 3-3: XS Field Production Station Overview

3.2 Problem Description

There are more than 10 gas lifting oil fields in PDO currently facing gas hydrate problems during each winter season (December, January and February). This results in a decline in well production and/or unscheduled deferment (Nengkoda et al., 2009). In this chapter, the XS field will be studied. Once XS field experience hydrate formation (at the gas lift manifolds and pipelines), leads to a well quit or production drop. This is mainly because the gas used for gas lifting is neither dehydrated nor dew pointed after being compressed and cooled in the compressors' after-coolers, and because high gas pressure from gas compressor discharge gets expanded through a gas lift chock valve (FCV) where it undergoes the Joule-Thomson cooling effect, these issues increase the chance of hydrate formation.

Even though there are two Gas Conditioning Units (GCUs) in XS Production Station (XSPS), they are designed to handle a maximum total capacity of 400,000 m³/d, which is lower than the gas lift requirement of greater than 600,000 m³/d (Petroleum Development Oman, 2016). As a result, condensation of water and hydrocarbons will occur during winter seasons when the ambient temperature falls below 5 °C (Nengkoda et al., 2009) in the bare steel pipelines from the station to the respective gas lift manifold's location. XSPS gas lift compressors discharge temperature (Figure 3-4) shows that it varies widely from the summer to the winter season. GL discharge temperature falls below 30 °C during winter. This low temperature at compressor discharge side can be further lowered by ambient temperature to below hydrate formation temperature (\approx 19 °C) once arrived at manifold sides.

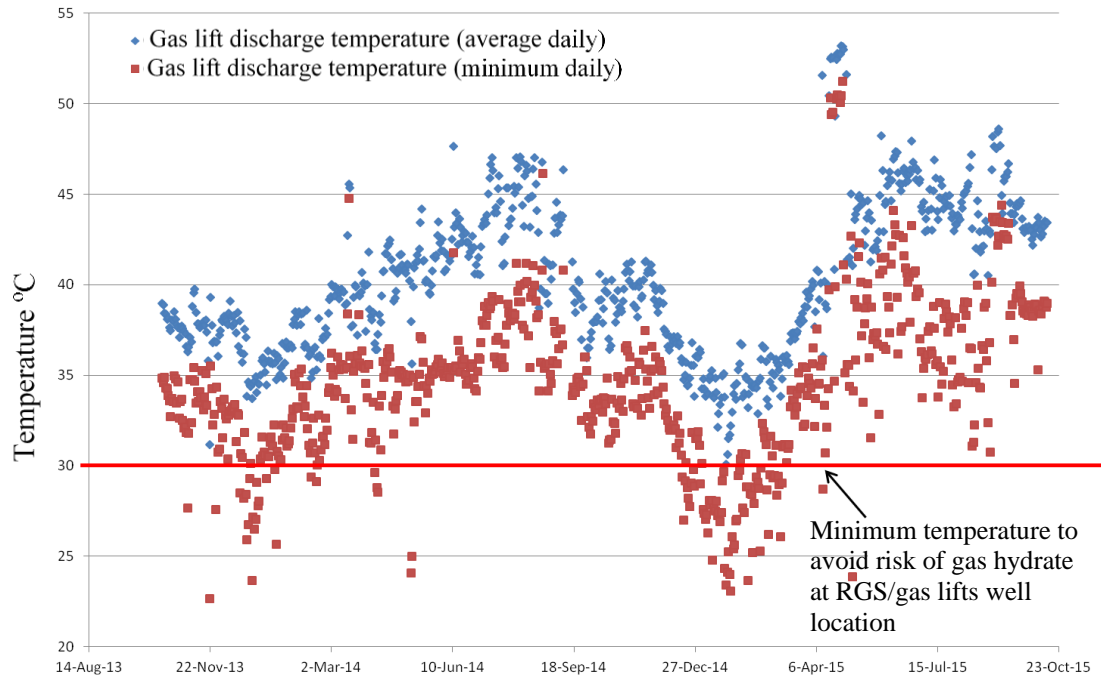


Figure 3-4: XS production station common gas lift compressors discharge temperature (Aug. 2013 to Oct. 2015)

Gas hydrates, which cause pipeline blockage (Figure 3-5) are ice-like crystalline solid structures consisting of water molecules and small natural gas molecules that are formed under high pressures and at low temperatures (Carroll, 2002, Eslamimanesh et al., 2012). Gas hydrates are normally formed at a low point in the flow line where water is likely to accumulate (Jamaluddin et al., 1991) as shown in Figure 3-6:



Figure 3-5: Gas hydrate blockage inside pipeline; after (Fraser, 2013)

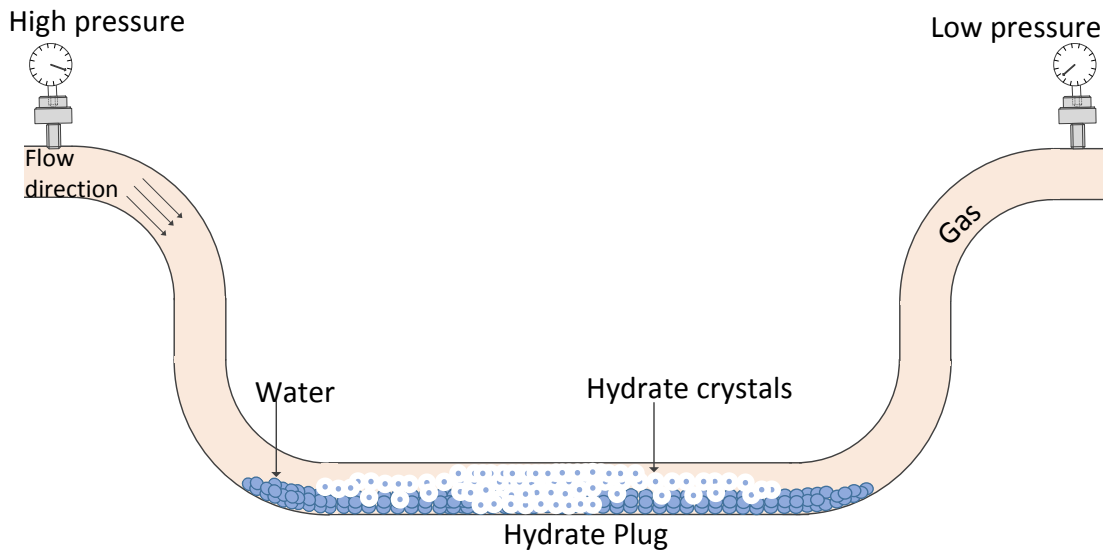


Figure 3-6: Hydrate formation at low point of flowline; adapted after (Jamaluddin et al., 1991)

Hydrate density is greater than those of typical fluid hydrocarbons, and this has practical consequences for flow assurance (pipeline blockage) as well as for safety concerns. In terms of safety concerns, as hydrate-specific gravity is typically 0.9 (compared to the 0.8 gravity of typical fluid hydrocarbon), this leads to hydrates travelling at a very high velocity of around 300 km/hour, which can cause pipeline rupture or the plug to erupt through pipeline bends (Sloan, 2003).

Hydrate phase envelope for the XS field (Figure 3-7) has been developed using Multiflash software (version 3.6, licensed to Curtin University), Peng-Robinson EOS and input data from XS field gas composition (Figure 3-9) and an operating pressure of 70 bar. The red area represents the hydrate-forming region, while the green area represents the non-hydrate-forming region. Therefore, at 70 bar and with the presence of water molecules, gas hydrates will form once temperature inside the flowline drops to 19.04 °C.

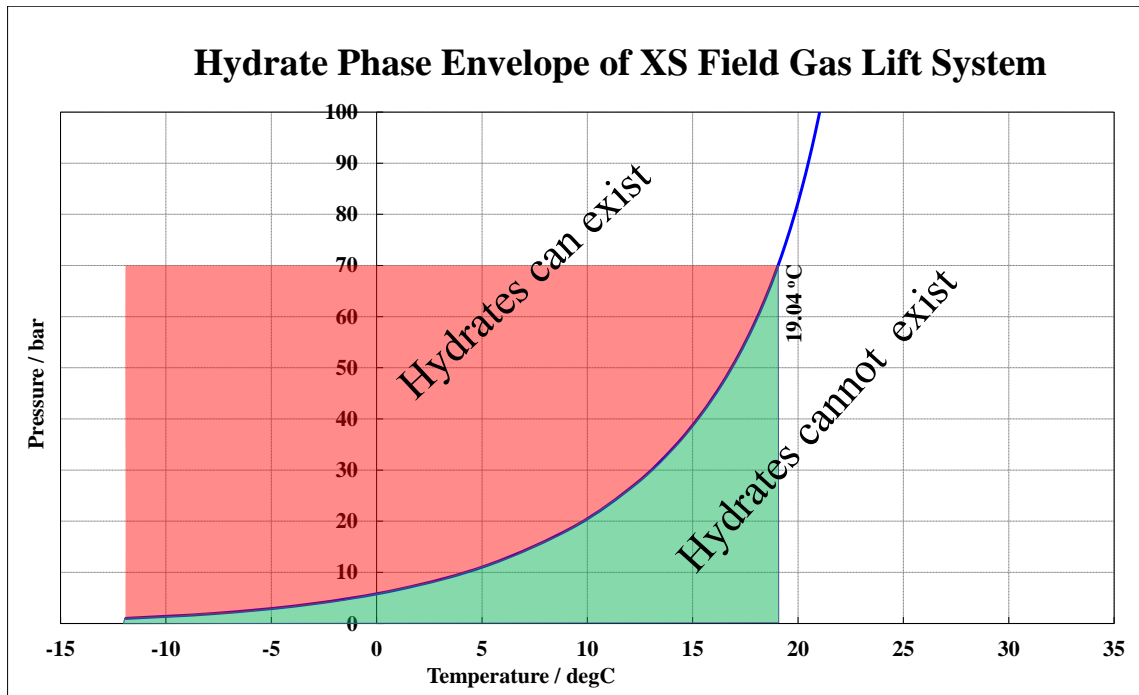


Figure 3-7: Hydrate Formation Phase Envelope for XS Field using Multiflash software P-R EOS. The coloured region is the operating envelope of pressure up to 70 bar; the red region is where hydrate can exist, and the green is where hydrate cannot exist.

The effect of different methanol injection percentages (0 mole % to 25 mole %) on the XS Field gas hydrate is illustrated in Figure 3-8. For the best effect, methanol must be injected upstream of the flow control valves to prevent hydrate formation. As methanol is injected at the gas lift manifold, it is mixed with the gas lift. This later gets mixed with the production of the well and gets lost with the hydrocarbon phases (Sloan, 2003). During winter, methanol injection doses should be closely monitored and adjusted to shift the hydrate formation curve to the left side (safe region) as per Figure 3-8 in order to avoid gas hydrate formation.

Hydrate Phase Envelope of XS Field Gas Lift System with Different Methanol Injection %

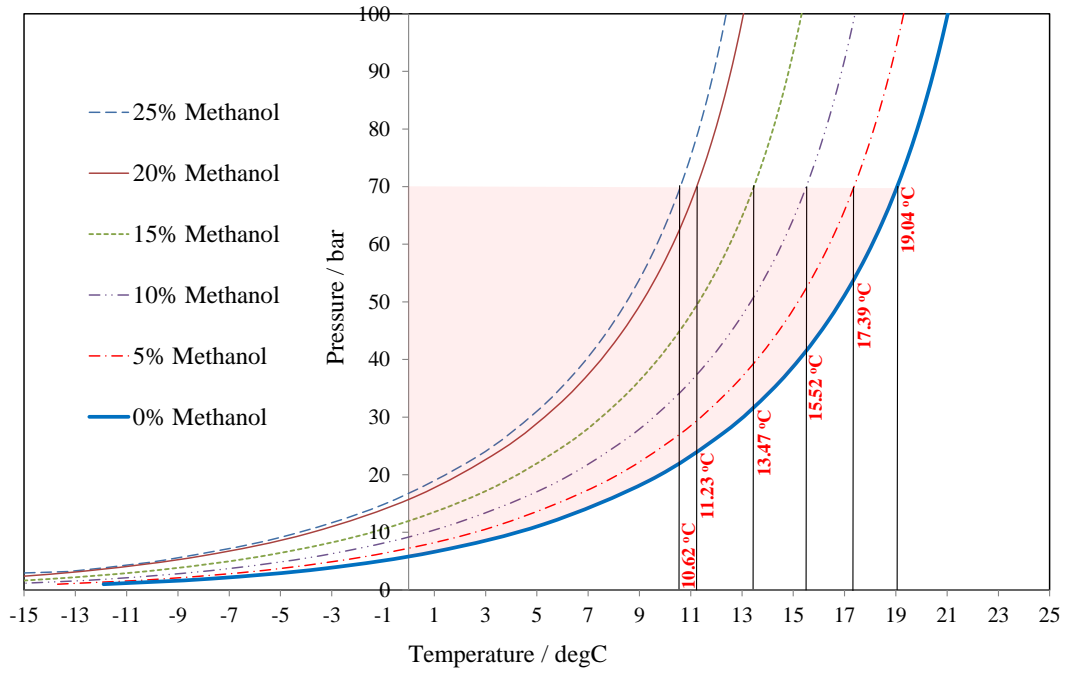


Figure 3-8: Hydrate formation phase envelope for XS field using Multiflash software P-R EOS with different methanol injection percentages, gas composition input extracted from Figure 3-9

Hammerschmidt (1939) developed a simple formula (with an average error of 5%) to roughly estimate the temperature shift of specific hydrate formation phase envelope based on methanol injection concentration (Bai et al., 2005).

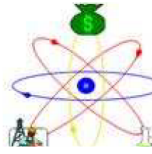
$$\Delta T = \frac{KW}{M(100-W)} = \frac{2335 W}{\frac{32.04}{18.01528} (100-W)} \quad \text{Eq 3-1}$$

Where ΔT : temperature shift, hydrate depression (°C)

K : constant (methanol = 2335)

W : concentration of inhibitor in weight percent in the aqueous phase

M : molecular weight of the inhibitor divided by the molecular weight of water.

Petroleum Development Oman
 Production Chemistry Laboratory
General Analysis Report - GAS
 Report Date : 18-Jul-2016

Parameters			
Area	South	(Sample collected from XS field)	
Field	XS	(XS Station)	
Facility	XS Station	(Gas Compressor Discharge)	
Sample Point	KXS36A_Out		
Sample Type	GAS		
Sampling Date/Time	03-June-15 13:00		
Components		Results	Units
Carbon Dioxide		0.44	mole%
Nitrogen		5.56	mole%
Methane		77.78	mole%
Ethane		8.03	mole%
Propane		5.13	mole%
i-Butane		1.10	mole%
n-Butane		1.42	mole%
i-Pentane		0.25	mole%
n-Pentane		0.24	mole%
n-Hexanes		0.05	mole%
Heptane		0.00	mole%
Octane		0.00	mole%
Nonane		0.00	mole%
Sampling Pressure	7050	Kpa	
Sampling Temperature	37.0	Deg.C	
Molecular Weight for the Gas	20.8	g/mole	PECOP3005
Calorific Value, Gross @ 15.6C & 101.325	43.4	MJ/m3	PECOP3005
Calorific Value, Net @ 15.6C & 101.325Kpa	38.9	MJ/m3	PECOP3005
Compressibility factor at 15C	0.998	--	PECOP3005
Compressibility factor at line condition	0.838	--	PECOP3005
Relative Density @ 15C; air =1	0.717	--	PECOP3005
Cp/Cv at line condition	1.245	--	PECOP3005
Gas Viscosity @ line conditions	0.013	cP	PECOP3005

Figure 3-9: XS Field gas analysis report (courtesy of PDO)

3.3 Hydrate Formation History

The compressed gas in both external compressors K-XS33A/B/C/D and PDO compressors K-XS35/05 distributed in six manifolds for gas lift wells. Three of the manifolds are located inside XSPS; A-XS16/30/64. The remaining three manifolds are located at remote gathering stations RGS 1 (A- XS68), RGS 2 (A- XS73) and RGS 3 (A-

XSYS). The RGSs are located outside XSPS. The distribution of the wells is represented in Table 3-1 (Petroleum Development Oman, 2016).

Table 3-1: Gas lift wells distribution

Manifold	Gas Lift Well Numbers			Total Gas Flow Distribution [Sm ³ /D]
A-XS16 At XSPS	W008	W086	W049	125000
	W087			
A-XS30 At XSPS	W029	W036	W068	84000
	W035	W088	W033	
A-XS64 At XSPS	W042	W034	W083	
	W044	W089	W053	180000
	W090	W062		
A-XS68 at RGS 1	W100	W048	W058	
	W014	W101	W064	88000
	W047	W057	W063	
A-XS73 at RGS 2	W070	W082	W099	68000
	W071	W084		
A-XSXS at RGS 3	W069	W079	W102	
	W078	W098	W103	86000

In general, the gas lift system is a closed loop system. Gas is received in the bulk/test separators and routed to gas lift compressors, which consist of three stages. There is a scrubber after the third-stage compressor to remove condensed water. The lift gas leaves the scrubber at around 50-70 bar and 25-50 °C (depending on compressor capacity and design). The amount of water condensed in each gas lift line was estimated at 0.1 barrels of water per day (BWPD). Hydrates forming in the gas lift system create back pressure, causing compressor discharge pressure to rise and excess gas to flare, which leads to reservoir depletion. Also, the operator needs to inject methanol to inhibit hydrate formation. As a result, energy and maintenance costs are increased (Fu et al., 2001).

The Sultanate of Oman is considered to be one of the hottest regions, especially in the desert areas where the oil/gas fields are located, where the temperature can reach above 50 °C during summer. However, during the winter season (November to February) ambient temperature can drop to -5 °C, especially between midnight and early morning. Hydrate formation/plugging in the gas lift lines during the winter season has been a

major problem plaguing the operation of most of the gas lifted wells in PDO. Figure 3-10 shows the history of total PDO hydrate deferment in barrels caused by hydrate formation during the winter seasons of 2013-2017.

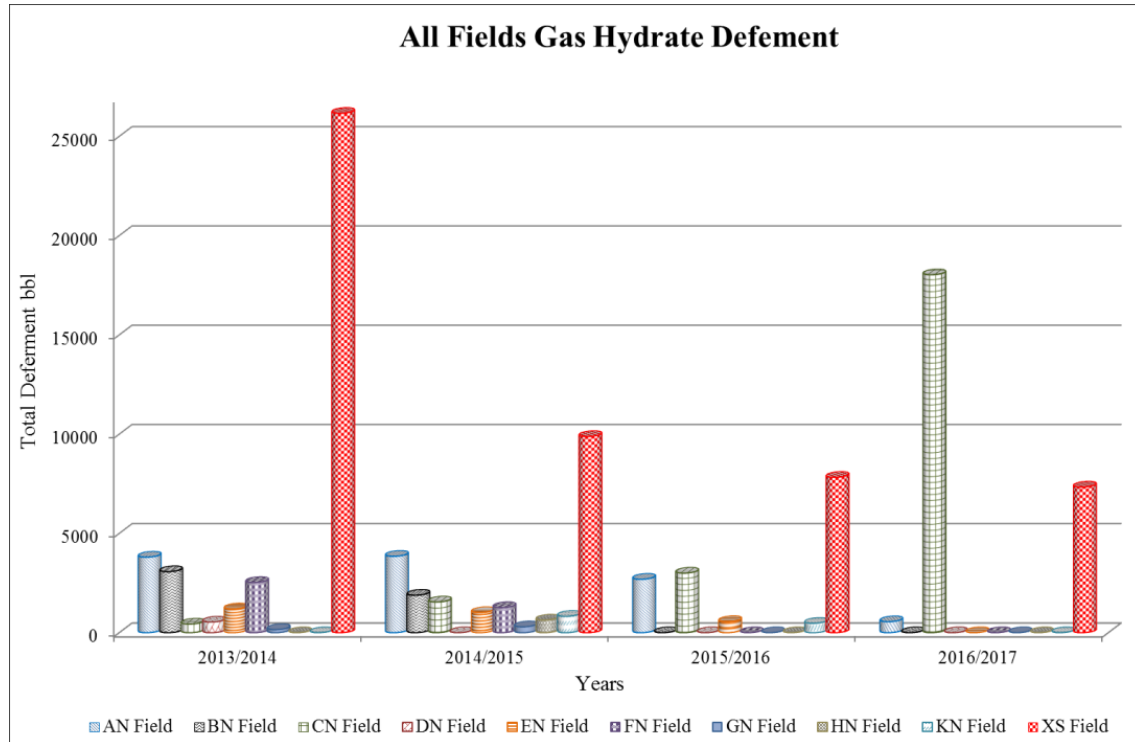


Figure 3-10: Total deferment of all PDO fields due to hydrate formation (during the winter season). Note: CN field shows high hydrate deferment in 2017 as a result of sending rich gas caused by a process upset (PDO deferment report-March-2017).

We can observe from Figure 3-10 that there is a tremendous amount of oil deferment because of hydrate blockages in the gas lift wells, with the XS field experiencing the highest deferment.

Figure 3-11 shows the history of the total XS field hydrate deferment in barrels because of hydrate formation during the winters of 2013-2017. Hydrate deferment has dropped tremendously from 2013 (26,159 bbl.) to 2017 (7336 bbl.). This is mainly because of various hydrate mitigation projects and techniques that were implemented in the XS field to tackle hydrate formation as explained in Section 3.5.

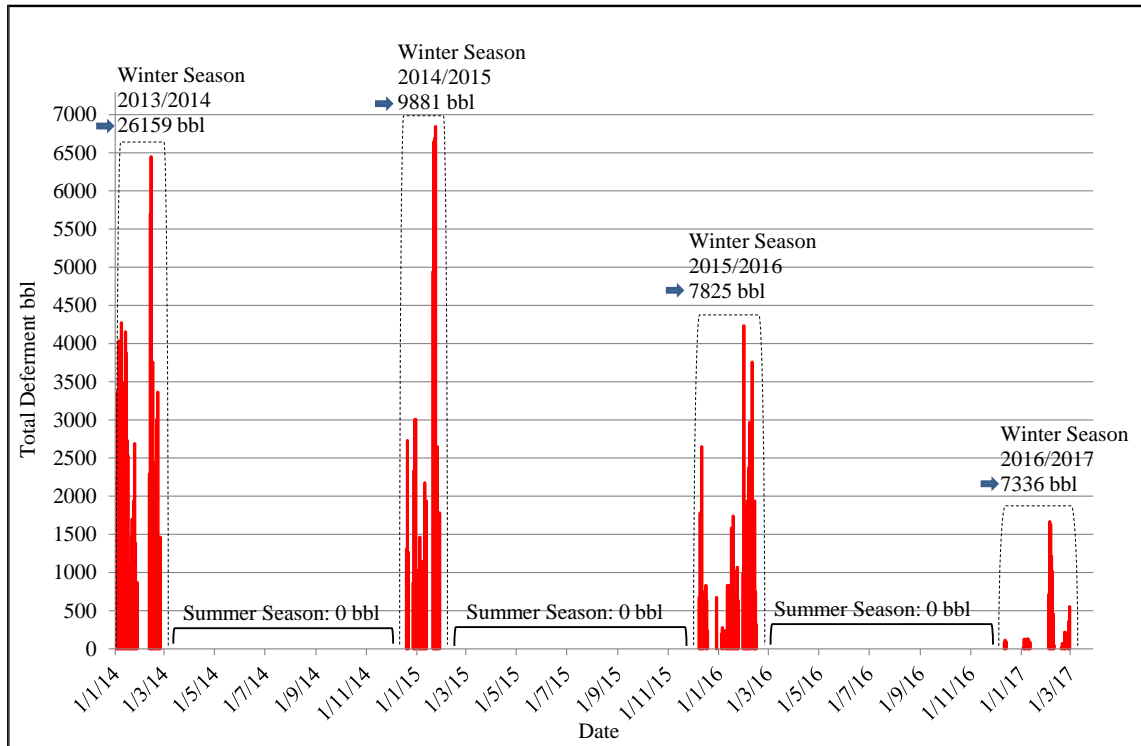


Figure 3-11: XS Field total deferment because of hydrate formation (where → for total reconciled deferment number) (PDO deferment report-March-2017)

3.4 Symptoms and Troubleshooting to Determine Hydrate Formation at XS Field Facility

It is worth noting that not all the wells affected by gas hydrate will face hydrocarbon production drop. Testing the wells that have suffered hydrate formation is the best way to determine the drop in production. However, because of the limitation of well-testing facilities, it is not feasible to test all the gas lift wells at the time of hydrate formation. Therefore, proper analyses of the station/manifold/wells trends is the best alternative.

Hydrate formation symptoms can be analysed by monitoring the pressure/flow/temperature parameters of affected flowline/wells. Below are some analyses examples from the XS field.

3.4.1 Gas Hydrate at Fuel Supply Line

Figure 3-12 shows operation trends of gas compressor discharge temperature, gas lift header pressure and fuel supply flow using PI ProcessBook. PI ProcessBook is widely

used in various process industries for past and real-time data management and visualisation, delivered by OSIsoft company (Reddi et al., 2010, OSIsoft, 2017, Vanus et al., 2015). The fuel line flow (used for various XS field gas requirements) fluctuates with gas compressor discharge temperature. Interestingly, fuel flow did not always experience gas hydrate with a temperature drop. The dashed blue square represents the period when hydrate did not form even though the temperature dropped to the hydrate formation region, while the black solid square line represents the period when hydrate was formed with a temperature drop.

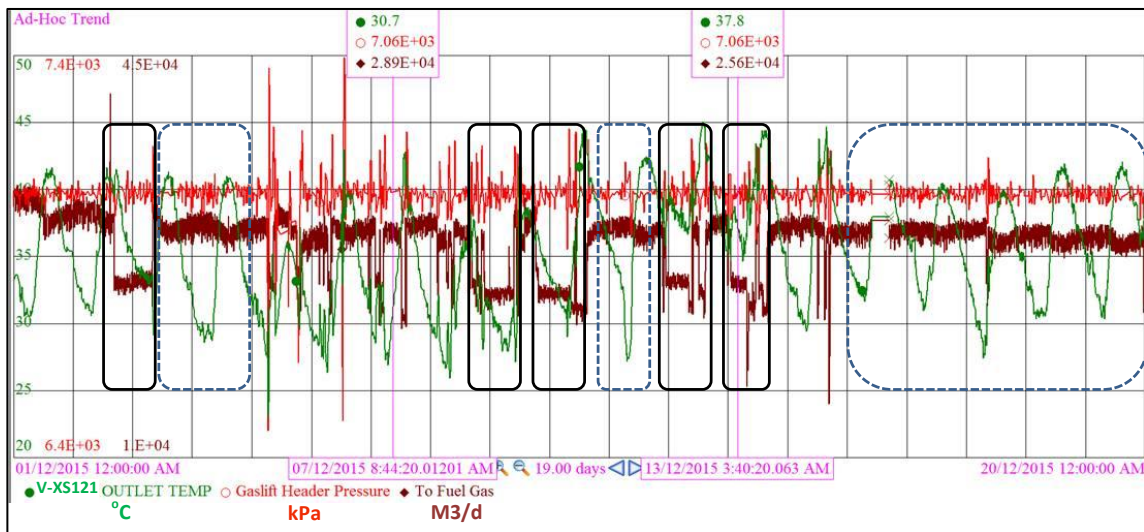


Figure 3-12: Hydrate formation monitoring at fuel supply line using PI ProcessBook (courtesy of PDO)

3.4.2 Flaring As a Result of Gas Hydrate

Figure 3-13 shows flare flows with gas compressor temperature and gas lift header pressure. Although the flow rate is fluctuating significantly, there is a clear trend of flare flow increases accompanying temperature drops. This is because of hydrate formation at the gas lift manifold resulting in an increase in station back pressure, which opens the gas to flare. Consideration should be taken to reduce flaring during the hydrate formation period by closing wells with a high gas/oil ratio (GOR).

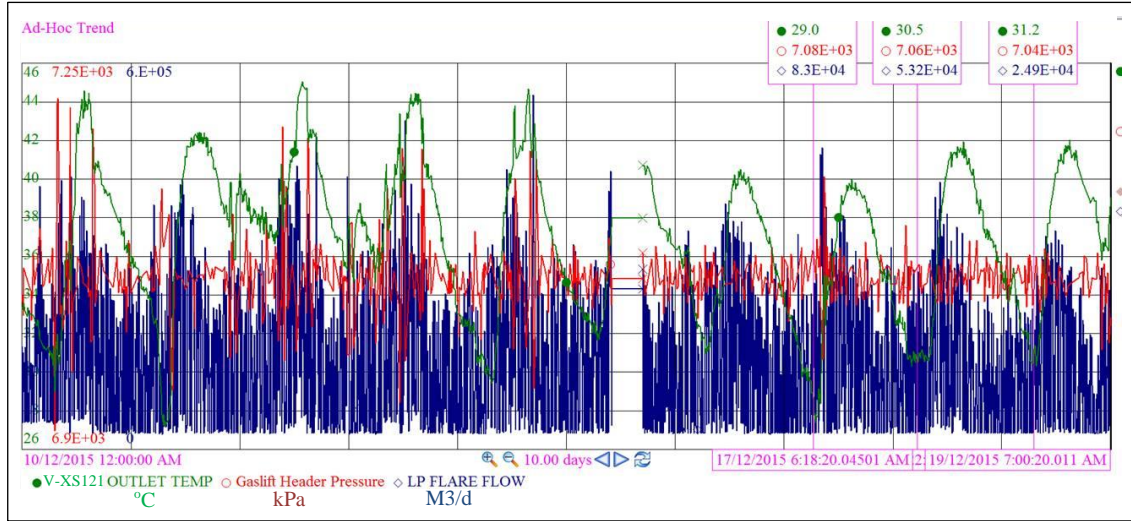


Figure 3-13: Flaring because of gas hydrate formation using PI ProcessBook (courtesy of PDO)

3.4.3 Analysing Gas Lift Well Trends Using Nibras (in-house) Monitoring Portal and PI ProcessBook

Gas lift wells parameters are transmitted live to Nibras monitoring tool (an in-house web-based portal) (Shihab et al., 2011, van den Berg et al., 2016) and PI ProcessBook. Parameters such as tubing head pressure (THP), casing head pressure (CHP), gas lift flow (m³/d), gas lift pressure, gas lift valve opening % position, etc. are used for well performance analyses and troubleshooting. Production drops (or well quits) of GL wells because of gas hydrate formation can be detected by proper monitoring of these parameters. Figure 3-14 shows THP (blue line), GL control valve position (green line) and GL flow (orange line) of well number W102. This well suffered from gas hydrate at 3:58 am. This is easily concluded from the sudden drop of GL flow from 30,000 m³/d to only 50 m³/d with an ambient temperature drop (< 19 °C). Once GL flow drops, the flow transmitter sends a signal to the GL control valve to open and supply more gas. But as there is hydrate blockage in the line, fully opening the control valve does not increase the GL flow. The shortage of gas flow to the well will drop the THP cause production drop or even well quit (Figure 3-15). Figure 3-16, which shows gas lift well parameters of W102 from 09/12/15-13/12/15 using PI ProcessBook software, shows this well frequently suffered from gas hydrate (three times during this period).

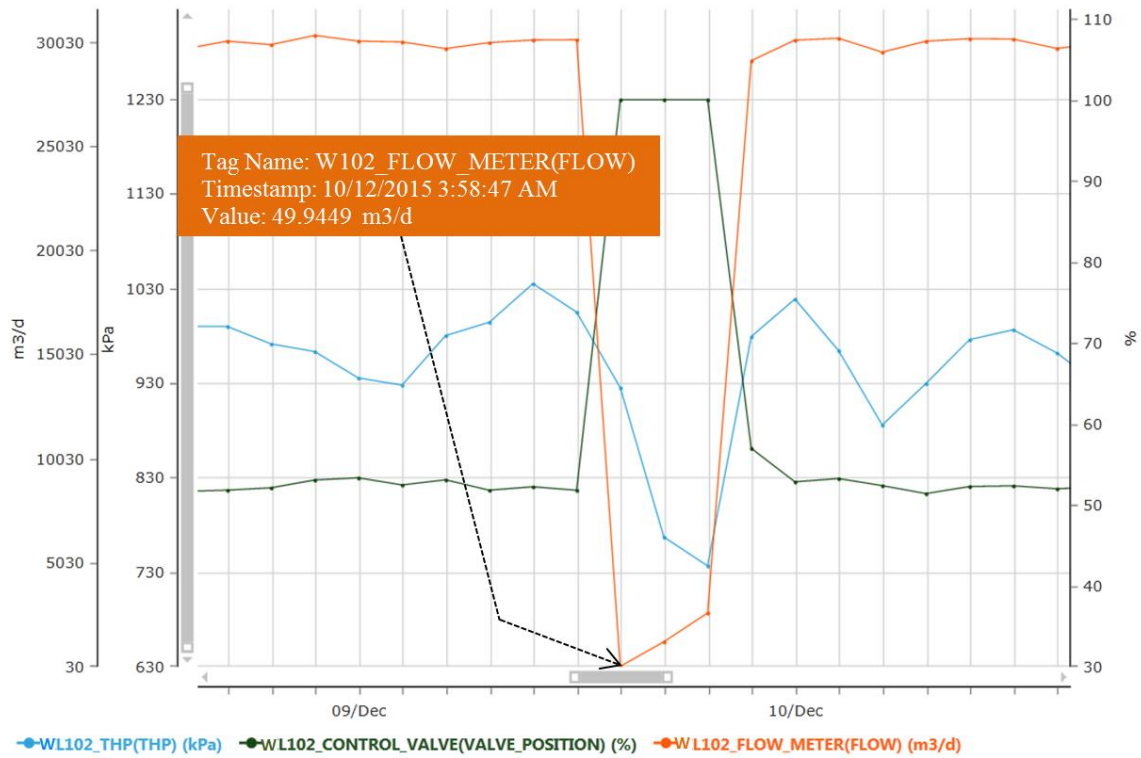


Figure 3-14: Gas Hydrate at W102 using Nibras tool (courtesy of PDO)

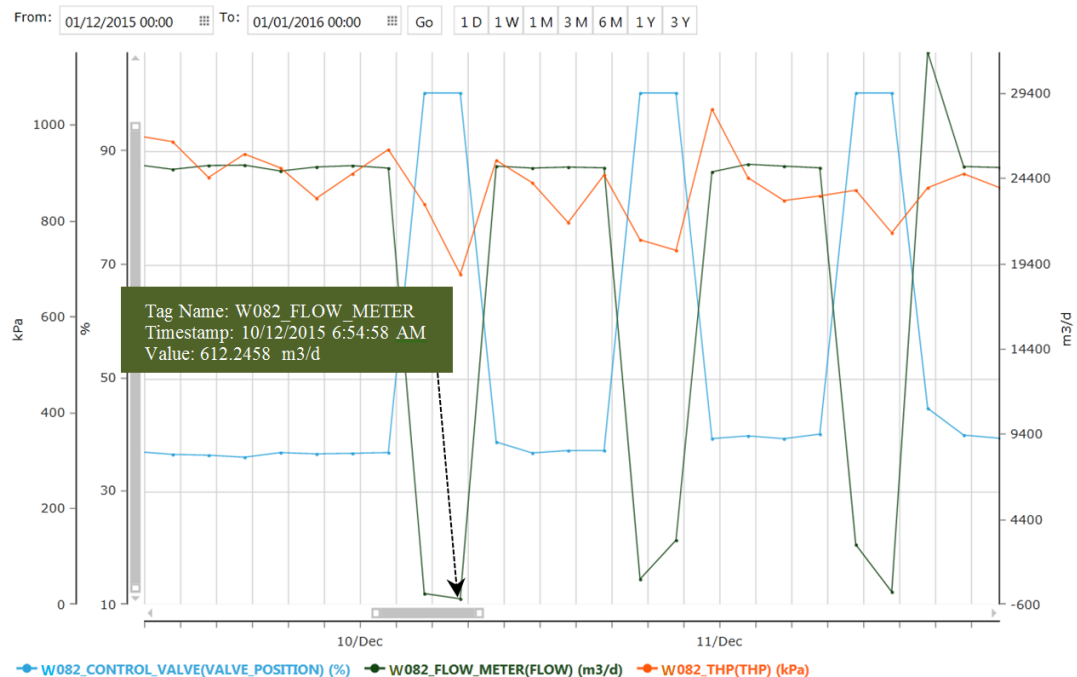


Figure 3-15: Gas Hydrate at W082 using Nibras tool (courtesy of PDO)

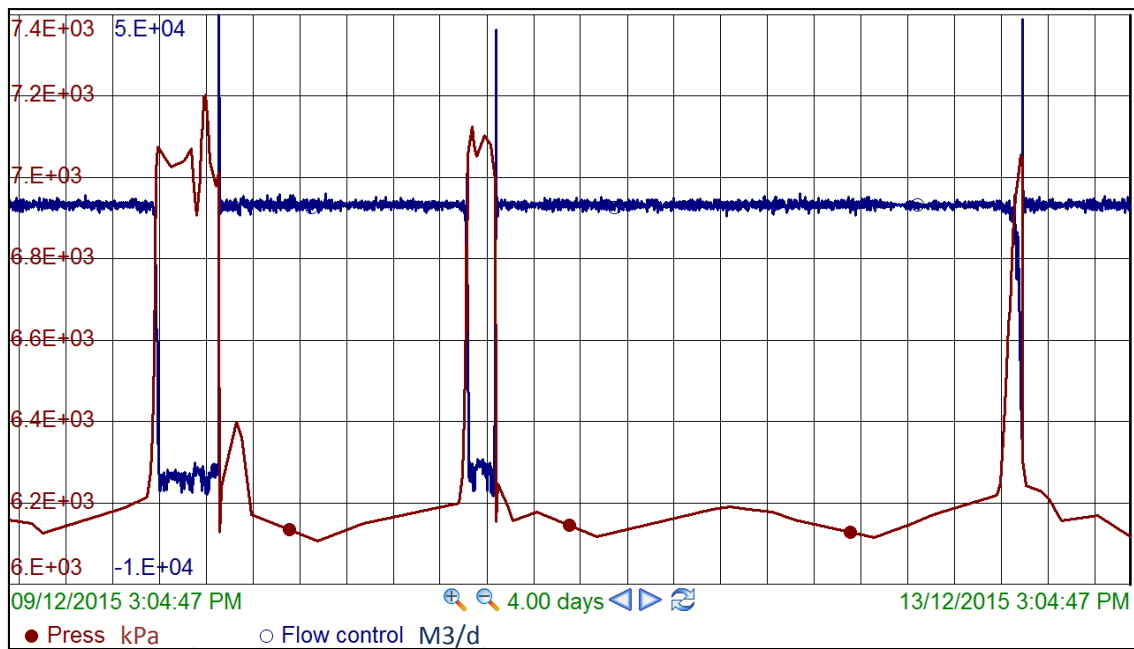


Figure 3-16: Gas Hydrate at W102 from 09/12/15-13/12/15 using PI ProcessBook (courtesy of PDO)

Figure 3-17 shows parameters trend of GL well W101 during winter. The THP drop indicates a production drop because of cutting GL gas supply. Analysing the trends shows that GL gas supply was stopped as a result of the control valve closing, not because of gas hydrate formation, as the control valve position went down to 0% even though the set point was at 15,000 m³/d. Further troubleshooting should be conducted for identifying the proper cause of control valve closing.

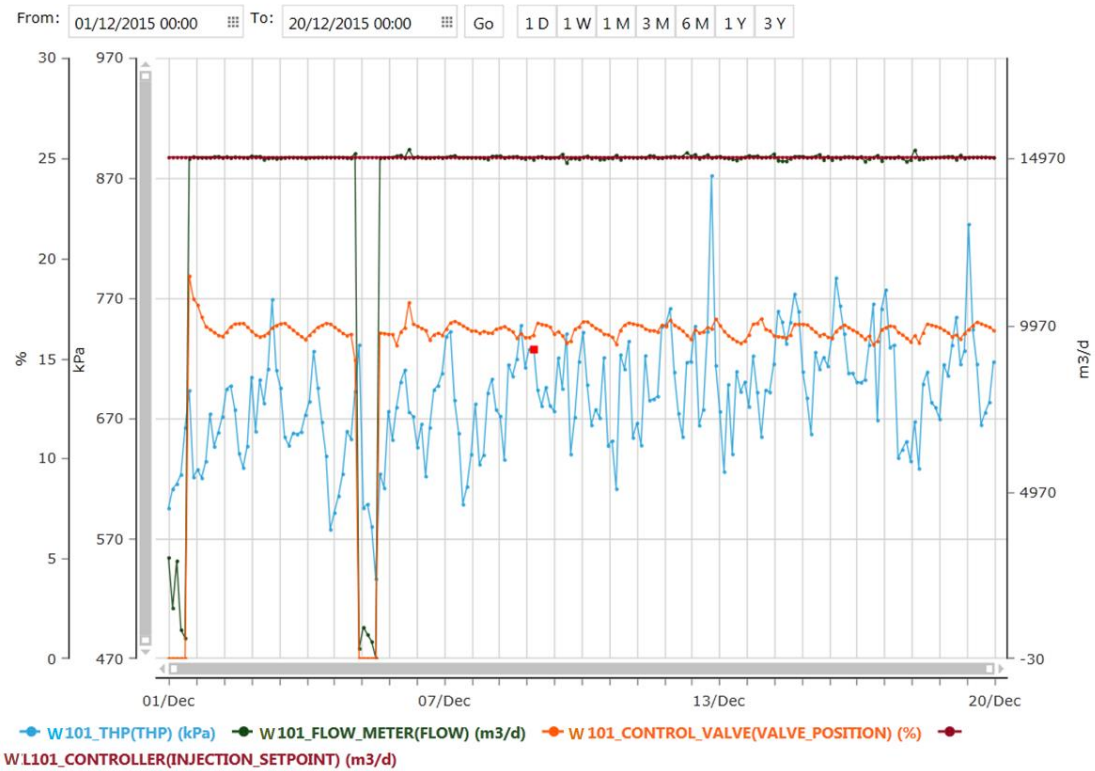


Figure 3-17: W101 well parameters using Nibras tool (courtesy of PDO)

Figure 3-18 shows parameters trend of GL well W071 during winter. The first hydrate formation (red dotted square) caused GL flow to drop from 28,100 m³/d to 3,792 m³/d, which caused THP to drop, which indicates a production drop. The second hydrate formation (black dotted square) did not cause a drop in THP. This is because of faster dissociation of the second gas hydrate formation, and the well was able to self-flow during this short period. This phenomenon of gas hydrate formation without affecting well production is also seen in Figure 3-19 of GL well W084.

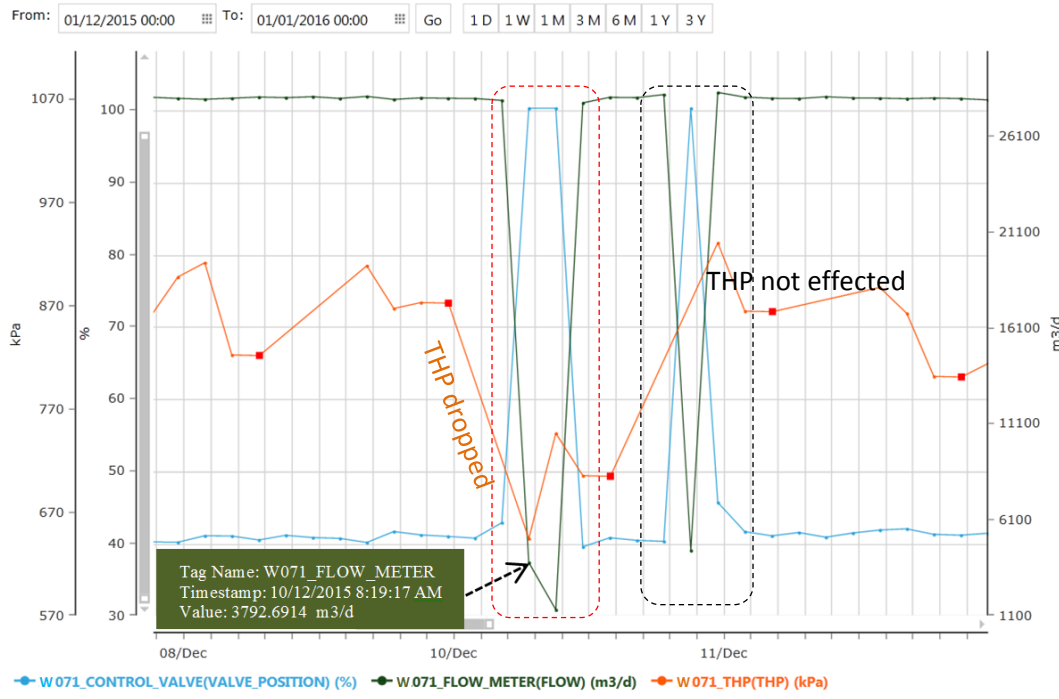


Figure 3-18 W071 using Nibras tool (courtesy of PDO)

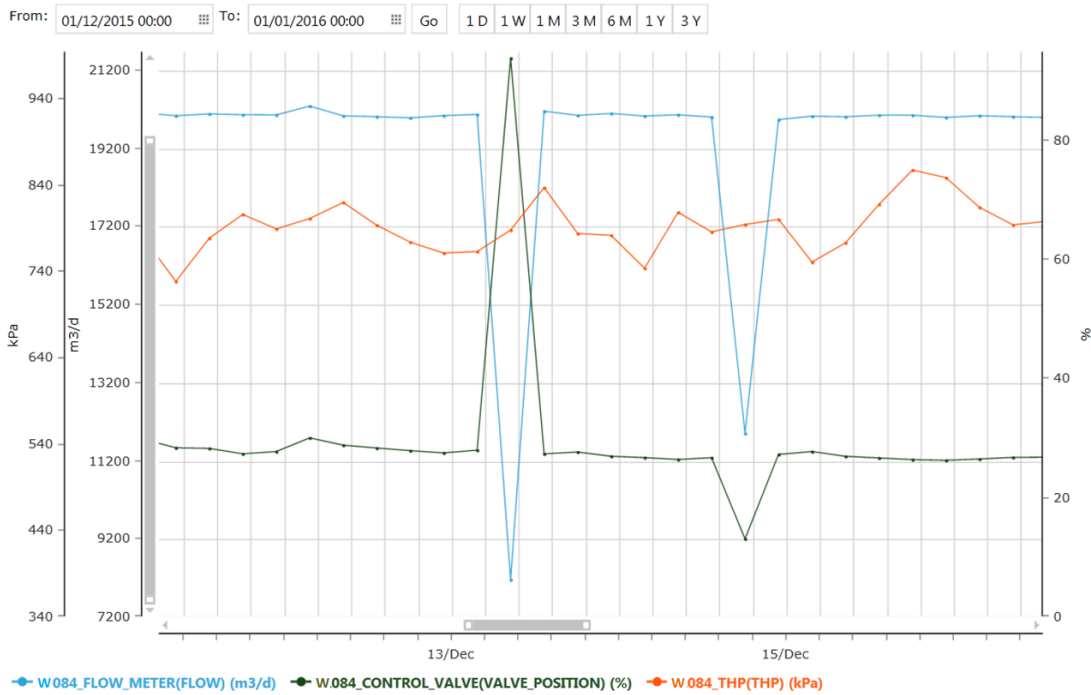


Figure 3-19 W084. This well shows that although there is hydrate, the well is still self-flowing as THP did not drop using Nibras tool (courtesy of PDO).

The performance of some of the GL wells is very sensitive to disturbance of the GL flow supply. Figure 3-20 and Figure 3-21 are examples of sensitive wells as the THP drops fast with the dropping of gas lift flow because of hydrate formation.

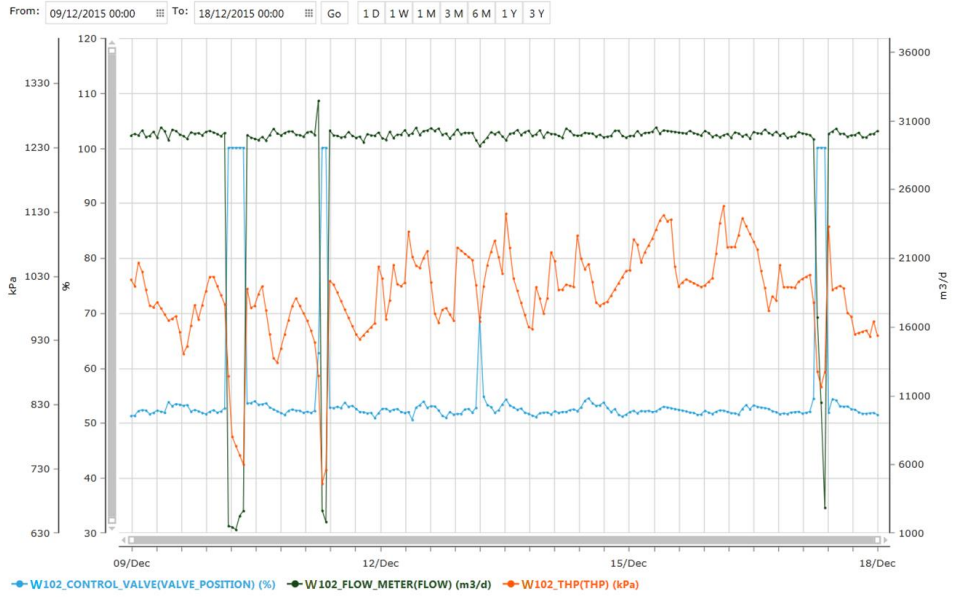


Figure 3-20: W102 is a very sensitive well. THP drops fast as gas lift flow drops because of hydrate formation using Nibras tool (courtesy of PDO).

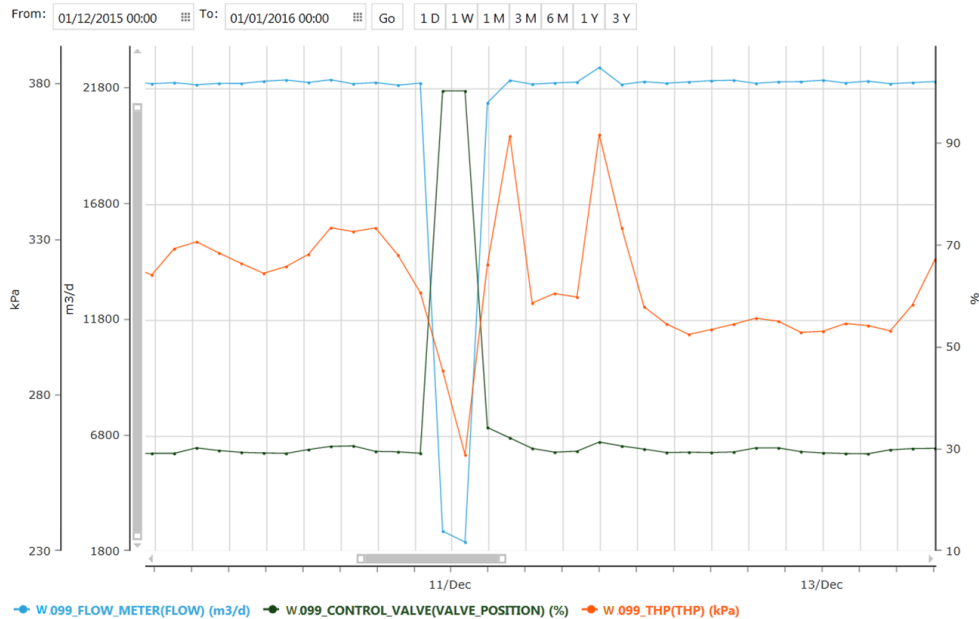


Figure 3-21: W099 is a sensitive well. THP drops fast as gas lift flow drops because of hydrate formation using Nibras tool (courtesy of PDO).

3.5 Thermodynamic Hydrate Inhibition and Dissociating Techniques:

There are four common methods of inhibiting and dissociating gas hydrates:

1. Removing one of the gas hydrate formation components (either the hydrocarbon or water).
2. Heating the system beyond the hydrate formation temperature point.
3. Decreasing the system pressure below hydrate stability point.
4. Injecting an inhibitor.

The above inhibition techniques are called thermodynamic, as they keep the system from approaching the thermodynamic stability region by changing the composition, temperature or pressure (Sloan, 1991, Carroll, 2014).

The above techniques have been recommended and implemented in the XS field to avoid hydrate formation and minimise deferment as discussed in Sections 3.5.1-3.5.6.

3.5.1 Installation of Rockwool Insulators

Good insulation will maintain the system temperature above the hydrate formation point and extend the cooldown time before reaching hydrate formation temperature. Insulation is not effective for a gas system with low thermal mass and where JT cooling will take place (Bai et al., 2005). Hydrate analyses were conducted for the XS field, and it was found that the hydrates frequently formed once the ambient temperatures dropped at the exposed (non-buried) 6-inch line upstream to RGS 1 and the combined 8-inch line upstream of RGS2 and RGS3. UNISIM software (a design modelling simulation software with simulation screenshots given in Figure 3-24 and Figure 3-25) (Lam et al., 2011, Unisim, 2017) was used to study the effect of installing Rockwool insulator (Figure 3-22) in these lines using the following basis and assumptions:

- Ambient temperature of 5 °C (extreme case condition).
- Ambient wind velocity of 2 m/s.
- Gas lift compressor discharge temperatures of 60 °C and 30 °C were simulated.
- For insulation, Rockwool properties are used (thermal conductivity (k) = 0.045 W/m.K)
- Gas lift pipeline length:
 - From station to RGS-1: 6" x 2.1 km

- From station to Multi-Phase Flow Meter (MFM) area (which splits to RGS-2/3): 8" x 2.4 km
- From MFM area to RGS-2: 6" x 1.7 km
- From MFM area to RGS-3: 6" x 1.1 km

Also, seven cases have been simulated and summarised in Table 3-2. Results demonstrate the effectiveness of the Rockwool insulators to minimise the gas lift temperature decrease with a drop of the ambient temperature at the RGSs as follows:

- Case 3: 60 °C compressor discharge temperature and 25 mm thickness Rockwool insulation. Arrival temperature can be maintained above hydrate region (only in RGS-2, it is marginally below hydrate temperature).
- Cases 4 and 5 of 30 °C compressor discharge temperature shows that a 25 mm Rockwool insulation is not enough to prevent hydrate formation (Case 4) while 50 mm Rockwool insulation preserves enough heat to prevent hydrate formation (Case 5).

Finally, a combination of Case 5 and Case 7 have been used in a field trial to maintain the temperature by installing the 50 mm Rockwool insulation as well as injecting methanol (Figure 3-23) to minimise hydrate formation. The Rockwool insulation was implemented in December 2014 (Petroleum Development Oman, 2016).



Figure 3-22: Rockwool Insulator

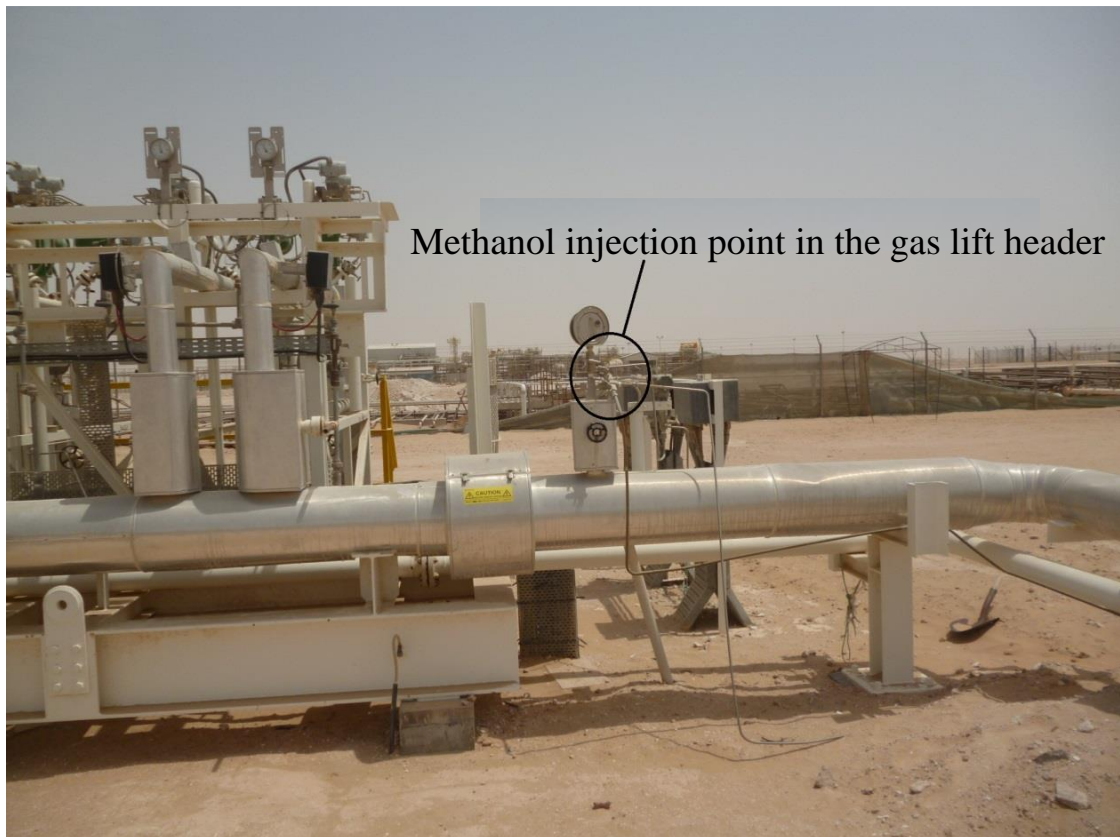


Figure 3-23: Methanol Injection Point (courtesy of PDO)

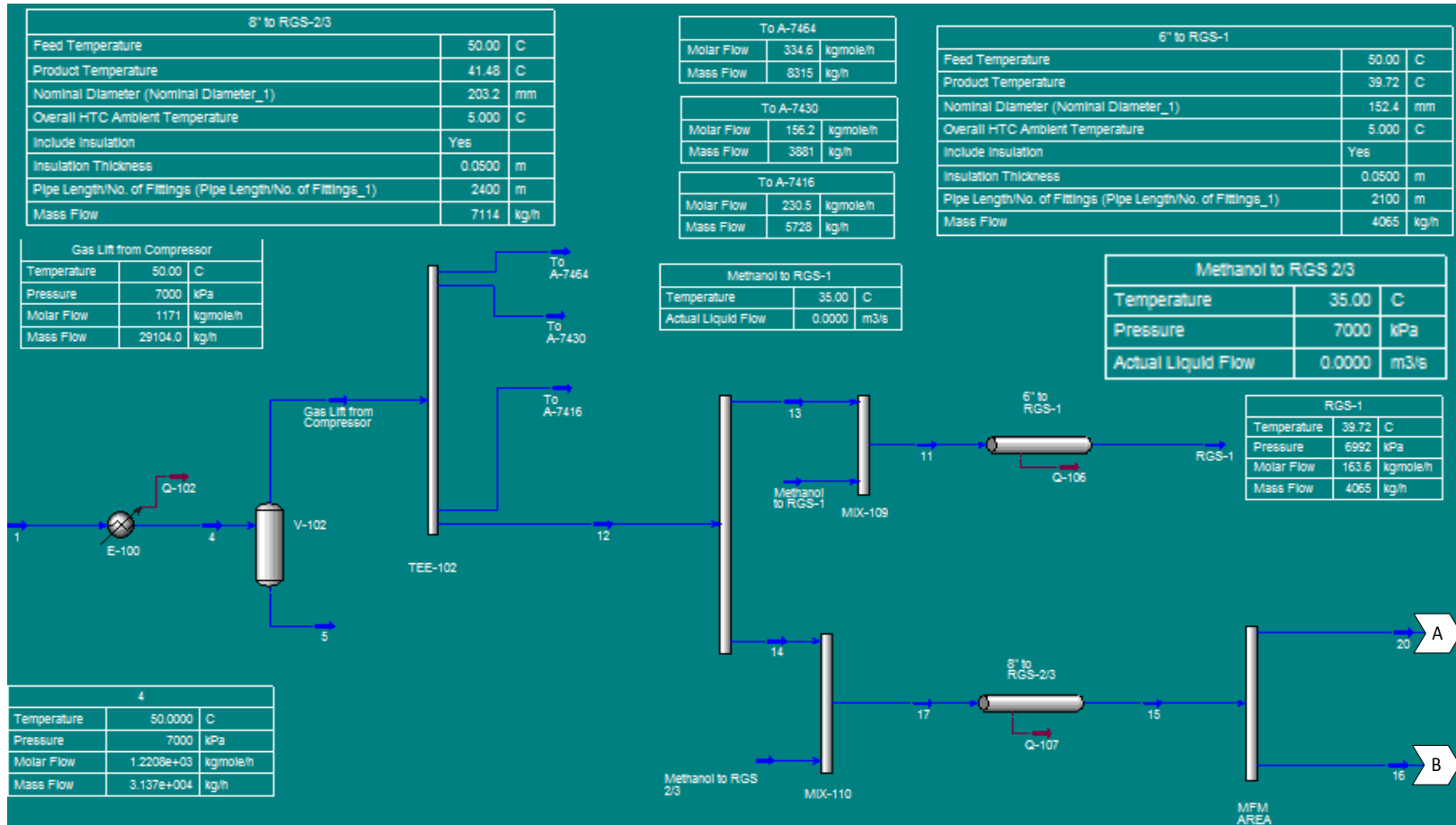


Figure 3-24: UNISIM Simulation Screenshot - Case 3 (process continued in Figure 3-25)

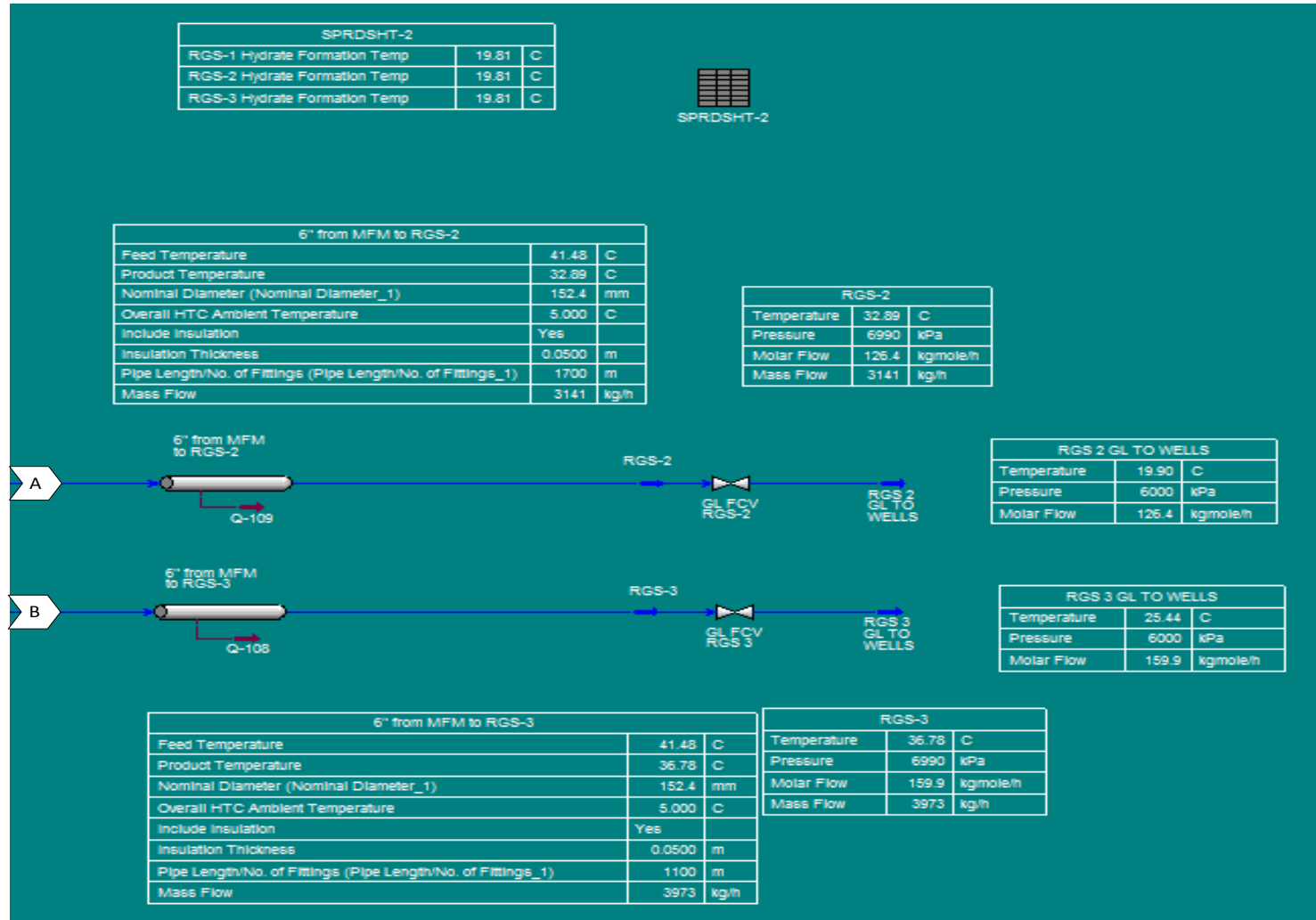


Figure 3-25: UNISIM Simulation Screenshot - Case 3 (process continued from Figure 3-24)

Table 3-2: Study Cases

Cases	Gas lift T from compressor	Ambient Temperature	Insulation (Rockwool)	Methanol injection upstream of RGS-1 flowline (at XS station)	Methanol injection upstream of RGS-2/3 flowline (at XS station)	RGS-1			MFM Area			RGS-2			RGS-3		
	°C	°C	mm	L/d	L/d	°C	Risk	°C	°C	Risk	°C	°C	Risk	°C	°C	Risk	
Case-1	60	5	NO	NO	NO	19.6	8.8	YES	19.3	12	YES	19.3	5.4	YES	19.3	6.6	YES
Case-2	30	5	NO	NO	NO	19.7	6.4	YES	19.4	7.5	YES	19.4	5.1	YES	19.4	5.5	YES
Case-3	60	5	25	NO	NO	19.6	41.2	NO	19.3	36	NO	19.3	18.4	YES	19.3	25.8	NO
Case-4	30	5	25	NO	NO	19.7	20.5	NO	19.4	20.9	NO	19.4	14.7	YES	19.4	17.3	YES
Case-5	30	5	50	NO	NO	19.7	23.7	NO	19.4	23.5	NO	19.4	18.9	YES	19.4	20.9	NO
Case-6	60	5	NO	446	924	4.9	8.8	NO	2.3	12	NO	2.3	5.4	NO	2.3	6.6	NO
Case-7	30	5	NO	222	415	3.3	6.4	NO	1.9	7.5	NO	1.9	5.1	NO	1.9	5.5	NO

Hydrates Formation Prediction Risk Legend:



3.5.2 Installation of Electrical Heat Tracing

Electrical Heat Tracing (EHT) installation is a rapidly developing technology and has been applied in many fields. Advantages of EHT include eliminating flowline depressurization, simplifying restart operations and quickly dissociating hydrate blockage (Bai et al., 2005). EHT was installed in 2015 at the locations illustrated in Figure 3-27 and Figure 3-32 to heat and maintain the gas temperature in the gas lift piping section. Maintaining the temperature of the wet gas inside the gas pipeline might help avoid reaching hydrate formation temperature when the ambient temperature drops. Field observation addressed that once the gas stream is overcooled, hydrate occurs even upstream of the RGS manifold that has been heat traced. The observations indicate that the temperature of the gas lift stream when approaching the RGS has already reached below the hydrate formation temperature because of ambient cooling in the pipelines. Furthermore, a performance test of EHT has been conducted at the site during the winter season of 2016 to ensure its functionality. It was confirmed that the EHT is working effectively. EHT was able to maintain the temperature of the wet gas inside the pipeline up to the upstream of the Flow Control Valve (FCV) of the individual GL lines (Petroleum Development Oman, 2016). Pressure reduction across the FCV causes temperature reduction because of the Joule-Thomson effect (Jamaloei et al., 2015), for which the EHT will not be a valid solution to maintain the FCV's temperature downstream. Figure 2-41 to Figure 3-29 show the manifold A-XS64 before and after EHT implementation.



Figure 3-26: A-XS64 gas lift manifold main header/flow control valves side before EHT implementation (courtesy of PDO)



Figure 3-27: A-XS64 gas lift manifold main header/flow control valves side after EHT implementation (courtesy of PDO)



Figure 3-28: A-XS64 gas lift manifold after flow control valves side before EHT implementation (courtesy of PDO)

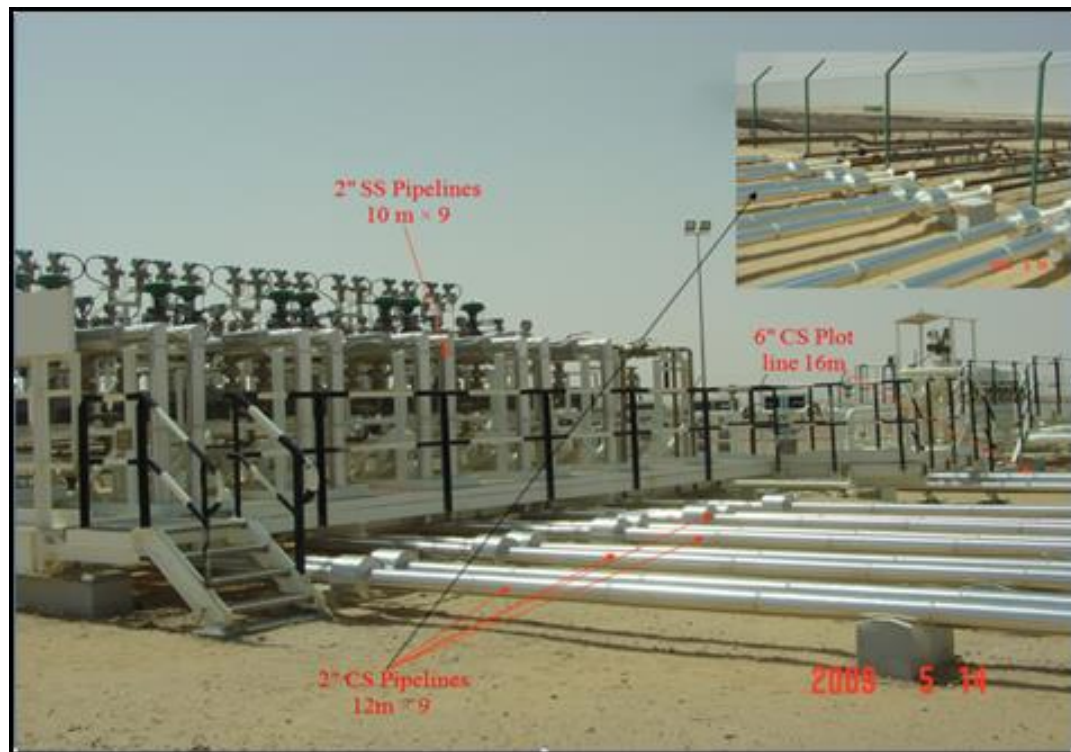


Figure 3-29: A-XS64 gas lift manifold after flow control valves side after EHT implementation (courtesy of PDO)



Figure 3-30: Heat-tracing coil with covered insulation across FCVs (courtesy of PDO)



Figure 3-31 Heat tracing panel (courtesy of PDO)

The locations where the EHT and the Rockwool insulators have been completed are shown in Figure 3-32 below.

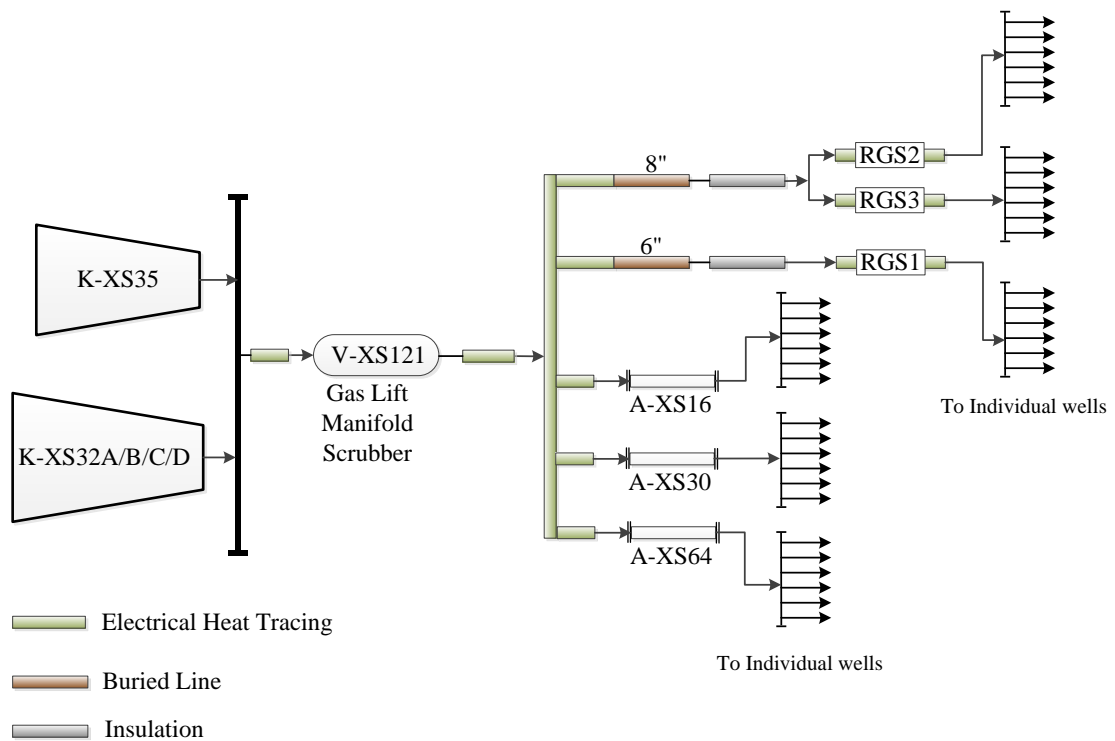


Figure 3-32 Rockwool insulation and EHT locations

3.5.3 Hot Gas Bypass across Third Stage Discharge Coolers of Reciprocating Compressor K-XS05

The temperature of the discharged gas from K-XS05 cannot be maintained because of the low ambient temperatures during winter. The discharge temperature of the third stage cooler E-XS14 reaches as low as 23 °C which is just above the hydrate formation temperature of 19 °C. Therefore, as a result of ambient cooling, the manifold area's temperature might drop below the hydrate formation temperature when the gas reaches it. A new temperature control proposal has been raised, and the design review and the HAZOP have been completed. The proposal will be implemented as described below and as represented by the red dotted line in Figure 3-33:

- Installation of temperature transmitter (XS-TIC-1681) on discharge line after third stage cooler E-XS14.

- Installation of temperature control valve (XS-TCV-1681) with new spool across third stage cooler E-XS14.

This proposal will allow bypassing the cooler when the ambient temperature drops in order to supply hot gas at around 50 °C to the gas lift manifold.

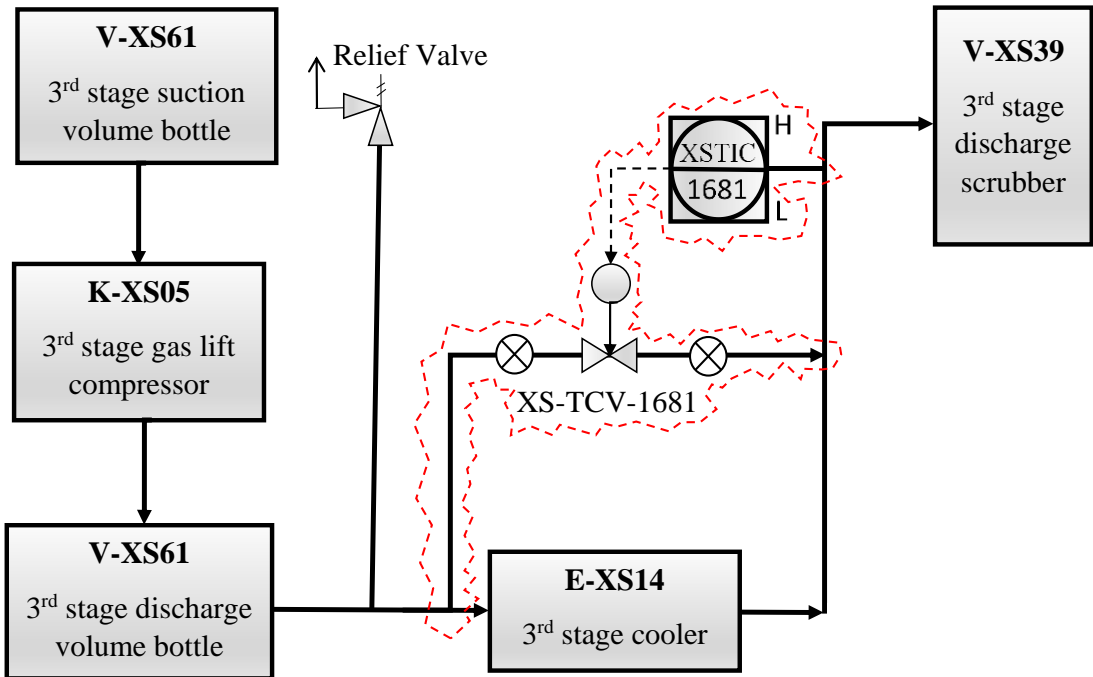


Figure 3-33: Proposed hot gas bypass across 3rd stage cooler E-XS14

3.5.4 After-Coolers Discharge Temperature Adjustment of the New GL Compressor K-XS35

Each of the four stages of the new GL compressor (K-XS35) is installed with an individual air cooler temperature control system (temperature transmitter with flow control valve). During the winter season, it is recommended to raise the temperature controller set point to 50 °C. This will improve the gas lift temperature leaving the station, thus minimising the chance of hydrate formation, as described in section 3.5.3.

3.5.5 Maintaining External Compressors K-XS33A/B/C/D Discharge Gas Temperature

As mentioned above, the temperature of the gas discharged from K-XS35 is always maintained at 50 °C throughout the winter. On the other hand, the temperature of the discharged gas from the external compressors (K-XS33A/B/C/D) cannot be

maintained at this temperature. As can be seen from Figure 3-34, the discharge temperature oscillates significantly between nighttime and daytime (with a minimum of 20 °C and a high of 50 °C). Therefore, the gas leaving the external compressors during the night has a very low temperature which will probably drop below the hydrate formation temperature as a result of ambient cooling at the common discharge header from which the gas will be distributed to the gas lifting manifolds.

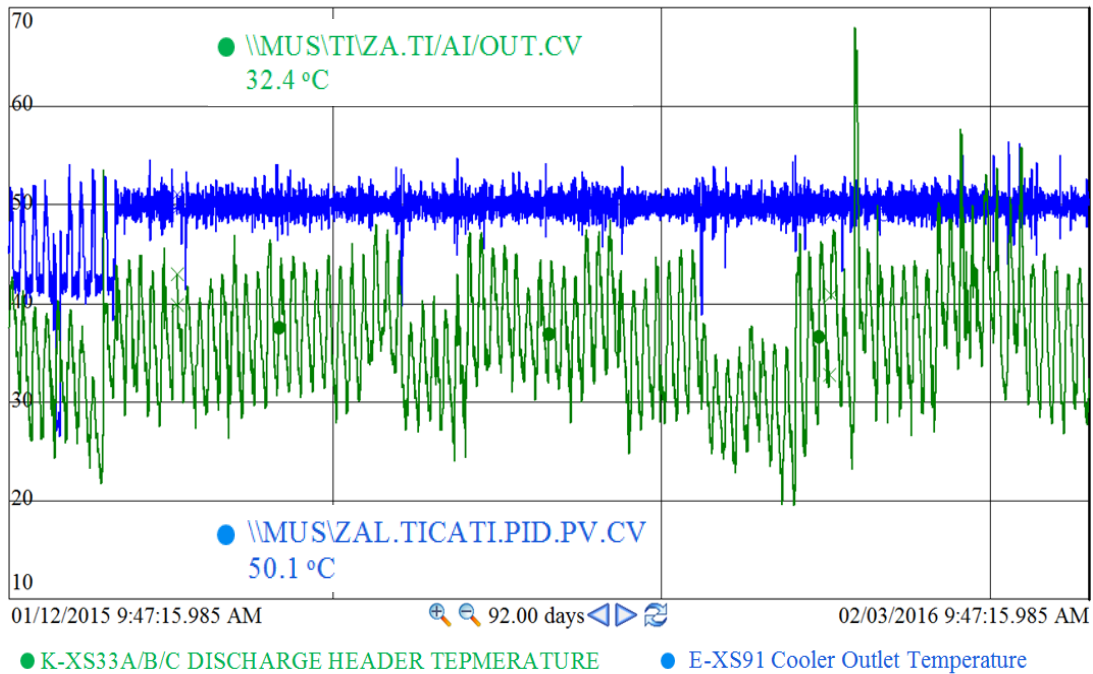


Figure 3-34: Temperature profile during winter using PI ProcessBook (courtesy of PDO)

It is strongly recommended to maintain a stable high discharge temperature of the external compressors (K-XS33A/B/C/D) at above 50 °C during the winter season, especially at night and into the early morning, by manually closing the louvers of the fourth stage fan, or installing a temperature control valve to partially bypass the cooler (Petroleum Development Oman, 2016).

3.5.6 Decreasing the system pressure below hydrate stability point

As gas hydrate formation is favoured at higher pressures and lower temperatures, a trial was performed to decrease the gas lift pressure by reducing the gas flow rate on three selected wells that frequently experience gas hydrate formation: W82, W87 and W102. Figure 3-35 shows W102 behaviour after decreasing the flow rate from

30,000 to 20,000 m³/d, which caused a pressure reduction of only 100 kPag. It was noticed that after this reduction, hydrates still formed (Petroleum Development Oman, 2016). This implies that a reduction of 100 kPag with this low ambient temperature is still not enough to prevent hydrate formation, as illustrated in Figure 3-7 of the hydrate formation phase envelope. Further reduction of pressure is required to prevent hydrate formation. This is not recommended, however, as this will also cause a reduction in well production.

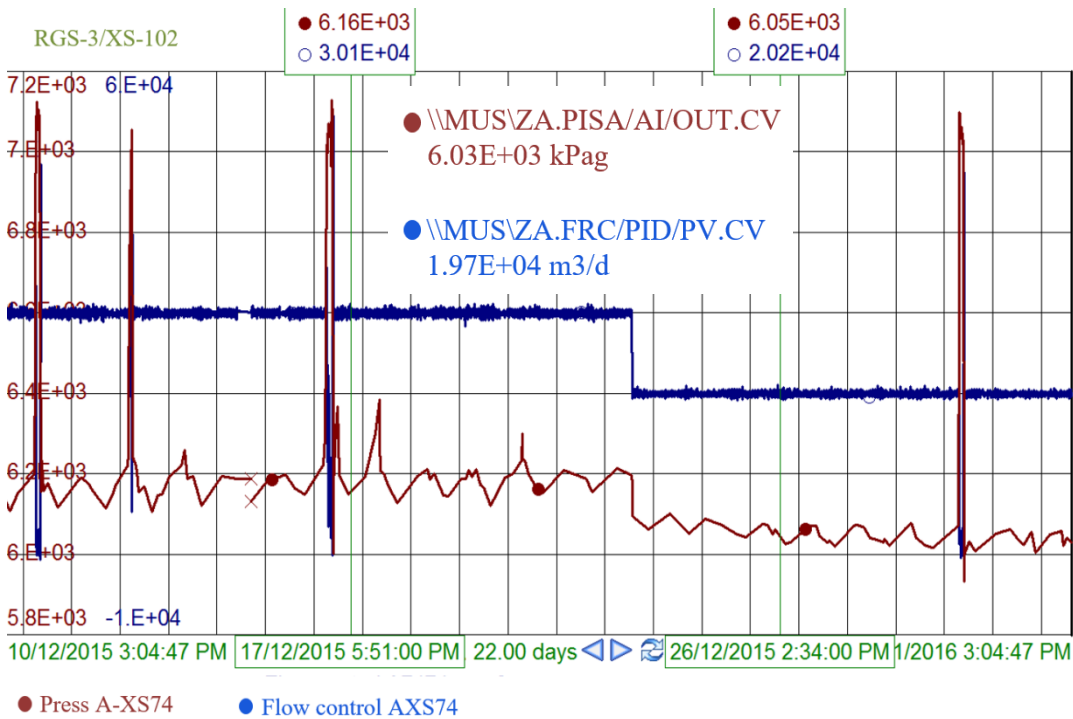


Figure 3-35: Trial of pressure reduction on W102 at RGS3 using PI ProcessBook (courtesy of PDO)

3.6 Conclusion and recommendations

In this chapter, gas hydrate problems and mitigation techniques at the gas lifting system of the XS field were analysed. Hydrate formation phase envelopes for the XS field using Multiflash software P-R EOS (Figure 3-7) and with different methanol injection percentage (Figure 3-8) was developed to enhance understanding of the problem. Figure 3-7 shows that in the presence of water molecules at 70 bar, gas hydrates will form at 19.04 °C. Analysing and troubleshooting of wells/facility parameters to determine gas hydrate formation were performed (Figure 3.4) which showed that gas hydrate formation will not always cause production to drop.

Four different thermodynamic hydrate inhibition and dissociating techniques were analysed. Long-term mitigation options such as gas lift heating or dehydration are not deemed viable because gas hydrate is only formed during the short winter season, and because of the field development plan for converting the GL wells to ESP wells which will reduce or eliminate gas lift requirement. The technique of heating the system above the hydrate equilibrium point was applied using EHT. EHT provided a good improvement to maintain the heat, but it was not good enough to prevent gas hydrate formation, especially with a high-temperature drop as a result of the JT effect at flow control valves. The system pressure was decreased by 100 kPag, but this was not enough to move the hydrate stability point. Further reduction of pressure is not recommended as this will decrease the well production. Methanol injecting (924 litres/day) was applied, commingled with other techniques as shown in Table 3-2 of the study cases. The mitigation techniques, together with the temperature control proposals and recommendations, helped to reduce the total XS field hydrate deferment from 26,159 bbl during winter 2013 to only 7336 bbl during winter 2017.

As hydrate formation still exists in the XS field, these points were recommended to help further reduce its impact:

- Check functionality and carry out proper maintenance for the EHT system before the winter season.
- Inject methanol on a daily basis during the low ambient temperature winter season.
- Carry out gas lift monitoring and optimisation, especially during winter time.
- Maintain a high stable compressor's discharge temperature of K-XS35/05 during the winter season of a range of 45-50 °C.
- Maintain a stable high discharge temperature of the external compressors (K-XS33A/B/C/D) to above 50 °C during the winter season, especially at night and into the early morning by manually closing the louvres of the fourth stage fan.
- Install a temperature control valve to the external compressors to partially bypass the cooler.
- Replace the existing methanol injection skids with a new permanent 8 m³ capacity skid to provide proper and adequate methanol injection doses to the

GL headers in XSPS, RGS1, 2 and 3 as well as to the individual flowlines, as per Table 3-3 below.

Table 3-3: Methanol Injection Connections

Location	Points of Supplement
XSPS	<ul style="list-style-type: none"> Injection to 6" gas lift piping to RGS1 Injection to 8" gas lift piping to RGS2/3 Injection on individual gas lift flowlines from manifold A-XS16/30/64
RGS1	Injection on 8" Header and individual gas lift flowlines from manifold at RGS1
RGS2	Injection on 8" Header and individual gas lift flowlines from manifold at RGS2
RGS3	Injection on 8" Header and individual gas lift flowlines from manifold at RGS3

Abbreviations

PDO	Petroleum Development Oman
GL	Gas Lift
DWD	Deep Water Disposal
GCU	Gas Conditioning Unit
SOGL	South Oman Gas Line
XSPS	XS field Production Station
HC	Hydrocarbon
RGS	Remote Gathering Station
EHT	Electrical Heat Tracing
FCP	Facility Change Proposal
FCV	Flow Control Valve
XSGP	XS field Gas Plant
API/CPI	Oil Water Separators/Corrugated plate interceptor
MFM	Multi-Phase Flow Meter

Chapter 4 Evaluation of Different Hydrate Prediction Software and Impact of Different MEG Products on Gas Hydrate Formation and Inhibition

4.1 Abstract

New hydrate profile correlations for methane gas hydrates were obtained computationally (using three different hydrate prediction software packages, Pipesim, Multiflash and Hysys) and experimentally (with three different MEG products from different suppliers). Methane gas with pure distilled water was the benchmark case used for the software comparison at pressures of 50 to 300 bar. In order to compare the hydrate inhibition performance of the MEG products, aqueous 10 wt% MEG solutions were tested using the isobaric method at a pressure range of 50 to 200 bar.

Furthermore, the kinetics of MEG hydrate inhibition were studied experimentally for methane gas using a stirred cryogenic sapphire cell. Hydrate formation start, hydrate dissociation initiation and hydrate dissociation end points were identified and analysed. The results were correlated with the hydrate formation start points predicted by three well known selected hydrate prediction software packages (which all use the Peng-Robinson equation of state). Moreover, the hydrate inhibition performance of the three MEG products was evaluated to determine the superior MEG product that provides the best hydrate inhibition performance.

Our analysis shows that the hydrate formation points predicted computationally are not identical to the hydrate formation start points measured in this work. Pipesim and Multiflash predicted results matching with the average curve of the experimental hydrate formation start and hydrate dissociation start points, and with a deviation value of 0.06 °C for Pipesim and a deviation value of 0.03 °C for Multiflash. However, Hysys predicted results almost identical with the experimental dissociation start points, and with an average deviation value of 0.54 °C.

The methane gas hydrate profiles for the three different MEG products (X-MEG, Y-MEG and Z-MEG) indicated that X-MEG was the most efficient inhibitor as it shifted the hydrate curve most to the left; X-MEG shifted the hydrate formation curve by an average temperature of 2.07 °C when compared to the benchmark curve

(100% water); while Z-MEG shifted the curve by an average temperature of 1.81 °C and Y-MEG shifted the curve by an average temperature of 1.71 °C.

We conclude that not all software packages predict the same results although they are all based on the same equation of state. Furthermore not all MEG products supplied have the same hydrate inhibition efficiency. Importantly, choosing the best MEG supplier will reduce the OPEX by reducing the amount of MEG used, and it will accommodate more relaxed operating conditions of lower temperatures and higher pressures.

4.2 Introduction

Gas hydrates are ice-like crystalline solids formed by water, as the host, and suitably sized gas molecules, as guests, such as methane, ethane, propane and carbon dioxide (Sloan et al., 2008a). Different gas hydrates form, depending on many factors such as; composition of the gas-water vapour, temperature and pressure. Typically gas hydrates form at high pressure and low temperature, i.e. when a gas stream is cooled below its hydrate formation temperature. However, hydrate formation is undesirable in the context of flow assurance as the formation of hydrate crystals could lead to a plugging of the flow lines and processing equipment, which reduce the line capacities or cause physical damage (Arnold et al., 1999, Sum et al., 2009). Thus identifying the precise hydrate formation conditions for each gas system is essential for designing the gas plants and setting the safe operating condition.

Thermodynamic inhibition is the favourable method used for preventing and delaying hydrate formation, and this hydrate formation can be predicted with software packages. Historically, Hammerschmidt developed the first calculation method used in the industry for predicting the inhibiting effect of thermodynamic inhibitors based on experimental results (Hammerschmidt, 1934). Subsequently, Robinson (1986) obtained experimental data on hydrate formation in the presence of methanol and glycol as thermodynamic inhibitors for various hydrocarbon gas systems. Robinson (1986) presented a computer program based on his equation of state (EOS) for the calculation of the depression of hydrate formation temperatures. It is to be noted that equations of state are used for all hydrate prediction models. This prediction of gas hydrate formation plays a significant role in terms of operating conditions and calculating the appropriate amount of the required thermodynamic

inhibitor. However, the presence of the inhibitor makes the prediction more challenging. Note that Monoethylene glycol and methanol are the most common inhibitors used in industry; these inhibitors work by producing strong hydrogen-bonds between their hydroxyl groups and water molecules that reduce the ability of the gas molecules to enter the water cage and form hydrate (Sloan et al., 2008a).

In this context, different methods have been proposed in terms of the hydrate formation prediction in the presence of inhibitors. These methods are divided into empirical methods (Carroll, 2014, Nielsen et al., 1983) or statistical methods (Van der Waals et al., 2007).

In this work, a new hydrate profile correlation for binary CH₄–H₂O systems was established for a pressure range of 50 to 300 bar using a stirred cryogenic sapphire cell and the isobaric test method. The results acquired experimentally were compared with the computational results and literature data. The analysis was conducted for experimental hydrate formation points, and correlated with the results predicted by the three software packages (which are all based on the Peng–Robinson EOS; (Peng et al., 1976, Davarnejada et al., 2014)). This comparison was conducted to help pre-estimate the actual hydrate formation points for the laboratory results for various operation conditions.

Finally, in this work, the hydrate inhibition performance of three MEG products was studied at a constant weight concentration of 10 wt% MEG and a pressure range of 50 to 200 bar. The results of these experiments will help to evaluate and pinpoint the best MEG supplied that provides superior hydrate inhibition performance.

4.3 Description of Equipment and Processes

4.3.1 Materials, Equipment and Testing Process

Three MEG products (from three different well-known MEG suppliers) were evaluated to identify which product provides the best hydrate inhibition performance. The physical properties of the products tested are listed in Table 4-1 MEG properties. Table 4-1. Due to the commercial reasons, the names of the three MEG suppliers are not mentioned, but instead, abbreviations (X-MEG, Y-MEG and Z-MEG) are used.

Table 4-1 MEG properties.

Supplier abbreviation	Molecular Formula	Melting Point °C	Boiling Point °C	Flash Point °C	Specific Gravity at 20 °C/20 °C	Vapour Density (Air =1)	Molecular Weight g/mol	H ₂ O content wt%
X-MEG	C ₂ H ₆ O ₂	-13	197	115	1.1153	2.14	62.08	0.10
Y-MEG	C ₂ HM ₆ O ₂	-13	197.6	111	1.1155	2.14	62.07	0.00
Z-MEG	C ₂ HM ₆ O ₂	-13	197	115	1.113	2.14	62.07	0.01

Methane gas (purity of 99.995 Mol%) and solution of 10 wt% MEG with 90 wt% distilled water mixtures were prepared using a high accuracy balance (accuracy of 1 mg for 1020 g; (Shimadzu, 2014)).

4.3.2 Experimental procedure

Experiments were conducted in a PVT cryogenic sapphire cell system, as shown in Figure 4-1. The sapphire cell has a volume capacity of 60 ccs. Prior to starting the experiments, pressure tests were conducted for the whole system by pressurising the system with N₂ gas up to 100 bar, and the pressure was held for half an hour to confirm no gas leaks were present.

Subsequently, gas samples were prepared by filling methane gas from a G size gas cylinder to four small gas bottles each having a capacity of 500 ml. The gas was then fed from the gas bottles to the piston pump using a pneumatic booster pump. The piston pump is designed to compress the gas up to 500 bar with a pressure accuracy of 0.1% (Shimadzu, 2014). Then 7 ml of the aqueous solution were filled into the cell. Note that the sapphire cell is fitted with a magnetic stirrer that is set at a constant speed of 530 RPM (300 mAmps) and with 2 Resistance Temperature Detectors (RTD PT100 sensors with 3 core Teflon tails, Model TC02 SD145; with temperature accuracy of ± 0.03 °C @ 0 °C; (Hinco, 2014)), one fitted at the top side of the cell to detect the gas temperature and the second at the bottom side to detect the liquid temperature. The sapphire cell temperature is controlled by the PC using Falcon-E4378-Curtin-Cryogenic Cell software (temperature range of +60 to -160 °C; (Shimadzu, 2014)).

The cell temperature was first set to a point well outside the expected hydrate formation zone (by around +5 °C) and then gradually lowered stepwise at a rate of 0.5 °C / 20 minutes to achieve homogeneous temperature conditions at each temperature step change. This resulted in a slow, homogeneous hydrate formation

process, which guarantees accurate detection (Haghghi et al., 2009). The gas hydrate formation start point was measured based on visual observations, Figure 4-3(a); and hydrate was left to form fully until complete blockage was achieved Figure 4-3 (b). Once complete hydrate formation was achieved, the cell temperature was raised again gradually at a rate of $0.5\text{ }^{\circ}\text{C} / 20$ minutes to achieve a homogeneous temperature at each temperature step change. The gas hydrate dissociation start point was again measured based on visual observations, and the hydrate was left to melt until full dissociation before the next experiment. All procedures were previously described in detail by AlHarooni et al. (2015).

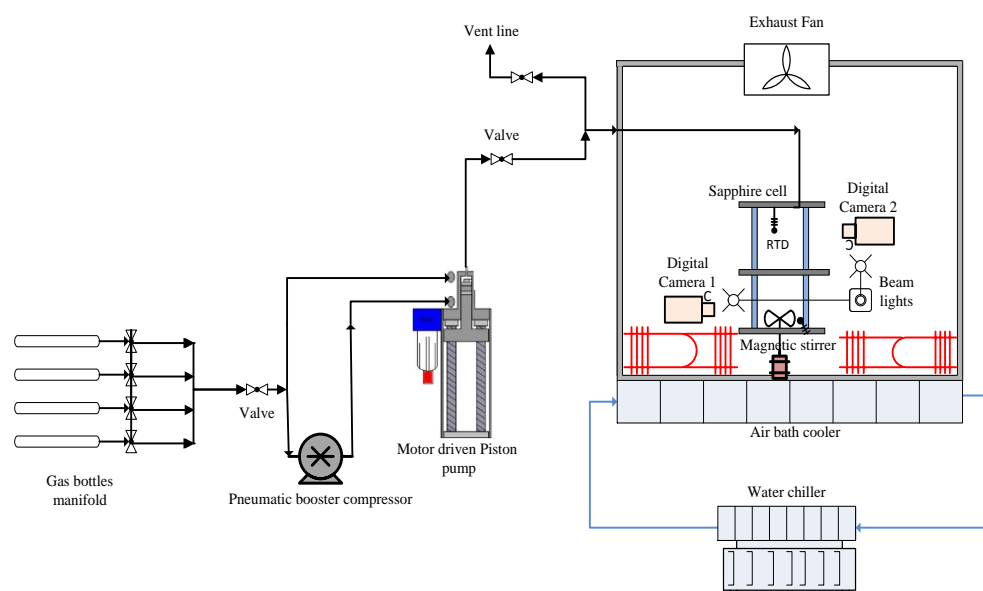
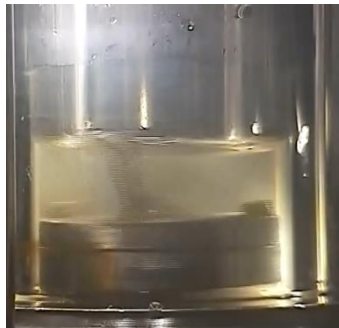


Figure 4-1 PVT sapphire cell layout.



Figure 4-2 PVT Cryogenic sapphire cell unit.

The first hydrate crystal was detected at the liquid/gas interface (Figure 4-3 (a)), consistent with Huo et al. (2001) and Taylor et al. (2007), and confirmed by Moon et al. (2003b) molecular dynamic simulation studies. Hydrates form at the vapor-liquid interface as this is the location with the highest concentrations of both, the host and guest molecules (Kashchiev et al., 2002).



(a) Start formation



(b) Full blockage

Figure 4-3 Hydrate formation stages.

4.4 Results and Discussion

Initially, the binary CH₄-H₂O hydrate profile was measured for a pressure range of 50 to 300 bar. The results were analysed and compared with literature data and the results predicted with the software packages. The accuracy and repeatability of data generated by this study was assessed, by repeating the experiment three times and conducting a statistical analysis that was compared to literature and software computed data. The experimental results for this work were found to be in excellent agreement with literature and software data (less than 1.3 °C difference). The Average Absolute Percentage Deviations (AAD%) were calculated using Eq 4-1:

$$AAD\% = \frac{1}{n} \sum_{i=1}^n \frac{|T_{exp} - T_{cal}|}{T_{exp}} \times 100 \quad \text{Eq 4-1}$$

Where T_{exp} is the experimental hydrate formation temperature and T_{cal} is the predicted hydrate formation temperature and n is the number of data points.

The AAD% was 8.84%; note that, the smaller the AAD%, the better the agreement. Based on the analysis of the repeatability of the generated experimental data, we estimate that the maximum experimental error is 1.92%, with a standard deviation (S) of S = 0.54 AlHarooni et al. (2015).

Hydrate formation/dissociation equilibrium curves are plotted in Figure 4-4. These experimental results were fitted with exponential curves (R^2 value > 0.97). From the graph it is clear that Sloan et al. (2008a) data present an almost complete match to our hydrate formation start points, while the rest of the literature data (Jager et al., 2001, Maekawa, 2001, Carroll, 2014, Lu et al., 2008) matches with our dissociation start points.

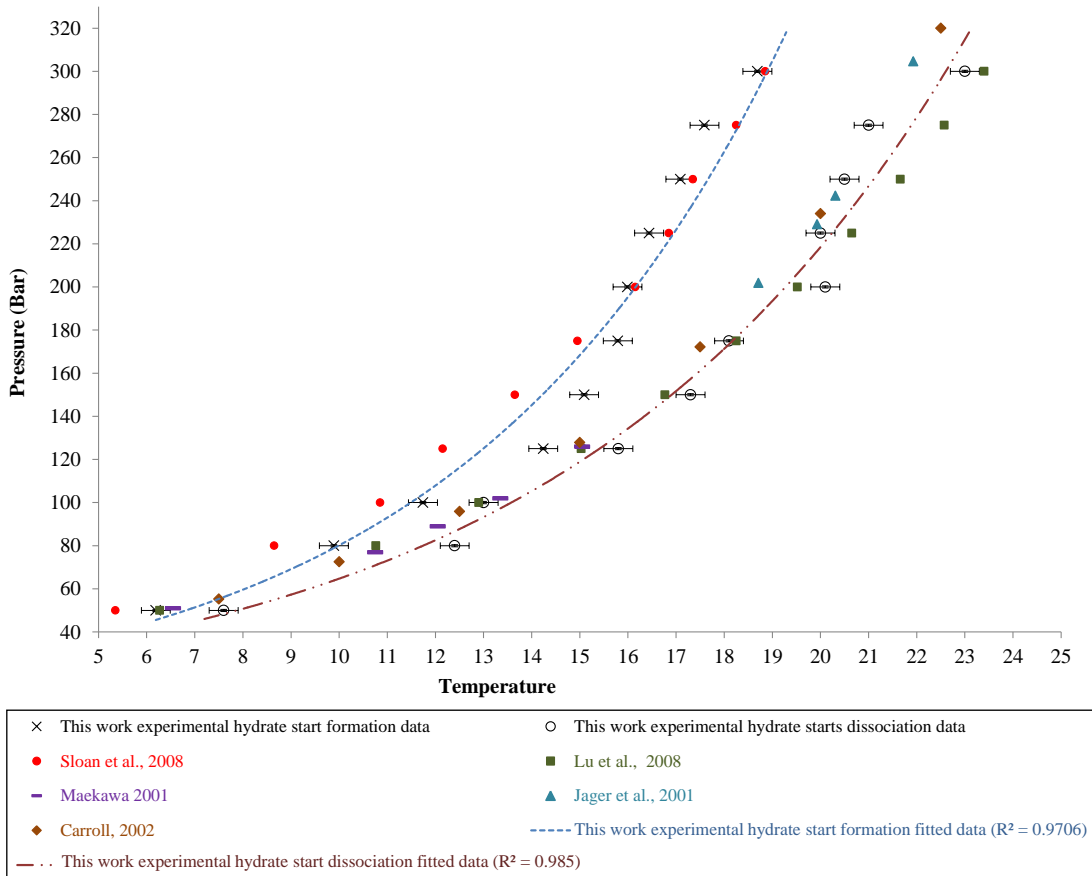


Figure 4-4 Hydrate formation / dissociation start points and literature data for binary CH₄-H₂O systems.

4.4.1 Comparison of computational results

Figure 4-5 compares the experimental hydrate formation profiles of formation start, dissociation initiation and dissociation end points with the results predicted by the three software packages. These results pinpoint where the software predictions are aligning with the experimental hydrate profile. The results show that the hydrate formation points predicted by Pipesim and Multiflash were almost identical with the experimental average points of start formation and start dissociation, which could be correlated with Eq 4-2:

$$P_{(A,B)} = 18.466 \times e^{0.1346 \times T_{(A,B)}} \quad \text{Eq 4-2}$$

Where $P_{(A,B)}$ is the pressure when using Pipesim and Multiflash and $T_{(A,B)}$ is the temperature when using Pipesim and Multiflash.

Pipesim had an average temperature deviation of 0.06 °C, and Multiflash had an average temperature deviation of 0.03 °C when compared to this correlation (Eq 4-2). Hysys predicted results almost matching with the fitted curve of the dissociation start points; which can be correlated via Eq 4-3:

$$P_{(C)} = 19.17 \times e^{0.1217 \times T_{(C)}} \quad \text{Eq 4-3}$$

Where $P_{(C)}$ is the pressure when using Hysys and $T_{(C)}$ is the temperature when using Hysys.

The Hysys predicted results had an average temperature deviation of 0.52 °C when compared to Eq 4-3. For both correlations (Eq 4-2 and Eq 4-3) the correlation coefficient was close to one ($R^2 > 0.98$). The two correlations are valid for the pressure range of 50 to 300 bar, at the respective temperatures of 6.8 to 22.6 °C.

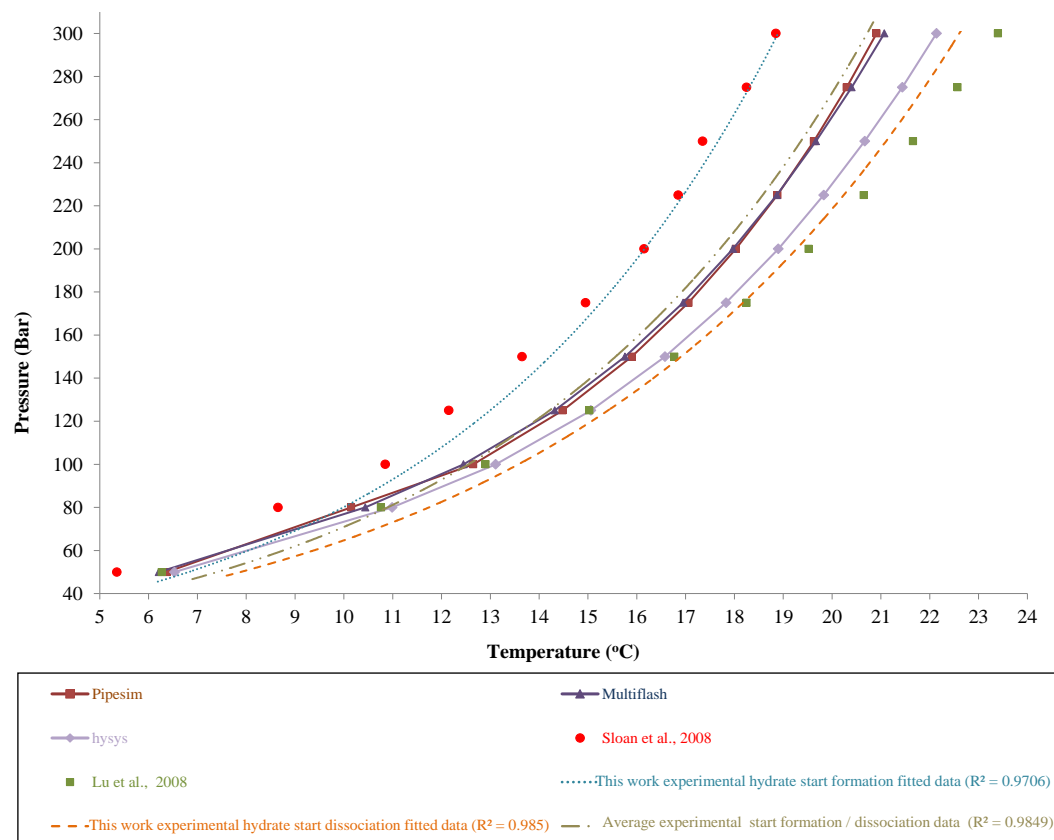


Figure 4-5 Hydrate Formation /Start Dissociation curves for binary CH₄-H₂O systems.

4.4.2 Influence of MEG product (MEG supplier) on methane hydrate formation

The rationale for conducting this experiment was to evaluate whether different MEG products (supplied by different manufacturers, but for the same MEG concentration) perform differently with respect to hydrate inhibition. Three major MEG products selected and abbreviated by X-MEG, Y-MEG and Z-MEG.

Hydrate formation curves for methane gas with aqueous MEG solutions (10 wt% MEG - 90 wt% distilled water) were then measured at pressures ranging from 50 to 200 bar at 25 bar intervals, Figure 4-6. A comparison of the results with data acquired for a methane gas-(100 %) water system revealed that X-MEG was the most efficient inhibitor, as it shifted the hydrate formation temperature most to the left, by an average temperature of 2.07 °C. Z-MEG was the second most efficient inhibitor, it shifted the curve to the left by an average temperature of 1.81 °C; while Y-MEG was least efficient, it shifted the curve by an average temperature of 1.71 °C to the left. Although the differences in temperature shifts among the three selected MEG products is small, this work does permit the selection of the best MEG product (i.e. X-MEG), thus enabling optimising the MEG injection doses.

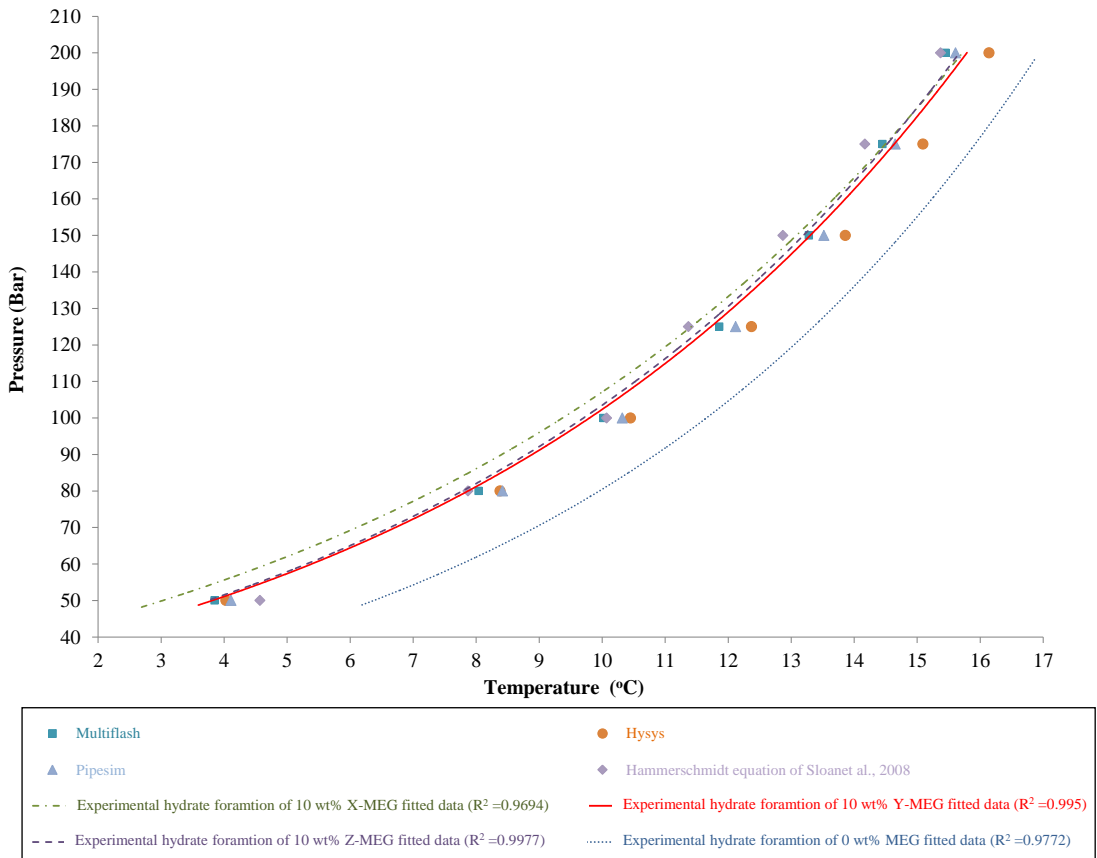


Figure 4-6 Hydrate formation curves for CH_4 – (10 wt% MEG solutions) of the three supplied MEG (X-MEG, Y-MEG, Z-MEG) and CH_4 -water.

4.5 Conclusions

New experimental data is reported for methane hydrate formation points measured under isobaric conditions in the presence of aqueous MEG solutions (0% and 10 wt% of MEG concentrations) over a wide pressure range (50-300 bar). Good agreement was observed between the experimental and literature data, Figure 4-4. The hydrate formation points were also predicted using three different software packages. The precise predictive power of the three hydrate prediction software packages (which use the Peng-Robinson EOS; (Peng et al., 1976, Davarnejada et al., 2014)) was tested by comparing their predictions with the experimental laboratory results. This helps pre-estimate the expected hydrate formation points for various operating conditions. All software packages (Pipesim, Multiflash and Hysys) showed some deviations from the hydrate formation experimental results. Pipesim and Multiflash predicted results which essentially matched with the average temperature of the hydrate formation start and hydrate dissociation start points. However, Hysys predicted results approximately identical to the hydrate dissociation start points.

We conclude that all software packages can be used as a tool to rapidly predict hydrate formation. However, no software accurately predicted the exact profiles and consideration needs to be taken for each software with their developed correlation (Eq 4-2 and Eq 4-3).

Furthermore, three MEG products (from three different major MEG suppliers) were compared with respect to their hydrate inhibition performance. X-MEG was the most efficient with a hydrate formation temperature reduction of 2.07 °C, the second best product was Z-MEG, which reduced the hydrate formation temperature by 1.81 °C, followed by Y-MEG, which reduced the hydrate formation temperature by 1.71 °C. Note that the greater the temperature reduction, the better the hydrate inhibition performance. Identifying the superior MEG product will help optimise the amount of injection doses used to tackle hydrate formation. We conclude that X-MEG is the best MEG tested.

Chapter 5 Inhibition Effects of Thermally Degraded MEG on Hydrate Formation for Gas Systems

5.1 Abstract

Mono-ethylene glycol (MEG) is used as a hydrate inhibitor in gas processing plants and transportation pipelines. Due to its high cost, large consumption rate, and its environmental impact, regenerating MEG is an economical and environmental solution. When heated to high temperatures at the reboiler, thermal degradation of MEG may occur during the regenerating process. In this work, the hydrate inhibition performance of MEG after it was thermally exposed to high temperatures has been evaluated. The experiments were conducted using pure methane gas in a stirred cryogenic sapphire cell under isobaric condition (constant pressure), for pressure ranges of 50–300 bar and using solutions of 25 wt% MEG with 75 wt% de-ionised Water. Experiments conducted using thermally exposed MEG to temperatures of 165 °C, 180 °C and 200 °C for durations of 4 and 48 h. The degradation products from these samples were then analysed by third party laboratories using two techniques: ion chromatography (IC) and high-performance liquid chromatography - mass spectroscopy (HPLC–MS). Results using both techniques showed that MEG was degraded when exposed to the above referenced temperatures and resulted in a formation of organic acids, such as glycolic, acetic, and formic acids. Another experimental study was conducted to study the kinetics of MEG hydrate inhibition for the binary CH₄–H₂O system. These experiments showed that difference between the hydrate start formation curve and the hydrate start dissociation curve (the metastable region) is narrow at lower pressures and that it widens as pressures increase. Similar trends were observed when the hydrate start formation and the hydrate end formation curves were compared. Evaluation of hydrate inhibition performance of the thermally degraded MEG samples established that all the samples resulted in increasing of hydrate formation temperatures. The findings of this study conclude that thermally exposed MEG causes a drop in hydrate inhibition performance due to thermal degradation effects.

5.2 Introduction

Crystalline solids of natural gas hydrates are made from water cavities (hosts) composed of hydrogen-bonded molecules and suitably sized gas molecules (guests)

combined under certain formation conditions. These formation conditions usually consist of low temperatures and high pressures. Common gas molecules are methane, ethane, propane, and carbon dioxide (Sloan et al., 2008a, Delli et al., 2014). Hydrates normally form when a gas stream cools below its hydrate formation temperature. At high pressures, a hydrate may form at temperatures well above 0 °C. Environmental conditions may contribute to undesirable hydrate formation depending on whether the facilities are sub-sea, platform based, or shore based. Hydrate will disturb flow assurance conditions due to the formation of crystals where the formed hydrate may plug the flow lines, chokes, valves, and instrument lines, causing a reduction in the line capacities and physical damage. These issues draw up the attention to gain a better understanding of the behaviour of gas hydrates (Arnold et al., 1999).

The risks of gas hydrate formation could be reduced by many techniques. These techniques include eliminating one of the hydrate formation elements. To eliminate hydrate formation element of the effect of low-temperatures for example, the production lines must be covered by thermal insulation or apply an effective heating system. The second hydrate formation element is the wet gas caused by water in the system. Wet gas can be removed by a dehydration process, such as tri-ethylene glycol (TEG) or mono-ethylene glycol (MEG) dehydration systems. The third hydrate formation element is the high operating pressure; lowering the pressure can prevent hydrate formation (Su et al., 2012). This option is used to remove hydrate blockage in the production system. Due to difficulties in eliminating the hydrate formation elements mentioned above, industry practises concentrate on injecting hydrate inhibitors upstream of the gas process. Calculating the hydrate injection amount and type is based on various parameters, such as the hydrate phase boundary, water saturation percentage, worst conditions of temperature and pressure and the amount of the inhibitor lost to non-aqueous phases. The current trends in the gas industry favour the use of MEG ($C_2H_6O_2$) rather than methanol (CH_3OH) for the newly developed gas plants (Chapoy and Tohidi, 2012, Seo et al., 2012). This preference is based on the fact that MEG is a non-flammable material with a high flash point of 111 °C, as opposed to methanol, which is highly flammable with a low flash point of only 11 °C. Given these facts, methanol presents a high safety risk during handling and storage. This is especially true with offshore installations having

limited areas. Furthermore, methanol burns with an invisible flame, making visual fire detection more challenging (Brustad et al., 2005). In contrast, losses of MEG due to the vapour phase are very small. It also has the advantage that it can be effectively recovered, regenerated and recycled. Therefore, precise knowledge of gas hydrate formation/dissociation conditions, as well as knowledge of phase behaviour of aqueous solutions of glycol, is essential to eliminate or avoid gas hydrate formation (Talatori et al., 2011). This precise knowledge will lead to a safer operation and more economical design of gas process facilities. (Chapoy and Tohidi, 2012).

Gas hydrate formation in the oil and gas systems (reservoir/wells, production process, flow lines and pipelines) may lead to very large production deferment, environmental damage and process safety concerns. Also, it is a serious flow assurance problem causing large economic losses due to the operational expenditures to remove the hydrate plug (Camargo et al., 2011, Tavasoli et al., 2011). Gas hydrate occurs in both oil and gas streams, especially in gas lifted wells (Nengkoda et al., 2009). It appears where low temperature and high differential pressure exist as the combination formula for hydrate formation (Malegaonkar et al., 1997). Preventing the formation of hydrates and the deferment caused by hydrate formation costs the offshore oil and gas industry up to 8% of their OPEX (Herath et al., 2015). Also Sloan (2003) stated that the worldwide estimation costs associated with gas hydrate inhibition are at 220 million dollars per year. Ongoing huge incremental operation costs of hydrate prevention and mitigation require urgent remedial actions(Nengkoda et al., 2009, Jensen et al., 2000).

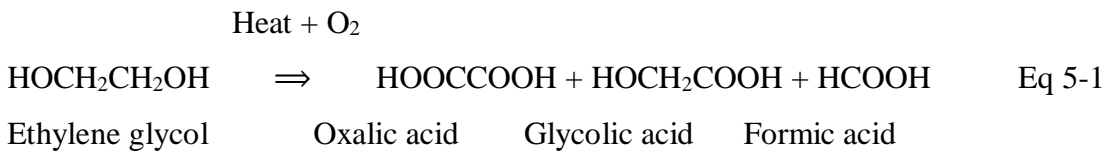
Hydrate formation and dissociation curves are primarily used to define the conditions (gas composition, temperature and pressure) that hydrate will form under. Hydrate formation curves can be derived from the experimental results, thermodynamic models, literature and prediction software (for this work, Peng-Robinson EOS is selected as the thermodynamic property model used for the prediction software). In the gas industry, these curves are typically used to ensure that the operating conditions of the transported fluid are within the hydrate free region as illustrated by Bai et al. (2005).

In the gas industry, MEG is regenerated in order to recover its large consumption in the field, its high cost and its impact on downstream processes. MEG is regenerated

by heating it to remove any surplus water and regain the high glycol purity for maximum recovery (Carroll, 2002, Psarrou et al., 2011). A basic MEG regenerator unit consists of a reboiler, a still column, a flash tank, and a surge drum (Bahadori, 2009). During the regeneration process, the water saturated MEG is separated by heating the solution utilising their different boiling points (At standard atmospheric pressure of 1 atmosphere, MEG boils at 197 °C while water boils at 100 °C). In order to have good quality MEG, its purity should be around 90 wt% (Carroll, 2002). In the gas industry, MEG is heated in the reboiler to a temperature that depends on the operating envelope of each specific unit. For example, some units are heated to around 95 °C (Diba et al., 2003), 140°C (Montazaud, 2011) or to 160 °C (Gonzalez et al., 2000) or higher. During the regeneration heating process, if MEG is overheated it will start to degrade into organic acids such as acetic acid (ethylic acid H₃C—COOH). When this happens, some fresh MEG needs to be injected to the MEG units to replace the degraded quantity (Montazaud, 2011). Hence, keeping the temperature below the degradation point is essential to maintain MEG quality and prevent the production of organic acid.

Most of the available literature on thermally exposed MEG has mainly been focused on MEG's effect on chemical decomposition aspects, such as what acidic products are formed from thermally degraded MEG and the effect on accelerating the corrosion of metallic components as stated by Rossiter Jr et al. (1985). The research by Rossiter Jr et al. (1985) focused on degradation products formed from the thermal oxidation of glycol according to three scenarios. First, glycol was diluted to 50 vol% and exposed to different temperature values (75 °C, 86 °C and 101 °C), which resulted mainly in the production of glycolic, oxalic, and formic acids. Second, the glycol was exposed to different temperatures in the presence of copper, which resulted mainly in the production of glycolic acid. Third, the glycol was exposed to different temperatures in the presence of aluminium, resulting mainly in the production of glycolic and lactic acid. These degradation products lead to the formation of organic acids, which decreased the solution's pH. Findings from this study indicate that thermal oxidation of glycol will reduce glycol quantity. This reduction in the quantity in turn leads to reduction in freezing inhibition efficiency. Thus, it is essential to monitor the amount of glycol in the system by determining the solution density as recommended by Rossiter Jr et al. (1985). Another study conducted by Rossiter et al. (1983) indicated that the main degradation products from

ethylene glycol solutions may include glycolic, oxalic, and formic acids as shown in Eq 5-1 below:



Psarrou et al. (2011) reported an experimental study for the MEG degradation at MEG reclaiming/regeneration conditions under total CO₂ equilibrium amount [(50–98) wt% MEG, (80–140) °C, (50 or 100) mmol Kg⁻¹ total alkalinity]. Observations from experiments performed by these researchers showed that the solution's colour changed to yellow as a sign of degradation. Ion chromatography report showed that glycolic and formic acids were the dominating MEG degradation products. Another experimental publication by Madera et al. (2003) on identifying the main products of glycol degradation using ion chromatography analysis found that the main products are formic, acetic, and glycolic acids. A study and analysis of the effect of thermal degraded MEG's on hydrate inhibition performance will provide new data to help understand its impact on flow assurance. To the authors' knowledge, such data is not yet available. Considering all of the above, studying gas hydrate inhibition profiles of MEG as fresh and as thermally exposed is essential for the process design. In this work, the thermal degraded MEG effects on hydrate inhibition are studied for exposure temperatures of 165 °C, 180 °C, and 200 °C and duration of 4 and 48 h.

5.3 Methodology

5.3.1 Materials and Equipment

Experiments were conducted using the cryogenic sapphire cell unit (capacity of 60 ccs). To avoid any error in preparing the gas composition for these experiments, only methane gas having a purity of 99.995% was used to maintain the same gas composition. The solution preparation was prepared based on a weight percentage of 25 wt% of pure MEG (Table 5-1) with 75 wt% de-ionised water using a high electronic balance with an accuracy of 1 mg for 1020 g. Pure nitrogen gas was used for purging.

5.3.2 General experiment procedure

The system, which consists of a sapphire cell, piston pump, gas sample bottles and the connecting tubing, was subjected to a pressure test prior to commencement of any experiment. The system was pressurised with nitrogen gas up to 100 bar and held for half an hour to confirm that there was no gas leak. The nitrogen gas from the cryogenic sapphire cell system was then vented into the atmosphere and then the cell was subjected to vacuum conditions using a vacuum pump. Gas samples were prepared by filling methane gas from a gas cylinder to four gas sample bottles. These sample bottles were then connected to the gas manifold. The desired gas volume was fed from the gas bottles to the piston pump using a pneumatic booster pump that is designed to boost the gas to pressure up to around 170 bar. The piston pump is motor driven and controlled by the computer available in the laboratory using Mint Workbench V-5-Gas pump-pressure software. The piston pump was designed to compress the gas up to 500 bar. The housing of the piston pump is equipped with a pressure sensor with an accuracy of 0.1%. The sapphire cell was drained and then filled with 7 mls of the required solution, which was prepared based on weight percentage concentration using the Eq 5-2 below:

$$M_1 \cdot C_2 = M_2 \cdot C_1 \quad (\text{Where } M \text{ is mass and } C \text{ is wt\% concentration}) \quad \text{Eq 5-2}$$

The gas was then routed directly from the piston pump to the sapphire cell by opening valve-6 (Figure 5-1). Of note here is that the sapphire cell came fitted with a magnetic stirrer. This stirrer was kept at a constant rotation of 530 RPM (330 mA) to maintain the same agitation rate for all experiments. Research done by Clarke et al. (2000) and Jensen et al. (2008) shows that the rate of gas hydrate formation is influenced by the change in the Reynolds number, caused in turn by changing the agitation rate. Obanijesu, Gubner, et al. (2014) also stated that an increase in agitation (stirring) rate could prolong the hydrate growth rate by both lowering start formation point and delaying complete solidification time. The sapphire cell was fitted with two resistance temperature detectors (RTD PT100 sensor with three cores Teflon tails). One RTD is placed on the top side of the sapphire cell to detect the temperature of the gas phase. The second RTD is placed on the bottom side to detect the liquid phase temperature to an accuracy of ± 0.03 °C. The cooling system efficiency is enhanced with the supply of chilled water to cool the refrigeration compressor. The sapphire cell chamber temperature is controlled by a computer software, with a

cooling range of +60 to -160 °C. The cell chamber temperature was first set to a point well outside the expected hydrate formation zone. The temperature was then controlled by a gradual stepwise decrease at a rate of around 0.5 °C per 20 min to achieve equilibrium conditions at each temperature step. This gradual control assured a homogeneous condition for slow hydrate formation/dissociation processes for accurate detection (Haghghi et al., 2009, Lee,Baek, et al., 2005). Sapphire cell parameters of temperature, pressure and stirrer current were recorded at an interval of 12 points per second through a computer software. The point at which gas hydrate started forming was noted based on visual observation and the hydrate left to form until complete blockage was achieved. Once there was complete hydrate blockage, the temperature in the cell was raised gradually by heating at a rate of around 0.5 °C per 20 min. The temperature at which gas hydrate started dissociation was recorded, subsequently the hydrate was left to melt until full dissociation occurred. Prior to each new experiment set, the sapphire cell was drained and cleaned. The cell was cleaned by a solvent (acetone) followed by de-ionised water to remove any contaminated solvent inside the cell. The vacuum pump was used to remove any fluid remaining inside the cell and was then fully dried by switching on the heater.

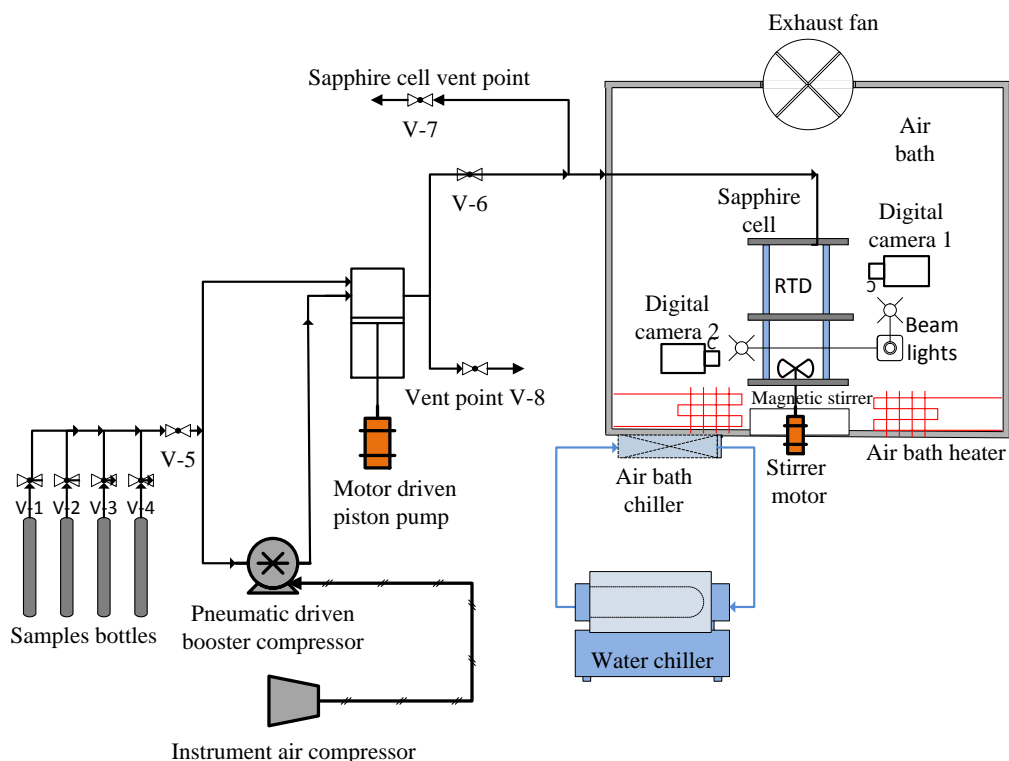


Figure 5-1 The PVT sapphire cell layout.

5.3.3 Testing methods

There are two types of experiment procedures that can be conducted to capture gas hydrate in the laboratory: the isochoric method (volume stays constant while pressure varies) and the isobaric method (pressure stays constant while volume varies). Mohebbi et al. (2012) stated that the rates of gas diffusion by the isochoric and isobaric test methods are nearly the same providing that the consumption rates are equal. The amount of consumed gas can be determined by the reduction of the reactor pressure (Mohebbi et al., 2012).

The isobaric method is one of the recognised methods in the study of hydrate formation. Malegaonkar et al. (1997) used the isobaric method to study methane hydrate formation to obtain the kinetic data of hydrate formations. For this work, each experiment set was done under a wide range of pressures, which extended from 50 to 300 bar. The isobaric method was selected here for the experiments at each pressure point to maintain the same rates of hydrates formation and dissociation. The pressure was maintained by the piston pump, which is controlled by a computer. Hydrates full profile were noted using the visual observation method. The visual observation method is an approved method used to determine hydrate profiles. It is widely used by various (Tohidi et al., 2001, Chen et al., 2010, Kondo et al., 2014, Vijayamohan et al., 2014, Windmeier et al., 2014b). Similarly, the natural gas production processing transport book by Rojey et al. (1997) mentions that the most common method for determining the point at which hydrates appear is the visual method. The hydrate profile images were recorded by two mounted cameras connected to a computer screen. Light beams were used for better vision quality.

5.3.4 Thermally degraded MEG samples preparation

During the preparation of thermal degraded MEG samples, a 2-l autoclave was used to heat the samples to the desired temperatures (135 °C, 165 °C, 180 °C, 185 °C and 200 °C) for duration of 4 and 48 h. These temperatures and duration were selected to replicate the normal industrial operational fluid temperatures up to the overheating temperature in the reboiler units to convert the rich MEG into lean MEG (Lehmann et al., 2014). Solutions were prepared by using 80 wt% lean MEG with 20 wt% deionised water as this is the typical concentration used for hydrate inhibition. Firstly, the sample was transferred inside the autoclave and then the autoclave's head and body were clamped and bolted. High purity nitrogen was then sparged through the

dip tube into the liquid phase for around 16 h, to reduce the oxygen concentration to less than 20 ppb to replicate the reboiler condition. The autoclave was then placed in a heating mantle and the heater turned on and set to achieve the desired temperature and duration. Once the proper heating duration was achieved, the heater was turned off and the sample was allowed to cool. The resultant test solution was transferred into glass bottles and stored under a nitrogen cap.

5.3.5 MEG degradation Identification Techniques

Samples of thermally exposed MEG to temperatures of 135 °C, 165 °C and 185 °C were selected for product identification. In general, a wide range of analytical instruments could be used to identify the MEG degradation products such as Fourier transform infrared spectroscopy (FTIR) (Smith, 2011), ultraviolet-visible spectroscopy (UV-vis), gas chromatography mass spectroscopy (GC-MS), nuclear magnetic resonance spectroscopy (NMR), gas chromatography flame ionization detector (GC-FID), high performance liquid chromatography (HPLC), mass spectroscopy (MS) and ion chromatography (IC). For this work, the thermally exposed MEG samples were analysed by a third party laboratory using two techniques: ion chromatography (IC) and high-performance liquid chromatography - mass spectroscopy (HPLC-MS). Ion Chromatography is a liquid chromatography method for the breakdown of ionic species in liquid solutions and able to measure concentrations of major anions. HPLC-MS is a technique that combines the physical separation capabilities of liquid chromatography (HPLC) with the mass analysis capabilities of mass spectrometry (MS). The use of HPLC-MS and IC for MEG degradation analysis has previously been described (Huang et al., 2009, Kadnar et al., 2003). These two techniques were selected due to their reputation and earlier literature references (Niessen et al., 1995, Schreiber et al., 2000).

Table 5-1 Mono-ethylene glycol properties characteristics at atmospheric pressure (Aylward et al., 2008, Braun et al., 2001).

Molecular formula	Solubility in water	Melting point °C	Boiling point °C	Flash point °C	Viscosity (25 °C) Pa.s	Density (25 °C) g/cm³	Molecular weight g/mol
C ₂ -H ₆ -O ₂	Miscible	-12.9	197.3	111	0.181	1.110	62.07

5.4 Results and discussions

5.4.1 Hydrate formation/dissociation behaviour of binary CH₄–H₂O system

The initial experiment was carried out to create a baseline for succeeding experiments. In general, this first experiment was meant to ensure several objectives; that the PVT sapphire cell unit and all its accessories could handle the operating pressure of 300 bar, that everything worked as per expected conditions, and finally that the experimental data was accurate. As such, the first experiment was conducted using methane gas (106.67 g) with a solution of 100 wt% de-ionised water (7 g), at a pressure range of 50–300 bar and at intervals of 25 bar. The hydrate profile points were recorded to be used later as the expected minimum points for the succeeding experiments. Inside the sapphire cell, hydrate formation temperature was detected at the liquid phase and the gas phase. A homogeneous temperature inside the sapphire cell was achieved and confirmed by ensuring that both thermocouples read the same temperature. Furthermore, the accuracy of the cryogenic sapphire cell experimental data was assessed by repeating the same experiment three times, the results of which being nearly identical. A maximum experimental error of 1.92% was generated from the statistical analysis.

The results were analysed and compared with literature and software (Hysys, Pipesim, and Multiflash). Statistical analysis shows that the experimental results are consistent with the literature and software. An average absolute percentage deviation (AAD %) of 8.45% was found when the experimental data were compared with the literature and software. In addition, the standard deviation (S) was calculated at \pm 0.48. By considering the acceptable margin of experimental errors, this statistical analysis indicates that the experimental data was accurate. The hydrate formation/dissociation locus curve is plotted in Figure 5-2. For a better analysis, these experimental results were smoothed by curve fitting with R^2 of more than 0.99. It has been noticed that the results of Sloan et al. (2008a) nearly match the experimental hydrate start formation curve, while the rest of the literature (Lu et al., 2008, Maekawa, 2001, Jager et al., 2001) and software more closely match the start dissociation curve.

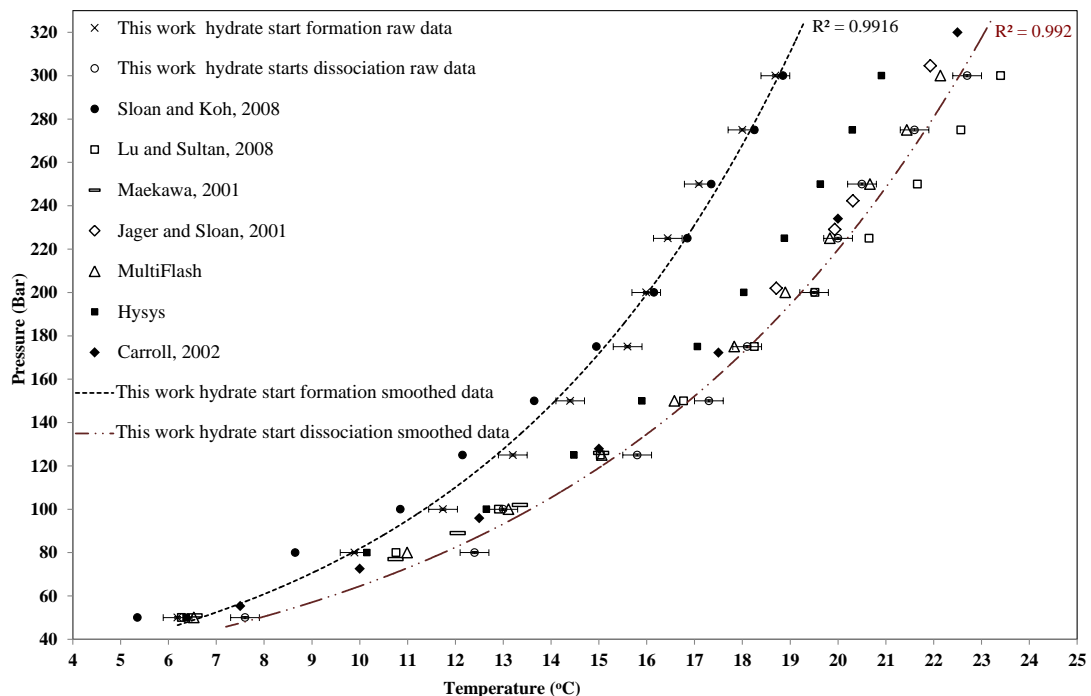


Figure 5-2 Hydrate locus of start formation /start dissociation and literature for binary $\text{CH}_4-\text{H}_2\text{O}$ system.

Further analysis of the full hydrate profile was conducted with points of end dissociation (Figure 5-3). The difference between the hydrate start formation point and the hydrate start dissociation point (ΔT_1) (Metastable region) shows a smaller difference at lower pressures ($\Delta T_1 = 1.41^\circ\text{C}$ at 50 bar), while the gap increases with an increase in pressures ($\Delta T_1 = 4.01^\circ\text{C}$ at 300 bar) (Figure 5-3). In addition, the difference between the hydrate start formation point and the hydrate end dissociation point (ΔT_2) shows the same phenomena: smaller difference at lower pressures ($\Delta T_2 = 3.51^\circ\text{C}$ at 50 bar) and a greater difference at higher pressures ($\Delta T_2 = 8.41^\circ\text{C}$ at 250 bar) (Figure 5-3). Additionally, higher pressures in the system resulted in higher hydrate formation temperatures. These findings correspond with the work of Bai et al. (2005). Furthermore, the dissociation temperature of hydrate is observed to be higher than the hydrate formation temperature, which indicates that hydrate dissociation requires a higher temperature than that of starting formation.

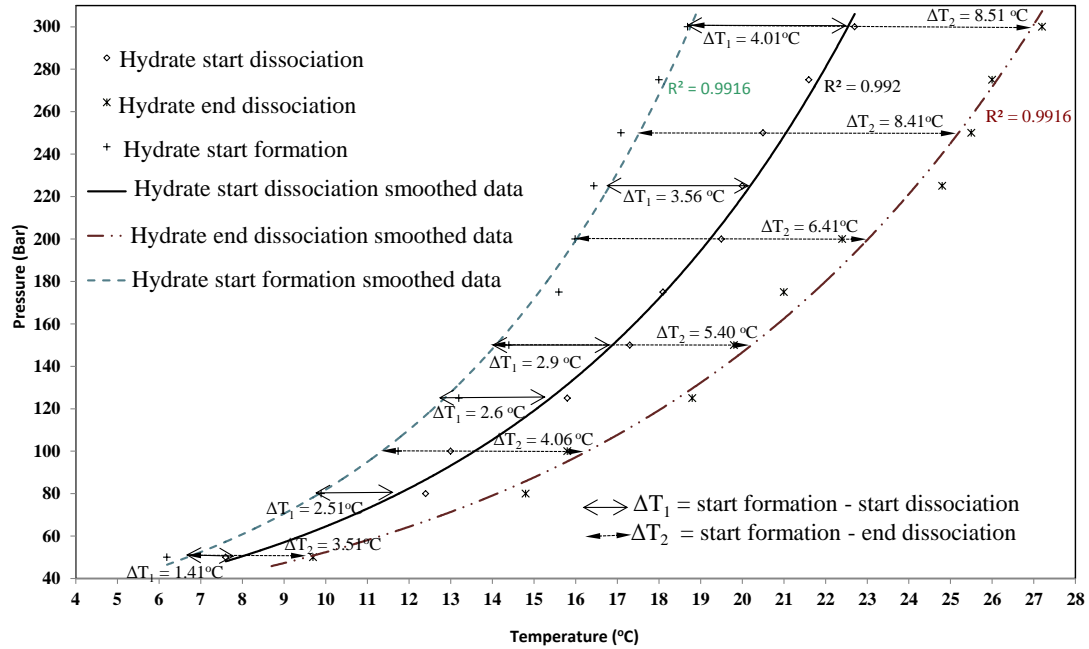


Figure 5-3 Hydrate locus curve for binary $\text{CH}_4-\text{H}_2\text{O}$ system of hydrate formation /start dissociation/end dissociation.

For the 100 bar pressure experiment, the hydrate nucleation pattern was analysed: First, hydrate crystals formed at a temperature of 11.7°C . The temperature was dropped to 11°C for 15 min after the first hydrate agglomerated with around 5% hydrate blockage (i.e., the amount of water percentage that converted to hydrate). After 30 min, the temperature was dropped to 9°C with hydrate blockage reaching around 15%. The hydrate formation pattern for this system shows that hydrates first stick to the surface area at the interface level, and then start to build up towards the centre of the sapphire cell, creating a thin hydrate layer. Later on, hydrates start to form towards the bottom of the cell. After 60 min, the temperature was dropped to 7.5°C with around 40% hydrate blockage. After 90 min, the temperature was dropped to 4°C with hydrate blockage reaching around 70%. After 120 min, the temperature dropped to 3.8°C with almost 85% hydrate blockage. Finally, the hydrate reached full blockage after 140 min at a temperature of 3.5°C (Figure 5-4).

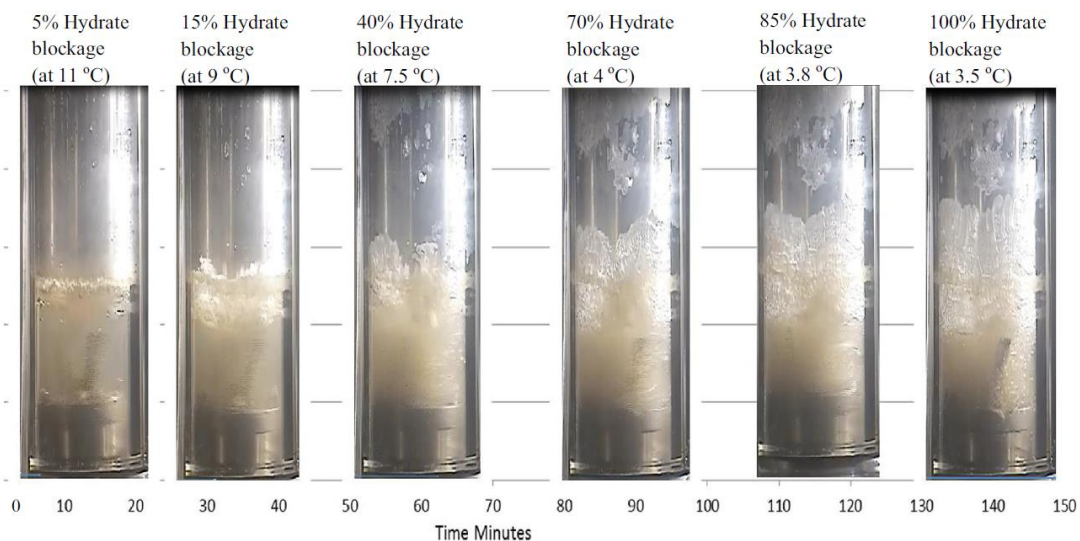


Figure 5-4 Hydrate formation pattern captured by the mounted camera (estimate driven from hydrate start nucleation till all water completely converted to hydrate).

5.4.2 MEG degradation products identification

The degradation products from thermally degraded MEG samples for both techniques show unconsented results in terms of products and concentrations. Specifically, the results from HPLC–MS (Figure 5-5) show that only two organic acids were detected (acetic and formic acid). In addition, it is evident from the results that the concentration of acetic acid increases with an increase in temperature that, in general, is expected. On the other hand, all samples show that formic acid has constant concentration of 10 ppm. It can be noticed that the HPLC–MS method has a minimum detection limit of only 10 ppm, hence any compounds below 10 ppm cannot be quantified.

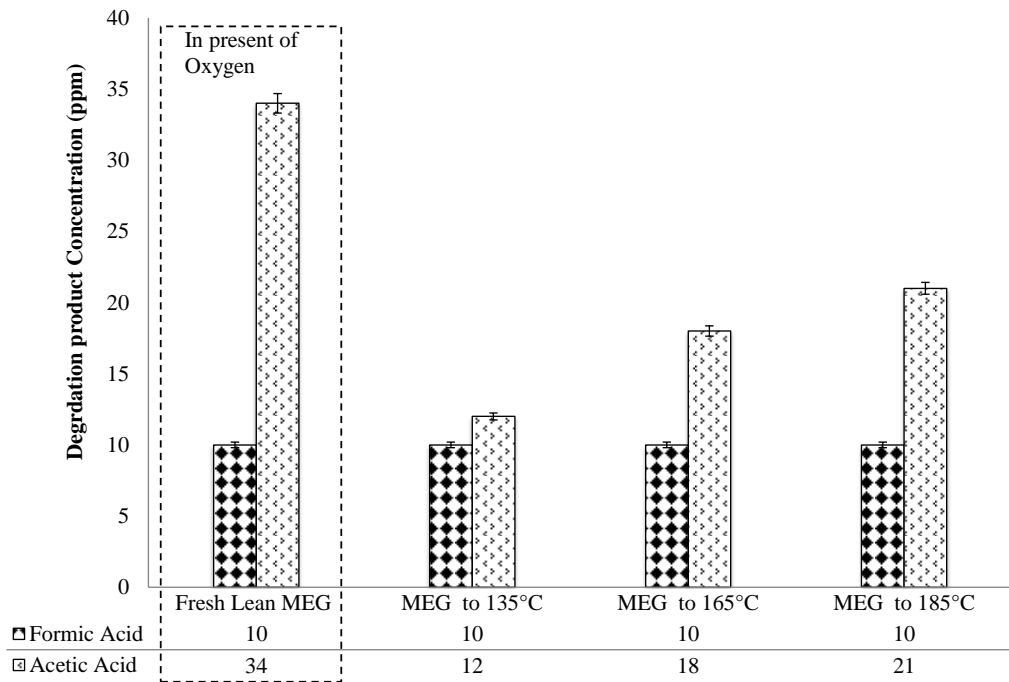


Figure 5-5 Degradation products identification using HPLC-MS technique for samples of thermally degraded MEG to 48 h.

The IC trend (Figure 5-6) shows disputed results as it indicates that the MEG degradation concentration increase as the temperature decreases. Such a trend clearly goes against expectations. IC was able to detect more organic products (glycolic acid, acetic acid, formic acid, and chloride) than HPLC-MS. Although the IC method shows high sensitivity in measuring organic acids up to 0.001 ppm, the presence of any single compound in higher concentration can influence the measurement of other compounds at lower concentrations.

Both identification techniques display almost similar results for the presence of acetic acid in the fresh lean MEG solutions that were not thermally exposed. The results possibly indicate the influence of oxygen from air ingress reacting with MEG to produce acetic acid. This might have occurred because the fresh solution samples were not purged with nitrogen to eliminate the dissolved oxygen. This corresponded with the work of Monticelli et al. (1988). In the gas field, the introduction of oxygen into the MEG process not only plays a role in degrading MEG, but also precipitates iron oxide which results in block nozzles in processing equipment. As such, dissolved oxygen should not be in contact with MEG. This can be achieved by various techniques such as: introducing a blanket gas (inert gas/hydrocarbon gas) or by dosing of an oxygen scavenger (Lehmann et al., 2014, Emdadul, 2012).

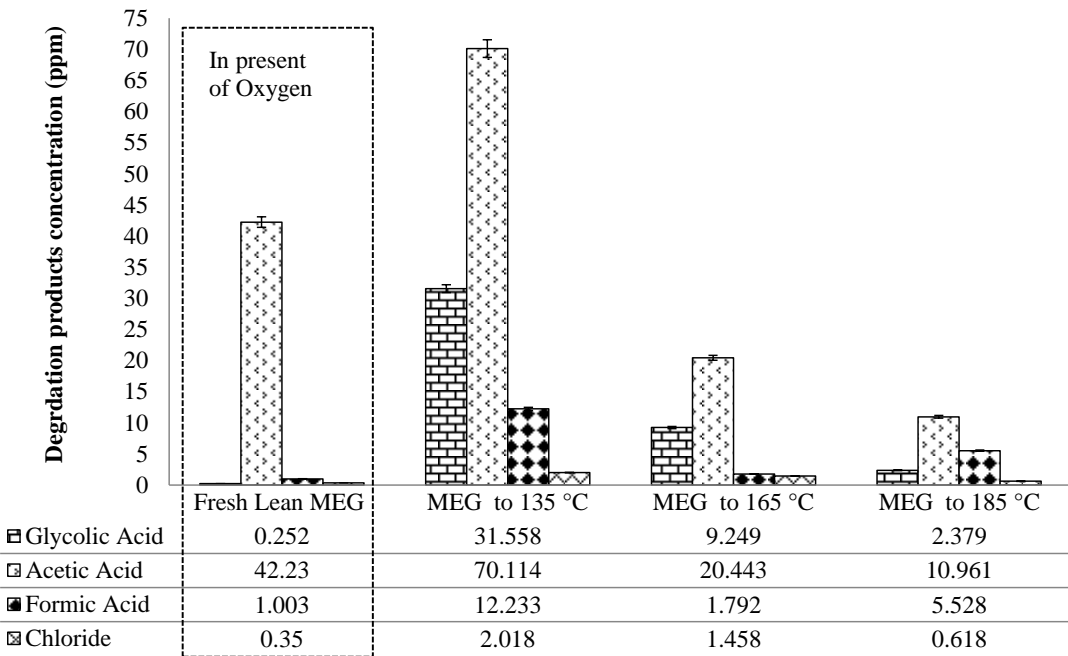


Figure 5-6 Degradation products identification using IC technique for samples of thermally degraded MEG to 48 h.

As can be seen from the visual observation of the samples (Figure 5-7), the resultant solution shows that MEG colour turns slightly yellow as the temperature increases. This colour change is a sign of degradation, as observed by Psarrou et al. (2011).

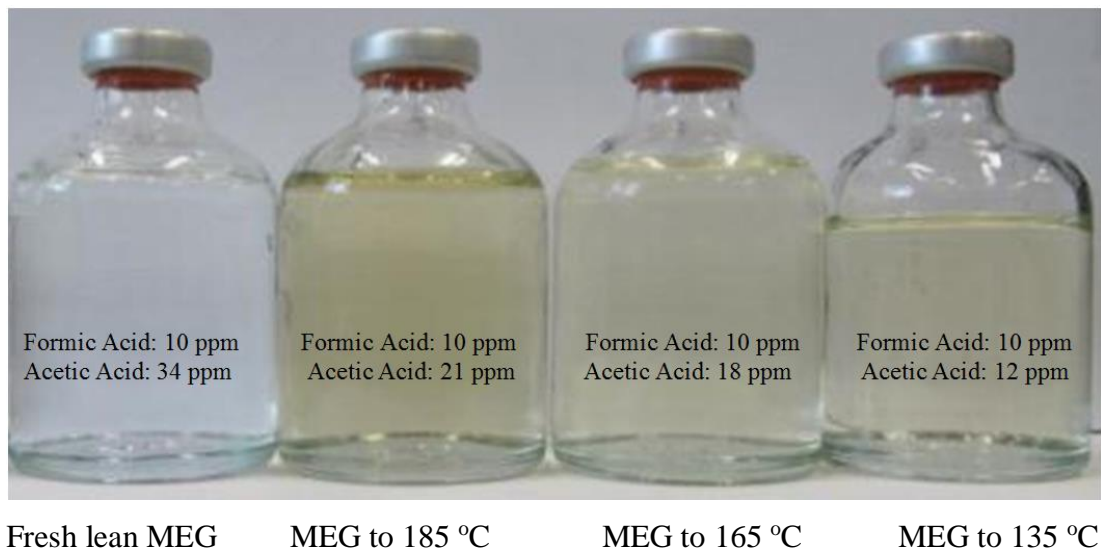


Figure 5-7 Various Sample bottles of thermally degraded lean MEG for 48 h.

5.4.3 Effect of thermally degraded MEG on hydrate inhibition performance

The objective of this section is to present results from the laboratory for the influence of the thermal thermally degraded MEG on the hydrate inhibition performance. After identifying the MEG degradation products raised from the thermally exposed MEG (section 5.4.2), the samples were analysed to evaluate their hydrate inhibition performance. Initially, the test was conducted using pure methane gas with a solution of 50 wt% pure MEG at 350 bars. For this high solution concentration, hydrate formation starts to form at -2.5°C . Based on these results, and to avoid testing hydrate formation below 0°C , the concentration of MEG was reduced. This was performed to accurately distinguish hydrate formation from ice, and avoid the analysis of the hydrate inside an ice formation region (below 0°C). So, the concentration turns into 25 wt% MEG (1.75 g), 75 wt% de-ionised water (5.25 g) and 100 % methane (106.67 g). The initial experiment with 25 wt% pure MEG (not degraded) was conducted and then used for comparison and evaluation. When compared to a solution of 100 wt% de-ionised water, the results of the pure 25 wt% MEG shifted the hydrate formation curve towards the left side by an average of 7.8°C (Figure 5-8). This temperature shift demonstrates the effect of MEG in inhibiting of hydrate, which is in line with the software, literature and consistent with the findings from (Kim et al., 2014a).

The full hydrate profile of the thermal degraded MEG samples were studied thoroughly by comparing the hydrate inhibition performance of degraded MEG with pure MEG, which were both at the concentration of 25 wt% (Figure 5-8). The results of the MEG sample, which was thermally exposed to 165°C for 4 h, show that the hydrate formation points deviated towards the right side of the hydrate curve by an average of 0.33°C . On the other hand, the 48 h sample deviated towards the right side by an average temperature of 0.72°C (Figure 5-8). This rise in the hydrate formation temperature indicates reduced inhibition performance of MEG due to the thermal degradation effect. As the MEG was exposed for longer durations, it showed a greater reduction in hydrate inhibition performance by shifting the curve more to the right.

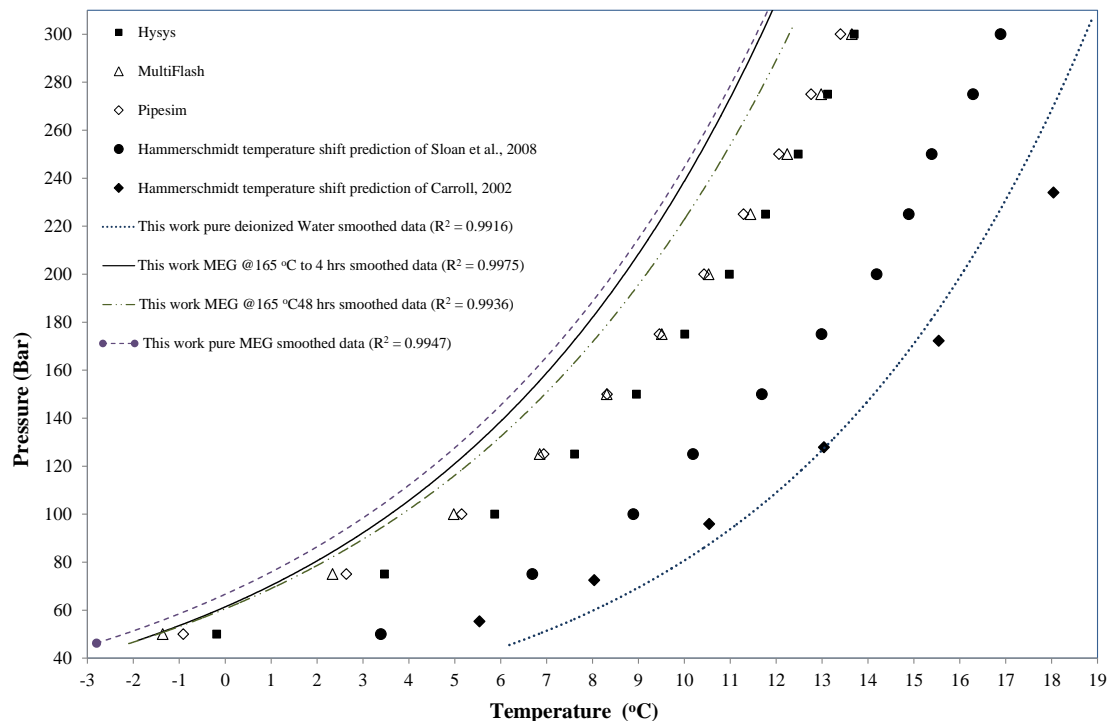


Figure 5-8 Hydrate locus of Methane with 25 wt% thermally degraded MEG to different exposure time. Hammerschmidt temperature shift prediction equation obtained from Bai et al. (2005).

For the second part, the effect of MEG being thermally exposed to different temperatures (165 °C, 180 °C and 200 °C for 48 h) was analysed using the same methodology as with the system of thermally exposed MEG to different durations. Results show that there is deviation in hydrate formation towards the right side of the hydrate curve (Figure 5-9, Table 5-2).

Table 5-2 Hydrate formation temperature deviation towards the right side of the hydrate curve.

48 h MEG exposure samples (25 wt%)	Average hydrate formation temperature deviation (°C)
165 °C sample	+ 0.72
180 °C sample	+ 1.07
200 °C Sample	+ 1.62

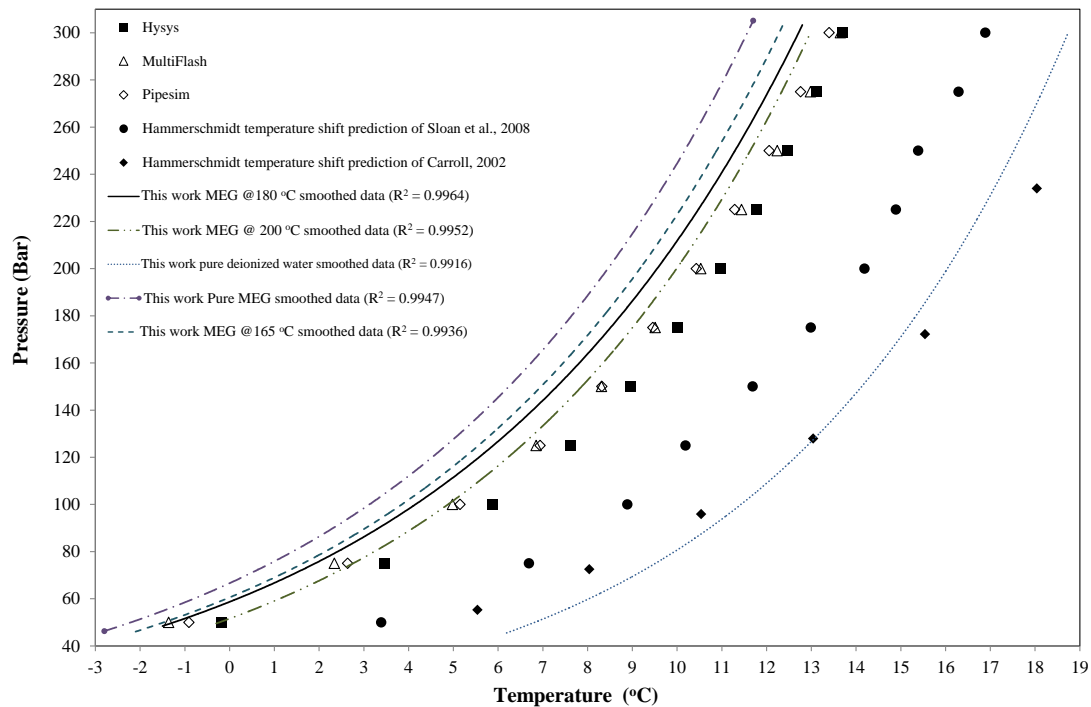


Figure 5-9 Hydrate locus of Methane with 25 wt% thermally degraded MEG to 48 h for different temperatures. Hammerschmidt temperature shift prediction equation obtained from Bai et al. (2005).

As shown in Table 5-2, as MEG was exposed to higher temperatures the hydrate formation temperature rose. This is a clear indication of the influence of MEG degradation on weakening MEG inhibition performance. Although there is a slight shift in hydrate formation temperature displayed in Table 5-2, it shows consistency in the results of the degradation effect.

The hydrate formation full profile patterns at 125 bar for the methane with a solution of 25 wt% of thermally degraded MEG to 180 °C were analysed (Figure 5-10), the observed hydrate pattern followed the same profile as explained in Figure 5-4 of section 5.4.1 above.

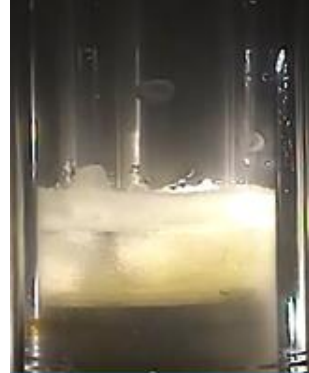
		
≈ 5% Hydrate blockage at t = 11 min	≈ 30% Hydrate blockage at t = 46 min	≈ 80% Hydrate blockage at t = 108 min

Figure 5-10 Captured images of hydrates formation of methane with 25 wt% of thermally degraded MEG to 180 °C at 125 bar.

5.5 Conclusion

In this work, new experimental data set have been reported for methane hydrate under isobaric condition in the presence of aqueous solutions of both pure and thermally exposed mono-ethylene glycol over a wide range of temperatures and pressures. The experimental results are in good agreement with the literature and software. Analysis of the full growth of hydrate formation for a solution of pure 100 wt% de-ionised water and pure 25 wt% MEG was conducted, with the results used as baseline data for the succeeding experiments. The hydrate profile reveals that the temperature gap between the hydrate formation point and the hydrate start dissociation/end dissociation points show a smaller gap at lower pressures and a higher gap at higher pressures. New hydrate full profile data have been obtained for the effect of thermally degraded MEG under different conditions of temperatures and duration on hydrate inhibition performance. The degradation products of MEG were analysed by independent laboratories using the IC and HPLC–MS methods. The main degradation products found were acetic acid, formic acid, and glycolic acids. Experiments were conducted to test hydrate inhibition performance of samples of thermally degraded MEG to 165 °C that were exposed to durations of 4 and 48 h. Results show that as MEG was exposed for higher temperature duration, the hydrate formation temperature raised which indicates a reduction in inhibition performance. Other experiments were conducted to test hydrate inhibition performance of samples of thermally degraded MEG that were exposed to different temperatures (165 °C,

180 °C, and 200 °C). These results show that as MEG was exposed to higher temperatures, hydrate formation temperature was subsequently raised, which is an indication of reduced hydrate inhibition performance. Extensive experiments should be conducted to find the point of non-thermal stability temperature, not to mention the means of preventing MEG degradation. In addition, the experiments should cover MEG samples that undergo greater exposure ranges, for both temperature and duration. These experiments will provide more data for the MEG regeneration units. In that vein, the gas industry needs to intensively investigate the proper means of correctly replacing the degraded MEG amounts. In conclusion, experiments need to be conducted to test if natural gas hydrates, along with thermally degraded MEG, will cause foaming or emulsion tendencies for the systems in the presence of different inhibitors and production chemicals.

Chapter 6 Effects of Thermally Degraded Monoethylene Glycol with Methyl Diethanolamine and Film-Forming Corrosion Inhibitor on Gas Hydrate Kinetics

6.1 Abstract (Figure 6-1)

Gas hydrate blockage and corrosion are two major flow assurance problems associated with transportation of wet gas through carbon steel pipelines. To reduce these risks, various chemicals are used. Monoethylene glycol (MEG) is injected as a hydrate inhibitor while methyl diethanolamine (MDEA) and film forming corrosion inhibitor (FFCI) are injected as corrosion inhibitors. A large amount of MEG is used in the field which imposes the need for MEG regeneration. During MEG regeneration, rich MEG undergoes thermal exposure by distillation to remove the water. This study focuses on analyzing the kinetics of methane gas hydrate with thermally exposed MEG solutions with corrosion inhibitors at 135–200 °C. The study analyses the hydrate inhibition performance of three different solutions at selected concentrations and pressures (50–300 bar), using a PVT cell and isobaric method. Results established that thermally degraded solutions cause hydrate inhibition drop. However, the inhibition drop was found to be lower than that of pure thermally degraded MEG, which is caused by the additional hydrate inhibition effects of MDEA and FFCI. In addition, hydrate phase boundaries and regression functions were reported to provide a deep insight into the operating envelope of thermally degraded MEG solutions.

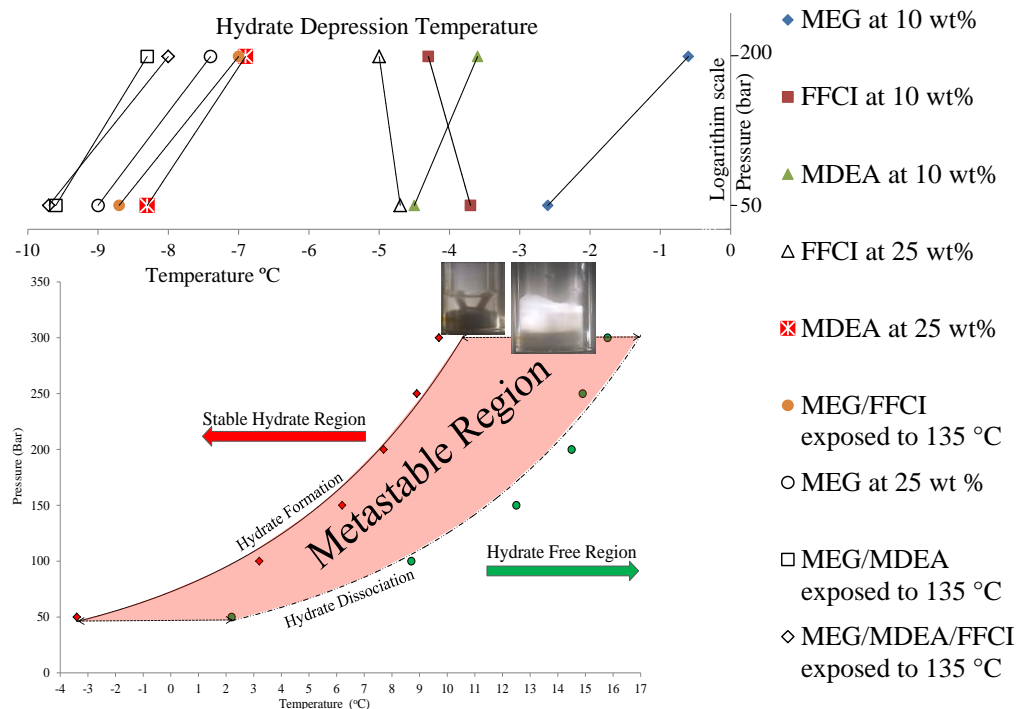


Figure 6-1 Abstract Graphics

6.2 Introduction

Gas hydrates (also known as clathrate-hydrates) are solid icelike compounds, which form various crystal structures. They are naturally found in marine sediments, especially in the upper few hundred meters of the sea-floor, (Xu et al., 1999, Dickens et al., 1997) and they can occur during gas production, processing, and transporting (Englezos et al., 1987a). Gas hydrate is created when water forms a cagelike structure around the guest molecules (such as methane, ethane, propane, isobutane, normal butane, nitrogen, carbon dioxide, hydrogen sulfide, etc.), particularly under favorable conditions of high pressure and low temperature (Yousif, 1994). It is well-documented that hydrate formation temperature increases proportionally with the increase of the operating pressure (Lunine et al., 1985, Englezos et al., 1987a, Sum et al., 1997, Sloan et al., 2008a). This is because the pressure effects are incorporated in the hydrate formation driving force, which is also demonstrated in this work. Gas hydrates can create serious flow assurance issues by plugging pipelines and jeopardizing the safety of processes and wellheads by causing leaks and ruptures (Sloan et al., 2008a).

Thus, precise knowledge of the thermodynamic stability of methane hydrates is crucial for flow assurance strategy, while monoethylene glycol (MEG) and corrosion

inhibitor additives influence this stability (Hoppe et al., 2006, Lehmann et al., 2014, Obanjesu,Gubner, et al., 2014). We thus investigated hydrate stability by analyzing the hydrate formation–dissociation profiles (i.e., the hydrate phase boundary) under isobaric conditions. Hydrate formation is defined as the intimal crystallization process (which includes nucleation and growth processes), which is controlled by heat and mass transfer, while hydrate dissociation is a sequence of lattice destruction (Bishnoi et al., 1996, Sloan et al., 2008a). The stable hydrate region is located to the left side of the hydrate formation curve in which hydrates are thermodynamically stable and will form. The hydrate–free region is located to the right of the hydrate dissociation curve, and this region is considered as a safe operating envelope where hydrate will not form unless subcooling is applied. The metastable region (also known as the induction region; the shaded region in

Figure 6-2) is where hydrate is not stable (Natarajan et al., 1994). However, it is highly recommended not to operate inside this metastable region because hydrate may occur at any point. If operation is taking place in this region, hydrate prevention measures should be considered. Identifying hydrate phase boundaries are therefore essential because they outline the safe operation region (Bai et al., 2005, Miers et al., 1907).

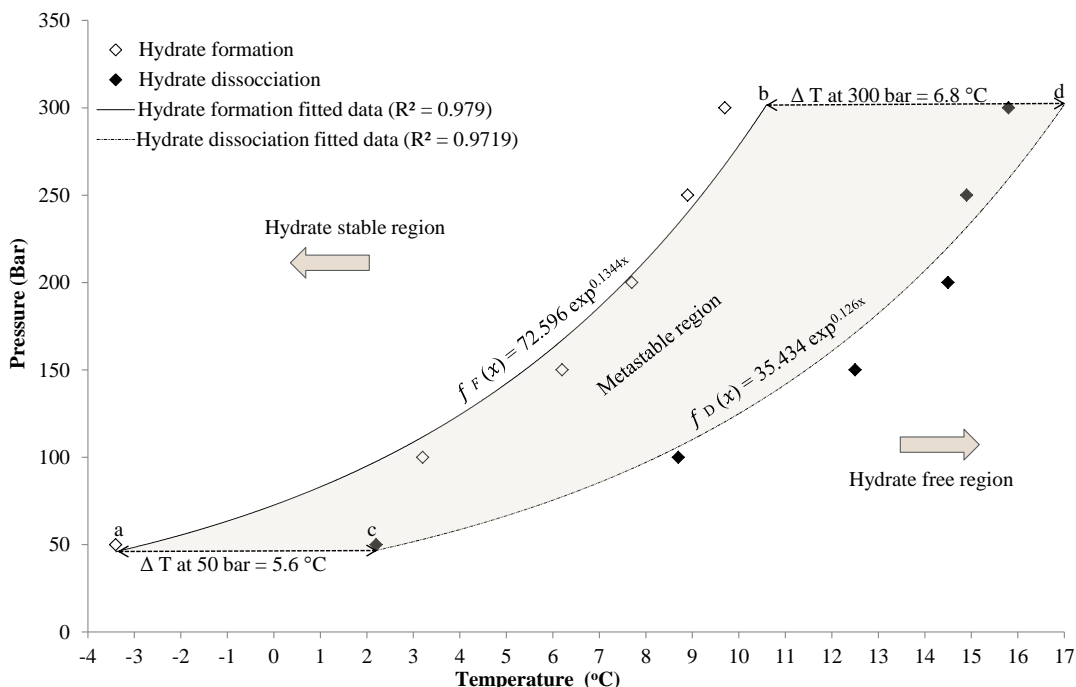


Figure 6-2 Methane gas hydrate phase boundaries of solution A exposed to 135 °C.

Because the tendency of the oil and gas industry to operate at conditions of high pressures and low temperatures in combination with transportation and processing of sour gases, flow assurance of these facilities is becoming more challenging so as to safely transfer hydrocarbon product with minimum deferment and asset damage. Under these operating conditions, gas hydrate and internal corrosion are the main problems in flow assurance apart from waxes, asphaltenes, and scale build up (Zerpa et al., 2010, Sloan, 2005). Hydrate and corrosion problems can be prevented by various techniques. However, applying some techniques could complicate other flow assurance aspects; for example, applying heat to prevent hydrate formation can increase corrosion rate by speeding up the chemical reactions (Melchers, 2003) and installing an internal liner to prevent corrosion can promote hydrate formation because of line pressure increase. Furthermore, some preventative techniques implicate huge CAPEX and could cause production shutdown (Moloney et al., 2008).

Monoethylene glycol (MEG) is an expensive chemical, and it is used as a thermodynamic hydrate inhibitor (THI). A large amount of MEG is consumed; therefore, recycling is an effective and economical solution for continuous long-term production (Brustad et al., 2005, Gizah et al.). Normally, MEG recycling involves regeneration and reclamation processes to remove water and soluble salts, respectively (Figure 6-3). During gas processing and production, various chemical additives, such as corrosion inhibitors, scale inhibitors, and oxygen scavenger, are injected together with MEG in the wet gas pipeline (Lehmann et al., 2014, Brustad et al., 2005, Lehmann et al., 2016, Salasi et al., 2017).

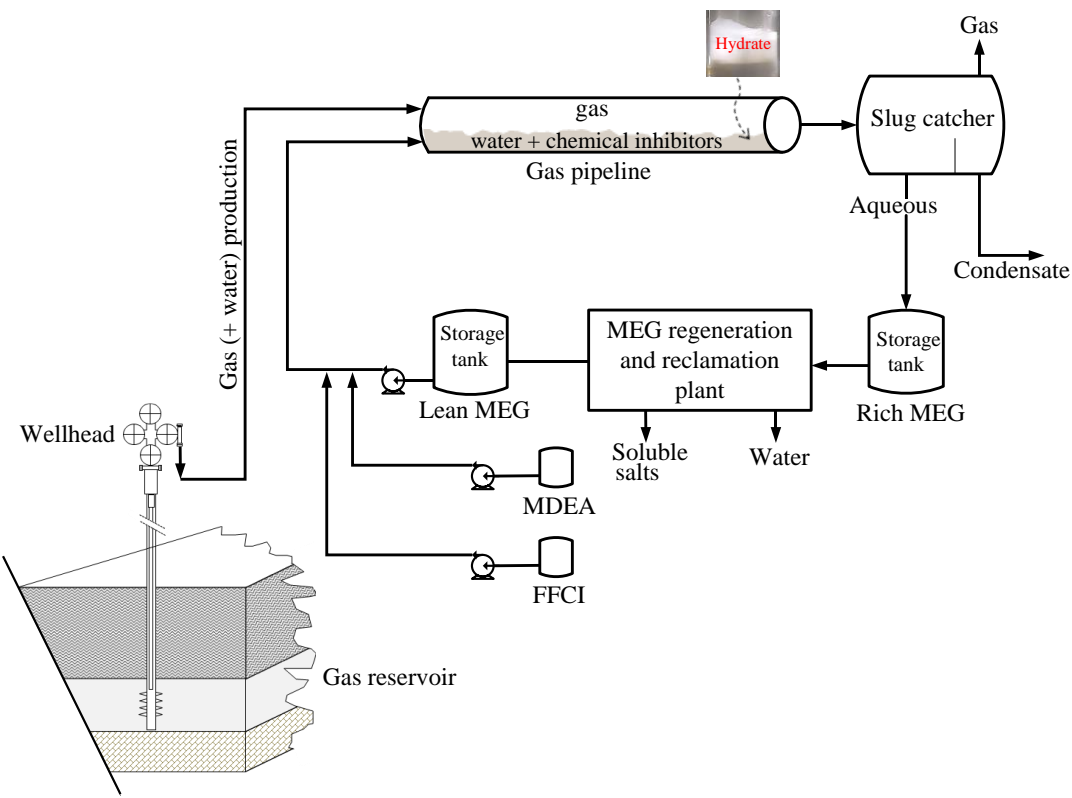


Figure 6-3 Overview of the MEG closed loop system.

During the MEG regeneration process, the incoming rich MEG solution (typically above 25 wt% MEG) is heated by a reboiler in a distillation column system to reconcentrate it to lean MEG (above 80 wt%, typically at 90 wt% MEG) (Zaboon et al., 2017). As a standard operation, the distillation column works above atmospheric pressure and temperatures ranging from 120–150 °C, depending on the incoming rich MEG concentration. Lean MEG from the regeneration unit is then routed to the reclaimer unit to flash the lean MEG solution to enhance MEG purity by removing salts and other contaminants. Reclamation is operated under vacuum (\approx 100–150 mbar) and at temperatures ranging from 125–155 °C, which helps to reduce the MEG viscosity and prevents fouling and deposition of the process equipment (Psarrou et al., 2011, Bikkina et al., 2012). The major challenge in the glycol regeneration and reclamation process is the thermal decomposition and degradation of MEG caused by reboiler overheating. Once MEG solutions are overheated, it undergoes thermal degradation resulting in fouling, foaming, corrosion and process upset (Bikkina et al., 2012, AlHarooni et al., 2015, Madera et al., 2003, Clifton et al., 1985).

Methyl diethanolamine (MDEA) solutions are used as an absorption solvent and sweetening agent to remove acid gases and carbon dioxide from natural gas. Such

MDEA solution have the advantages of reducing corrosion rate, stabilization, and relatively low reaction heat (Liu et al., 2015, Qian et al., 2010, Herslund et al., 2014). Film forming corrosion inhibitor (FFCI) solutions are used to reduce corrosion by forming a protective film inside the pipeline wall. Basically, there are four classifications of corrosion inhibitors: anodic inhibitors, cathodic inhibitors, mixed inhibitors, and volatile corrosion inhibitors. FFCI fall under the mixed inhibitors classification because they work by slowing both the cathodic and anodic reactions. They are typically film-forming compounds that create a barrier between the surface metal and the acidic solution. Various FFCI formulations have been developed by many commercial chemical providers and are typically complex mixtures. These mixtures contain film-forming inhibitor molecules (e.g., polymerizable acetylenic alcohols, quinoline-based quaternary ammonium compounds and various nitrogen heterocycles), an oil phase, a solvent package, and surfactants to assist dispersion of the inhibitor in the acid (Barmatov et al., 2015, Barmatov et al., 2012, Cicek et al., 2011). A FFCI is used as an additional or alternative corrosion control method when the risk of scaling is high (Dugstad et al., 2004, Davoudi, Heidari, et al., 2014).

Corrosion inhibitors such as MDEA and FFCI are widely used with MEG in numerous gas field applications, especially the ones that contain high amounts of H₂S, (Dugstad et al., 2003) such as the South-Pars gas field which is the world's largest gas field with twin 109 km 32 in. diameter gas pipelines. South Pars is a gas condensate moderately sour reservoir field. In this field, a solution of "70 wt% MEG + 4 wt% MDEA" is used for hydrate control and corrosion inhibition (Glenat et al., 2004, Bonyad et al., Davoudi, Heidari, et al., 2014). Moreover, MDEA has global application in several fields in Norway, Italy, Netherlands, and France (Olsen, 2006). The choice of using either MDEA or FFCI is based on the assessed corrosion protection strategies, which depend mainly on the reservoir water breakthrough, emulsion level, scaling rate, corrosion rate, environmental issues, iron production due to corrosion, and handling of corrosion products in the MEG process plant (Glenat et al., 2004, Dugstad et al., 2004). In some applications, injection of FFCI alone cannot provide adequate corrosion control; then pH adjustments may be injected commingled with FFCI to facilitate corrosion protection (Latta et al., 2013, Halvorsen et al., 2006). In principle, several strategies are considered for corrosion and hydrate protection: "MEG + full pH stabilization", "MEG + FFCI" and 'MEG +

partial pH stabilization + FFCI” (Anne Marie K. Halvorsen, 2007, Hagerup et al., 2003, Halvorsen et al., 2003, Halvorsen et al., 2006, Lehmann et al., 2014).

Several studies on MEG degradation have been conducted on corrosion rate, acidic degradation products, effect of temperature, and effect of oxidation with presence of metals and changes in pH values (Clifton et al., 1985, Rossiter Jr et al., 1985). However, little attention has been given to the effect of thermally degraded MEG solutions on gas hydrate thermodynamics. The closest literature is associated with our previous work (AlHarooni et al. (2015)) of pure thermally degraded MEG. This lack of information makes it difficult to predict the hydrate profile. To determine the extent to which degraded MEG will affect hydrate inhibition, we analyzed methane gas hydrate formation profiles for a variety of solutions of thermally degraded MEG with corrosion inhibitors (MDEA-FFCI) at a pressure range from 50 to 300 bar using the isobaric method. Analyzing the gas hydrate formation profiles by the isobaric method is one of the recognized methods (Kashchiev et al., 2002, Arjmandi et al., 2005, Wu et al., 2013, Najafi et al., 2014, AlHarooni et al., 2015). Furthermore, the effect of pure MDEA and FFCI on gas hydrate inhibition was analyzed at different concentrations (5–25 wt%) for a pressure range from 50 to 200 bar.

6.3 Experimental Methodology

6.3.1 Equipment and Materials

Hydrate formation and dissociation tests were carried out using a PVT sapphire cell unit (Figure 6-4). The sapphire cell has a volume capacity of 60 ccs, an operating temperature range from +60 to -160 °C, and an operating pressure up to 500 bar. The sapphire cell is equipped with a variable speed magnetic stirrer (0–1600 rpm rotating range) and two mounted cameras for viewing and recording. Furthermore, the unit is equipped with three temperature sensors (RTD PT100 sensor with three core Teflon tails, model TC02 SD145; accuracy of ± 0.03 °C): one temperature sensor to measure the temperature of the air bath surrounding the cell, one to measure the cell gas temperature, and one to measure the cell liquid temperature. The sapphire cell pressure is measured with a pressure transducer (model WIKA S-10; accuracy of ± 0.5 bar). Temperature, pressure, and stirrer current were recorded at 12 points per second through the computer’s Texmate Meter Viewer software.

In this research, the following materials were used: methane gas (purity = 99.995 mol%; obtained from BOC Company, Australia), MEG (purity = 99.9 mol%; obtained from Chem-supply Pty Ltd.); deionized water (electrical resistivity of 18 $\text{M}\Omega\cdot\text{cm}$ at 25 °C); nitrogen gas (purity = 99.99 mol%; obtained from BOC Company, Australia) for purging purpose; and FFCI and MDEA (purity \geq 99 mol%; obtained from Sigma-Aldrich Co. LLC).

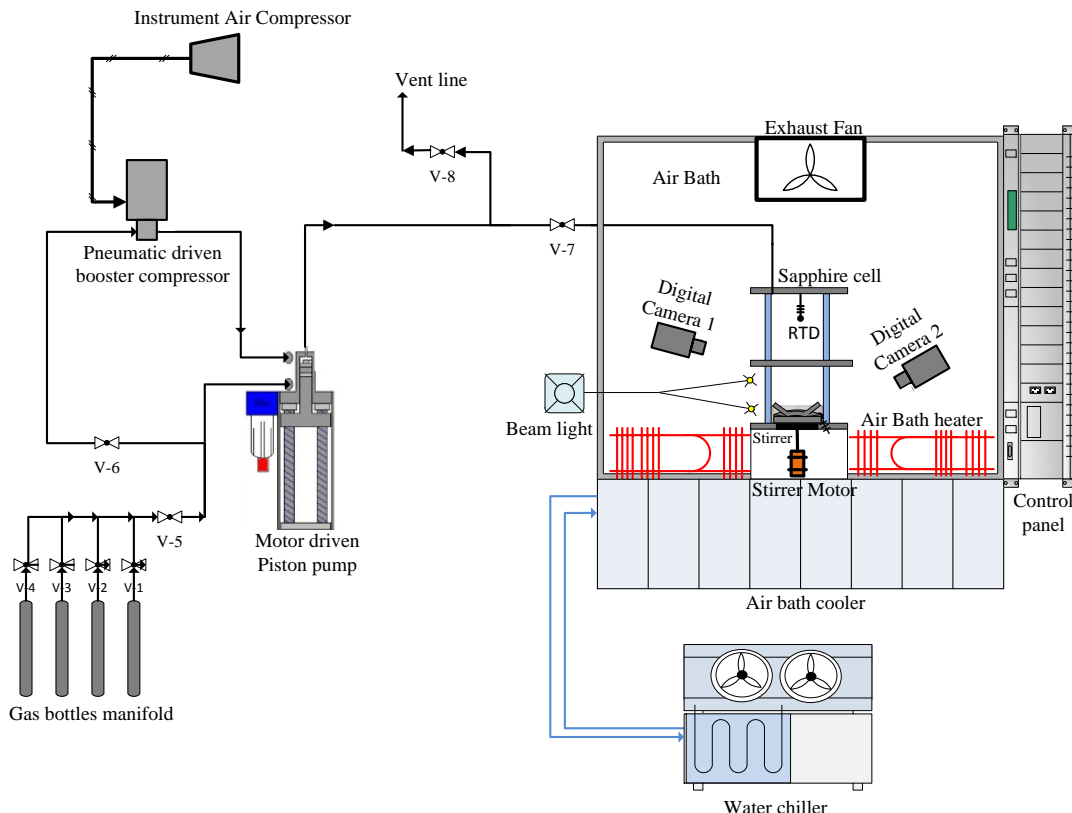


Figure 6-4 Schematic of the PVT unit.

The experimental solutions (Table 6-1 and Table 6-2) were prepared in the laboratory by mixing the ingredients in a glass beaker with a magnetic stirrer, and were weighed precisely using a high-accuracy self-calibration electronic balance (SHIMADZU UW/UX with a minimum display accuracy of 1 mg for 1,020 g).

6.3.2 Preparation of Thermally Exposed (Degraded) MEG Samples

The composition of the thermally exposed lean MEG solution (80 wt% MEG / 20 wt% deionized water) with MDEA and FFCI and their respective exposure temperatures were prepared as shown in Table 6-1. The MEG regeneration and reclamation operating temperature depends on many factors such as water

percentage, salt content, acidity, and associated components. The MEG solutions exposed to 135 and 165 °C were selected to reflect normal and worst case operating scenarios of the reboiler unit, while solutions exposed to 185 and 200 °C were selected to reflect the normal and worst case operating scenarios of the reclamer unit (Lehmann et al., 2014, Bikkina et al., 2012, Psarrou et al., 2011, King et al., 2015).

Table 6-1 Solution Matrix for Thermally Exposed Samples (AlHarooni,Pack, et al., 2016).

Solution	aqueous composition	exposure temperatures	exposure duration
A	lean MEG (80 wt % MEG / 20 wt % deionized water): 93.3 wt % MDEA: 6.7 wt%	135 °C	
B	lean MEG (80 wt % MEG / 20 wt % deionized water): 99.85 wt % FFCI (1500 ppm): 0.15 wt %	165 °C 185 °C	240 h
C	lean MEG (80 wt % MEG / 20 wt % deionized water): 93.16 wt % FFCI (1500 ppm): 0.15 wt % MDEA: 6.69 wt %	200 °C	

Solutions (A, B and C (AlHarooni,Pack, et al., 2016)) were prepared using an autoclave apparatus (high- temperature–high-pressure reactor) [Model 4532, 2 liters 316L (Parr Instrument Company)] as illustrated in Figure 6-5 and by the work of Pojtanabuntoeng et al. (2014). The solutions, once transferred into the autoclave, were sparged with high-purity nitrogen until the oxygen concentration dropped to 20 ppb. Subsequently, a heat jacket was placed around the autoclave and the system was heated to preselected temperatures for a set duration as shown in Table 6-1. After the heating process was completed, samples inside the autoclave were left to cool to room temperature, and then the solutions were transferred and stored in glass vials in an oxygen-free environment under a nitrogen cap to prevent oxidation reactions (Han et al., 1997).

Before the hydrate performance test was conducted, the solutions of Table 6-1 were further diluted with deionized water as shown in Table 6-2 to reflect the solution average concentration after the injection points during gas transportation. Typically, injected lean MEG concentration is 90 wt%, but it can get diluted to below 40 wt%.

inside the pipeline with water produced from the wells (Dugstad et al., 2003, Kim et al., 2014b, Halvorsen et al., 2009).

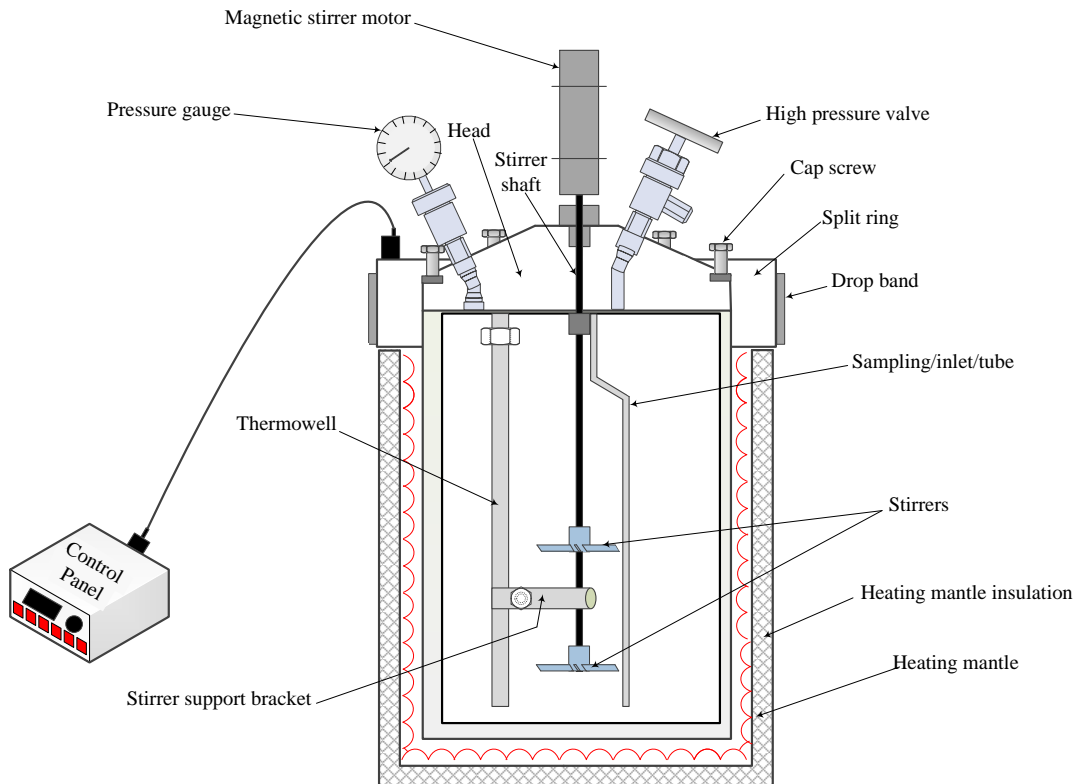


Figure 6-5. Schematic of the autoclave.

Table 6-2 Solution Matrix for Gas Hydrate Inhibition Performance Test (AlHarooni, Pack, et al., 2016).

solutions	diluted aqueous composition
A	deionized water (78 wt % = 5.46 g) MEG (20 wt % = 1.4 g) MDEA (2 wt % = 0.14 g)
B	De ionized water (79.99 wt % = 5.60 g) MEG (20 wt % = 1.4 g) FFCI (375 ppm = 0.01 wt% = 0.000656 g)
C	De ionized water (77.99 wt % = 5.46 g) MEG (20 wt % = 1.4 g) FFCI (0.01 wt % = 375 ppm = 0.000656 g) MDEA (2 wt % = 0.14 g)

6.3.3 Experiment Procedure

Prior to the experiment, the entire PVT unit was subjected to a pressure test using nitrogen gas at 100 bar (held for 1 h). The unit was vented, and the sapphire cell was thoroughly cleaned by acetone followed by cleaning with deionized water. Then the entire system was flushed twice with methane gas. Subsequently, the cell was injected with 7 ml of solution, and then methane gas was added by a piston pump at constant pressure mode (Wu et al., 2013, Najafi et al., 2014). Methane gas was loaded to the sapphire cell unit by a pneumatic booster pump to boost the gas from the four gas bottles (each having a capacity of 500 ml) to the electrically driven piston pump. Then, the piston pump is used to pressurize the sapphire cell to the required pressure. The piston pump is motor driven and is controlled by Mint Workbench V-5-Gas pump-pressure software (Figure 6-4).

The fluids were continuously agitated by the magnetic stirrer (at a constant rate of 530 rpm). The cell temperature was then gradually decreased at step changes of 0.5 °C / 20 min, which allowed sufficient time to achieve homogeneous temperature conditions for each temperature change. As hydrate started to form (Figure 6-6), it was left to continue forming until all liquid was fully converted to hydrate (Figure 6-7). Then, the dissociation process was started by gradually increasing the temperature at step changes of 0.5 °C / 20 min. Three sets of experiments were repeated four times to evaluate reproducibility. Before the experiments were repeated, the temperature was first raised to above 30 °C (which is significantly above the equilibrium temperature), and then step cooling commenced to avoid any influence of hydrate memory effect (Sefidroodi et al., 2013, Del Villano et al., 2011, Lee et al., 2006, Sadeq et al., 2017). More details on the experimental procedure are given elsewhere (AlHarooni et al., 2015, Sadeq et al., 2017).

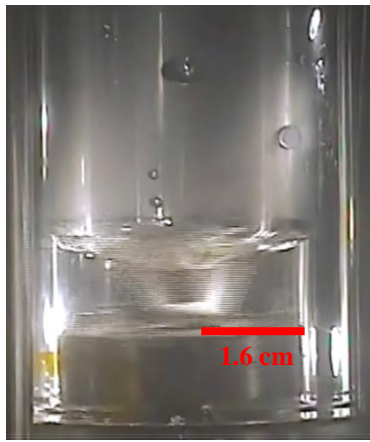


Figure 6-6. Start hydrates formation.

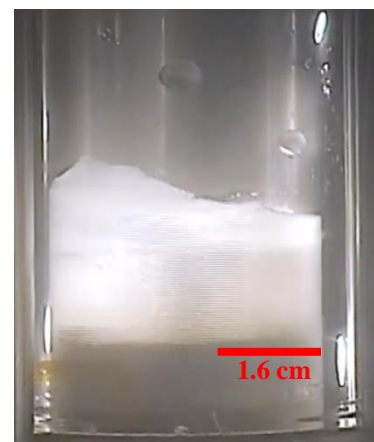


Figure 6-7. Hydrates full blockage.

6.3.4 Consistency of Results and Phase Boundary

Reproducibility of the experimental results is challenging when simply applying a subcooling process. The driving force for gas hydrate formation is not only a function of subcooling, but also a combination of many variables, such as cooling rate, water history, mixing efficiency, pressure stability, fluids compensation, etc. Arjmandi et al. (2005) conducted a study based on the work of Kashchiev et al. (2002) to analyze the driving force ($\Delta\mu$) of pure gas hydrate formation at isobaric conditions; they determined the driving force as

$$\Delta\mu = \Delta s_e \Delta T \quad \text{Eq 6-1}$$

where ΔT is the subcooling temperature and Δs_e is the entropy change in the transfer of one gas molecule from the hydrate crystal to the gaseous phase, which given by

$$\Delta s_e = n_\omega(P, T_e) s_\omega(P, T_e) - s_h(P, T_e) + s_{gg}(P, T_e) \quad \text{Eq 6-2}$$

where s_{gg} is the entropy per gas molecule in the gas phase, T_e the hydrate equilibrium temperature at pressure P , s_ω the entropy per water molecule in the water phase, s_h the entropy per hydrate-building unit in the hydrate crystal, and n_ω the number of water molecules at the given pressure and temperature.

Replicating the same hydrate formation points is challenging because of various factors contributing to the driving force as per Eq 6-1 and Eq 6-2. The hydrate formation experiments for solution A that were thermally exposed to 135, 165, 185 and 200 °C at a pressure of 200 bar and stirrer rotation rate of 530 rpm were

statically analyzed (each experiment was repeated three times); and we found that repeatability of hydrate formation points was good with a standard deviation value of ± 0.39 .

Once the hydrate formation–dissociation points were experimentally determined, the results were then compared to those in the literature and results predicted by Hysys software using the highly recommended equation of state (Peng–Robinson equation) (Peng et al., 1976, Hemmingsen et al., 2011) as shown in Figure 6-8.

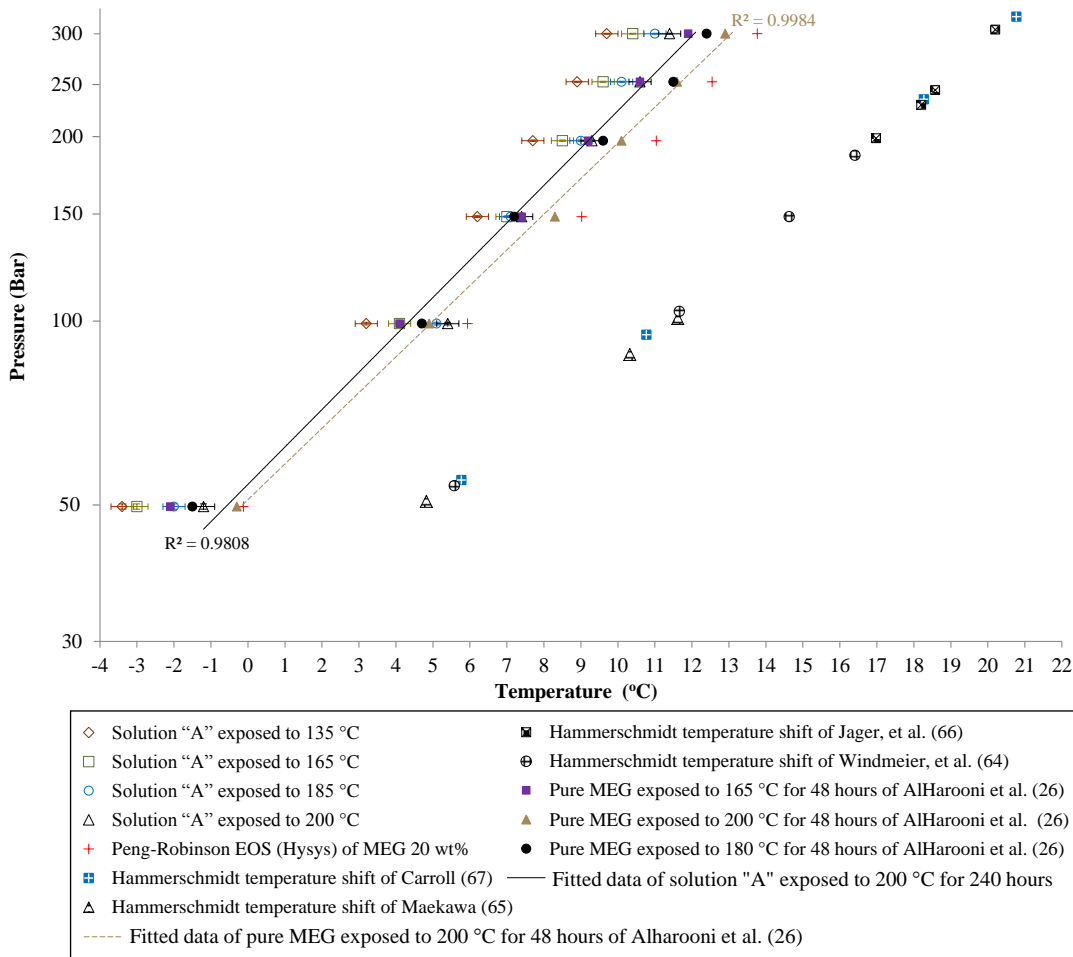


Figure 6-8 Hydrate formation locus of methane gas with solution A and literature data [with data of thermally degraded pure MEG (without MDEA or FFCI)], plotted using a semilogarithmic scale, as the logarithm of the hydrate formation locus has almost linear behavior.(Mohammadi et al., 2009) Literature data for pure MEG (without additives) is added to the figure for comparison (Windmeier et al., 2014a, Sloan et al., 2008a, Maekawa, 2001, Jager et al., 2001, Carroll, 2014, AlHarooni et al., 2015). The Hammerschmidt temperature shift prediction equation was obtained from Bai et al. (2005).

Metastable regions (6.4.4) were established by plotting the area bounded by the hydrate formation and hydrate start dissociation curves. Specifically, the metastable regions were computed by the definite integrals of the area under the curves for the four hydrate formation–dissociation temperatures as per below Eq 6-3

$$\text{Metastable region} = \int_a^c (f_F(x) - P_{min}) dx + \int_c^b (f_F(x) - f_D(x)) dx + \int_b^d (P_{max} - f_D(x)) dx \quad \text{Eq 6-3}$$

where; P_{min} is the minimum pressure, P_{max} the maximum pressure, a the hydrate formation temperature at P_{min} , b the hydrate formation temperature at P_{max} , c the hydrate start dissociation temperature at P_{min} , d the hydrate start dissociation temperature at P_{max} , $f_F(x)$ the hydrate formation curve function and $f_D(x)$ (AlHarooni,Pack, et al., 2016) the hydrate dissociation curve function.

For

Figure 6-2, the metastable region of methane gas hydrate of solution A exposed to 135 °C was computed as

$$\begin{aligned} \text{Metastable region} &= \int_{-3.4}^{2.2} (72.596 \exp^{0.1344x} - 50) dx \\ &+ \int_{2.2}^{10.6} (72.596 \exp^{0.1344x} - 35.434 \exp^{0.126x}) dx \\ &+ \int_{10.6}^{16.9} (300 - 35.434 \exp^{0.126x}) dx = 1519.05 \text{ bar.}^\circ\text{C} \end{aligned} \quad \text{Eq 6-4}$$

6.4 Results and Discussions

The study of the thermally degraded MEG (pure) on hydrate inhibition by AlHarooni et al. (2015) confirmed that MEG thermal degradation decreases the performance of hydrate inhibition by different rates depending on the degradation level. The higher the thermal exposure temperature, the higher the reduction of the inhibition performance. This is mainly due to the formation of degradation products: formic acid, acetic acid, and glycolic acid (AlHarooni et al., 2015, AlHarooni,Pack, et al., 2016). Further gas hydrate experiments were conducted for analyzing the nucleation behavior of methane gas hydrate with pure MDEA and FFCI solutions at different

concentrations and pressure ranges. These experiments were conducted to assess the effect of MDEA and FFCI on the MEG hydrate profile.

There is a lack of literature in the area of hydrate phase boundary of the thermally degraded MEG with MDEA and FFCI. The hydrate phase boundaries were plotted to fill this gap and to enhance the knowledge of thermodynamic stability of gas hydrate under these degradation conditions, which is crucial to flow assurance strategies.

6.4.1 Effect of Thermally Degraded MEG on Hydrate Inhibition Performance

It is worth noting here that there is a lack of data in the literature of hydrate kinetics of thermally degraded MEG with inhibitors, and the only literature reports are from our previous works AlHarooni et al. (2015) and AlHarooni,Pack, et al. (2016). Therefore, it is vital to generate referenced experimental data for these solutions; allowing the investigation of inhibitor characteristics and the validation of predictive models. Furthermore, this study also provides input information to flow assurance engineers in terms of predicting hydrate inhibition drift once MEG is overheated during the MEG regeneration and reclamation process. We thus tested methane gas hydrate formation characteristics for thermally exposed MEG–MDEA–FFCI solutions (Table 2) for a pressure range from 50 to 300 bar. Literature and Hysys software results (Peng–Robinson EOS) show some deviation from this work. This is mainly because no consideration has been given to MEG thermal degradation and additions of corrosion inhibitors, as referenced in Figure 6-8.

The results clearly show that thermally degraded MEG with additives (MDEA and/or FFCI) inhibited hydrates more efficiently than MEG without additives, as shown in Figure 6-8 to Figure 6-12. This is mainly due to the additional inhibition effect of the MDEA and FFCI, as discussed in 6.4.2 and 6.4.3.

While the results for the hydrate inhibition performance of solution A exposed to 200 °C (solid line) are compared with that of thermally degraded pure MEG (without MDEA or FFCI) (dashed line), Figure 6-8, it is evident that solution A caused the hydrate formation points to deviate toward the left side of the curve by an average of 0.85 °C, which indicates better hydrate inhibition performance. Exposing the solution to higher temperature, shifted the original methane hydrate phase boundary to lower pressure and higher temperature which indicates a drop of the inhibition performance. This is due to the increase in the amount of complex degradation

products (such as formic acid, acetic acid, and glycolic acid) in the solution by thermal degradation; (AlHarooni et al., 2015, Liu et al., 2015, Psarrou et al., 2011, Madera et al., 2003, Rossiter Jr et al., 1985, Rossiter et al., 1983, AlHarooni, Pack, et al., 2016) see also the work of Chakma et al. (1997) and Chakma et al. (1988) who identified MDEA degradation products.

6.4.1.1 Solution A

Results for the influence of solution A (deionized water 78 wt%, MEG 20 wt%, and MDEA 2 wt%) on methane gas hydrate formation is illustrated in Figure 6-9. Results were fitted with a polynomial curve, $R^2 > 0.997$. Solution A exposed to 135 °C showed the best inhibition performance compared to those exposed to higher temperatures (165, 185 and 200 °C), as hydrate formation process become more active with solutions exposed to higher temperatures, as indicated in Figure 6-9 and Table 6-3.

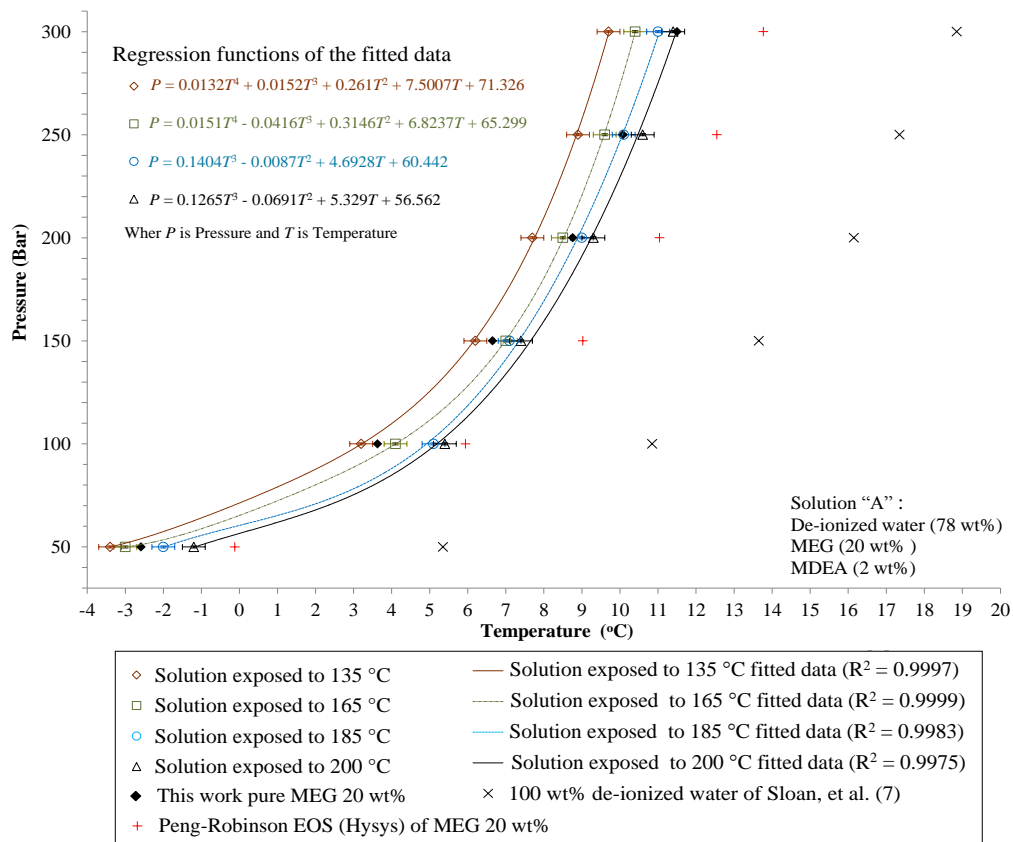


Figure 6-9 Hydrate formation locus of methane gas with solution A and regression functions of fitted data.

Table 6-3. Solution A: Hydrate Depression Temperature^a Due to Thermal Degradation

pressure (bar)	hydrate depression temperature (ΔT_d)			
	from 135 to 165 °C	from 165 to 185 °C	from 185 to 200 °C	from 135 to 200 °C
300	+ 0.7	+ 0.6	+ 0.4	+ 1.7
250	+ 0.7	+ 0.5	+ 0.5	+ 1.7
200	+ 0.8	+ 0.5	+ 0.3	+ 1.6
150	+ 0.8	+ 0.1	+ 0.3	+ 1.2
100	+ 0.9	+ 1.0	+ 0.3	+ 2.2
50	+ 0.4	+ 1.0	+ 0.8	+ 2.2
Average	+ 0.7	+ 0.6	+ 0.4	+ 1.8

^aA higher positive depression temperature (ΔT_d) corresponds to a lower inhibition performance

Solution A exposed to 165 °C induced an increase of hydrate formation temperature (average of 0.7 °C) compared to the same solution exposed to 135 °C. Hydrate formation temperature of the solution exposed to 200 °C induced an increase of hydrate formation temperature of an average of 1.8 °C compared to the same solution exposed to 135 °C. The solution exposed to 185 °C also showed similar behavior (Table 6-3). A higher hydrate formation temperature corresponds to a higher drop of hydrate inhibition performance. The effect of MDEA as an inhibitor has been noticed here (solution A) when compared with pure MEG without MDEA that was thermally exposed to the same temperature. This is due to the function of MDEA as hydrate inhibitor (Hossainpour, 2013, Davoudi, Heidari, et al., 2014). To study this further, we investigated how pure MDEA behaves as a gas hydrate inhibitor (section 6.4.2).

Throughout the gas hydrate experiments, hydrate nucleates were found to first stick to the liquid–gas interface, resulting in an accumulation of hydrate crystals on the cell wall near the interface level (Figure 6-10), consistent with Huo et al. (2001) and Taylor et al. (2007) and also consistent with the molecular dynamic simulation studies of Moon et al. (2003b). Hydrates form at the vapor–liquid interface because of the minimum in Gibbs free energy of nucleation (ΔG) and the high host and guest molecule concentration (Kashchiev et al., 2002).

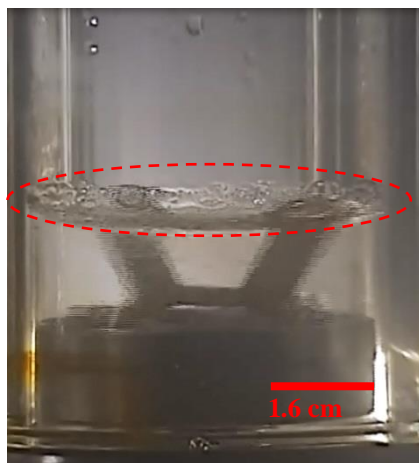


Figure 6-10 Hydrate formation at liquid–gas interface.

6.4.1.2 Solution B

Understanding the effect of thermally exposed solution of MEG with FFCI is of interest because of their wide use in tackling both gas hydrate and internal corrosion during various stages of hydrocarbon production (Liu et al., 2015, Anne Marie K. Halvorsen, 2007). The effect of thermally exposed MEG with additives on the kinetics of hydrate inhibition is poorly understood theoretically. In this section, experimental evaluation of hydrate formation for thermally exposed solution of MEG at 20 wt% with FFCI additive at 375 ppm (solution B) was conducted.

Results for solution B showed behavior similar to that of solution A. A noticeable increase in hydrate formation temperature occurred for the samples that were exposed to higher temperatures, which indicates a drop of inhibition performance as illustrated in Figure 6-11. This is due to the reduction of MEG purity by the increase of organic product concentration in the solution (Rossiter Jr et al., 1985, AlHarooni et al., 2015).

Solution B exposed to 135 °C showed better inhibition performance compared to those exposed to higher temperatures (165, 185 and 200 °C), as the hydrate formation process becomes more active with solutions exposed to higher temperatures, as shown in Figure 6-11 and Table 6-4.

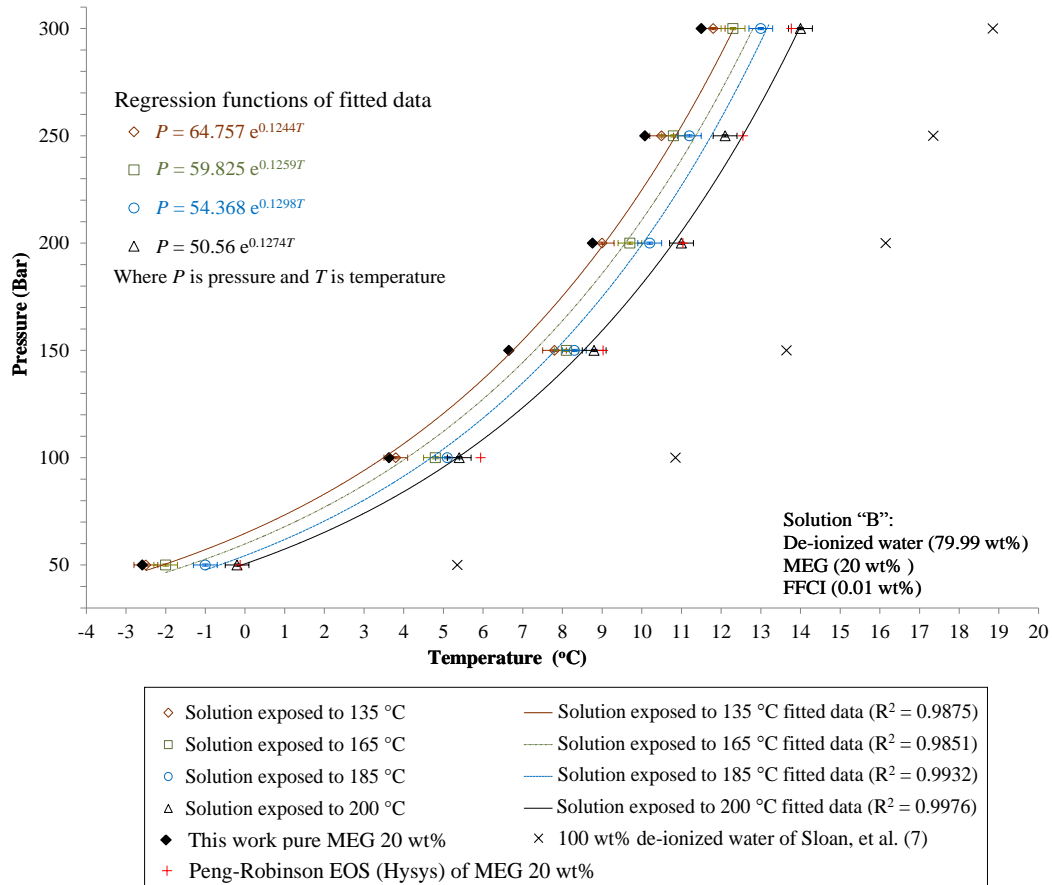


Figure 6-11 Hydrate formation locus of methane gas with solution B and regression functions of fitted data.

Table 6-4. Solution B: Hydrate Depression Temperature Due to Thermal Degradation^a

pressure (bar)	hydrate depression temperature (ΔT_d)				
	from 165 °C	to 185 °C	from 165 °C	to 200 °C	from 135 °C to 200 °C
300	+ 0.5		+ 0.7	+ 1.0	+ 2.2
250	+ 0.3		+ 0.4	+ 0.9	+ 1.6
200	+ 0.7		+ 0.5	+ 0.8	+ 2.0
150	+ 0.3		+ 0.2	+ 0.5	+ 1.0
100	+ 1.0		+ 0.3	+ 0.3	+ 1.6
50	+ 0.5		+ 1.0	+ 0.8	+ 2.3
Average	+ 0.6		+ 0.5	+ 0.7	+ 1.8

^aA higher positive depression temperature (ΔT_d) corresponds to a lower inhibition performance.

The influence of thermal degradation of a solution exposed to 165 °C compared to a solution that is exposed to 135 °C shows an increase of hydrate formation temperature of an average of 0.6 °C. The influence of thermal degradation on solution B exposed to 200 °C compared to a solution that was exposed to 135 °C shows an increase of hydrate formation temperature of an average of 1.8 °C, which corresponds to a drop of inhibition performance. Solution B exposed to 185 °C also showed similar behavior, as shown in Table 6-4.

6.4.1.3 Solution C

The use of solution C (MEG 20 wt %, MDEA 2 wt %, and FFCI 375 ppm) in the context of corrosion and hydrate controls is relevant to some specific cases such as sweet fields; during a changeover program of MEG/MDEA to MEG/FFCI modes, or vice versa; and in cases when MDEA alone cannot provide full corrosion control (Olsen, 2006, Latta et al., 2016, Glenat et al., 2004, Lehmann et al., 2014).

As presented in Figure 6-12 , the hydrate formation profile followed the pattern of solutions A and B, that is, formation temperature increased with increasing exposure temperature for the pressure range 50–200 bar. In general, solution C showed hydrate inhibition performance that was better than that of solutions A and B i.e., it shifted the hydrate curve to the left side by an average of 0.5 and 1.6 °C, respectively, caused by the synergistic inhibition effects of MEG, MDEA, and FFCI (Hossainpour, 2013, Davoudi, Heidari, et al., 2014). Inhibition effects of MDEA and FFCI have been demonstrated by the laboratory experiments in sections 6.4.2 and 6.4.3. At this point, no immediate explanation can be given for the FFCI inhibition phenomenon because its chemical composition is proprietary.

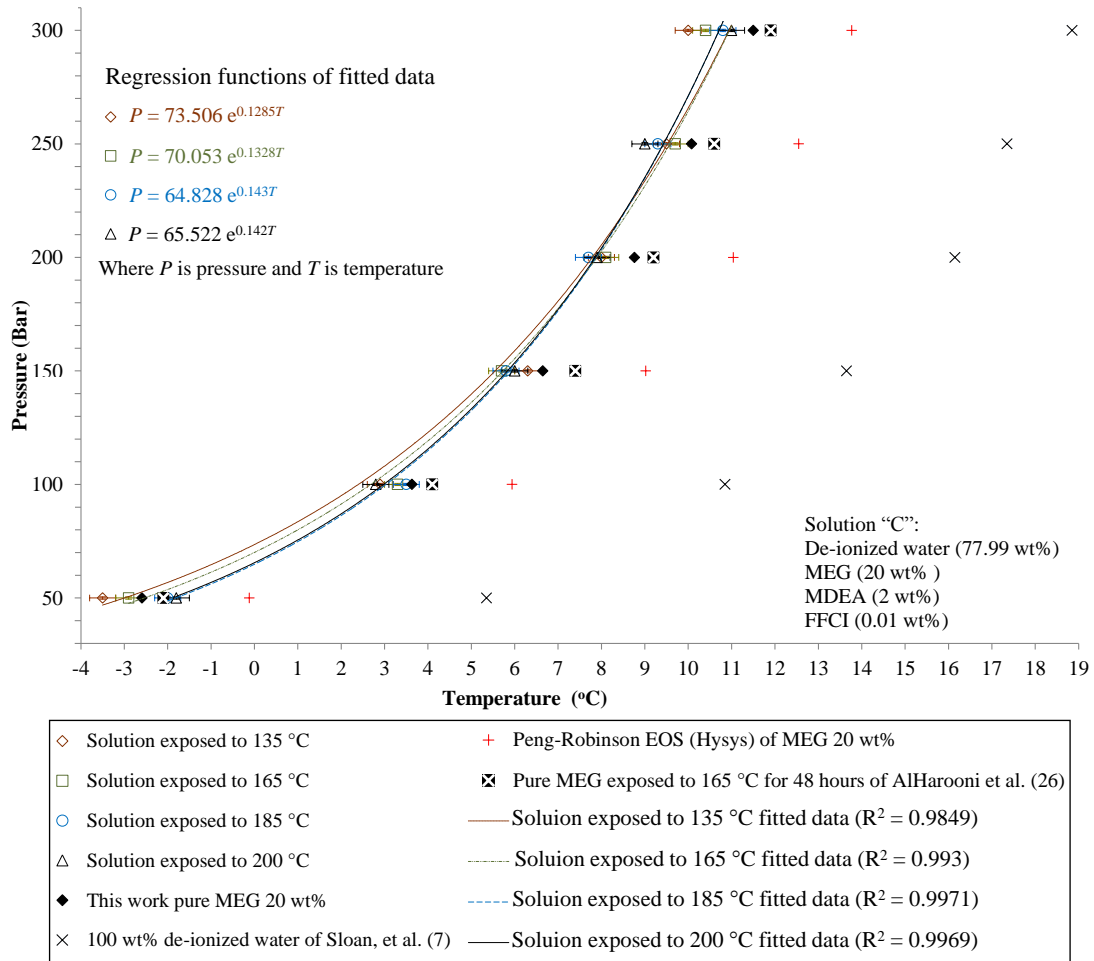


Figure 6-12 Hydrate formation locus of methane gas with solution C and regression functions of fitted data.

6.4.2 Effects of Pure MDEA on Gas Hydrate Formation

MDEA reacts exothermally with CO₂ and acids and thus generates heat, which has the potential to dissociate hydrate. Moreover, MDEA is highly soluble in water and so acts as a hydrate inhibitor. Once MDEA comes in contact with water, it creates strong hydrogen bonds, making the water cage less accessible for the guest gas molecule, which reduces the hydrate formation tendency (Hossainpour, 2013). The function of MDEA is to raise the pH by capturing H⁺ ions, thereby increasing the bicarbonate content of the medium. MDEA also captures the positive charge on the hydrogen of the neighboring water molecules, forms a strong hydrogen bond between MDEA and the water molecule, and thus functions as a thermodynamic inhibitor, which opposes the conversion of water molecules to hydrate (Davoudi, Heidari, et al., 2014).

Various MDEA concentrations in deionized water (5, 10, 15 and 25 wt %) were tested at pressures from 50 to 200 bar with methane gas to evaluate the hydrate inhibition performance (Figure 6-13). We observed a direct proportional relationship between MDEA concentrations and hydrate formation temperature. As MDEA concentration was increased, hydrate inhibition increased by shifting the hydrate formation curve to the left. However, pure MEG showed inhibition performance that was better than that of pure MDEA (Figure 6-13).

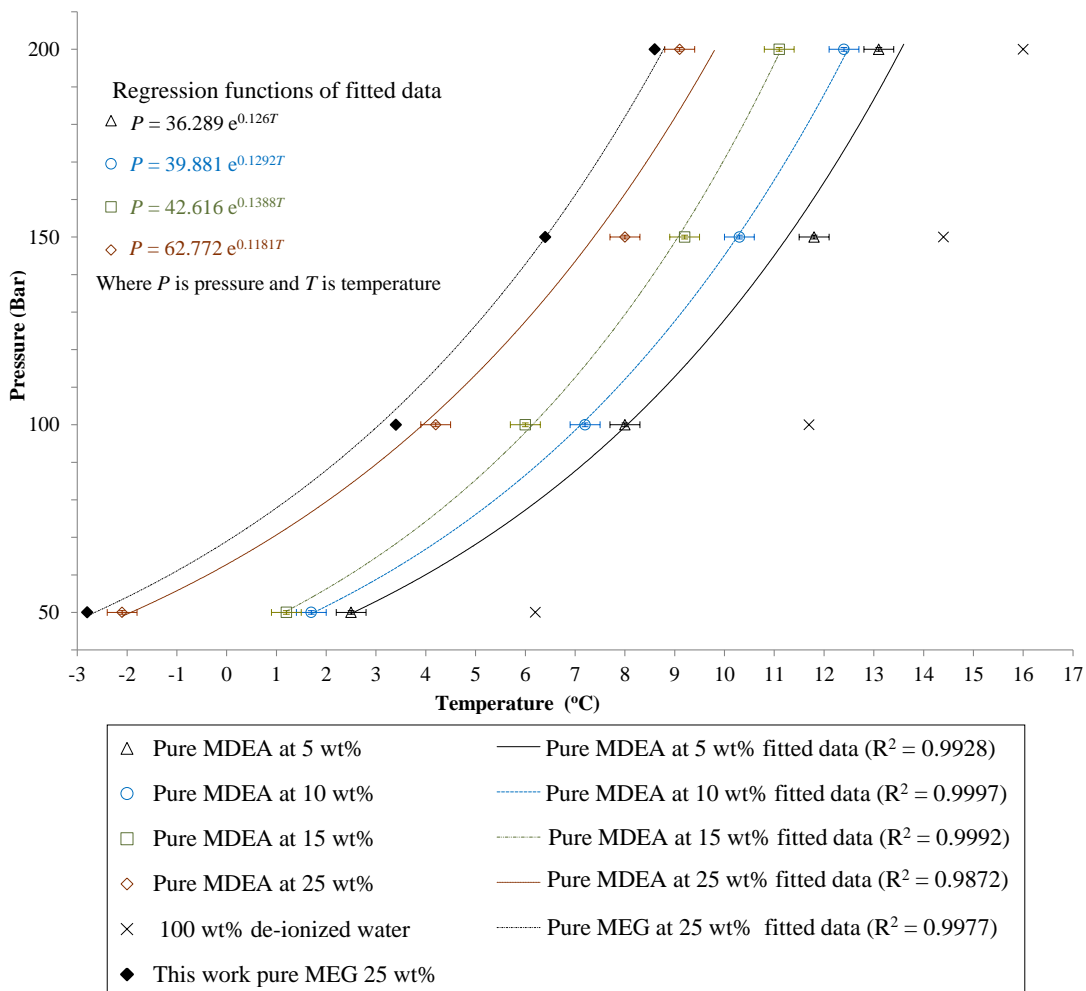


Figure 6-13 Hydrate formation locus of methane gas with pure MDEA at different concentrations and regression functions of fitted data.

6.4.3 Effects of Pure FFCI on Gas Hydrate Formation

Various FFCI concentrations (5 wt%, 10 wt%, 15 wt% and 25 wt% in deionized water) were tested at pressures from 50 to 200 bar with methane gas to evaluate FFCI hydrate inhibition characteristics. A directly proportional relationship between FFCI

concentration and methane hydrate formation temperature has been observed, Figure 6-14.

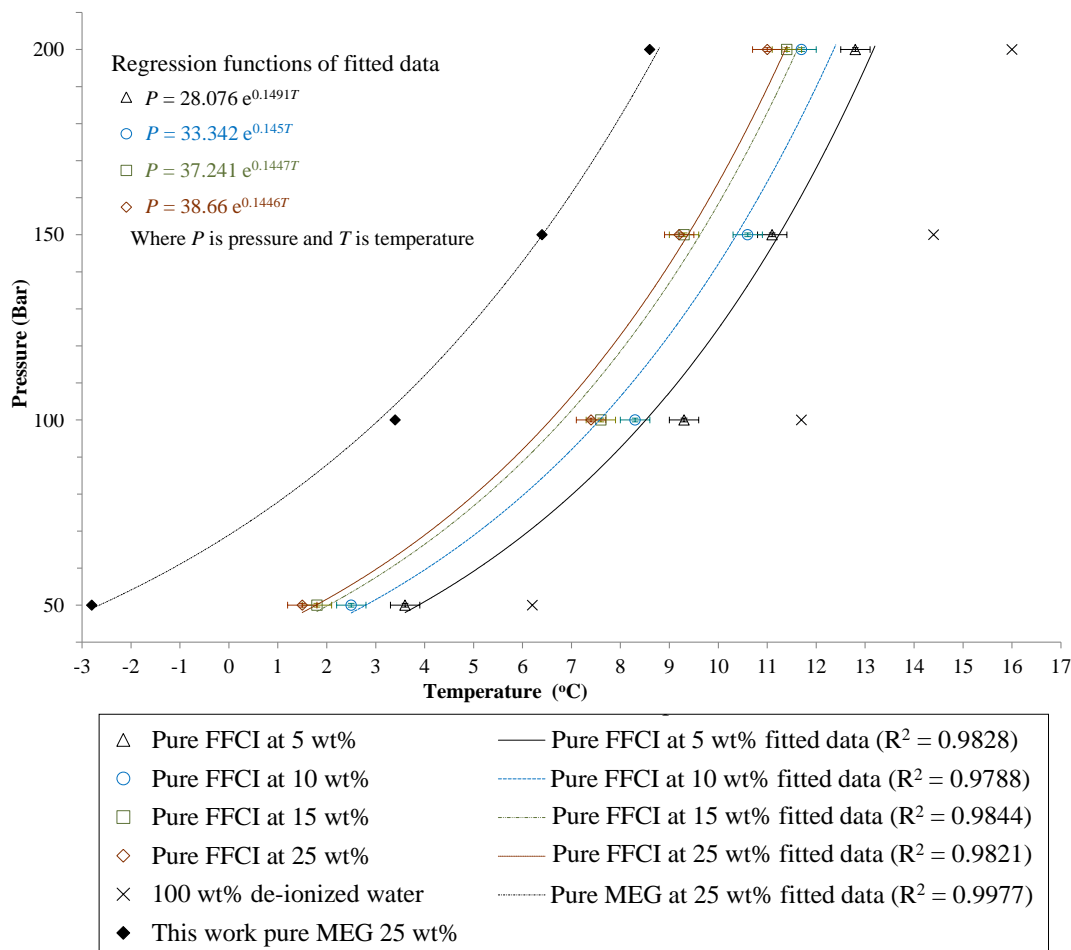


Figure 6-14 Hydrate formation locus of methane gas with pure FFCI at different concentration.

Overall, MDEA showed better hydrate inhibition performance than FFCI. Furthermore, it has been observed that FFCI has an antiagglomeration effect as it delays the time of full blockage by approximately 40% when compared to MDEA. Moreover, the hydrate inhibition performance of MDEA, FFCI, and other solutions (different composition and thermal exposure) was compared with that of 100 wt% deionized water at pressures from 50 to 200 bar (Table 6-5). When the results of the hydrate depression temperature of Table 6-5 are analyzed, it is observed that, at a concentration of 10 wt%, FFCI showed hydrate inhibition performance that was better than that of pure MEG but less than that of MDEA. As concentration increased to 25 wt%, pure MEG showed hydrate inhibition performance that was better than

that of pure MDEA and FFCI. Solution A and C showed superior hydrate inhibition performance (average ΔT_d of -8.7 °C).

Table 6-5. Methane Gas Hydrate Depression Temperature (given in ΔT_d versus deionized water) of Various Solutions at Different Pressures (sorted from poorest to highest inhibitor)^a

solutions	ΔT_d	pressure (bar)					average ΔT_d
		50	100	150	200		
pure MEG at 10 wt %	°C	-2.6	-2.1	-0.9	-0.6	-1.6	
pure FFCI at 10 wt %	°C	-3.7	-3.4	-3.8	-4.3	-3.8	
pure MDEA at 10 wt %	°C	-4.5	-4.5	-4.1	-3.6	-4.2	
pure FFCI at 25 wt %	°C	-4.7	-4.3	-5.2	-5.0	-4.8	
pure MDEA at 25 wt %	°C	-8.3	-7.5	-6.4	-6.9	-7.3	
solution B exposed to 135 °C	°C	-8.7	-7.9	-6.6	-7.0	-7.6	
pure MEG at 25 wt %	°C	-9.0	-8.3	-8	-7.4	-8.2	
solution A exposed to 135 °C	°C	-9.6	-8.5	-8.2	-8.3	-8.7	
solution C exposed to 135 °C	°C	-9.7	-8.8	-8.1	-8.0	-8.7	

^aThe higher the negative “ ΔT_d ” value corresponds to a better inhibition performance.

In this context, Obanijesu, Gubner, et al. (2014) conducted experimental work to evaluate the influence of various types of corrosion inhibitors on hydrate formation (2-mercapto pyrimidine, cetylpyridinium chloride, dodecylpyridinium chloride, thiobenzamide, benzyl dimethyl hexadecyl ammonium chloride), and they concluded that corrosion inhibitors do promote hydrate formation because of their surfactant properties and ability to form hydrogen bonding, which results in increasing gas contact with water molecules to assist in hydrate formation. The findings are in contrast with our findings for FFCI, as we found that adding FFCI inhibits hydrate formation by shifting the hydrate formation curve to the left (Figure 6-14). This is probably due to the difference in chemical compositions and inhibition physiognomies of the FFCI compared to the traditional corrosion inhibitors used in their experiments.

6.4.4 Hydrate Phase Boundary

Accurate knowledge of the thermodynamic stability of methane hydrates is crucial to flow assurance strategy. Consequently, we analyzed the hydrate phase boundary of thermally degraded MEG solutions.

Figure 6-2, and Figure 6-15 to Figure 6-17 show the hydrate phase boundaries for methane gas with solution A (thermally exposed at 135 to 200 °C), while Figure 6-18 and Figure 6-19 show results for solutions B and C (thermally exposed to 185 °C). The hydrate dissociation curve functions ($f_D(x)$) are obtained from AlHarooni,Pack, et al. (2016).

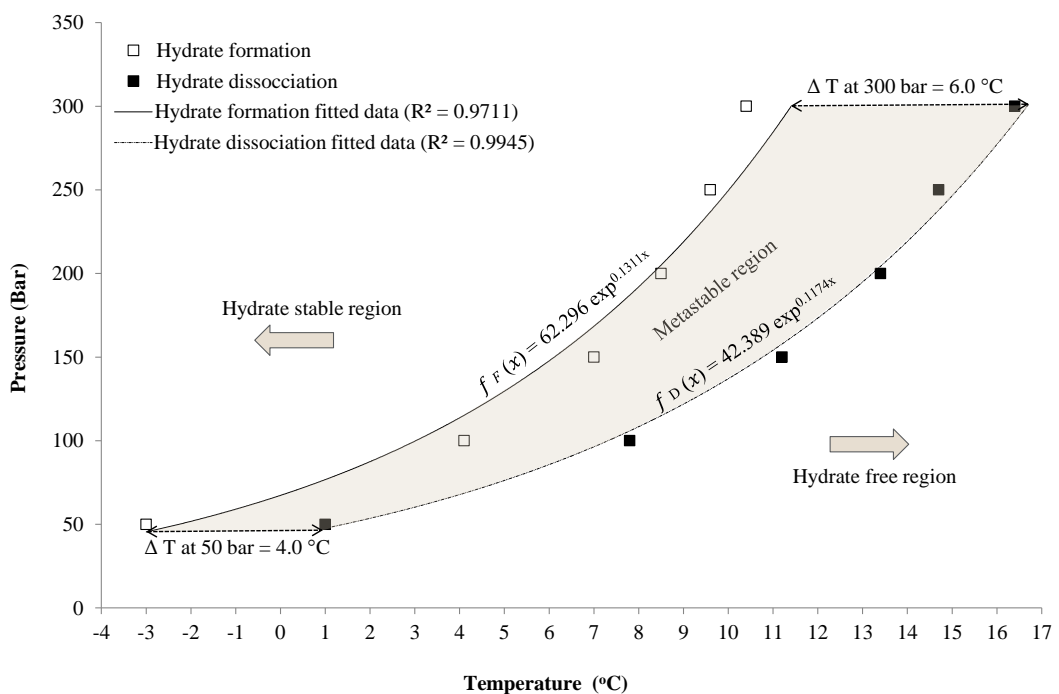


Figure 6-15 Methane gas hydrate phase boundaries of solution A exposed to 165 °C.

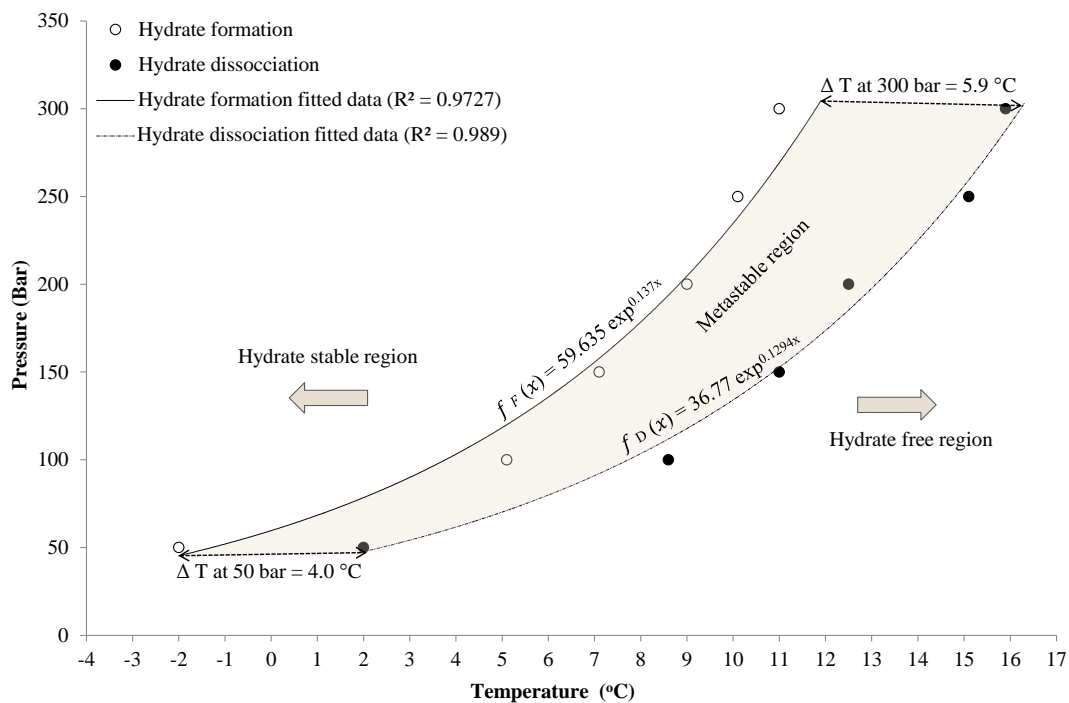


Figure 6-16 Methane gas hydrate phase boundaries of solution A exposed to 185 °C.

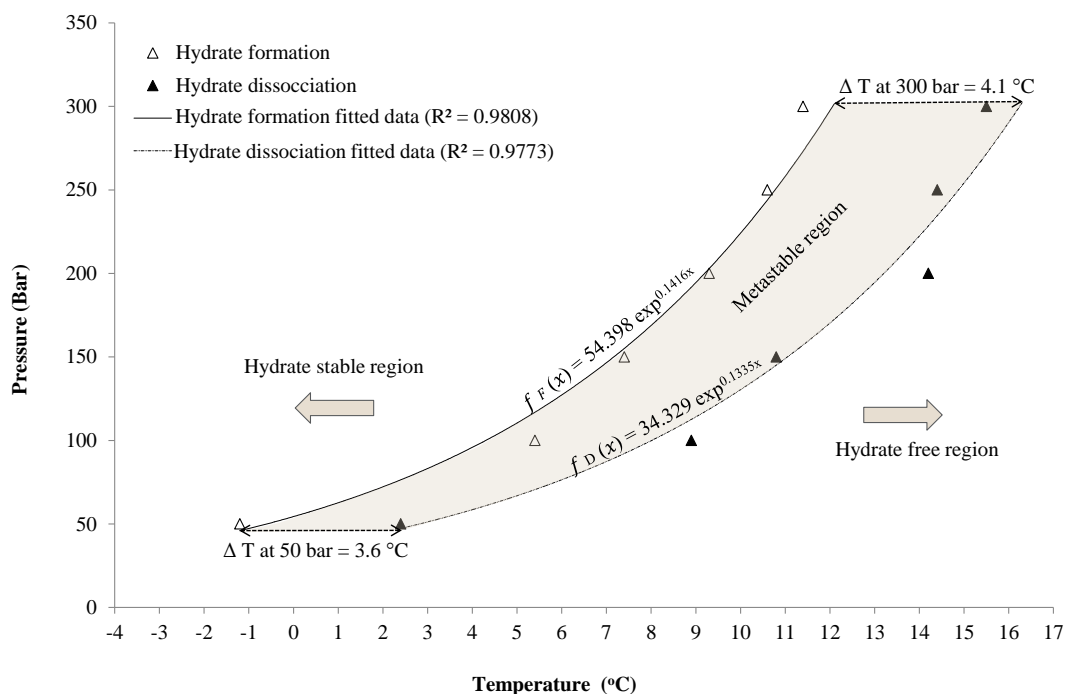


Figure 6-17 Methane gas hydrate phase boundaries of solution A exposed to 200 °C.

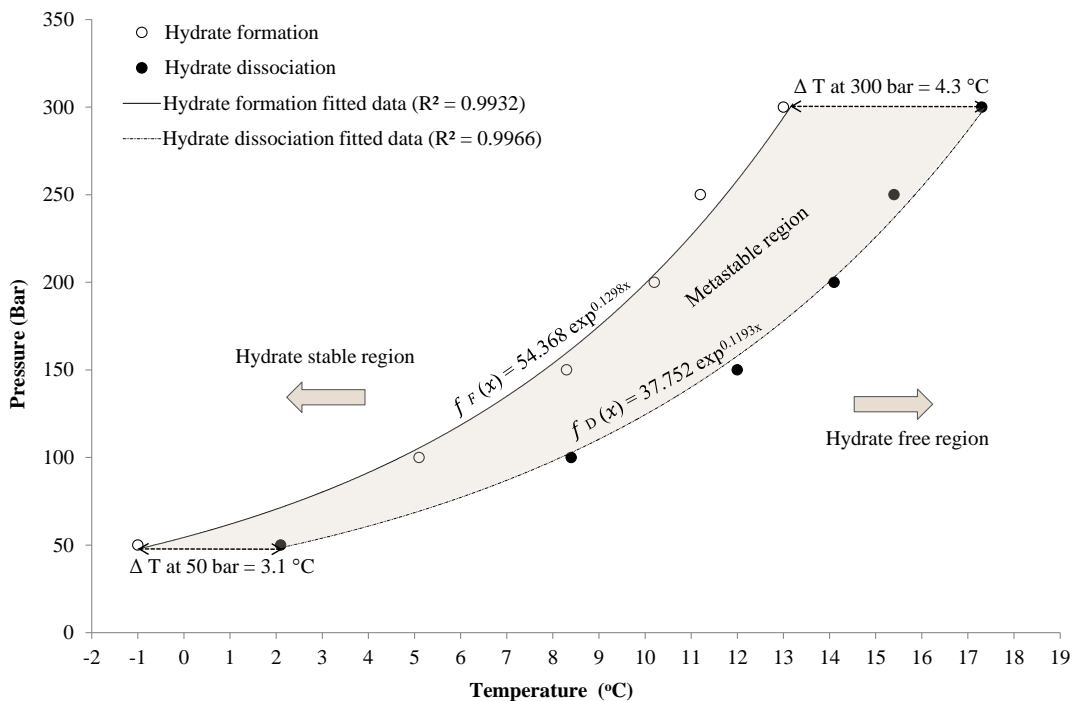


Figure 6-18 Methane gas hydrate phase boundaries of solution B exposed to 185 °C.

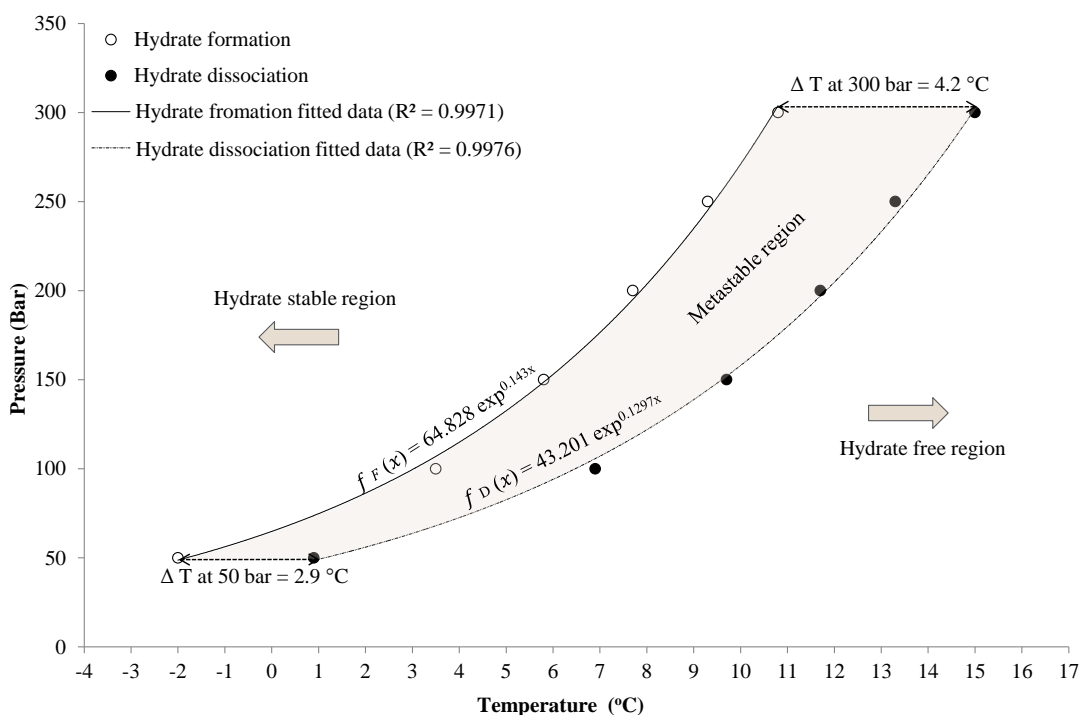


Figure 6-19 Methane gas hydrate phase boundaries of solution C exposed to 185 °C.

Generally, the metastable region was less pronounced at lower pressures [ΔT (hydrate formation temperature – hydrate dissociation temperature) at 50 bar is 5.6 °C, Figure 6-2] and more pronounced at higher pressures (ΔT at 300 bar is 6.8 °C,

Figure 6-2). Consequently, the hydrate dissociation temperature was higher than the hydrate formation temperature, consistent with Riestenberg et al. (2003) and Bai et al. (2005). This is because hydrate dissociation is endothermic, essentially requiring additional heat to break the hydrogen bonds and the van der Waals interaction forces between the water and gas molecules (Sloan et al., 2008a).

A summary of the hydrate phase boundaries is tabulated in Table 6-6. The table compares the calculated area of each metastable region. Interestingly, the size of the metastable region area varies inversely with exposed temperatures; the areas were larger for solutions exposed to lower temperatures (lower degradation) and smaller for solutions exposed to higher temperatures (higher degradation).

Table 6-6. Phase Boundary Region Areas (Figure 6-2 and Figure 6-15 to Figure 6-19)

solutions	metastable region areas (bar. $^{\circ}$ C)
Figure 6-2 :solution A exposed to 135 $^{\circ}$ C	1519.05
Figure 6-15: solution A exposed to 165 $^{\circ}$ C	1191.65
Figure 6-16: solution A exposed to 185 $^{\circ}$ C	1034.30
Figure 6-17: solution A exposed to 200 $^{\circ}$ C	975.89
Figure 6-18: solution B exposed to 185 $^{\circ}$ C	944.88
Figure 6-19: solution C exposed to 185 $^{\circ}$ C	942.10

6.5 Conclusions

The effect of thermally exposed MEG-additive mixtures on the kinetics of gas hydrate inhibition is poorly understood. However, MEG-MDEA and FFCI formulations are very significant, especially for sour gas fields (for both corrosion and hydrate control). Thus, we investigated the influence of thermally degraded MEG, MDEA, and FFCI mixtures on gas hydrate inhibition. Specifically, hydrate profiles and regression functions for methane gas were reported using the isobaric method for various mixtures for a pressure range from 50 to 300 bar, also with pure MDEA and FFCI at various concentrations (5, 10, 15 and 25 wt %) and a pressure range from 50 to 200 bar. The MEG formulations were thermally exposed to 135,

165, 185 and 200 °C for 240 h (Table 6-1 and Table 6-2). The results showed that thermally degraded MEG with corrosion inhibitors (MDEA and FFCI) reduces the performance of hydrate inhibition to different degrees depending on the thermal degradation level. The higher the exposure temperature, the higher the reduction in the inhibition performance (Table 6-3–Table 6-5). This is mainly due to the formation of acidic degradation products during thermal exposure (AlHarooni et al., 2015, AlHarooni,Pack, et al., 2016).

Thermally degraded MEG with additives (MDEA and/or FFCI) inhibited hydrate formation more efficiently than thermally degraded MEG without additives. Solution C (MEG–MDEA–FFCI) showed the best hydrate inhibition performance, because of the additional synergistic hydrate inhibition effect of both MDEA and FFCI, (Hossainpour, 2013, Davoudi,Heidari, et al., 2014) followed by solution A (MEG–MDEA) and then solution B (MEG–FFCI). Solution A showed better inhibition than solution B because of the higher hydrate inhibition effect of MDEA compared to FFCI. The hydrate depression temperature caused by MEG thermal degradation was around + 2 °C (Table 6-3 and Table 6-4) and showed a consistent hydrate profile; MEG exposed to higher temperatures reduced inhibition efficiency due to the degradation effect. However, although the magnitudes of these differences in hydrate depression temperature are small, they provide valuable information for the design of MEG plants, evaluating the corrosion control of the organic acids developed from the thermal degradation process and calculating MEG injection rate. The MEG injection rate is calculated intentionally with big margin based on the worst case scenario, including the highest of seasonal temperature variation, pressure variation, change of gas composition, change of water content, and change of lean MEG concentration. Including the MEG degradation phase boundary shift will provide a useful factor to maintain the MEG injection margin (Bonyad et al., 2011).

Furthermore, we observed a direct proportional relationship between pure MDEA and FFCI concentrations and hydrate inhibition, i.e., as concentration increased, hydrate inhibition performance increased. This relationship proves that they function as a thermodynamic hydrate inhibitor (Figure 6-13 and Figure 6-14). However, thermodynamic hydrate inhibitor function of MDEA is better than that of FFCI but less than that of pure MEG, as can be clearly established from Table 6-5. Solution of 25 wt% MDEA shows less hydrate depression temperature by 0.9 °C compared to 25

wt% MEG (i.e., equivalent to 89% performance of MEG), while the solution of 25 wt% FFCI shows less hydrate depression temperature by 3.4 °C compared to 25 wt% MEG (i.e., equivalent to 58% performance of MEG). The reported hydrate phase boundary shifts of MDEA and FFCI are considered as newly reported data to the best of our knowledge; in that vein, further investigations should be conducted to test the thermodynamic functions of MDEA and FFCI in the presence of pure MEG. Findings from these tests influence the calculation of MEG injection rate for hydrate control and calculating hydrate phase boundary. Interestingly, FFCI showed antiagglomeration effects as it delayed the time of full blockage (compared to MDEA by almost 40%).

In addition, because there is a lack of literature in the area of hydrate phase boundaries of gas hydrate with thermally degraded MEG–MDEA–FFCI formulations, hydrate phase boundaries were plotted to enhance the knowledge of thermodynamic stability of gas hydrates for these mixtures. This is crucial to outline the flow assurance strategy for safe operation. Generally, the metastable regions were smaller at lower pressure and broadened as pressure increased. The area covered by each metastable region was calculated, and interestingly the metastable region varied inversely with exposure temperature, i.e., larger areas were found for solutions exposed to lower temperatures and smaller areas for solutions exposed to higher temperatures.

In summary, this study has brought a new focus to the relationship between gas hydrate profiles for thermally degraded MEG formulated with corrosion inhibitors (MDEA–FFCI) and for pure MDEA and FFCI. These results show that exposing MEG solutions to higher temperatures (> 135 °C) leads to an increase in the hydrate formation temperature (thus reducing hydrate inhibition performance). We conclude that MDEA and FFCI corrosion inhibitors also react as thermodynamic hydrate inhibitors.

ABBREVIATIONS

- MEG = Mono-ethylene Glycol
- MDEA = Methyl Di-Ethanolamine
- FFCI = Film Formating Corrosion Inhibitor
- CAPEX = Capital Expenditure Cost
- EOS = Equation Of State
- PPM = Part Per Million
- PVT = Pressure Volume Temperature
- RTD = Resistance Temperature Detector.
- THI = Thermodynamic Hydrate Inhibitor

Chapter 7 Analytical Techniques for Analyzing Thermally Degraded Monoethylene Glycol with Methyl Diethanolamine and Film Formation Corrosion Inhibitor

7.1 Abstract (Figure 7-1)

Gas hydrate formation and corrosion within gas pipelines are two major flow assurance problems. Various chemical inhibitors are used to overcome these problems, such as monoethylene glycol (MEG) for gas hydrate control and Methyl Diethanolamine (MDEA) and film formation corrosion inhibitor (FFCI) for corrosion control. As an economical solution, MEG is regenerated due to the large volume required in the field. MEG regeneration involves thermal exposure by traditional distillation to purify the MEG. During this process MEG is subjected to thermal exposure and so might be degraded. This study focuses on evaluating six analytical techniques for analyzing the degradation level of various MEG solutions consisting of MDEA and FFCI that were thermally exposed to 135 °C, 165 °C, 185 °C and 200 °C. The analytical techniques evaluated are pH measurement, electrical conductivity, change in physical characteristics, ion chromatography (IC), high performance liquid chromatography – mass spectroscopy (HPLC-MS), and gas hydrate inhibition performance (using 20 wt% MEG solutions with methane gas at pressure from 50 to 300 bar). Most of the analytical techniques showed a good capability, while electrical conductivity showed poor result for solution without MDEA and IC showed poor results for solution exposed to 135 and 165 °C. The primary aim of this paper is thus to provide the industry with a realistic evaluation of various analytical techniques for the evaluation of degraded MEG solutions and to draw attention to the impact of degraded MEG on gas hydrate and corrosion inhibition as a result of the lack of quality control.

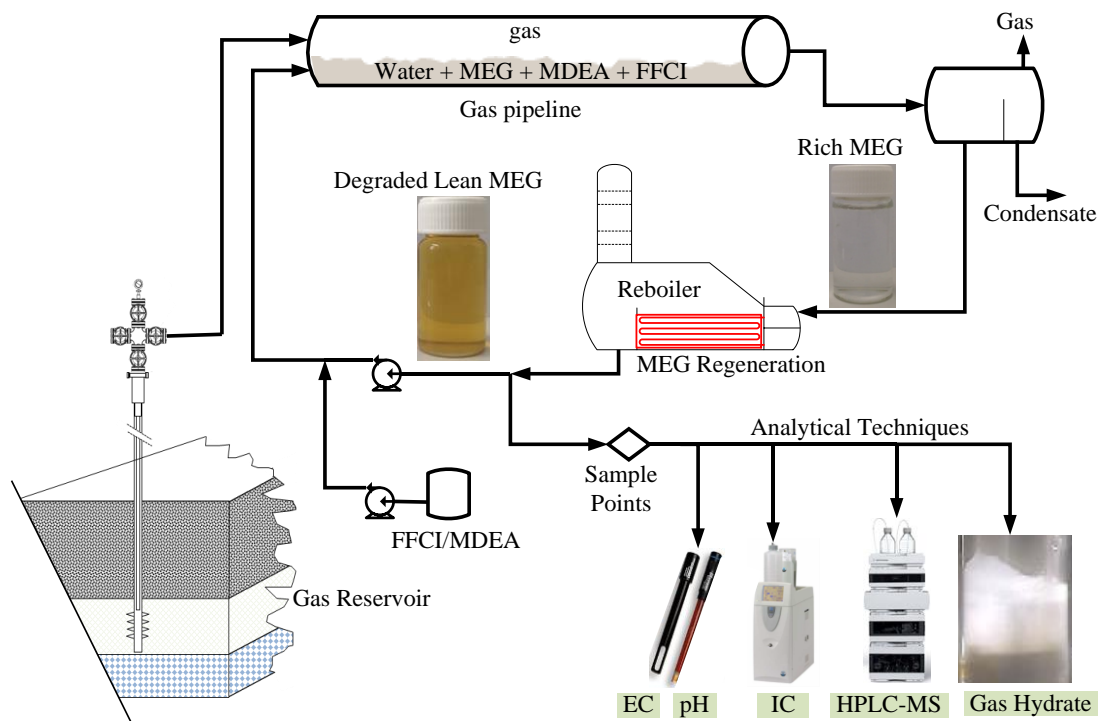


Figure 7-1 Abstract Graphics

7.2 Introduction

Transportation of wet gas in carbon steel pipelines results in hydrate and internal corrosion flow assurance challenges. Gas hydrates occur under high pressure–low temperature conditions, when water forms a cagelike structure around the guest molecules (e.g., methane, ethane, propane, nitrogen, isobutane, normal butane, hydrogen sulfide, carbon dioxide, etc.), (Yousif, 1994). The main cause of the corrosive nature of various produced fluids, including formation brines, organic acids, and acid gases (H_2S and CO_2) (Sandengen et al., 2007, Menendez et al., 2014, Davoudi, Heidari, et al., 2014).

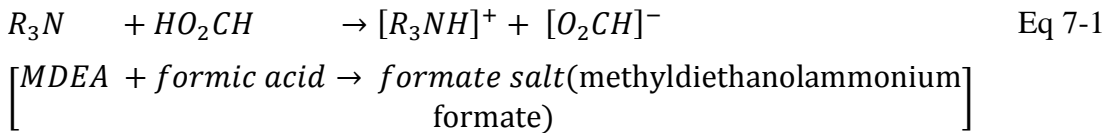
To avoid hydrate formation, thermodynamic hydrate inhibitors (such as monoethylene glycol (MEG)) are used. Internal corrosion can be controlled by implementing corrosion control strategies such as injection of film formation corrosion inhibitors (FFCIs) or pH stabilizers (e.g. methyl diethanolamine (MDEA)). Hydrate and corrosion inhibitors are used in the gas field separately or comingled (especially for wet sour gas fields), as shown in Figure 7-2. When they are used together, it is recommended to perform compatibility tests to evaluate any undesirable effect (e.g., foaming, emulsification, or promotion of hydrate formation or corrosion), (Menendez et al., 2014, Moloney et al., 2009, Achour et al., 2015).

The most commonly used corrosion control method is pH stabilization, where MDEA is added to the lean MEG solution to lower the corrosion rate by formation of a protective FeCO_3 layer on the pipeline wall (Dugstad et al., 1994, Zheng et al., 2016). However, MDEA increases the scaling rate of the process facilities (Hajilary et al., 2011). Thus, selection of MDEA and/or FFCI depends on several factors, including water breakthrough, emulsion formation, scaling and corrosion rate. Commonly, FFCI is used during field start up and when there is a significant risk of scale build up (Glenat et al., 2004, Dugstad et al., 2004, Davoudi, Heidari, et al., 2014).

When gas field facilities operate at gas hydrate formation conditions, typically a large amount of MEG is injected. To help counteract the high cost of this injection, MEG regeneration and reclamation are used to remove water and soluble salts in order to have economical solutions for sustainable production (Brustad et al., 2005, Gizah et al.) (Figure 7-2).

The rich MEG solution received from the pipeline (~ 25–60 wt% MEG) is heated in a distillation column to reconcentrate it to 80–90 wt% MEG for reinjection. Typically, the distillation column operates just above the atmospheric pressure and temperatures ranging from 120 to 150 °C. The lean MEG (above 80 wt%) from the regeneration unit is then routed to the reclaimer unit, which operates under vacuum (~ 150–100 mbar) and at temperatures ranging from 125 to 155 °C. The reclaimer increases MEG purity by removing salts and other contaminants, which prevents fouling and deposition of the process equipment (Psarrou et al., 2011, Bikkina et al., 2012). The main challenge during MEG (regeneration/reclamation) is thermal MEG degradation caused by reboiler overheating. Thermal degradation causes various problems such as fouling, efficiency drop, foaming, pH drop, and corrosion (Bikkina et al., 2012, AlHarooni et al., 2015, Madera et al., 2003, Clifton et al., 1985). For instance, it has been reported by Clifton et al. (1985) that after heating ethylene glycol for 140 days at different temperatures (75, 86, and 101 °C), the pH value dropped from 7.8 to 4.8 at 75 °C, to 4.3 at 86 °C, and to 2.4 at 101 °C. Such drops in pH indicate that the solution undergoes a degradation process. This means that MEG cannot be recycled via the normal process and that further processing, such as activated charcoal filtration or vacuum distillation, is required (Elhady, 2005). However, MDEA has a good thermal stability and so can be regenerated with MEG, thus reducing the complexity of pH neutralization (Lehmann et al., 2014).

Amine (e.g., MDEA) solutions are used in gas processing as a sweetening agent and absorption solvent to reduce the corrosion rate by removing acid gases (such as H₂S and CO₂) from the produced gas (Liu et al., 2015, Qian et al., 2010, Herslund et al., 2014). Acids in the pipeline come either directly from the reservoir fluid or stem from degraded MEG (e.g., acetic and formic acids). In addition, research conducted by Choi et al. (2010) and Cummings et al. (2007) confirmed that absorber reactions of acids and MDEA result in the formation of stable salts as shown below:



Another concern associated with MDEA besides salt formation is foam formation, as observed in this work. Foaming can cause solution loss, off-specification product gas, high operating costs and production decline (Liu et al., 2015). Foaming does not occur in the clean uncontaminated MDEA, but is caused by contaminants (e.g., feed gas, water, oxygen ingress, and acidic degradation and corrosion products) (Kohl et al., 1997, Al Dhafeeri, 2007). In this work, foaming was observed for the MEG–MDEA solutions both at atmospheric and at high pressure conditions. In addition, the quantity of organic acids developed by MEG degradation increased proportionally with increasing exposure temperature, which in turn also increased foaming levels (Yanicki et al., 2006).

In general, there are three main amine degradation processes: (1) oxidative, (2) reaction with CO₂, and (3) thermal degradation. An experimental study conducted by Chakma et al. (1997) evaluated the degradation mechanism of MDEA under CO₂ blanketing and thermal exposure up to 230 °C. They found that MDEA degrades when it reacts with CO₂ and water as per Figure 7-2 below:



The rate of the MDEA degradation is slower when exposed to temperatures below 120 °C while it increases with increasing temperature. Chakma et al. (1997) advised not to exceed 120 °C of MDEA reboiler temperature. Liu et al. (2015) conducted an investigation on the effect of degradation products on the foaming behavior of a 50 wt% MDEA solution. They concluded that MDEA degradation products promote

foam formation and that the foam properties were also influenced by viscosity, surface tension, density, and pH values.

Film forming corrosion inhibitors (FFCIs) are essentially cationic species which are widely used in the oil and gas industry (Graham et al., 2002). Phosphate esters are the main FFCI types used in the hydrocarbon industry (Alink et al., 1999), however, specific FFCI chemical formulations are typically confidential (Moore et al., Achour et al., 2015). Thus Achour et al. (2015) analyzed the chemical composition of a common FFCI using liquid chromatography mass spectroscopy (LCMS), and they detected 32 compounds, which confirms the complexity of FFCI formulations. In this work, the FFCI components have not been investigated, but we rather focused on analyzing its effect on gas hydrate performance and how it contributes to thermal degradation when mixed with MEG and MDEA.

Electrical conductivity measurement, i.e. the ability of an aqueous solution to carry an electrical current, is an extremely widespread and useful monitoring method, especially for quality control purposes. Reliable and accurate electrical conductivity measurements depend on a number of factors, such as the concentration and mobility of ions, the presence of organic alcohols and sugars, the valence of ions, temperature, etc. (Cammann et al., 2000). Bonyad et al. (2011) analyzed salt-organic inhibitor concentrations via electrical conductivity measurements for samples taken from a MEG regeneration unit, offshore platform inlet and slug-catcher outlet.

Degraded MEG solutions and corrosion inhibitors additives influence the thermodynamic gas hydrate stability (Hoppe et al., 2006, Lehmann et al., 2014, Obanijesu,Gubner, et al., 2014). In this research, the hydrate dissociation profile was analyzed, as hydrate dissociation is a sequence of lattice destruction (Bishnoi et al., 1996, Sloan et al., 2008a) considered as the thermodynamic equilibrium point and is repeatable (Tohidi et al., 2000).

Several MEG degradation studies focused on corrosion rate, identification of degradation products, thermal exposure effects, changes in pH values, and the effect of oxidation (Clifton et al., 1985, Rossiter Jr et al., 1985). In this research, monitoring and identifying the extent to which MEG degrades due to different temperatures and once mixed with FFCI and MDEA is studied. We evaluated six analytical techniques in terms of their efficiency to monitor and identify degradation levels of thermally exposed MEG–corrosion inhibitor (MDEA–FFCI) formulations. The six analytical techniques are pH measurement, electrical conductivity, changes

in the physical characteristics, ion chromatography (IC), high performance liquid chromatography–mass spectroscopy (HPLC–MS), and gas hydrate inhibition performance.

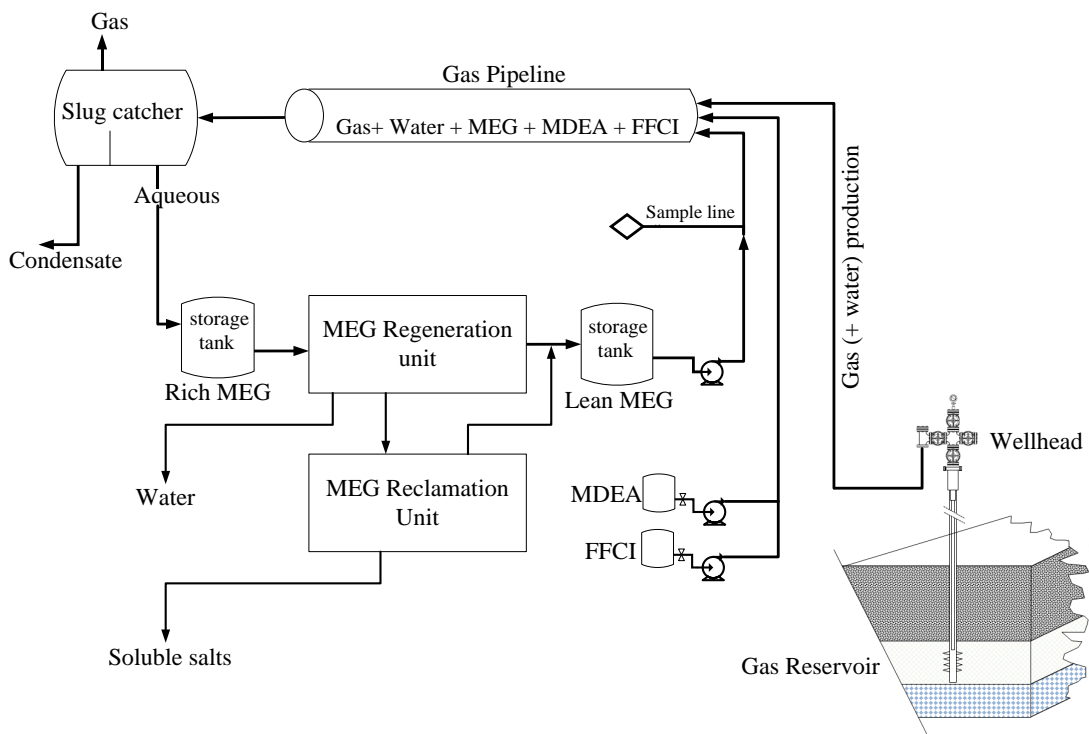


Figure 7-2 Overview of the MEG closed loop system.

7.3 Experimental Methodology

7.3.1 Materials

Monoethylene glycol (MEG) (obtained from Chem-supply Pty Ltd. with purity of 99.9 mol%); film forming corrosion inhibitor (FFCI) (obtained from Baker Hughes), methyl diethanolamine (MDEA) (obtained from Sigma-Aldrich Co. LLC. with purity of ≥ 99 mol%), methane (obtained from BOC Company, Australia, with purity of 99.995 mol%), deionized water (obtained from a reverse osmosis system with electrical resistivity of $18 \text{ M}\Omega\cdot\text{cm}$ at 25°C), and nitrogen (obtained from BOC Company, Australia, with purity of 99.99 mol%).

MDEA is a clear, pale yellow liquid with odor similar to ammonia, miscible with water, alcohol, and benzene; more properties of MDEA and MEG are shown in Table 7-1.

Table 7-1 MEG and MDEA Properties at Atmospheric Pressure (Aylward et al., 2008, Braun et al., 2001).

Name	Chemical Formula	Structure	Solubility in water	Melting Point °C	Boiling Point °C	Flash Point °C	Viscosity mPa.s (at 20 °C)	Density (at 20 °C) g/mL	Molar weight g/mol
MEG	C ₂ H ₆ O ₂		Miscible	-12.9	197.3	111	16.1	1.1132	62.07
MDEA	C ₅ H ₁₃ NO ₂		Miscible	-21.0	247.1	127	101	1.038	119.16

7.3.2 Experimental Procedure

7.3.2.1 Equipment

7.3.2.1.1 Autoclave

Thermal exposures of MEG solutions were prepared using a high temperature/high pressure autoclave (Model 4532, 2 L 316L by Parr Instrument Company); Figure 7-3.

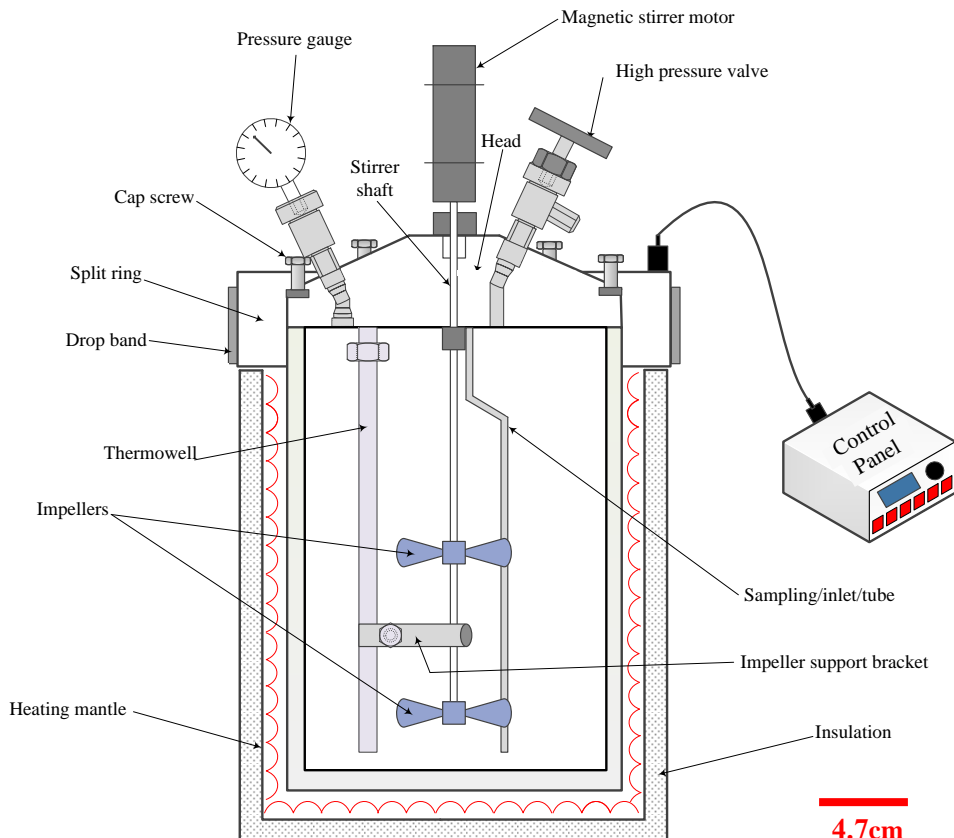


Figure 7-3 Autoclave sketch

7.3.2.1.1 Sapphire Cell Unit

The hydrate dissociation experimental setup used in this study has been described earlier elsewhere (AlHarooni et al., 2015). Briefly, the main part of the setup is the sapphire cell with a capacity of 60 cm³ (Figure 7-4), which operated from 50 to 300 bar pressure and at temperatures from +40 to -5 °C. The sapphire cell has a variable speed magnetic stirrer (operated at 530 rpm) used to ensure the fluid is sufficiently mixed to rapidly reach equilibrium conditions. Three platinum resistance thermometers (PT100 sensor with three core Teflon tails, model TC02 SD145; accuracy of ± 0.03 °C) were inserted, one to measure the air bath temperature, one at the top section of the sapphire cell to measure the gas temperature, and one at the bottom section of the sapphire cell to measure the solution temperature. The pressure in the vessel was measured with a pressure transducer (model WIKA S-10; accuracy of ± 0.5 bar). Stirrer current, pressure, and temperature parameters were recorded to a computer via Texmate Meter Viewer software at an interval of 12 points/second.

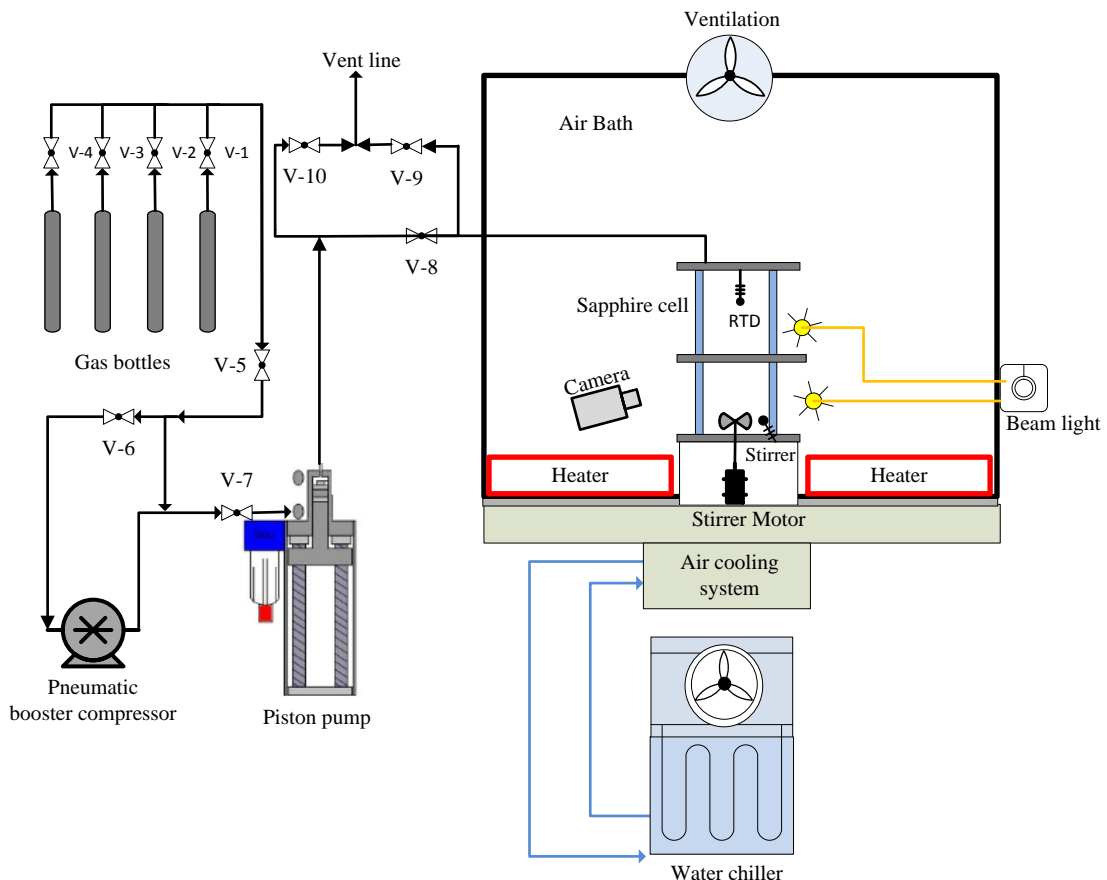


Figure 7-4 Cryogenic sapphire cell schematic.

7.3.2.2 Preparation of Thermally Exposed MEG Solution Samples

MEG/MDEA/FFCI solutions (Table 7-2) were prepared in a glass beaker with a magnetic stirrer using a high accuracy self-calibration electronic balance (SHIMADZU UW/UX with a minimum display accuracy of 1 mg for 1020 g).

The autoclave was filled with approximately 800 mL of the test solution and sparged with high purity nitrogen for 10–12 h to reduce the oxygen concentration to below 20 ppb which is confirmed by a portable oxygen analyzer (Hach Orbisphere model 3655, measurement range 0 ppb to 20 ppm, resolution 0.001 ppm, accuracy \pm 1%). Then, the autoclave was placed into a heating jacket and the solution was heated for 240 h at specified temperatures (Table 7-2); these temperatures represent typical MEG regeneration and reclamation field operating conditions (Lehmann et al., 2014, Bikkina et al., 2012, Psarrou et al., 2011).

The temperature of the solution was maintained with a temperature controller (Parr reactor controller model 4848, accuracy of \pm 0.03 °C). After thermal exposure, the solution was left to cool to room temperature, and was transferred into glass vials in an oxygen-free environment (i.e., under a nitrogen cap) to prevent further oxidation reaction. Photographs of the exposed solutions were then taken with a consistent set angle, background, and illumination.

Table 7-2 Solutions Tested and Thermal Exposure Conditions ^a

Solution	composition
“I”	MEG: 74.64 wt% Deionized water: 18.66 wt% MDEA: 6.7 wt%
“II”	MEG: 79.88 wt% Deionized water: 19.97 wt% FFCI (1500 ppm): 0.15 wt%
“III”	MEG: 74.53 wt% Deionized water: 18.63 wt% FFCI (1500 ppm): 0.15 wt% MDEA: 6.69 wt%

^a All solutions were exposed to 135, 165, 185 and 200 °C for 240 h.

For the hydrate inhibition tests, the thermally exposed solutions were diluted with deionized water to reduce the MEG concentration to 20 wt% (Table 7-3). This MEG

concentration reflects average MEG concentrations inside the gas pipeline. Usually, lean MEG (90 wt%) gets diluted by produced water to below 40% (Dugstad et al., 2003, Kim et al., 2014b, Halvorsen et al., 2009)

Table 7-3 Hydrate Performance Test Solutions

Solution	Diluted aqueous composition
“I”	Deionized water (78 wt% = 5.46 g) MEG (20 wt% = 1.4 g) MDEA (2 wt% = 0.14 g)
“II”	Deionized water (78 wt% = 5.60 g) MEG (20 wt% = 1.4 g) FFCI (375 ppm) = 0.0375 wt% = 0.000656 g)
“III”	Deionized water (78 wt% = 5.46 g) MEG (20 wt% = 1.4 g) FFCI (375 ppm = 0.000656 g) MDEA (2 wt% = 0.14 g)

7.3.2.3 pH Measurements

pH values were measured with a Thermo Scientific Orion 5-Star pH/RDO/conductivity portable meter (accuracy ± 0.002) with built in temperature compensation. For the tests, the pH probe was inserted into the enclosed sample vial at room temperature under nitrogen sparging. The pH probe was left inside the sample vial for at least 20 min to obtain stable readings. Duplicate pH readings of each sample were taken and found to be almost matching (within variance of ± 0.04). However, the presence of MEG and additives can cause a bias in the pH readings due to interference with the liquid junction potential of the electrode. This bias was adjusted following the Sandengen et al. (2007) methodology. The actual pH was calculated first by obtaining the $\Delta \text{pH}_{\text{MEG}}$, which is given by Sandengen et al. (2007)

$$\Delta \text{pH}_{\text{MEG}} = \text{pH}_{\text{RVS}} - \text{pH}_{\text{measured}} \quad \text{Eq 7-3}$$

where

$$\begin{aligned} \text{pH}_{\text{RVS}} = & 4.00249 + 1.0907w_G + 0.9679 w_G^2 + 0.3430z + \\ & 0.03166 w_G z - 0.8978 w_G^2 z + 7.7821 \left\{ \ln \left(\frac{T}{\theta} \right) - z \right\} + \\ & 9.8795 w_G^3 \left\{ \ln \left(\frac{T}{\theta} \right) - z \right\} \end{aligned} \quad \text{Eq 7-4}$$

where $z = T - \left(\frac{\theta}{T}\right)$, $\theta = 298.15$, and w_G is the weight fraction of MEG.

For pure MEG of 80 wt%, pH measured at 28 °C was found as 5.08. $\Delta \text{pH}_{\text{MEG}}$ for pure MEG of 80 wt% was found as

$$\Delta \text{pH}_{\text{MEG}} = \text{pH}_{\text{RVS}} - \text{pH}_{\text{measured}} = 5.49 - 5.08 = 0.41 \quad \text{Eq 7-5}$$

The actual pH value for each MEG in the solution sample is denoted by $\text{pH}_{\text{calculated}}$ and obtained as below:

$$\text{pH}_{\text{calculated}} = \text{pH}_{\text{measured}} + \Delta \text{pH}_{\text{MEG}} \quad \text{Eq 7-6}$$

The above-mentioned steps were repeated for each sample, and results are represented in Figure 7-6. Before taking each measurement, the probe was rinsed with deionized water and dried before each use. The objective of this exercise was to establish a concept of whether monitoring the pH values will provide an indication of degradation level of the thermally degraded MEG solutions.

7.3.2.4 Electrical Conductivity Measurements

A Thermo Scientific Orion 5-Star pH/RDO/Conductivity portable meter was used to measure the electrical conductivity of the thermally exposed MEG samples. The electrical conductive meter was calibrated and adjusted before taking the reading, as per the user guide, with conductivity standard solutions of 0.01 M KCl (1.413 mS/cm) and 0.1 M KCl (12.88 mS/cm) (Ameta et al., 2013).

The measurements were conducted at room temperature by inserting the electrical conductivity probe inside the sample vial for 15 min until a stable reading was reached.

7.3.2.5 Degradation Product Identification Techniques

Furthermore, the products of thermally exposed test solutions were analyzed by ion chromatography (IC) and high performance liquid chromatography - mass spectroscopy (HPLC-MS) (Huang et al., 2009, Kadnar et al., 2003, Schreiber et al., 2000, Niessen et al., 1995, Gil et al., 2000, Hess et al., 2004, Chandra et al., 2001). For the HPLC-MS technique, an in-house method was used (SGS Method HPLC-MA-1425.LIQ 01 using a mass spectrometry detector)(AlHarooni et al., 2015). The

IC technique was carried out on a Metrohm system (Metrohm 930 compact IC). The samples were first separated into their components using a 250-4 mm ion-exclusion column at standard conditions. Prior to separation, the samples were diluted with deionized water by a factor of 10 and filtered through a 0.10 µm filter, using the Metrohm in-line ultrafiltration unit. Eluent of sulfuric acid having 0.5 mmol/L was used. In order to minimize errors on dilution, an in-line dilution Metrohm method was used (Madera et al., 2003). Although the IC method has a high sensitivity in measuring organic acid concentrations down to 0.001 ppm, the presence of a single highly concentrated compound can interfere with the accurate measurement of other more lowly concentrated compounds.

7.3.2.6 Gas Hydrate Inhibition Tests

A full description of the gas hydrate test procedure is given elsewhere (AlHarooni et al., 2015, AlHarooni,Barifcani, et al., 2016). Prior to starting an experiment, the cell was pressurized with methane gas and vacuumed twice. Then, 7 mL of the solution was injected into the sapphire cell. The cell was pressurized with methane gas to the desired pressure using an electric piston compressor, and cell pressure was maintained during the experiment (Wu et al., 2013, Najafi et al., 2014). Moreover, the solution was continuously agitated with a magnetic stirrer at a rate of 530 rpm. To achieve a homogeneous temperature profile, the cell temperature was gradually decreased in steps of ~ 0.5 °C every 20 min. Once hydrates started to form (Figure 7-5A), the hydrate formation was monitored until full conversion to hydrate (Figure 7-5B). Subsequently, temperature was gradually increased in steps of 0.5 °C every 20 min until the hydrate started to dissociate. All hydrate dissociation points were then measured for each solution.

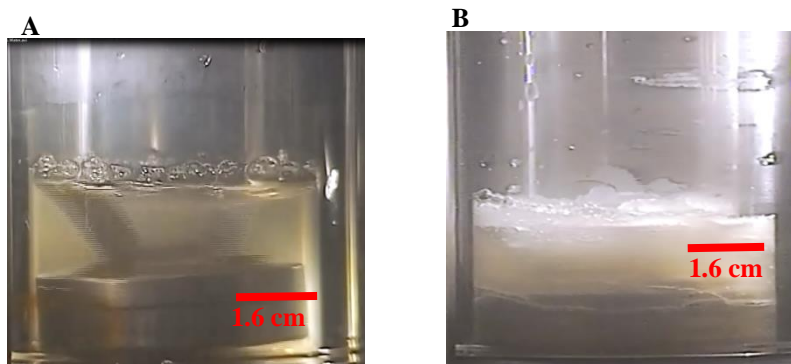


Figure 7-5 (A) Hydrate formation. (B) Hydrate fully converted

The repeatability of the experiments was tested by repeating the same measurements for solution “I” at 200 bar (thermally exposed to 135, 165, 185 and 200 °C), and good reproducibility was achieved with a standard deviation of ± 0.39 .

7.4 Results and Discussion

Various experimental methods were used in order to analyze if thermally degraded solutions could be appropriately monitored, identified, and evaluated. These techniques were:

1. pH measurement.
2. Electrical conductivity measurements.
3. Physical characteristics.
4. Product identification by IC.
5. Product identification by HPLC-MS.
6. Gas hydrates inhibition performance.

7.4.1 pH Measurements

Rossiter et al. (1983) conducted pH measurements to monitor the quality of MEG solutions which were heated to 100 °C for 15 days. They found that as the amount of degradation products increased, the pH value decreased; the initial pH value of the aqueous MEG solution of 9 mol/L (50 vol%) was 8.0, and it reduced to 6.7 after heating. The pH value dropped further to 6.6 and 4.9 in the presence of aluminum and copper metals, respectively. In our work, pH values were measured before and after thermal exposure (Figure 7-6). A pH buffering effect of MDEA was evident for solution “I” (MEG / deionized water / MDEA) and solution “III” (MEG / deionized water / MDEA / FFCI). MDEA essentially masked the change in pH that may have been caused by the organic acids (which are formed by thermal MEG degradation) as it reacts with acids to form salts by the absorber reactions (Choi et al., 2010, Cummings et al., 2007). For solution “I”, exposure temperatures slightly reduced the pH values (by 0.29, when heated to 135 °C, and by 0.56 when heated to 200 °C). For solution “II” (MEG / deionized water / FFCI) without MDEA, a significant drop in pH value was measured: the pH dropped by 3.6 when heated to 135 °C and by 4.04 when heated to 200 °C. Solution “III” behaved similarly to solution “I”: pH dropped only by 0.25 when heated to 135 °C, and by 0.51 when heated to 200 °C.

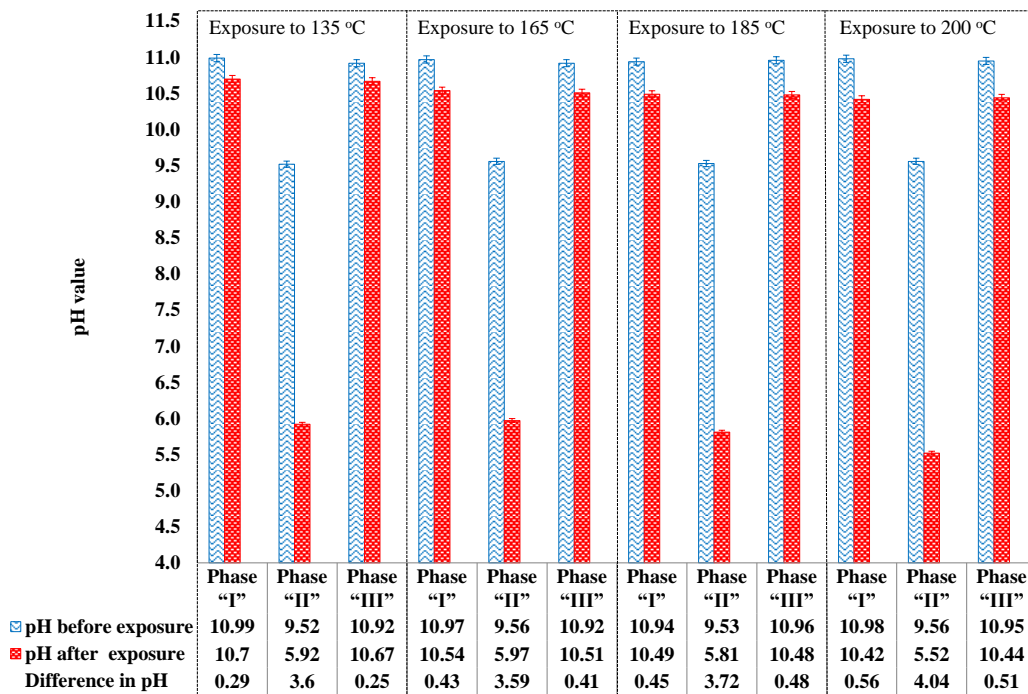


Figure 7-6 pH values as a function of exposure temperature for Table 7-2 solutions.

We thus conclude that the pH values correlate highly with the MEG thermal degradation level and thus can be used as a monitoring tool, consistent with Stewart et al. (2011), Clifton et al. (1985) and Monticelli et al. (1988).

7.4.2 Electrical Conductivity Measurements

Electrical conductivity is a recognized measurement tool for MEG degradation (Mrklas et al., 2004). Thus, electrical conductivities for solutions I–III were measured and found to respond proportionally to the exposure temperature (Figure 7-7), electrical conductivity increased with increasing thermal exposure temperature. MDEA reacts with acids and forms salts (Choi et al., 2010, Cummings et al., 2007), so that the electrical conductivities increase. Specifically, the electrical conductivity of solution “I” exposed to 135 °C was 46.7 µS/cm, and reached 149.5 µS/cm for 200 °C exposure temperature. Solution “III” showed a similar behavior, at nominally lower values: when exposed to 135 °C, 33.1 µS/cm were measured, while, for a temperature of 200 °C, 122.6 µS/cm were measured. Furthermore, there is an average difference of about 20.4 µS/cm between the conductivities of solutions I and III (Figure 7-7).

However, the electrical conductivity of solution “II” showed overall lower conductivities when compared to solutions “I” and “III”, and only minor conductivity increases were measured when temperature increased: 5.4 µS/cm were

measured for the solution exposed to 135 °C, and 15.73 $\mu\text{S}/\text{cm}$ for the solution exposed to 200 °C (Figure 7-7).

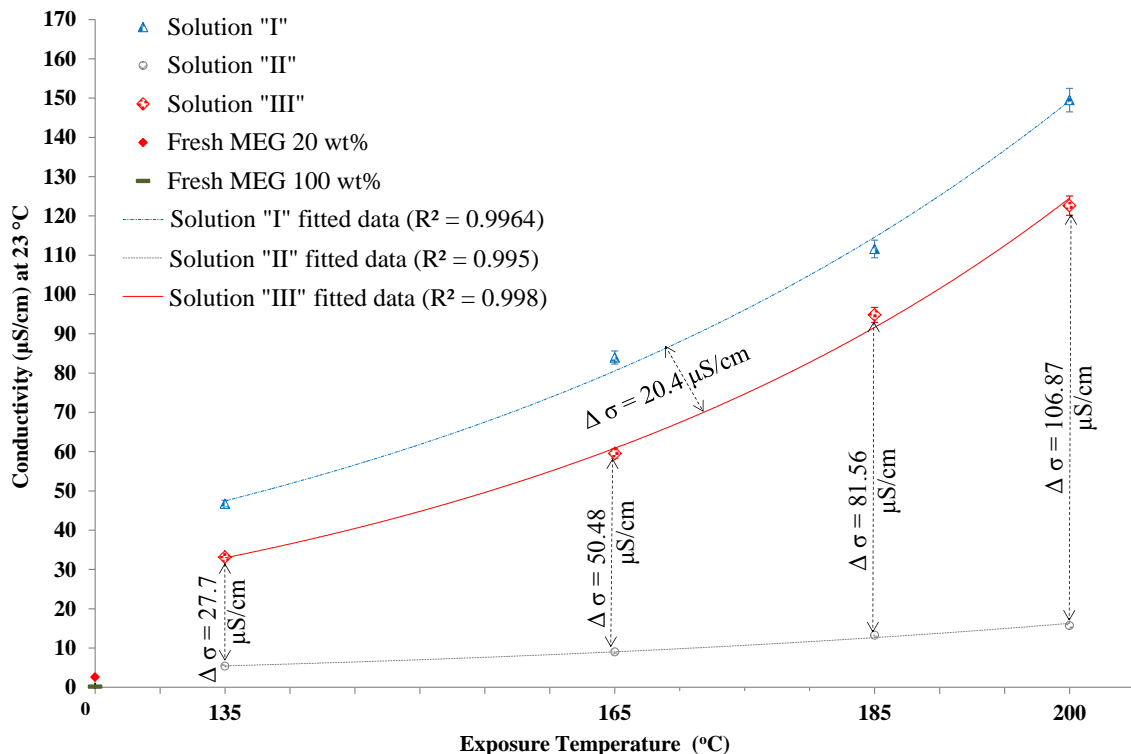


Figure 7-7 Electrical conductivity as a function of exposure temperature for solutions I–III (Table 7-2)

Furthermore, solutions “I” and “III” had higher electrical conductivities due to the presence of MDEA: MDEA forms salts when reacting with organic acids formed in the degradation process (such as formic acid ($\sigma = 5.18 \text{ mS}/\text{cm}$ at 18 °C) or acetic acid ($\sigma = 1.32 \text{ mS}/\text{cm}$ at 18 °C)) (Kidnay et al., 2011, Huang et al., 2007). Thus, the electric conductivity increased due to an increase in salts concentration caused by the reaction of MDEA with acids (eq 1). This is consistent with the measurements of Hille (2001). Hence, the electrical conductivity can be used as a MEG degradation monitoring tool, especially in the presence of MDEA.

7.4.3 Physical Observations

7.4.3.1 Physical Characteristics

The MEG solution in the presence of FFCI–MDEA underwent substantial changes in physical characteristics due to thermal exposure. The MEG–MDEA solution developed a pungent foul odor and the color changed from transparent and colorless

(Sorensen et al., 1999) to dark brown, consistent with previous observations (Chakma et al., 1997). Photographs of the solutions are shown in Figure 7-8. However, none of the samples experienced any phase separation, gunk, or solid deposition, consistent with Bikkina et al. (2012) observations. Besides that, the addition of FFCI turned the solutions even darker brownish. Furthermore, it is clear that higher exposure temperatures turned the samples' colors even darker (Figure 7-8). Thus, color change is a sign of degradation, as observed by Madera et al. (2003), Kadnar et al. (2003), and Chakma et al. (1997) and we conclude that a simple visual inspection of the solutions is the easiest way to assess MEG degradation.

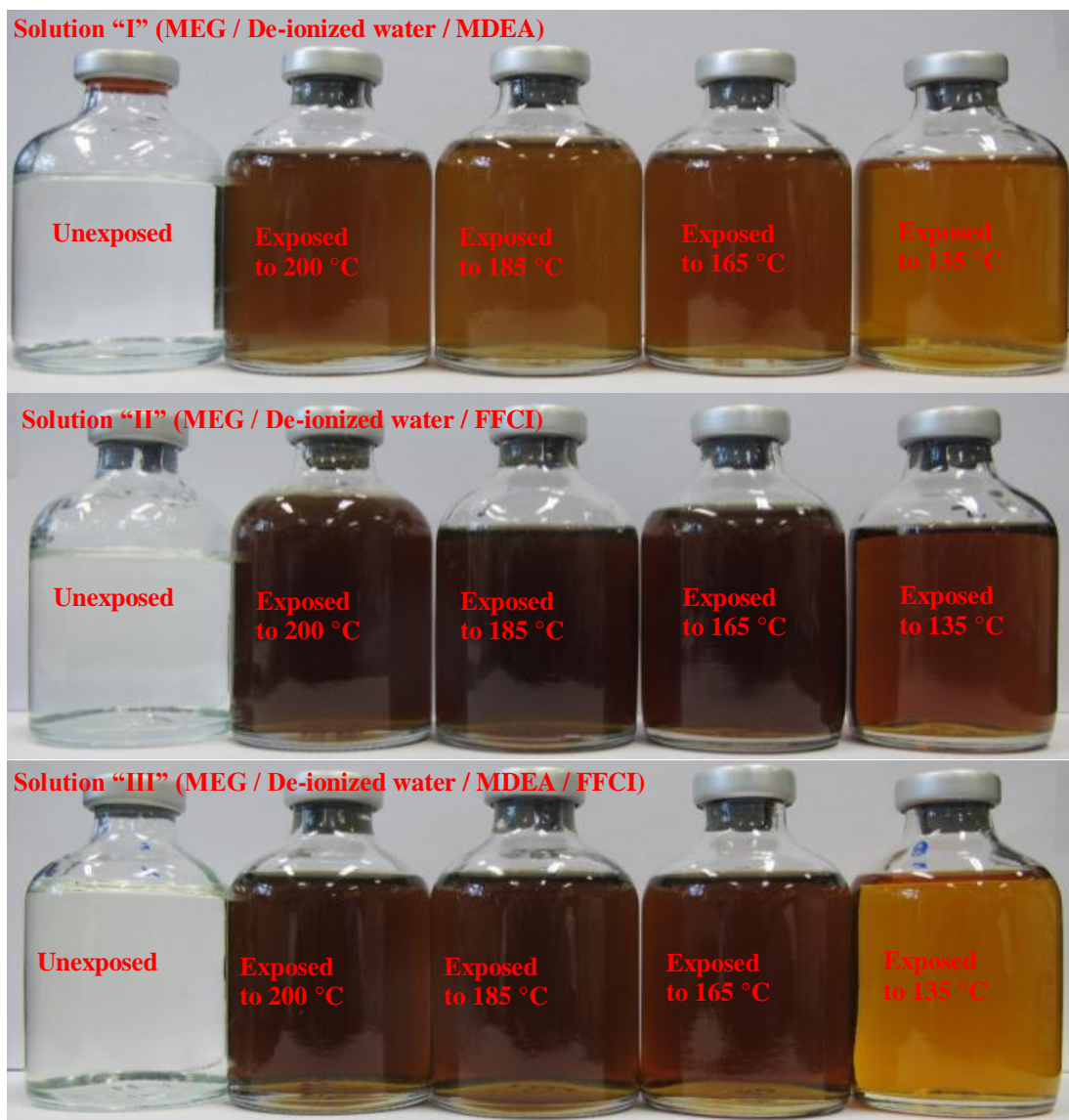


Figure 7-8 MEG solutions after heat treatment. Higher temperatures lead to more degradation (= darker color).

7.4.3.2 Foam Formation

Once MEG–MDEA solutions were diluted with deionized water (to 20 wt% MEG concentration), foam formation was observed to take place when the solutions were agitated (both at atmospheric pressure inside the glass vials or when pressurized with methane gas inside the sapphire cell); see Figure 7-9. Foaming can be caused by the introduction of different contaminants, such as acidic degradation products, mixing with feed gas, water, and oxygen ingress (Kohl et al., 1997, Al Dhafeeri, 2007). Furthermore, there is a direct relationship between the foam volume and the amount of methane converted to hydrate. Foaming accelerates hydrate formation and diminishes hydrate inhibitor performance. This can be explained by the increase in the water/gas interfacial area in the foam (Lekse et al., 2007, Pakulski, 2007). Moreover, the foam volume broke down as hydrate started to form. This is consistent with observations made by Mori et al. (1989).

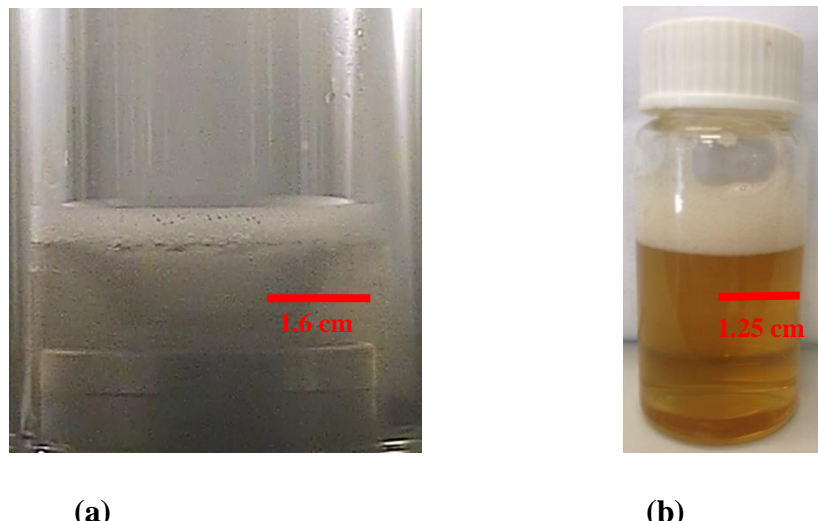


Figure 7-9 Foam formation in solution “I” thermally exposed to 200 °C.

7.4.4 Identification of MEG Degradation Products

7.4.4.1 Ion Chorography (IC)

All thermally exposed samples were analyzed with ion chromatography (IC), and three degradation products were identified: glycolic acid, acetic acid, and formic acid (Figure 7-10). IC was able to detect these species even at very low concentrations (down to 0.183 ppm).

Fresh MEG samples (unheated, at room temperature, 22 °C) showed inconsistent results when compared with the rest of the samples. This is due to the fact that the fresh MEG samples were exposed to oxygen they thus degraded by oxidation. MEG degradation due to oxidation is discussed by Monticelli et al. (1988). In case of solution “I” (MEG /deionized water / MDEA), the glycolic acid concentration increased dramatically when the solution was exposed to higher temperatures (185 °C and 200 °C). The formic acid concentration increased moderately as temperature increased. No acetic acid was found in samples exposed to 135 °C and 165 °C, while samples exposed to 185 °C and 200 °C contained high acetic acid concentrations (109 and 88 ppm, respectively) Figure 7-10.

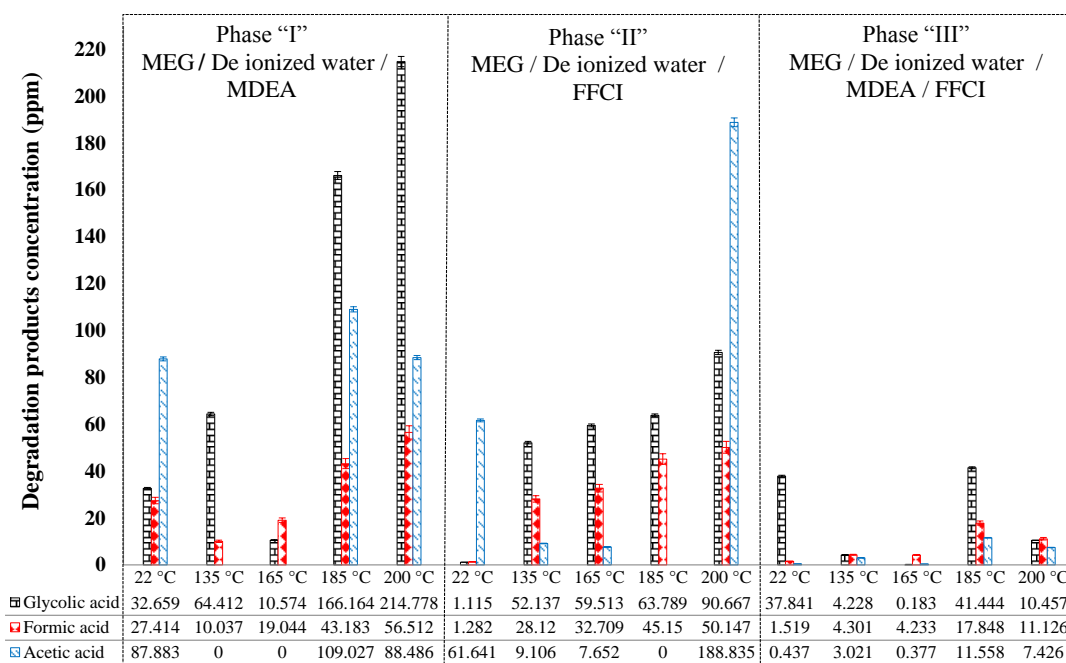


Figure 7-10 Degradation product concentrations in thermally exposed MEG solutions measured via IC.

In the case of solution “II” (MEG /deionized water / FFCI), the glycolic acid concentration increased moderately as the solution was exposed to higher temperatures (135–200 °C), but overall lower concentrations of solution “I”. The formic acid concentration also increased moderately as exposure temperature increased. No acetic acid was found in the sample exposed to 185 °C, while the samples exposed to 200 °C showed a high concentration of 188 ppm.

In solution “III” (MEG /deionized water / MDEA / FFCI), the glycolic acid concentration did not increase significantly with increasing temperature. When exposed to 185 °C, a maximum concentration of 41 ppm was measured. Generally,

the formic and acetic acid concentrations were lower than in solutions “I” and “II”. It is worth noting that glycolic acid was the most frequently measured organic acid.

7.4.4.2 High Performance Liquid Chromatography–Mass Spectroscopy (HPLC–MS)

HPLC–MS detected only formic and acetic acids (Figure 7-11), while clearly higher organic acid concentrations were measured for higher exposure temperatures. However, HPLC–MS did not detect any product at concentrations less than 10 ppm. Specifically for solution “I”, formic acid concentration increased when the solution was exposed to higher temperatures except for the solution exposed to 200 °C. In solution “II”, formic acid concentration was always ~30 ppm except for 135 °C exposure temperature, where only 10 ppm were measured. Solution “III” had always a formic acid concentration of 36 ppm, except for 135 °C exposure temperature, which resulted in only 10 ppm. The acetic acid concentration increased as temperature increased; it increased from 47 ppm for solutions exposed to 135 °C to 76 ppm for solutions exposed to 200 °C. Overall, acetic acid concentrations increased as exposure temperatures were increased.

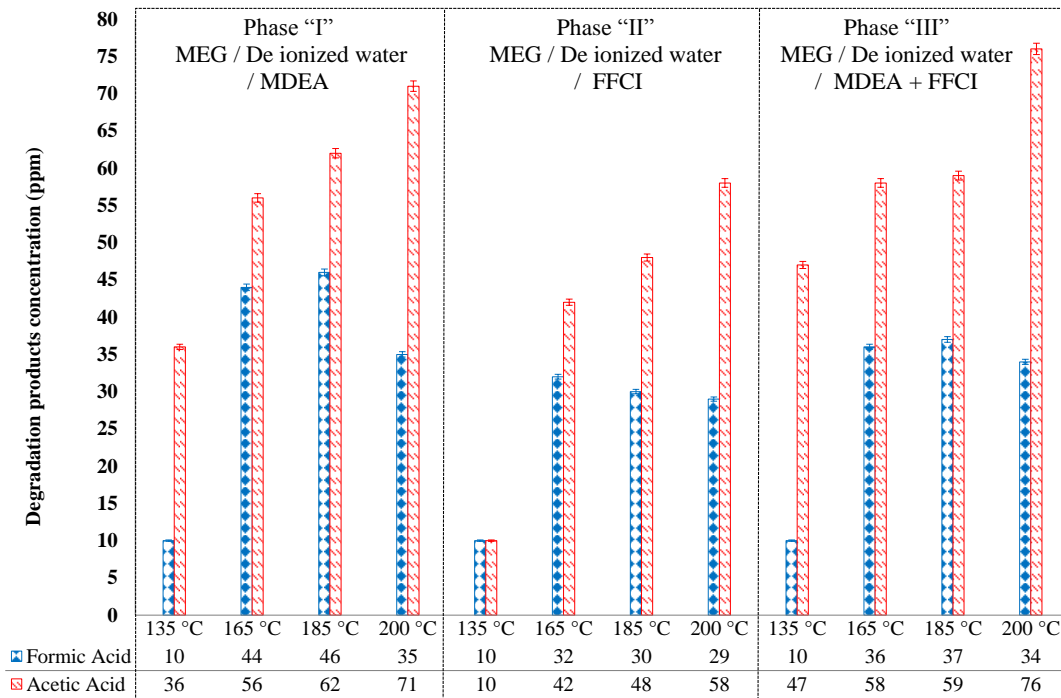


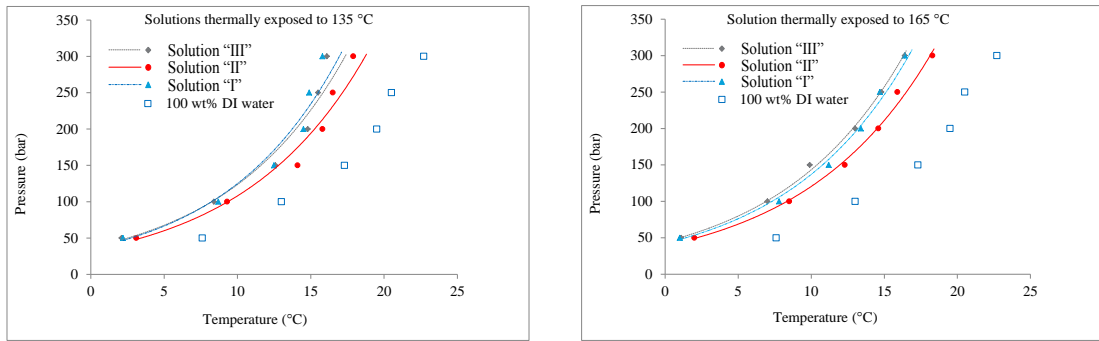
Figure 7-11 Degradation product concentrations in thermally exposed MEG solutions measured via HPLC–MS.

Although an in-line dilution method was used in order to minimize errors on dilution by manual handling, IC showed different results than HPLC-MS. This could be due to the fact that eluents lose their strength and concentration over time or due to the excess of organic ions which may severely disturb the chromatographic run, both by masking parts of the chromatogram and by influencing the shapes of the early eluting peaks (Rossiter Jr et al., 1985). The presence of any single compound in higher concentration (e.g., glycolic acid) can significantly influence the quantification of other less concentrated compounds (Rossiter Jr et al., 1985).

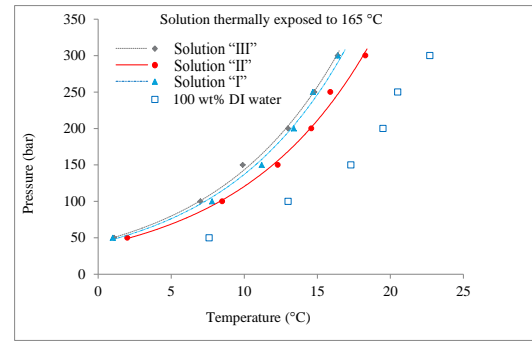
7.4.5 Hydrate Inhibition Performance Test

The work of AlHarooni et al. (2015) established that thermal exposure to high temperatures ($> 135^{\circ}\text{C}$) affects the gas hydrate inhibition performance of MEG solutions. This effect mainly depends on the thermal degradation level; the gas hydrate inhibition performance decreases with increasing exposure temperatures, mainly due to generation of organic acids (Psarrou et al., 2011, Clifton et al., 1985, AlHarooni et al., 2015). Here we further analyze methane gas hydrate dissociation points and how they are affected by thermally exposed MEG solutions, for a pressure range from 50 to 300 bar.

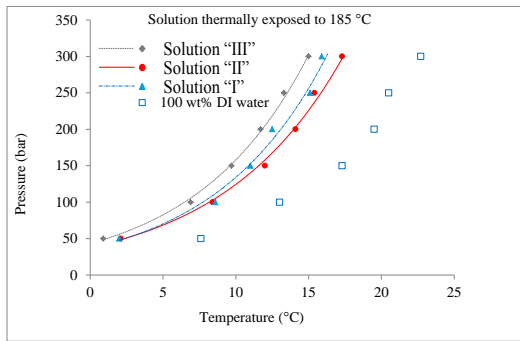
Results are summarized in Figure 7-12. In general, solution “III” showed superior hydrate inhibition performance in terms of shifting the hydrate curve most to the left side, followed by solution “I” and “II”. In Table 7-4 the methane gas hydrate dissociation temperature shifts of thermally exposed MEG solutions versus a baseline of deionized water are tabulated. For a 185°C exposure temperature, solution “III” shifted the hydrate curve by 7.2°C , solution “I” by 5.9°C , and solution “II” by 5.2°C . This is mainly due to the synergistic MEG–MDEA hydrate inhibitor effects in solutions “I” and “III” (Hossainpour, 2013, Davoudi, Heidari, et al., 2014). Solutions exposed to lower temperatures showed better inhibition performance, which is due to their lower organic acids concentration (Clifton et al., 1985, AlHarooni et al., 2015) (Figure 7-12, Table 7-4). Hence, hydrate inhibition analysis can be used to evaluate MEG degradation levels, especially for solutions exposed above 135°C .



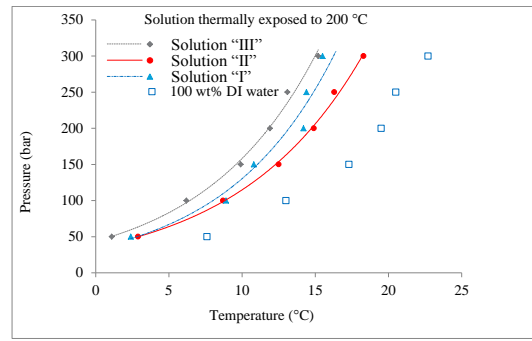
(a) Solutions thermally exposed to 135 °C.



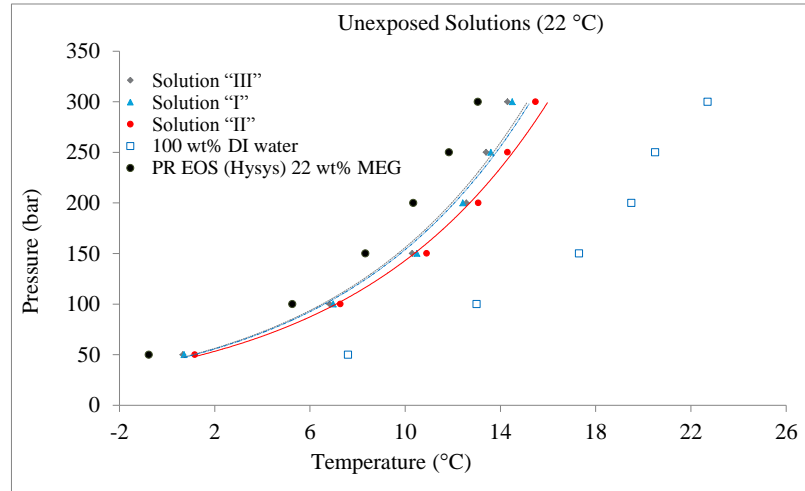
(b) Solutions thermally exposed to 165 °C.



(c) Solutions thermally exposed to 185 °C.



(d) Solutions thermally exposed to 200 °C.



(e) Unexposed solution (22 °C).

Figure 7-12 Hydrate dissociation curves of methane–MEG solutions for different thermal exposure temperatures; solid curves represent fitted data ($R^2 > 0.98$).

Predictions using the Peng–Robinson EOS (Aspen Hysys software, version 7.2, Licensed to Curtin University of Technology) and literature results showed some variance from this work, as referenced in Figure 7-13. This is primarily due to the

fact that no factor effect of MEG thermal degradation and corrosion inhibitors was applied.

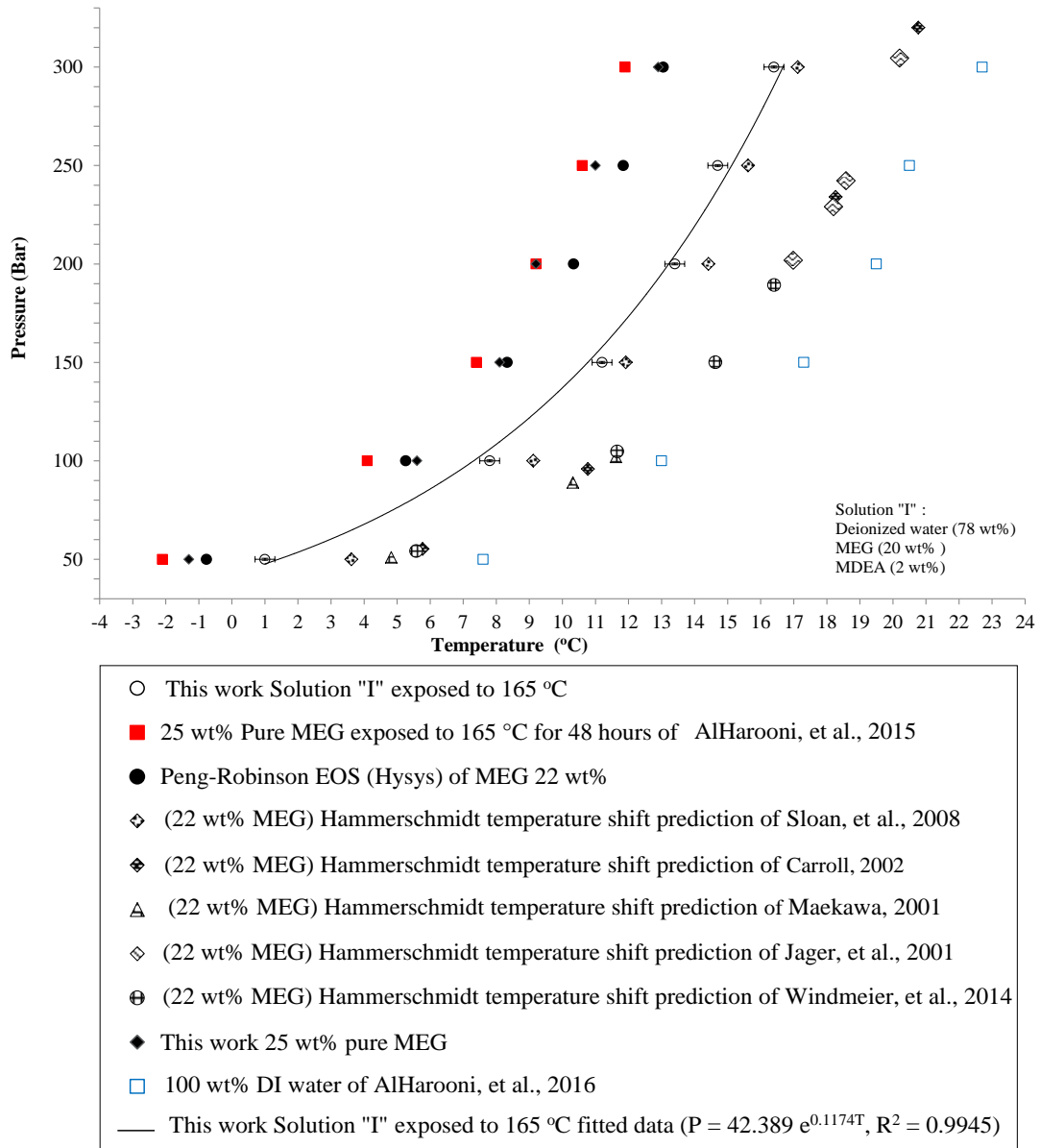


Figure 7-13 Methane-solution "I" hydrate dissociation curve with literature (Sloan et al., 2008a, Carroll, 2002, Maekawa, 2001, Jager et al., 2001, Windmeier et al., 2014a, Peng et al., 1976, Hemmingsen et al., 2011, AlHarooni, et al., 2015, AlHarooni, Barifcany, et al., 2016).

Table 7-4 Gas Hydrate Dissociation Temperature Shift of Methane–MEG Solutions Versus Baseline of Methane–Deionized water (Δ °C) and the Regression Functions of the Fitted Data^a

Exposure Temperature	Solutions	Regression functions	Δ °C	Pressure (bar)							Average Δ °C
				50	100	150	200	250	300		
Unexposed (22 °C)	“III”	$P = 43.596 e^{0.1275T}$	°C	-6.9	-6.2	-7.0	-6.9	-7.1	-8.4	-7.1	
	“I”	$P = 43.161 e^{0.1271T}$	°C	-6.9	-6.0	-6.8	-7.1	-6.9	-8.2	-7.0	
	“II”	$P = 41.665 e^{0.1234T}$	°C	-6.4	-5.7	-6.4	-6.4	-6.2	-7.2	-6.4	
135 °C	“III”	$P = 36.982 e^{0.1207T}$	°C	-5.5	-4.6	-4.7	-4.7	-5.0	-6.6	-5.2	
	“I”	$P = 35.434 e^{0.126T}$	°C	-5.4	-4.3	-4.8	-5.0	-5.6	-6.9	-5.3	
	“II”	$P = 33.474 e^{0.1172T}$	°C	-4.5	-3.7	-3.2	-3.7	-4.0	-4.8	-4.0	
165 °C	“III”	$P = 44.561 e^{0.1169T}$	°C	-6.5	-6.0	-7.4	-6.5	-5.7	-6.3	-6.4	
	“I”	$P = 42.389 e^{0.1174T}$	°C	-6.6	-5.2	-6.1	-6.1	-5.8	-6.3	-6.0	
	“II”	$P = 39.26 e^{0.1122T}$	°C	-5.6	-4.5	-5.0	-4.9	-4.6	-4.4	-4.8	
185 °C	“III”	$P = 43.201 e^{0.1297T}$	°C	-6.7	-6.1	-7.6	-7.8	-7.2	-7.7	-7.2	
	“I”	$P = 36.77 e^{0.1294T}$	°C	-5.6	-4.4	-6.3	-7.0	-5.4	-6.8	-5.9	
	“II”	$P = 37.752 e^{0.1193T}$	°C	-5.5	-4.6	-5.3	-5.4	-5.1	-5.4	-5.2	
200 °C	“III”	$P = 43.835 e^{0.1284T}$	°C	-6.5	-6.8	-7.4	-7.6	-7.4	-7.5	-7.2	
	“I”	$P = 34.329 e^{0.1335T}$	°C	-5.2	-4.1	-6.5	-5.3	-6.1	-7.2	-5.7	
	“II”	$P = 35.628 e^{0.117T}$	°C	-4.7	-4.3	-4.8	-4.6	-4.2	-4.4	-4.5	

^aP is pressure and T is the temperature. A higher negative “ Δ °C” value corresponds to a higher dissociation temperature.

7.5 Conclusions

During the MEG regeneration process, MEG is subjected to thermal exposure and degraded once overheated. The influence of thermally degraded MEG solutions with MDEA and FFCI on gas hydrate inhibition is of key importance for both hydrate and corrosion control, and it is poorly understood. MEG degradation causes the formation of acids, which leads to corrosion and reduction of hydrate inhibition performance. This would impact the operation cost and the systems shelf-life (Davoudi,Safadoust, et al., 2014). For this an experimental methodology was developed to thermally expose the solution aliquots (exposure temperatures 135 °C, 165 °C, 185 °C, 200 °C) for 240 h. This study provided realistic evaluation of six independent chemical and physical analyses to measure MEG solutions degradation level and its impact on gas hydrate inhibition during gas transportation.

Measured pH values correlated with the MEG thermal degradation levels and thus can be used as a monitoring tool, consistent with Stewart et al. (2011), Clifton et al. (1985) and Monticelli et al. (1988). MDEA masked this drop in pH and raised the electrical conductivity. Electrical conductivities also steadily rose with increasing thermal exposure temperatures. This is due to an increase in salts concentration, generated by the reaction between MDEA and organic acids (which are formed by the thermal degradation process) (Hille, 2001). Hence, the electrical conductivity can also be used as a MEG degradation monitoring tool, especially for solutions containing MDEA.

Furthermore, the solutions underwent changes in physical characteristics, including color, smell, and foam formation due to thermal exposure. Visual inspection of the samples showed that the solutions turned brownish as degradation increased due to harsher thermal exposure conditions. In addition, foam formation was observed on diluted MEG–MDEA solutions at both atmospheric and high pressure conditions. The foam volume started to disintegrate when hydrate started to form. IC and HPLC–MS were used to identify and quantify the presence of the formed organic acids (degradation products). Three reaction products were identified by IC: glycolic, acetic, and formic acids. IC was able to detect products at very low concentration (down to 0.183 ppm), while HPLC–MS detected only two reaction products—formic and acetic acids—and HPLC–MS did not detect products below 10 ppm.

However, HPLC–MS showed a clear pattern for all test solutions: higher acetic acid concentrations were obtained for higher exposure temperatures.

Finally, the influences of thermally degraded MEG solutions on gas hydrate inhibition were analyzed for a pressure range from 50 to 300 bar. The results showed that thermally degraded MEG with corrosion inhibitors (MDEA and FFCI) significantly reduced the hydrate inhibition performance. In general, as the exposure temperature increased, the inhibition performance dropped; this is mainly due to the formation of acidic degradation products during thermal exposure. Interestingly, solution “III” demonstrated the best inhibition performance. This is mainly due to the synergistic hydrate inhibition effects of MEG, MDEA, and FFCI (Hossainpour, 2013, Davoudi, Heidari, et al., 2014).

Table 7-5 evaluates the six analytical techniques used in terms of their strength in identifying, monitoring and quantifying the MEG degradation level. Of the six methods reviewed, pH, physical change, HPLC-MS and gas hydrate methods are most effective, due to consistency across all solutions and exposure temperatures. Electrical conductivity measurements showed excellent results for MDEA solutions. IC provided acceptable results especially for solution exposed to higher temperature, as shown in Table 7-5. The thermal degradation of aqueous glycol solutions is a complex process, producing different reaction products in solution depending upon reaction conditions (Rossiter Jr et al., 1985). The excess of organic ions may severely disturb the chromatographic run, especially when eluents start losing their strength and concentration, both by masking parts of the chromatogram and by influencing the shapes of the early eluting peaks (Rossiter Jr et al., 1985). The existence of some organic acids (e.g., glycolic acid) in high concentration will affect the ability of IC to determine the lower concentration compounds.

The study of thermal degradation of MEG/MDEA/FFCI solutions is of key importance for the sour gas fields for both hydrate and corrosion control (Glenat et al., 2004, Davoudi, Heidari, et al., 2014, Davoudi, Safadoust, et al., 2014)

In summary, we conclude that exposing MEG solutions to higher temperatures ($> 135^{\circ}\text{C}$) leads to increased degradation levels thus reducing hydrate inhibition performance and increasing the risk of corrosion. Also results demonstrated that the presence of oxygen in the system causes degradation. Exclusion of higher temperatures and oxygen from the system is an effective means of suppressing degradation.

Table 7-5 Evaluation of Analytical Techniques for Measurement of Thermal Degradation of MEG Solutions.

Analytical techniques	Solution “I”	Solution “II”	Solution “III”
pH meter	Good	Excellent	Good
Electrical Conductivity	Excellent	Not suitable	Excellent
Physical change	Good	Good	Good
IC	Suitable for samples exposed to 185 °C and 200 °C.	Good	Suitable for samples exposed to 185 °C and 200 °C.
HPLC–MS	Good	Good	Good
Gas Hydrate	Good	Good	Good

Furthermore, the analytical techniques show an acceptable measure (as outlined in Table 7-5) in identifying and evaluating the MEG degradation level. We found that pH, HPLC–MS, and gas hydrate formation measurements and simple visual inspection of the samples give a good indication of the MEG degradation level, while electrical conductivity measurement is suitable for solutions with MDEA. The degradation levels have been quantified into five levels (0–4) using four analytical technique indicators, as illustrated in Figure 7-14. The degradation level scale can be used in conjunction with Table 7-5. As the MEG solution approaches higher degradation levels (> 1), the flow assurance strategies must be reviewed (with the option of replacing recycled MEG) in terms of MEG doses and corrosion protection strategies, based on the operating envelope and material specification of each field. This is essential to ensure achieving optimal production performance and maintaining asset integrity. Moreover, as the MEG solution approaches higher degradation levels (3–4), recycled MEG is highly recommended to be replaced by fresh MEG; this is not only to prevent gas hydrate blockage and corrosion rate in the gas pipeline but also to prevent fouling and deposition of the process equipment (Psarrou et al., 2011, Bikkina et al., 2012).

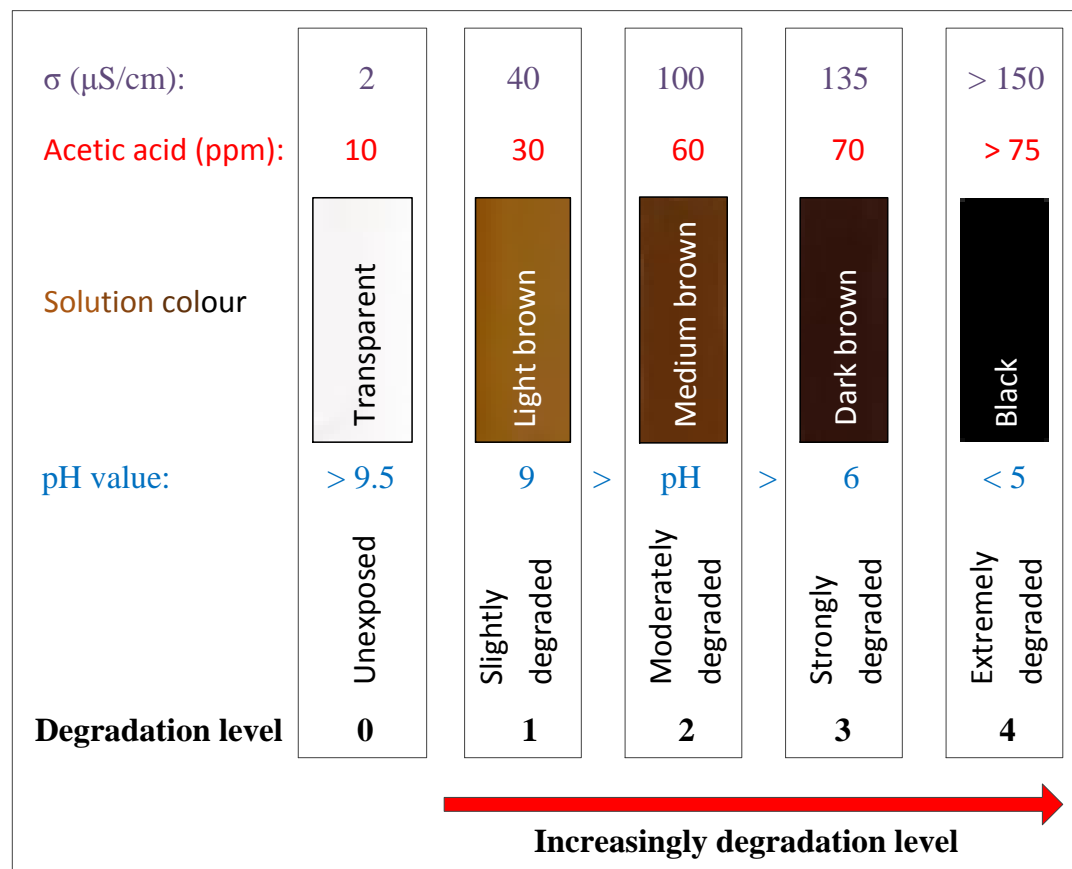


Figure 7-14 Degradation level scale of MEG solutions (to be used in conjunction with Table 7-5)

ABBREVIATIONS

- MEG: Monoethylene Glycol
- MDEA: Methyl diethanolamine
- FFCI: Film Forming Corrosion Inhibitor
- PVT: Pressure Volume Temperature
- HPLC-MS: High Performance Liquid Chromatography - Mass Spectroscopy
- IC: Ion Chromatography
- LCMS: Liquid Chromatography Mass Spectroscopy
- EOS: Equation Of State
- PPM: Part Per Million
- RTD: Resistance Temperature Detector.

Chapter 8 Influence of Regenerated Mono-ethylene Glycol on Natural Gas Hydrate Formation

8.1 Abstract (Figure 8-1)

The key objective of this study is to investigate the efficiency of thermodynamic hydrate inhibition of Monoethylene glycol (MEG) solutions collected from a MEG regeneration/reclamation pilot plant, simulating six scenarios of the start-up and clean-up phases of a typical gas field. The scenarios contain complex solutions of condensates, drilling muds/well completion fluids with high concentrations of divalent-monovalent ions, particulates, and various production chemicals, which can result in various system upsets in MEG plant. MEG was regenerated and reclaimed at a recently constructed closed-loop MEG pilot plant that replicates a typical field plant. During MEG plant operation, feed-rich MEG is separated, cleaned, and heated so that water in it is evaporated and purified for re-use. In this study, equilibrium conditions of natural gas hydrates in the presence of 20 wt % of regenerated and reclaimed MEG solution at a pressure range of 65 to 125 bar were reported. The equilibrium data were measured in a PVT sapphire cell unit using an isochoric temperature search method. The measured data were compared with the literature and theoretical predictions to investigate the influence of regenerated/reclaimed MEG on gas hydrate inhibition performance. A better understanding of the efficiency of regenerated complex MEG solutions on hydrate phase equilibria forms a basis for improved system design, operations, and calculating required MEG dosages for hydrate inhibition.

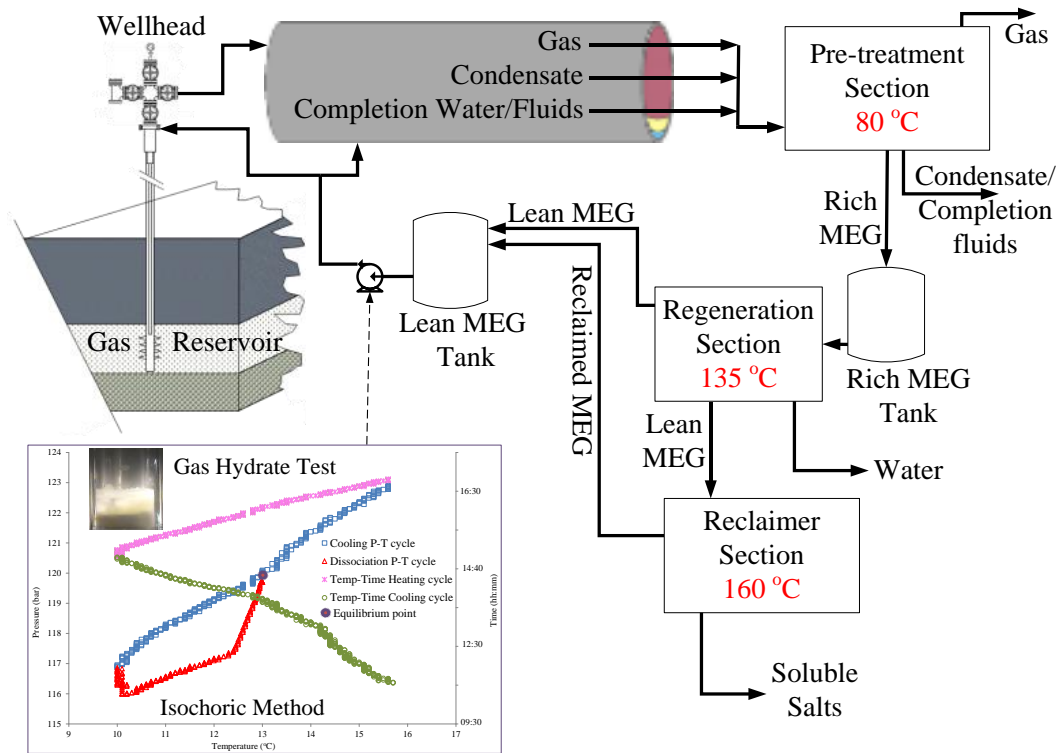


Figure 8-1 Abstract Graphics

8.2 Introduction

In hydrocarbon production, ethylene glycols are used primarily as thermodynamic hydrate inhibitors, or as a hygroscopic liquid for gas dehydration for absorbing water associated with natural gas (Emdadul, 2012, Arnold et al., 1999). Gas hydrates, which are also known as gas clathrates, resemble ice and form in the presence of water at specific conditions of high pressure and low temperature (Sloan et al., 2008a, He et al., 2011). Gas hydrates become crystallized by entrapping guest molecules in a hydrogen-bonded network of water (Sloan, 2003, Tariq et al., 2016). Guest molecules of natural gas are mainly of methane, with other guests such as carbon dioxide, ethane, and propane (Jin et al., 2016, Tariq et al., 2016). Favorable conditions for gas hydrates often exist in gas pipelines and during gas processing; therefore, gas hydrates are considered as a serious flow assurance problem (Sloan, 2003). Monoethylene glycol (MEG) is becoming more favored in the use as hydrate thermodynamic inhibitors than other inhibitors such as methanol because of its better hydrate suppression performance, (Haghghi et al., 2009) less loss to the gas phase and more operationally and environmentally friendliness (Brustad et al., 2005). Considering the large quantities required for operation, MEG regeneration is the most reliable and cost-effective method to recycle the used MEG to clean

contamination with minimum loss (Teixeira et al., 2016, Lehmann et al., 2014, Arnold et al., 1999).

MEG regeneration is used widely and in different fields, such as Reliance KG-D6 (India), Statoil's Ormen Lange and Asgard B (Norway), Conoco Phillip's Britannia Satellites (UK), BP's Shah Deniz (Azerbaijan), Woodside Pluto (Australia), South Pars gas field, and most of the gas-condensate fields in the North Sea and the deeper parts of the Gulf of Mexico (Lehmann et al., 2014, Babu et al., 2015).

MEG regeneration and reclamation poses ongoing operational challenges in the oil and gas industry, especially during the field start-up phase where the incoming rich MEG may contain a large volume of drilling mud and completion fluids that require special separation treatment (Latta et al., 2013). To assist in understanding these operational challenges and concerns, a MEG pilot plant that replicates the functionality of actual MEG facilities was constructed at the Curtin Corrosion Engineering Industry Centre (CCEIC) to generate pilot data replicating field operation conditions (Zaboon et al., 2017). The MEG regeneration and reclamation pilot plant was designed as a MEG closed-loop system with a design capacity of 1-4 kg/hour of lean MEG production. A schematic of the MEG pilot plant is given in Figure 8-2.

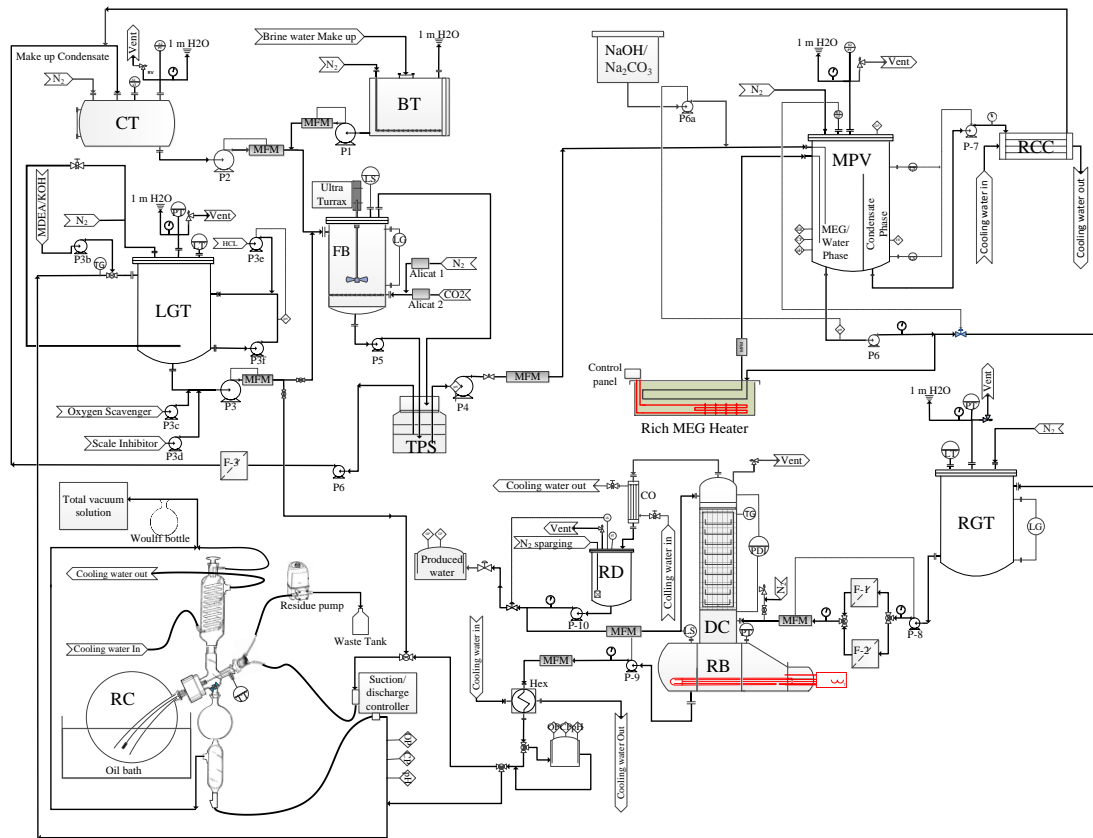


Figure 8-2 MEG pilot plant schematic.

A better understanding of the MEG closed-loop processes and their consequences on the process units is essential to flow assurance and process and will give engineers a better understanding of MEG plant operations at various conditions, such as during the field clean-up stage. The pilot plant bridges the gap between individual laboratory-scale tests and a comprehensive testing practice correlated to field conditions. The facility is designed to simulate specific production fluids that represent industrial-scale MEG systems, such as condensate, drilling mud, brines and formation water. Also, the facility has the capability to simulate condensate carryover from a three-phase separator (TPS) to a MEG pretreatment vessel (MPV), optimizing salt removal and performing production chemical additive compatibility. The use of MEG in wellheads and gas pipelines as a hydrate formation suppressor has been well established in recent years. The lean MEG, typically with a concentration of 80 to 95 % MEG (Nazzer et al., 2006, Halvorsen et al., 2006), is injected at the wellhead and then enriched with the produced/formation fluids and soluble salts as it travels through the production pipeline. Also, scale inhibitors, pH

stabilizers (such as NaOH/KOH or Methyl Di-Ethanolamine (MDEA)), and film forming corrosion inhibitor (FFCI)) are commonly injected in the pipeline (AlHarooni et al., 2017). For the initial startup with potential for back production of completion fluids, or during formation water breakthrough, the corrosion inhibitor strategy of FFCI is selected, reducing the risk of scale formation (Lehmann et al., 2014, Halvorsen et al., 2006, Halvorsen et al., 2009). Water, completion fluids, inhibitors, and salts are then separated from the rich MEG by regeneration and reclamation to produce lean MEG for re-injection. MEG regeneration is the process whereby only water is evaporated, and MEG is discharged as a liquid (Carroll, 2002). The downside of this configuration is that any chemicals or salts are carried out with the lean MEG. These chemicals/salts may deposit and result in accelerating equipment corrosion, reducing the heat transfer rate (because of fouling of salts on heat exchanger surfaces) and polluting MEG over time (Emdadul, 2012). The reclamation is a configuration of evaporating both water and MEG, whereby salts and chemicals are separated (Akpbio, 2013). Depending on the contamination amount and the allowable salt level in the MEG to be injected, reclamation can be run either in continuous (full reclamation) or partial slip-stream modes (Son et al., 2000). In this study, the slip-stream mode is selected and is used widely in different fields such as Ormen Lange, Norway (Norske Shell), and Snøhvit, Norway (Statoil) (Brustad et al., 2005, Christiansen, 2012). The processed lean MEG is then sent back to the well head by designated lines for reinjection. Although continuous MEG recycling (injection/regeneration) is the most reliable and cost-effective solution for hydrate management, recycling is a complex process comprising various physical and chemical processes. The degree of complexity in a closed-loop MEG regeneration system is significant, because of the presence of various chemical additives and salts. The combined effect of these components (especially drilling mud and salts) has led to a number of issues that have contributed to shutdowns, resulting in loss of production (Babu et al., 2015, Son et al., 2000). Some of these issues are summarized below.

- Hydrocarbon carry-over along rich MEG to the regenerator, causing damage to column internals and packings (Emdadul, 2012).
- High level of soluble salts in the rich MEG, causing severe fouling of regenerator column and heat exchangers (Nazzer et al., 2006).

- Scale formation on hot surfaces of the glycol reboiler, which leads to the formation of hot spots, resulting in MEG losses because of thermal degradation (Teixeira et al., 2016).
- Foaming and emulsion tendencies because of condensate carryover(Alhseinat et al., 2014) and the improper selection of non-compatible chemicals in the case of corrosion inhibitors, pH stabilizers, oxygen scavengers, and scale inhibitors (Lehmann et al., 2014).
- Collapse of packing in the distillation column (DC) caused by entrainment of a high quantity of condensate in rich MEG and the occurrence of various scale depositions (accelerated by the returning lost mud fluid from the reservoir) such as Calcium Sulfates, Barite (BaSO_4), Halite (NaCl), or Calcite (CaCO_3) (Kan et al., 2011, Babu et al., 2015).

These interactions do have some effect on the purity of the final MEG product function and, therefore, its hydrate inhibition performance. The need to understand the mechanism driving these interactions and their effects on hydrate inhibition has become critical to solving the operational challenges encountered during operating service. Models have been developed to simulate the depression of hydrate equilibrium points by increasing the MEG concentrations from a simple correlation (Bai et al., 2005, Hammerschmidt, 1939). to thermodynamic models.(Haghghi et al., 2009) Most of the thermodynamic models can simulate the hydrate depression to high accuracy, but no published thermodynamic models are capable of predicting hydrate depression and equilibrium data with high accuracy for regenerated/reclaimed MEG (with different incoming solutions). This is because the fluid phase equilibrium models cannot precisely evaluate the interactions between regenerated MEG components (MEG/salts/organic acids) and water, leading to inaccurate predictions of water fugacity/activity in the aqueous phase.(Mohammadi et al., 2009) At each equilibrium point, a hydrate will form if the fugacity of water in a hydrate lattice is lower than the fugacity of water (f_w^{Aq}) in liquid state, as per below equation: (Hemmingsen et al., 2011)

$$f_w^{\text{Aq}} = x_w^{\text{Aq}} \gamma_w^{\text{Aq}} f_w^o \quad \text{Eq 8-1}$$

Where, x_w^{Aq} is the mole fraction of water in the aqueous phase, f_w^o the fugacity of pure water, and γ_w^{Aq} is the activity coefficient of water in the aqueous phase.(Hemmingsen et al., 2011) For contaminated water (in the presence of

regenerated MEG), the pure water fugacity will be affected by the fugacity of the water/liquid and water/vapor phases, leading to the inaccurate prediction of hydrate equilibrium points, as per the below equation: (Sloan et al., 2008a)

$$f_w^H = f_w^V = f_w^L \quad \text{Eq 8-2}$$

Where f_w^H is fugacity of water/hydrate, f_w^V is fugacity of water/vapor, and f_w^L is fugacity of water/liquid phase. A lack of phase equilibrium data therefore exists for regenerated MEG solutions exposed to different operating solutions. This information is provided here by obtaining hydrate equilibrium points and regression functions for systems of natural gas inhibited by different scenarios of regenerated MEG. The right prediction of the hydrate equilibrium locus of natural gas with various solutions from the MEG regeneration and reclamation significantly enhances the provision of answers to the operator's concerns, and provides proper input for calculating the quantity of MEG required to shift the hydrate stability region outside the operating condition range (Creek, 2012).

During well drilling, a drilling mud is used to accommodate various functions, such as carrying away cuttings from the well, controlling formation pressure by providing a seal-off, controlling hydrostatic pressure to prevent a kick or blowout, minimizing formation damage, and facilitating cementing and completion (Abraham, 1933). The use of Oil-based drilling muds is common in deep formation drilling to overcome high pressure and high temperature conditions (Davies et al., 1984, Cranford et al., 1999). Oil-based drilling muds have many favorable characteristics, such as better thermal stability, and inherent protection against acid gasses (e.g. CO₂ and H₂S) and corrosion; they also improve lubricity and reduce the stuck pipe problems (Boyd et al., 1985, Amani et al., 2012). In addition, oil-based drilling mud prepared with brine also helps to reduce the risk of gas hydrates formation (Grigg et al., 1992).

The MEG pilot plant was used to simulate six MEG scenarios of fluids coming from the field during start-up/clean up phase (containing completion fluids and drilling muds; refer to section 8.3.3). In particular, the focus of this study was to compare the hydrate inhibition performance of final MEG products obtained from different scenario runs collected from the reboiler and reclamer output of the MEG pilot plant.

The oil-based drilling muds and well completion fluids contain high concentrations of divalent-monovalent ions, particulates, and various production chemicals, which can result in various system upsets in the MEG regeneration plant. This work has analyzed the partitioning of the drilling muds into condensate and MEG phases. It has also investigated the effectiveness of demulsifiers to break emulsions. Demulsifiers are generally formulated with surfactants, flocculants, wetting agents, and solvents such as benzene, toluene, xylene, short chain alcohols, and heavy aromatic naphtha (Laurier, 1992). Demulsifiers work by neutralizing the effect of emulsifying agents that stabilize emulsions. They are surface active components that enhance water droplet coalescence, migrating to the interface to accelerate emulsion separation. Demulsifier effectiveness depends on pH, salt content, and temperature (Kokal, 2002, Laurier, 1992). A demulsifier is a complex chemical and wide varieties are available; it is vital to select the right one for the process (Kokal et al., 2000).

General information about MEG regeneration and reclamation can be found in the literature. Most of the flow assurance reported research related to MEG plants is focused on scale (Baraka-Lokmane et al., 2013, Yong et al., 2015, Babu et al., 2015, Emdadul, 2012, Baraka-Lokmane et al., 2012) and corrosion (Lehmann et al., 2014, Gonzalez et al., 2000, Baraka-Lokmane et al., 2013, Psarrou et al., 2011, Bikkina et al., 2012). It appears from the literature that research knowledge of regenerated/reclaimed MEG kinetics performance on natural gas hydrate is currently limited, especially the study of MEG regenerated from the start-up/clean-up phase of a gas field. It has therefore been our goal to evaluate the natural gas hydrate equilibrium depression of different MEG samples collected from the reboiler and reclaimer outlets from different scenarios. This has assisted in the calculation and adjustment of the MEG dosing amount to prevent hydrate formation. The first part of this paper presents the MEG regeneration and reclamation for six scenarios, while the second part analyzes the effect of final MEG products collected from reboiler/reclaimer outlets in different scenario runs on gas hydrate inhibition performance.

8.3 Methodology

8.3.1 MEG Pilot Plant

Drilling mud is supplied by M-I SWACO (a Schlumberger company). It is an oil-based drilling mud that contains a large amount of calcium in terms of an internal calcium chloride brine phase plus calcium carbonate and calcium hydroxide solids acting as weighting and bridging agents. The suspension fluid is a NaCl/KCl MEG-water brine (80/20 MEG/water brine). The gravel pack carrier fluid contains acetic acid, caustic soda, NaCl, KCl, NaBr, and some other components. The drilling mud is well stirred for five minutes (using an Ultra-turrax model homogenizer at 1000 rpm) before dosing to a feed-blender. Demulsifier and oxygen scavenger supplied by Baker Hughes. Methyl diethanolamine (MDEA) (obtained from Sigma-Aldrich Co. LLC with a purity of ≥ 99 mol %), condensate fluid used was IsoparTM M (distillates (Petroleum), hydrotreated light) by ExxonMobil Chemical, CO₂ (purity 99.9 mol%, supplied by BOC Company, Australia) and N₂ generated by Nitrogen generator (Atlas Copco, model NGP 10⁺ and filtered by Donaldson ultra filter system with purity of ≥ 99.9 mol %).

Laboratory analyses to measure ionic concentrations were performed using Inductively Coupled Plasma Optical Emission Spectrometry (ICP-OES) (Perkin Elmer Optima 8300), and organic acids were measured using Ion Chromatography (IC) (Metrohm 930 compact IC) (AlHarooni,Pack, et al., 2016, AlHarooni et al., 2015). On-line measurements of temperature, electrical conductivity (EC), pH, and dissolved oxygen were obtained from the Programmable Logic Control (PLC) system that synchronized the data from the M800 PROCESS transmitter system (by Mettler-Toledo Company). Furthermore, the pH and EC of the reboiler and reclainer samples were measured using a Thermo Scientific Orion 5-Star pH/RDO/conductivity portable meter (accuracy ± 0.002) (AlHarooni,Pack, et al., 2016). pH readings were adjusted as per the work of AlHarooni,Pack, et al. (2016) utilizing the methodology developed by Sandengen et al. (2007). The salt-laden rich MEG composition used for preparing the solutions of different scenarios (section 8.3.3) was prepared as per Table 8-1 below.

Table 8-1 Salt-laden rich MEG composition^a

Material	Amount
NaCl	1.6 wt %
KCl	0.5 wt %
Water	24.5 wt %
MEG	73.4 wt %
Oxygen Scavenger	25 ppm
MDEA	6.4 mmol/kg
Acetic Acid	60 ppm

^a Other salts component arises from the drilling mud.

8.3.2 Gas Hydrate Experiment

A synthetic gas (with high methane content) (Ogawa et al., 2009) representing typical real natural gas composition (Lee et al., 2011, Wu et al., 2007, Ahmad Syahrul, 2009, Akpabio, 2012) that will form structure II hydrate (Ebeltoft et al., 2001) (preparation tolerance $\pm 2\%$, prepared by BOC Company, Australia) was used for the gas hydrate test (Table 8-2). Nitrogen gas (purity = 99.99 mol %; obtained from BOC Company, Australia) was used for the purpose of purging. A refractometer (device type Atago PAL-91S) (Zaboon et al., 2017) was used to measure the MEG concentration from the regeneration and reclamation outlet samples. Deionized water (obtained from a reverse osmosis system with an electrical resistivity of $18 \text{ M}\Omega\cdot\text{cm}$ at 25°C) was used to dilute the collected MEG samples from the regenerated/reclaimed MEG plant to 20 wt %. 7 mL ($\approx 11\%$ volume of the cell) of the diluted samples injected into the sapphire cell. This MEG concentration was selected to represent the average solution concentrations inside the gas pipeline (Ebeltoft et al., 2001) during field start-up with high water cut,(Swanson et al., 2005) as the lean MEG is diluted by the produced water to below 40% (Dugstad et al., 2003, Wu et al., 2007, Kim et al., 2014b, Halvorsen et al., 2009).

Table 8-2. Composition of the synthetic natural gas for the gas hydrate test

Synthetic natural gas component	Mole percent
Methane	79.10%
Carbon Dioxide	2.50%
iso-Pentane	1.70%
n-Pentane	1.70%
iso-Butane	2%
n-Butane	2%
Propane	4%
Ethane	7%
Total	100%

8.3.3 Scenarios

The following scenarios have been simulated in the MEG pilot plant using a 50:50 wt % ratio of rich MEG to condensate, rich MEG at 74.5 wt % concentrations, and the assumption that sand/fines are negligible:

- A: Rich MEG + drilling mud (no brine, and no condensate).
- B: Salt-laden rich MEG + drilling mud (0.6 wt %) (no condensate)
- C: Salt-laden rich MEG + drilling mud (0.6 wt %) + condensate.
- D: Salt-laden rich MEG + drilling mud (1.2 wt %) + condensate.
- E: Salt-laden rich MEG + drilling mud (0.6 wt %) + condensate + demulsifier (at 1000 and 2000 ppm).
- F: Salt-laden rich MEG + drilling mud (1.2 wt %) + condensate + demulsifier (at 2000 ppm).

The salt-laden rich MEG solution used in the above scenarios was prepared according to the rich MEG composition presented in Table 8-1. Each scenario run was performed twice (except scenario A, which was only performed once) to observe results repeatability.

8.3.4 MEG pilot plant operating philosophy

The closed-loop MEG regeneration pilot plant (Figure 8-2) is controlled by a PLC system comprising three operational areas: pre-treatment (with feed blending),

regeneration, and reclamation (Baraka-Lokmane et al., 2013, Yong et al., 2015). For the purpose of simulating a typical field rich MEG clean-up phase (section 8.3.3), the salt-loaded rich MEG was premixed and put in the brine tank (BT). A glass vessel acting as a TPS was placed between the feed blender and the MPV. The rich MEG taken from the TPS represents the composition of the rich MEG leaving the primary liquid/liquid separator, both in terms of condensate content and emulsion (Figure 8-10 and Figure 8-11). Thus, in these experiments; the BT was utilized as a salt-loaded rich MEG feed, the condensate tank (CT), feed blender (FB), and TPS vessels to create a defined condensate carry-under into the MPV, and the rich glycol tank (RGT) and filters for particle precipitation and separation. The distillation column (DC) (fitted with two sections, one meter each of three-inch diameter of structural packing DN 800 with 5 KW electrical reboiler at the bottom) (Zaboon et al., 2017) was used to concentrate the rich MEG to lean MEG, and the reclaimer (20 L HEIDOLPH) to remove dissolved salts. The FB is a 15 L stainless steel 316 vertical cylindrical vessel, installed with a shear stress mixer (which can go up to 7000 rpm) to form a homogenized emulsion. The TPS is a 20 L vertical glass vessel that acts as the stabilizer feed separator (to separate flashed gasses, liquid hydrocarbon, and rich MEG). The MPV is a 31 L stainless steel 316 vertical cylindrical vessel with a glass viewing strip (Figure 8-3).

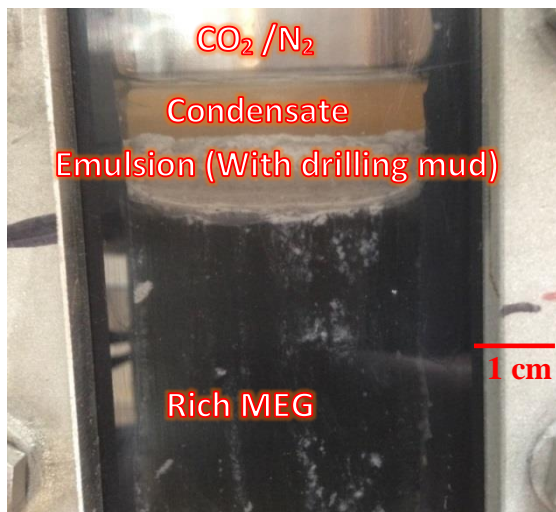


Figure 8-3. MPV viewing strip.

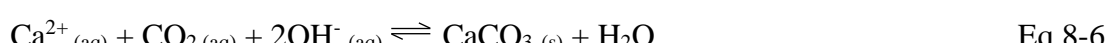
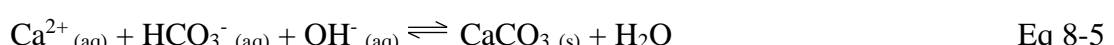
A rich MEG mixture was first prepared separately in the BT (100 L PVC Water/BT with floor-mounted Nitrogen sparge). For proper mixing, the drilling mud was mixed with the condensate and added to a separate feed-vessel, which was agitated using a

magnetic stirrer to keep the solids in suspension. Solutions from BT, the drilling mud feed vessel, and the CT (31 L stainless steel 316 horizontal cylindrical vessel) were routed to the FB. The solution of the FB was sheared at 5000 rpm and then routed to the TPS, prior to entering the MPV. The solution is sheared to replicate the agitation caused by different parameters such as pressure drop in the process, wellhead valves, mechanical chokes/orifice plates (for flow restriction and flow measurement), two-phase (gas/liquid) flow in trunk lines/separators, changing flow regimes, and pumping (Kokal et al., 2000). All the vessels in the pilot plant were run at 100 kPa pressure and the CO₂ content of the sparging gasses was, therefore, adjusted to provide the correct amount of dissolved CO₂ in the various vessels. Mass flow pumps were controlled by PLC via feedback from mass flow meters to ensure accurate mass ratios in the feed. The drilling mud/condensate solution was pumped at a constant flow rate of 5 kg/hour to the feed-blending vessel, and all other mass flows were adjusted accordingly. To maintain a 50:50 wt % ratio, the total feed into the feed blender was maintained at around 10 kg/hour. From the FB, the solution was transferred to the TPS. The rich MEG was then pumped from the bottom of the TPS into the MPV at a flow rate of 4 to 6 kg/hour, while the condensate was pumped from the condensate phase, and filtered and stored in the CT. The rich MEG alkalinity (i.e. ability to absorb protons) (Montazaud, 2011) was increased by adding 1 mol/L (80 ml/h) NaOH (Sykes et al., 2016) solution via a dosing pump, with the aim of forcing precipitation of scale forming salts in the MPV to protect the downstream regeneration equipment.

Equations (Eq 8-3 and Eq 8-4) (Flaten et al., 2010, 2009, Flaten et al.) below shows that water in contact with carbon dioxide (CO₂) produce carbonic acid (H₂CO₃) and pH is lowered (pH ≈ 4.2) (Toews et al., 1995, Wurts et al., 1992, Kalka, 2017).



Adding alkalinity (NaOH) until the pH of 9.6 shifts the reaction to the right thus promote calcium carbonate precipitation(MacAdam et al., 2004) as per below equations (Eq 8-5 and Eq 8-6) (Yong et al., 2015, Baraka-Lokmane et al., 2012):



The best way to remove scale-forming salts and clean the solution is to increase the temperature and allow sufficient residence time (Montazaud, 2011). On the other hand, reducing the alkalinity downstream of the MPV is essential, as high alkalinity increases the risk of calcium and iron carbonate precipitation in the process, injection points and pipeline, for example if formation water is produced (Flaten, 2010).

To achieve proper separation temperature, the rich MEG in the MPV was kept circulating through the rich MEG heat exchanger (RMH); once a temperature of 80 °C was reached, the rich MEG was pumped to the RGT via the temperature control valve. Once the RGT reached minimum fill height, the rich MEG was transferred to the reboiler by a pump through dual 10-micron sock filters. Filters were used to help minimize foaming and sludge build-up in the reboiler (Sykes et al., 2016, Pauley et al., 1991). The reboiler temperature was set at 135 °C to provide the necessary heat for the DC to operate, and thus evaporate water and concentrate the MEG to around 90 wt % (Montazaud, 2011, AlHarooni et al., 2017). The water vaporization process (MEG concentration) can be accelerated by increasing the reboiler operating temperature but may lead to MEG degradation (Dugstad et al., 2004, AlHarooni, Pack, et al., 2016, AlHarooni et al., 2015). To minimise the required operating temperature the reboiler was operated at atmospheric pressure. Reboilers are rarely operated under vacuum in the field (except in some cases of full stream reclaimer), because of the added complexity and increasing the chance of air sucking from the atmosphere (from weak joints or leaks). Inducing oxygen to the MEG loop leads to MEG degradation (Arnold et al., 1999).

The vapor (boiled water with a small amount of MEG) from the DC enters the overhead reflux condenser (CO). The CO provides cooling/condensation via a counter-current flow using chilled water supplied by the water chiller, thus improving the water/glycol separation and so minimizing glycol loss (Jonassen, 2013, Richardson et al., 1986). The condensed vapors then fall into the reflux drum (RD). The distillation system was operated at total reflux until a steady state was reached (after 1.3 hours). Once a steady state was achieved, the sump and feed pumps were started, to allow for continuous regeneration. Lean MEG concentration was monitored using the mass-flow meter density, the amount of produced water, and the refractometer. Once a sufficient amount of lean MEG was produced, the

reclaimer was partially filled with lean MEG and operated at 100 mbar pressure, 30 RPM, and oil bath temperature set to 160 °C. The temperature of the wet vapor leaving the reclaimer sump was around 125 °C. Reclaimers are operated under a considerable vacuum to reduce the processing temperatures and the consequential risk of MEG degradation, which, if allowed to occur, leads to a hydrate inhibition performance drop, (AlHarooni et al., 2015) a sharp rise in MEG losses, and equipment fouling (Sykes et al., 2016). Lean MEG was kept routed to the sump until salt crystallization was observed (Figure 8-15).

8.3.5 Gas Hydrate Experiment

8.3.5.1 Cryogenic Sapphire Cell Unit

Gas hydrate equilibrium measurements were carried out in a transparent cryogenic sapphire cell unit (AlHarooni, Barifcani, et al., 2016) (Figure 8-4), 60 cm³ volume, high operating pressure (maximum 500 bar), and a built-in variable speed magnetic stirrer (operated at 530 rpm) to agitate the solution. The cell chamber temperature (range +60 to -160 °C) was controlled using an electric heater and refrigeration system, enhanced with a supply of chilled water. The temperature of the gas phase and the liquid phase were respectively measured via platinum resistance thermometers (PT100 sensor with three core Teflon tails, model TC02 SD145, accuracy of ±0.03 °C). Sapphire cell pressure was measured with a pressure transducer (model WIKA S-10; accuracy of ±0.5 bar). The schematic diagram and full unit details have been described elsewhere (AlHarooni et al., 2015, Sadeq et al., 2017, AlHarooni, Pack, et al., 2016).

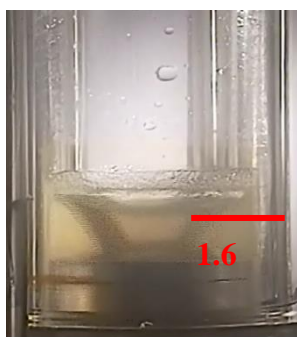


Figure 8-4. Hydrate Formation.

8.3.5.2 Hydrate Equilibrium Detection Method

Hydrate equilibrium (dissociation) points were detected by analyzing pressure versus temperature trends using an isochoric method (temperature search method) (Zang et

al., 2017, Fonseca et al., 2011, Chapoy et al., 2008, Rovetto et al., 2006, Tohidi et al., 2000). An isochoric method was conducted by pressurizing the cell to the required pressure, closing the inlet valve to keep the volume constant while the temperature was varied (Luna-Ortiz et al., 2014, Tohidi et al., 2000, Zang et al., 2017).

Experiments were conducted by first injecting 7 mL of test solution, pressurizing the cell with natural gas to the required pressure (i.e. 65, 85, 105 and 125 bar), setting the initial temperature at a value outside hydrate formation point (by around 8 °C), and then closing the inlet valve (to keep the volume constant). The cell was cooled to a high sub-cooling temperature and then monitored for hydrate formation. Once hydrate was formed, cooling was maintained until around 60% of the solution had converted to hydrate. The hydrate formation point was identified both by visual observation and by a sudden drop in pressure (caused by gas consumption, as the gas is enclathrated into the hydrate lattice) (Rovetto et al., 2006). The cell was heated slowly in steps of (\approx 0.5 °C/30 minutes) (Tohidi et al., 2000) to allow adequate time to achieve a steady equilibrium state. Once hydrate started to dissociate, heating was continued until most of the hydrate was dissociated, which was observed visually. The hydrate dissociation point is considered as the thermodynamic equilibrium point, because of its accurate repeatability, while the hydrate formation point is influenced by many factors, such as degree of sub-cooling, rate of cooling, memory effect, purity of solution, etc (Tohidi et al., 2000). The hydrate equilibrium point was identified from the pressure versus temperature trends for each experimental run. The pressure variation with temperature change and time were synchronized at an interval of 12 points/second to a computer using Texmate Meter-Viewer software. The hydrate equilibrium point (●) is identified as the intersection of the hydrate dissociation curve (Δ) with the cooling curve (□), as illustrated in Figure 8-5 and by Sloan et al. (2008b). The intersection (equilibrium) point is also found to be coincident with visual observation of hydrate dissociation points within an average error deviation of $\pm 1.01\%$.

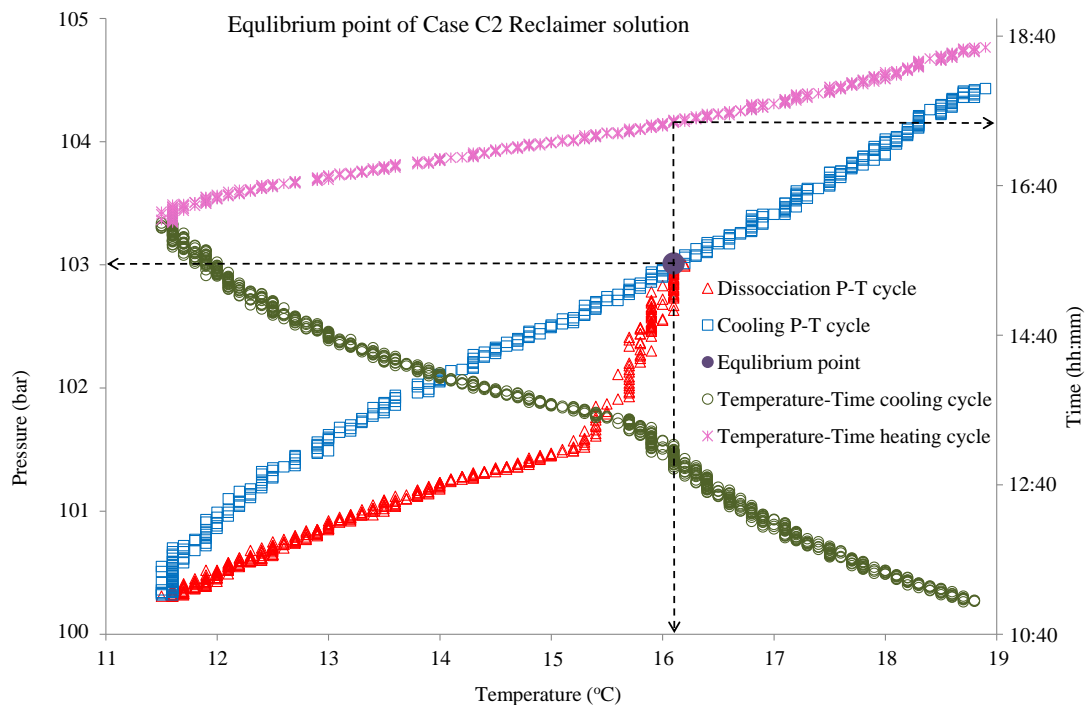


Figure 8-5 An example of an isochoric temperature search method used for identifying the equilibrium point of reclaimed solution of scenario C2.

The accuracy of the equilibrium-generated data was evaluated by repeating the 20 wt % fresh MEG and the 100 wt % deionized water experiments three times; the repeated experiments showed a high accuracy, with a maximum experimental error of 1.65% and standard deviation (SD) of ± 0.19 . Hydrate equilibrium points were generated using the highly-recommended equation of state by Peng-Robinson (PR) (Peng et al., 1976, Hemmingsen et al., 2011) (Aspen HYSYS (version 8.6) and Multiflash (version 3.6) software). Both software demonstrated a high level of agreement with the experimental results. Aspen HYSYS predicted results with an average temperature deviation of ± 0.65 °C while Multiflash predicted results with an average temperature deviation of ± 0.44 °C. Equilibrium data in the literature showed higher deviation from this work than the software, as referenced in Figure 8-6. This is primarily because the literature used a slightly different natural gas composition. The equilibrium data of Smith et al. (2016), who used almost the same gas composition as in our work, showed excellent matching results, with an average temperature deviation of only ± 0.28 °C. For a clear comparison, Figure 8-6, plotted using a semi-logarithmic scale to illustrate data consistency, as the logarithm of the

hydrate equilibrium locus (pressure versus temperature), has approximately liner behavior (Mohammadi et al., 2009).

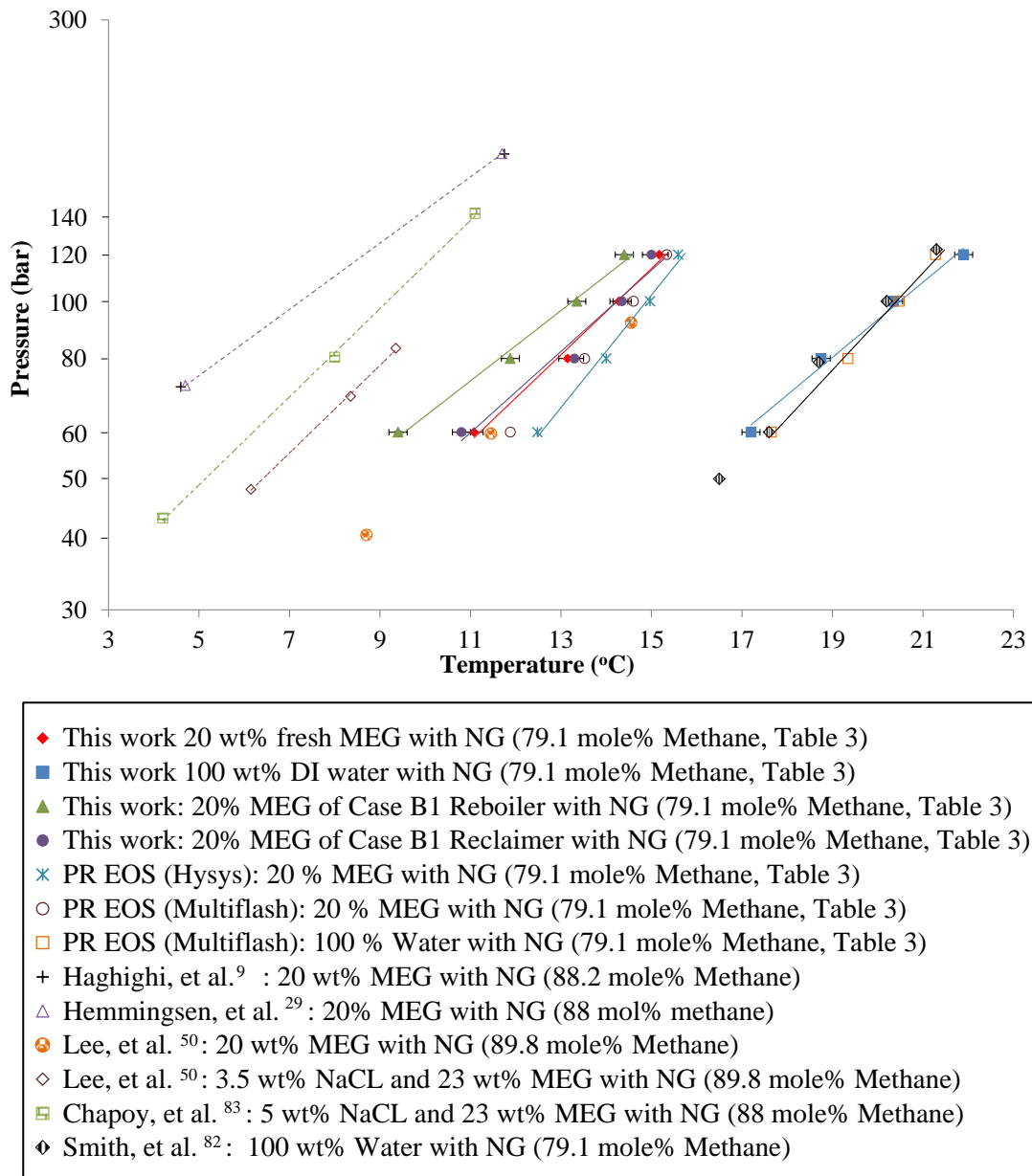


Figure 8-6. Equilibrium curve of natural gas with 20 wt % solution of scenario B1 (salt-laden rich MEG + drilling mud (no condensate)), literature data added for comparison. (Hemmingsen et al., 2011, Chapoy,Mazloum, et al., 2012, Haghghi et al., 2009, Lee et al., 2011, Smith et al., 2016)

8.4 Results and Discussion

8.4.1 MEG Pilot Plant

8.4.1.1 Pretreatment

The pretreatment section was run at atmospheric pressure and the CO₂/N₂ sparge gas concentration was adjusted using a mass flow controller (Alicat, MCS series by Alicate scientific, USA), to 6.2 mol % (of CO₂ in N₂) for FB, 5.8 mol % for TPS, and 3.5 mol % for MPV, to replicate field conditions. This section is designed to remove drilling mud, condensate, and low soluble/divalent salts and minerals (Kim,Lim, et al., 2017). Divalent-monovalent cation concentrations for each MEG pilot plant scenario run are illustrated in Figure 8-7, Figure 8-8, and Figure 8-9 for BT, TPS, and MPV respectively. The divalent-monovalent cation concentrations of BT are for the MEG solution prior to mixing with drilling mud, while for TPS they are from after the FB, where all incoming fluids are blended using a stress mixer at 5000 rpm. The MPV is injected with NaOH and purged with CO₂ to precipitate divalent cations in the solution, such as Ca²⁺. It can be seen clearly from Figures 7 and 8 that almost 74% of the Ca²⁺ has been precipitated in the MPV. To maximize removal of Ca²⁺ and other divalent ions, adjustment to a sufficient injection rate of NaOH is required. Removing divalent cations in the pretreatment section is vital, as recycling them in the MEG loop may lead to scaling, not only in the MEG plant but also downstream, at the MEG injection points situated at the wellheads and pipelines (Baraka-Lokmane et al., 2012, Baraka-Lokmane et al., 2013).

In terms of total cations movement from TPS to MPV, scenario runs of C1, D1, C2, F1, and B1 showed cations were migrated from TPS to the MPV (MEG outlet) by 47%, 23%, 11%, 0.6%, and 0.5% respectively. On the other hand, less cations migrated from TPS to MPV for scenario runs of F2, D2, E2, E1, and B2 by 8%, 8%, 2.2%, 0.9%, and 0.4% respectively (Figure 8-8 and Figure 8-9). It was observed during the operation that the dissolved oxygen level kept fluctuating, indicating that dissolved oxygen was not fully replaced by the sparging gas mixtures concentration (CO₂/N₂) and not fully captured by the oxygen scavenger. Dissolved oxygen concentration must be maintained or kept below the detrimental level of 20 ppb (Salasi et al., 2017).

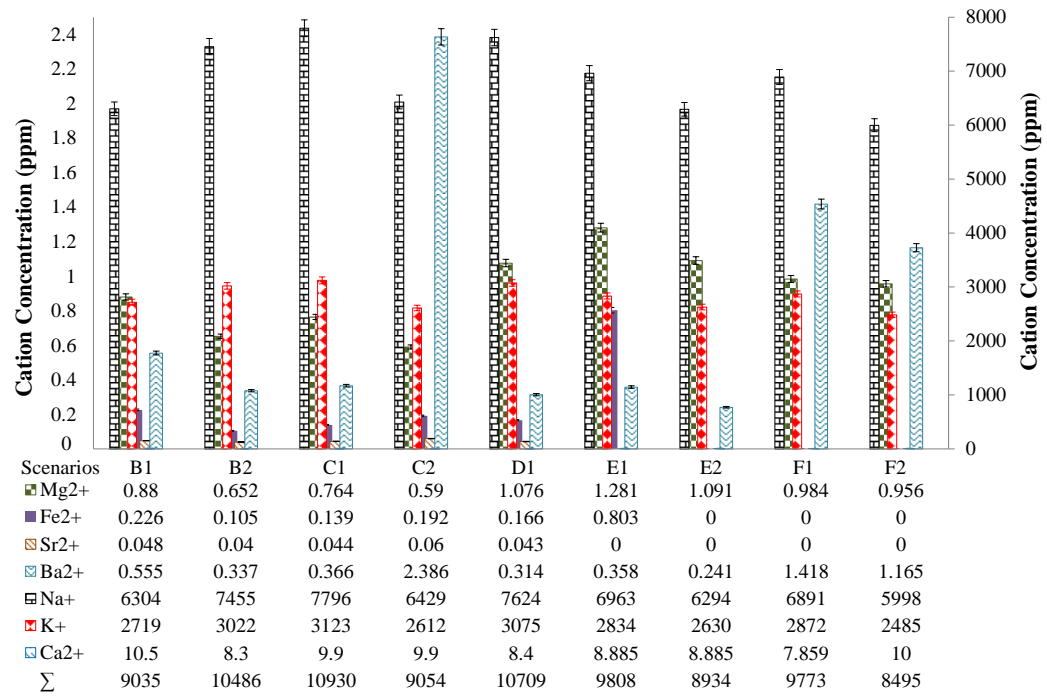


Figure 8-7. Brine Tank divalent-monovalent cation concentrations (ppm). Note: Na⁺, K⁺ and Ca²⁺ follow right-hand axis.

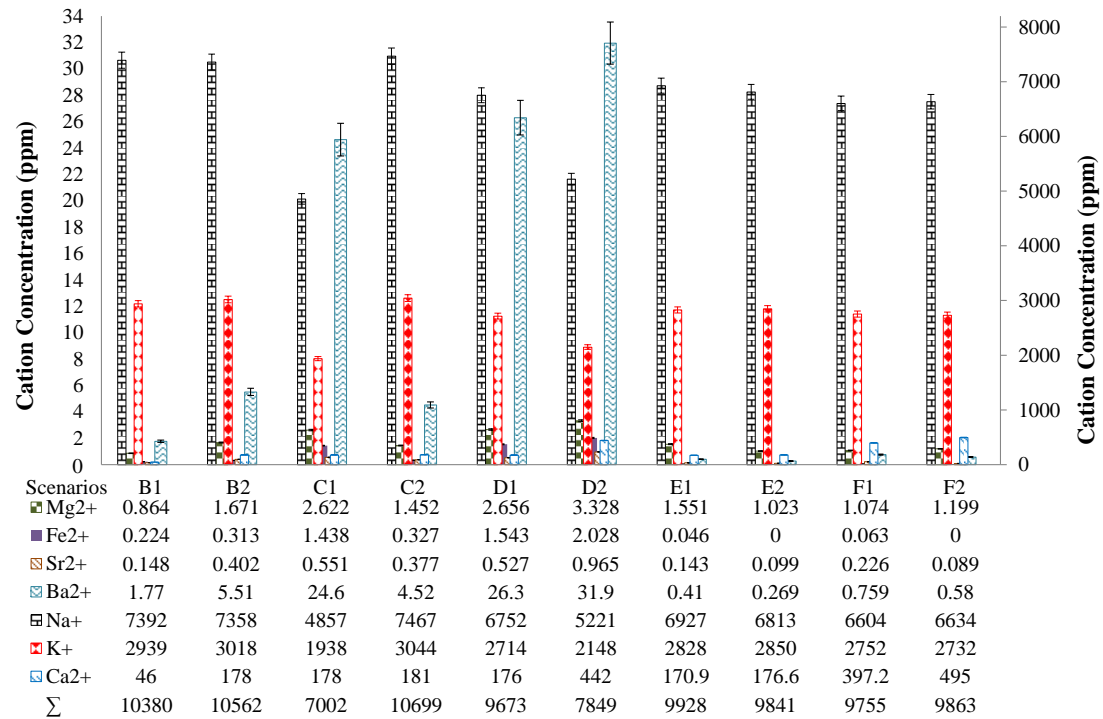


Figure 8-8. Three phase separator divalent-monovalent cation concentrations (ppm). Note: Na⁺, K⁺ and Ca²⁺ follow right-hand axis.

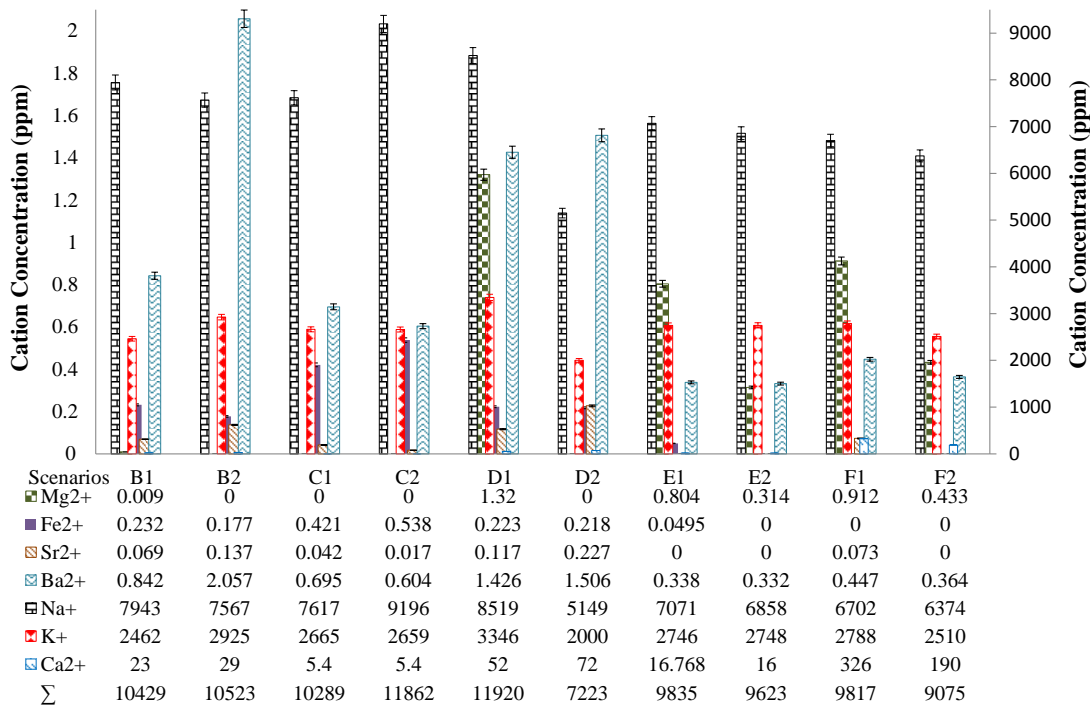


Figure 8-9. MEG Pre-treatment Vessel divalent-monovalent cation concentrations (ppm) at MEG outlet. Note: Na⁺, K⁺, and Ca²⁺ follow right-hand axis.

A base scenario, of clean fluid (rich MEG + condensate) without drilling mud, showed good separation in the TPS, and a clear white emulsion was formed at the interface level with clear MEG/condensate phases (Figure 8-10). However, solutions with drilling mud and without demulsifier did not undergo full emulsion separation (scenarios A-D). Drilling mud increases emulsion formation, leading to condensate carryover into the MPV (Figure 8-3 and Figure 8-11). The rich MEG and condensate phases remained cloudy, demonstrating that the drilling mud had no clear tendency to partition either in the condensate or the MEG phase. Adding a demulsifier led to faster emulsion breakdown in the TPS, and reduction in the drilling mud carry-over to the MPV. The addition of 2000 ppm demulsifier (scenarios E and F) resulted in a clear condensate phase, pushing the drilling mud to the interface portion. The addition of 1000 ppm demulsifier resulted in the same performance as the 2000 ppm, but with around 35% less drilling mud pushed to the interface portion.

The rich MEG phase from the MPV was circulated to the heat exchanger set at 80 °C to accelerate chemical precipitate of divalent ions.(Latta et al., 2016) A high temperature increases the thermal energy of the droplets, which enhances drop collisions and settling rates. It also reduces the interfacial viscosity and increases

MEG/condensate emulsion separation.(Kokal, 2002, Jones et al., 1978) The dual effect of temperature and demulsifier resulted in a better separation. The rich MEG leaving the MPV was clear, indicating that a high volume of the drilling mud stayed in the MPV, having accumulated in the interface portion (Figure 8-3)



Figure 8-10 TPS: Base scenario: clean fluid.

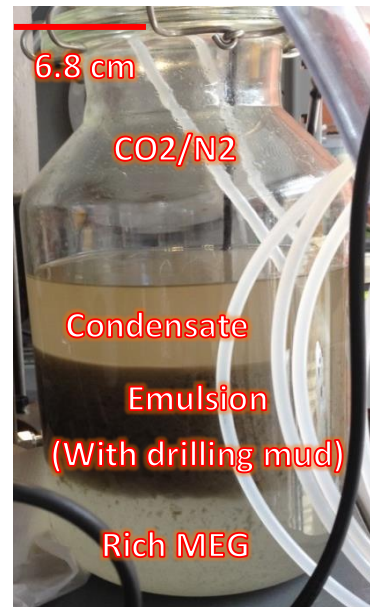


Figure 8-11 TPS: with drilling mud.

8.4.1.2 Regeneration

The solution leaving the MPV towards the RGT was found to be almost free from hydrocarbon (condensate). This means the pre-treatment section was well designed and operated to accommodate and separate the incoming condensate (Latta et al., 2013). Contamination of drilling mud was found in the RGT, indicating that mud did not take full separation during the pre-treatment section. Traces of mud are further separated before routing to the reboiler, using a 10-micron filter. The reboiler housing was made from glass, for visual observation, and, during the operation, no scaling was observed on the reboiler heating elements. It was, however, observed that the rich MEG in the reboiler became turbid when the temperature exceeded 80 °C (Figure 8-12). As the reboiler was operated at 135 °C and for short periods (≈ 4 hours), there might not have been sufficient time to develop a visible scale layer on the heating elements. However, from Table 8-3 it can be noted that calcium is precipitating out in the regeneration system as the amount of dissolved calcium ions was reduced during MEG regeneration (the exception being scenario F2). In general,

caution should be taken when operating at high temperature, as it have some negative effects, such as increasing the operation cost, scale deposition and corrosion rate (Kokal, 2002).

Table 8-3. Ca^{2+} concentration and % precipitated before and after reboiler

	Scenario B		Scenario C		Scenario D		Scenario E	
Runs	1	2	1	2	1	2	1	2
Ca^{2+} concentration in feed to RB (ppm)	17	24	8.3	6.6	44	99	63	84
Ca^{2+} concentration after RB (ppm) (in LGT)	5.8	19.8	2.9	3.5	2.3	63	3.9	67
Ca^{2+} Precipitating %	65.9	17.5	65.1	47.0	94.8	36.4	93.8	20.2

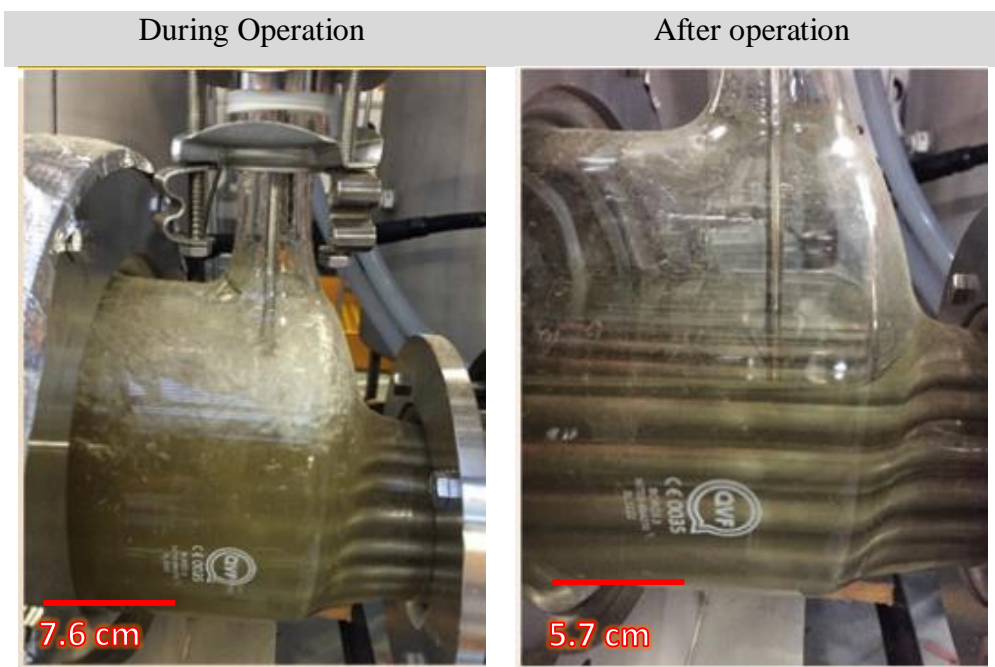


Figure 8-12 Reboiler vessel during and after operation of scenario E.

Analysis of the divalent cation concentrations (Figure 8-13) of the rich MEG in the RGT showed that Ca^{2+} ion concentrations varied between 7 to 300 ppm, corresponding to a removal rate of 23-95% (comparing to TPS divalent ion concentrations). Also, comparing the divalent cation concentrations (Figure 8-14) of the MEG solution in the LGT with RGT shows that Ca^{2+} ion concentrations vary between 2 and 300 ppm, corresponding to a removal rate of 18-99 ppm % (except for

scenario F2). The pH value of the lean MEG was observed to increase to values around 11.3 (Figure 8-19). A pH value of 7.0 to 8.5 is recommended to prevent corrosion/scale formation in a plant (Gonzalez et al., 2000). When comparing the alkalinity values of the feed MEG and lean MEG (Figure 8-19), the increase in pH can be explained by; the transformation of bicarbonate to carbonate when the dissolved CO₂ boils off in the DC and by the reduction (separation) of condensate. The relationship between dissolved CO₂ and pH for 80 wt % MEG solutions with 50 mmol/L alkalinity has been presented elsewhere, by Seiersten et al. (2015). After a steady state of 1.6 hours of reboiler operation, solution samples were collected for laboratory analysis and gas hydrate experiments.

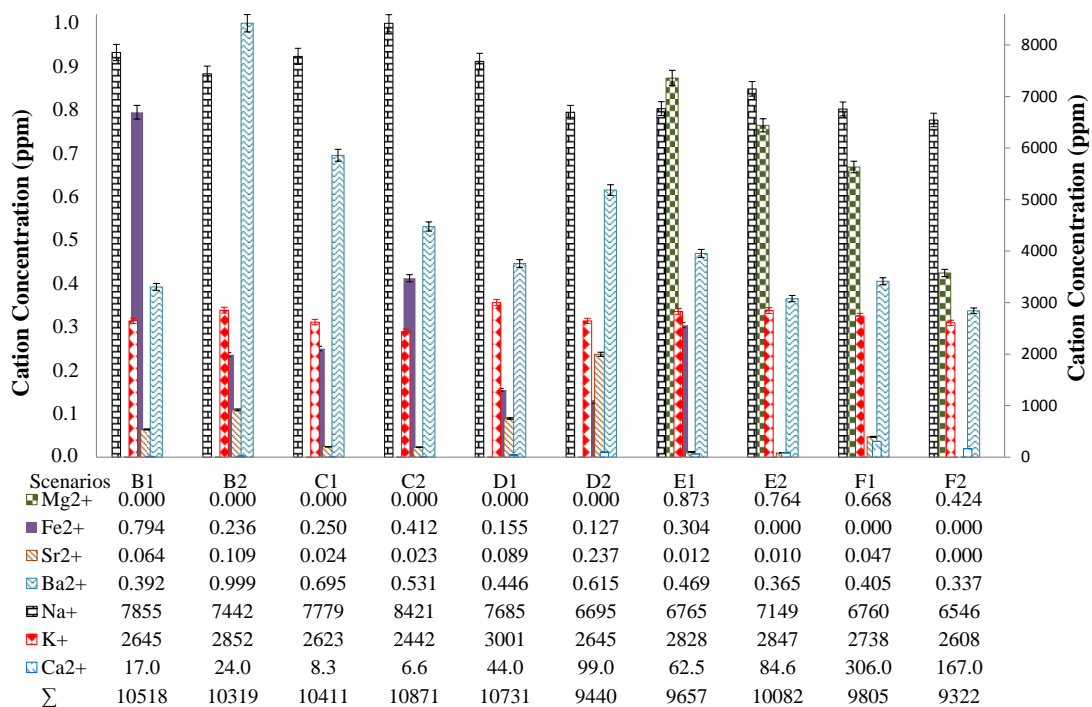


Figure 8-13 Rich Glycol Tank divalent-monovalent cation concentrations (ppm).

Note: Na⁺, K⁺, and Ca²⁺ follow right-hand axis.

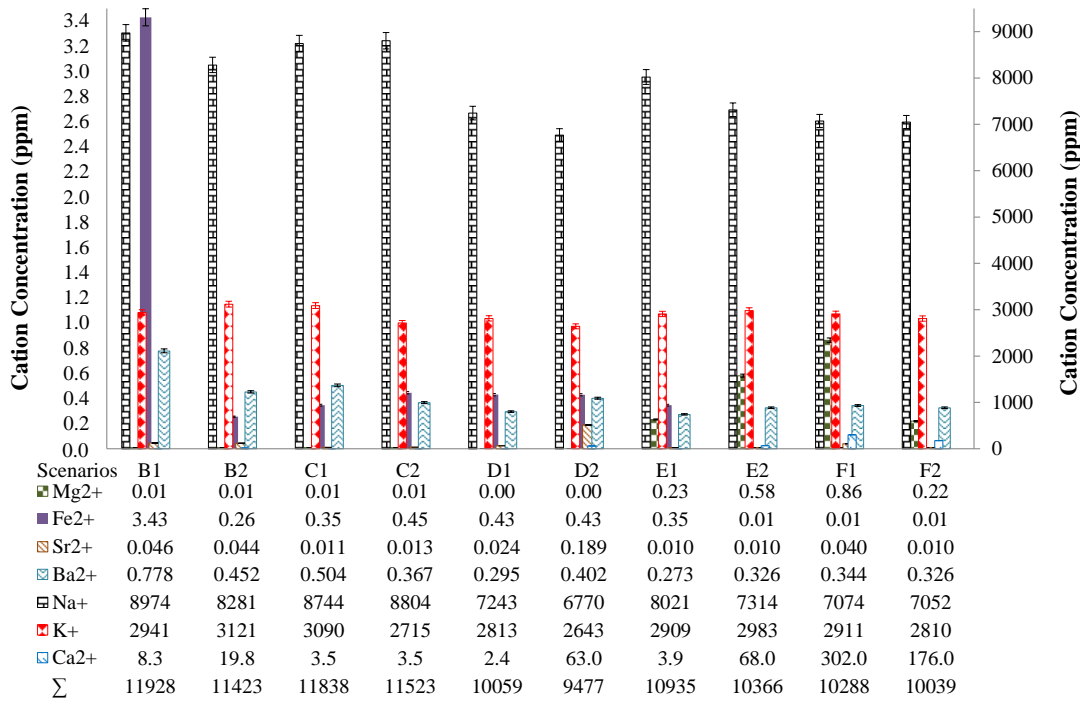


Figure 8-14 Lean Glycol Tank divalent-monovalent cation concentrations (ppm).

Note: Na⁺, K⁺, and Ca²⁺ follow right-hand axis.

8.4.1.3 Reclamation

A slip stream reclamation concept was implemented (a semi-continuous mode) for all scenarios run. In this concept, water is first separated in the regeneration unit, then part of the re-concentrated MEG is routed to the reclainer where high soluble salts of monovalent cations (NaCl and KCl) are removed, while some level of high soluble salts is tolerated (≈ 20 g/l) (Jeon et al., 2014, Baraka-Lokmane et al., 2012). As can be seen from Figure 8-14, high quantity of the divalent cations were removed, while monovalent cations (Na⁺ and K⁺) still exist at high concentrations. This indicates that most of the low soluble salts (salts of divalent cations) were precipitated in the pretreatment section as required (Baraka-Lokmane et al., 2012). As the reclamation was run in a semi-continuous mode, the fill height of the reclainer evaporation flask was maintained by adding solution from the LGT automatically. Reclamation of the salty lean MEG precipitates out high soluble salts and accumulate in the bottom of the flask. The formed salt crystals are monovalent (NaCl and KCl). The vapour flowed overhead to the condenser and was pumped out as salt free lean MEG to the LGT (Latta et al., 2016). The experiment was ended when the evaporation flask contained a large amount of precipitated salts (Figure 8-15).

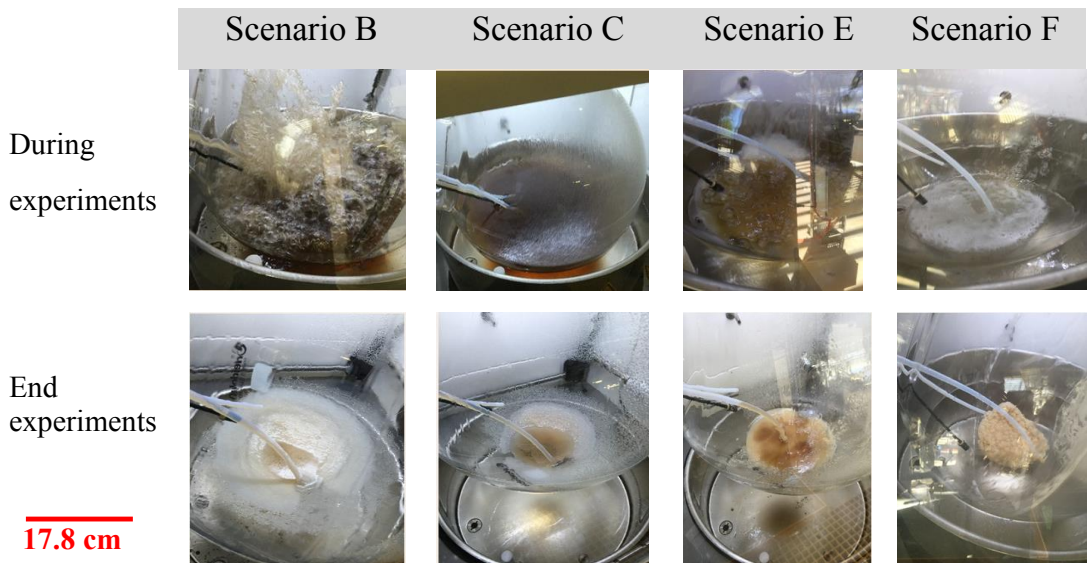


Figure 8-15 Salts precipitated in the reclaimer.

During reclamation, the first salt precipitation was observed when the lean MEG was concentrated by a factor of three, and the remaining water content in the slurry was as low as 7%. A significant portion of the monovalent ions was removed during reclamation (> 97%). Table 8-4 shows the monovalent cations percentage precipitation in reclaimed MEG, for each scenario run. The liquid phase of the slurry in the reclaimer had viscosity values up to 50 mPa-s at 20 °C and up to 6 mPa-s at 75 °C; this high viscosity is because of the solution containing high salt-saturated MEG and the precipitated salts.

Table 8-4. Reclaimer divalent-monovalent cations partition.

Scenarios	B 1	B2	C1	C2	D1	D2	E1	E2	F1	F2
	98									
Precipitation %	.5	97.1	99.2	99.9	98.6	97.9	98.8	98.9	97.1	99.9

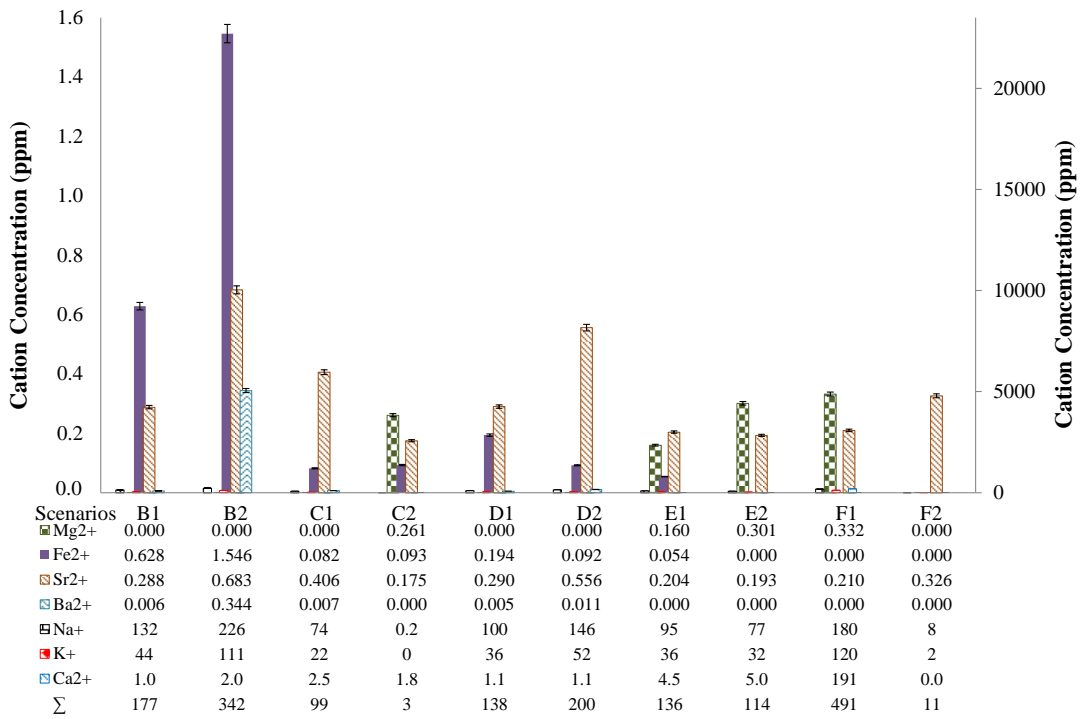


Figure 8-16. Reclaimer condensed side divalent-monovalent cation concentrations (ppm). Note: Na⁺, K⁺, and Ca²⁺ follow right-hand axis.

Electrical conductivity (σ), which is the ability of a solution to carry an electric current (Cammann et al., 2000), is a well-recognized measurement for evaluating salt concentrations in the MEG solution (Bonyad et al., 2011, AlHarooni, Pack, et al., 2016). Thus, electrical conductivities for scenarios were measured (Figure 8-17) and found to respond proportionally to the cations concentration. The electrical conductivity of scenario B2 showed the highest value (8620 μ S/cm), corresponding well to the high cation concentrations (15231 ppm), followed by scenario F1. Electrical conductivities increased dramatically as the solution moved from the reboiler to reclaimer condensed side, and then to the reclaimer slurry side (Figure 8-17). A big difference in electrical conductivity of the MEG solution at both reclaimer outlets gives a direct indication of high salt precipitation at the slurry side compared to condensed side. This gives a good indication of the salt extraction efficiency, and of the reclaimed MEG quality.

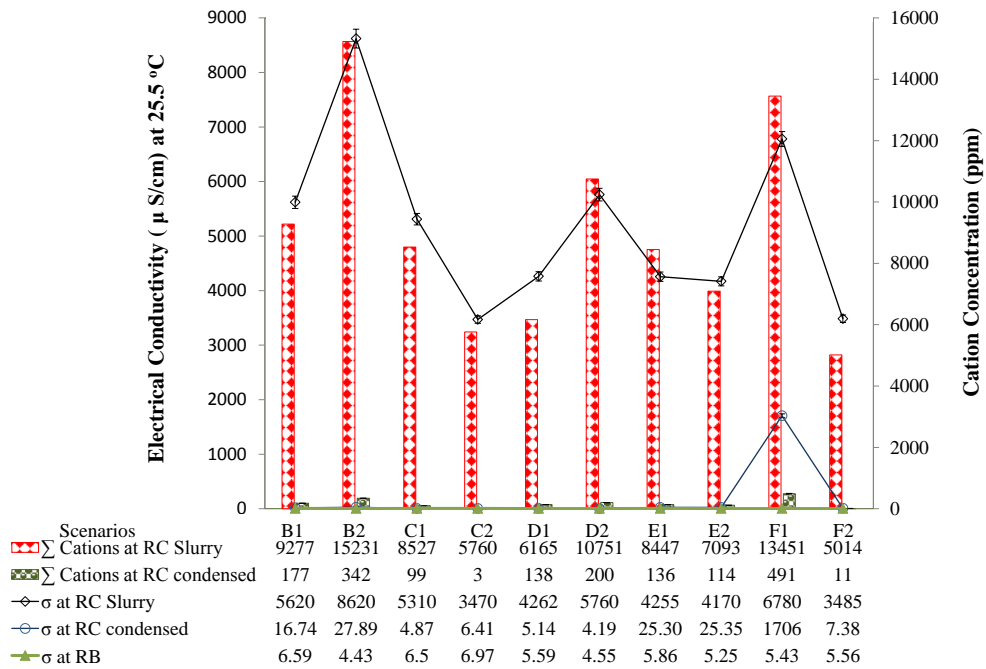


Figure 8-17. Reclaimer (RC) condensed/slurry sides total divalent-monovalent cation concentrations (ppm) corresponding with electrical conductivities (μ S/cm) of reclaimer condensed outlet, reclaimer slurry outlet, and reboiler outlet. Note: total cation concentrations follow right-hand axis.

Figure 8-18 illustrates the MEG concentration for all scenarios, measured at the outlets of BT (73.4 wt %), RGT, RB, and RC. It demonstrates the removal of water performance during MEG plant operation. It can be seen that MEG concentration of 73 wt % from the RGT was increased in reboiler to 87 wt % (scenario D2). MEG concentration is further increased in the reclaimer up to 91 wt % (scenario F1). The MEG solution samples from outlets of RB and RC were diluted with deionized water to 20 wt% and used for the gas hydrate experiments.

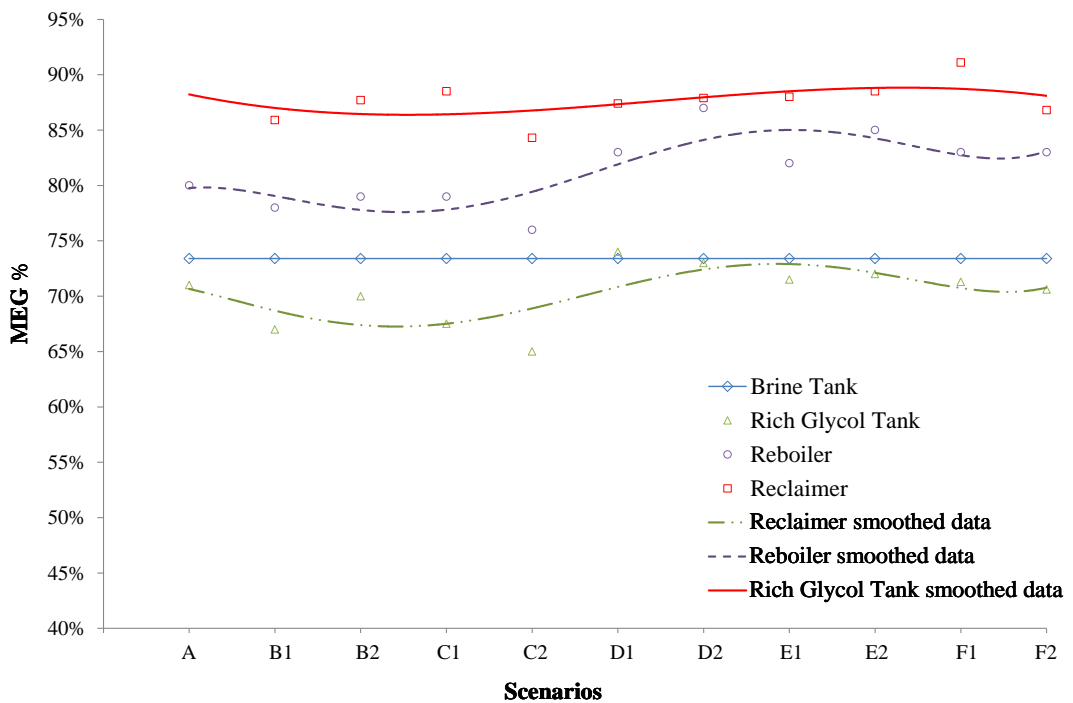


Figure 8-18 MEG wt % concentration.

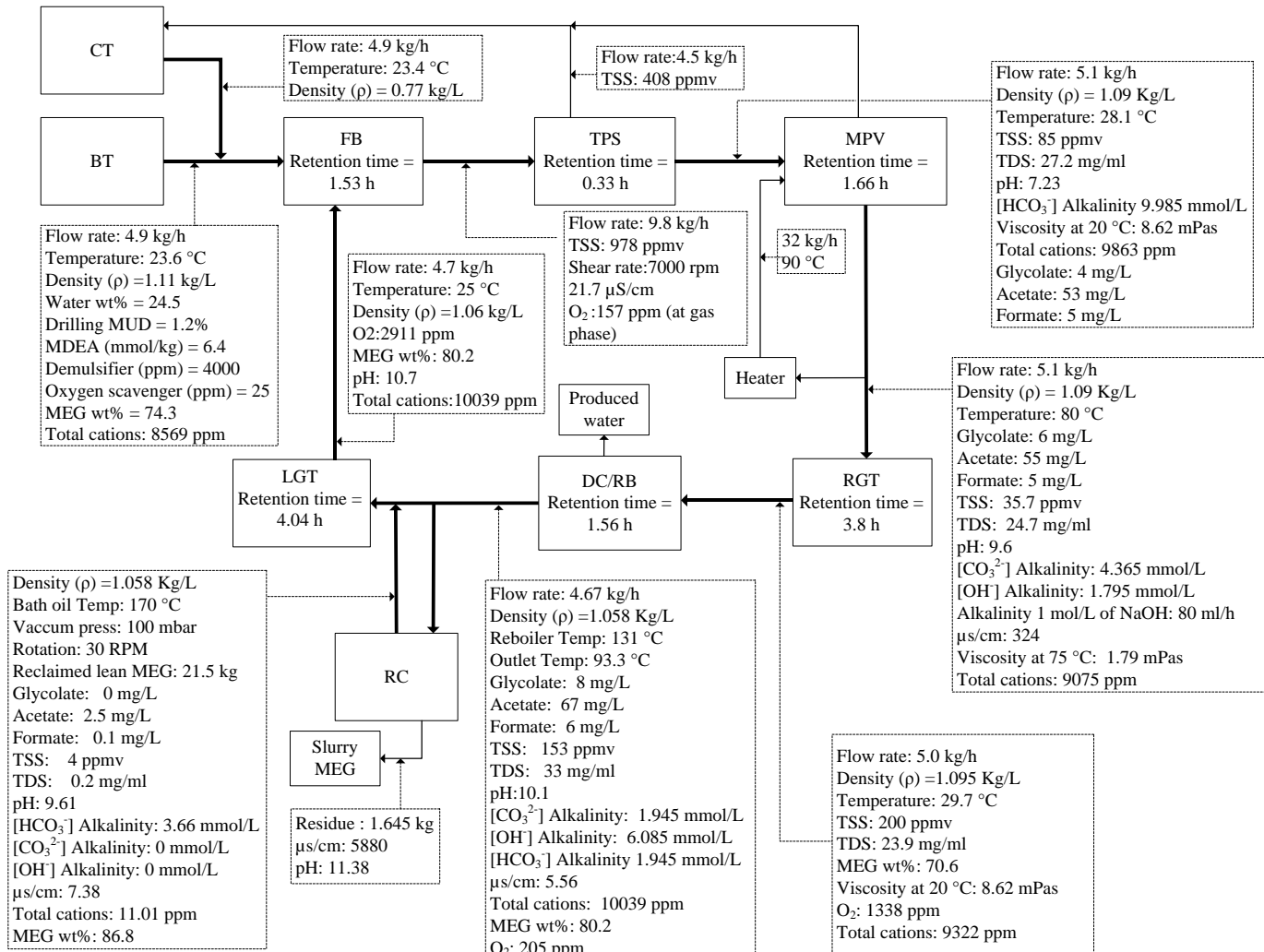


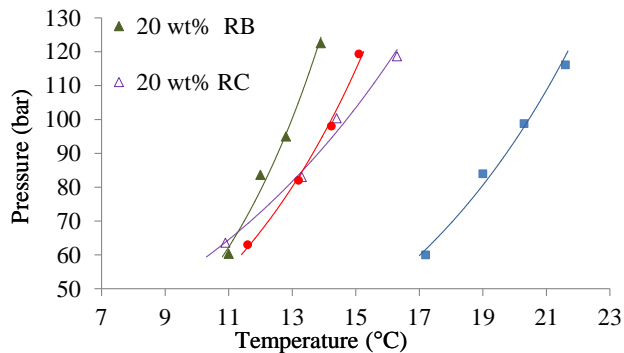
Figure 8-19. Experimental data and operating conditions of scenario "F2". Total operation time: 12.92 hours.

8.4.2 Gas Hydrate Inhibition Test

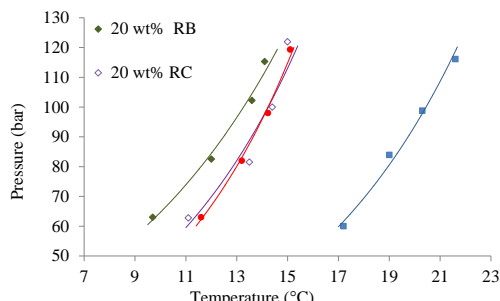
The gas hydrate equilibrium data of natural gas with 20 wt % from different MEG samples (collected from reboiler and reclaimer), compared to 20 wt % of fresh MEG and 100 wt % deionized water, are plotted in Figure 8-20 (a-i). The data fit correlates well with reboiler results ($R^2 > 0.99$) and reclaimer results ($R^2 > 0.97$). The hydrate depression temperature and the regression functions of the fitted data were reported Table 8-5 in and Table 8-6. For a given pressure, the hydrate depression value (ΔT_d) was determined as below (Eq 8-7):

$$\Delta T_d = T_{equ} (20 \text{ wt \% MEG}) - T_{equ} (100 \text{ wt \% water}) \quad \text{Eq 8-7}$$

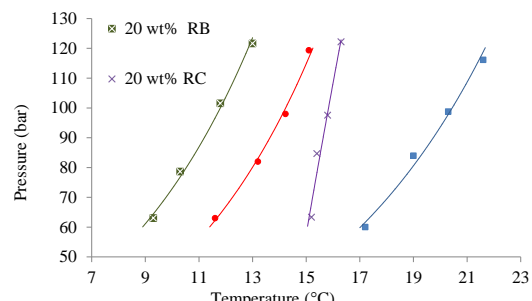
Where $T_{equ} (20 \text{ wt \% MEG})$ is the hydrate equilibrium temperature measured at 20 wt % of MEG and $T_{equ} (100 \text{ wt \% water})$ is the hydrate equilibrium temperature measured at 100 wt % water. A higher negative “ ΔT_d ” value corresponds to a higher depression (higher equilibrium shift).



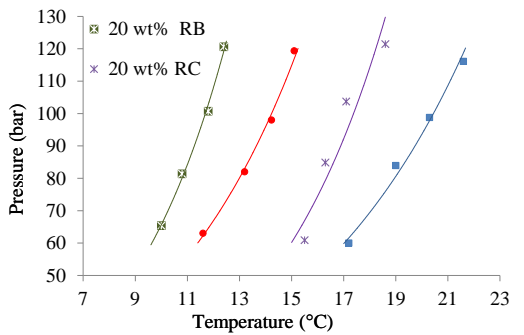
(a) Scenario A



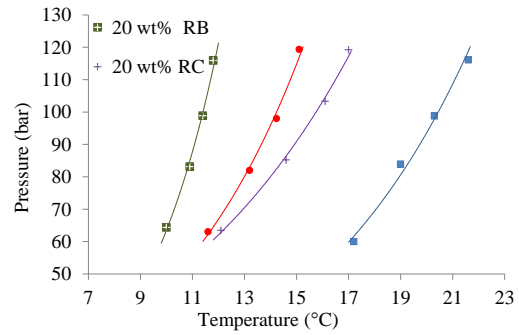
(b) Scenario B1



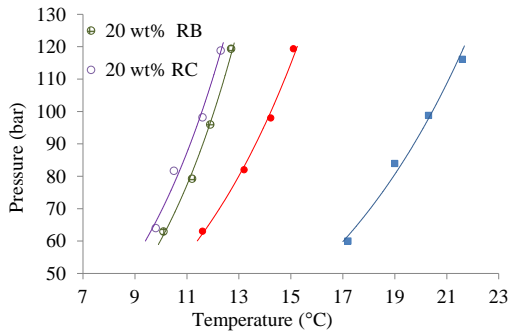
(c) Scenario B2



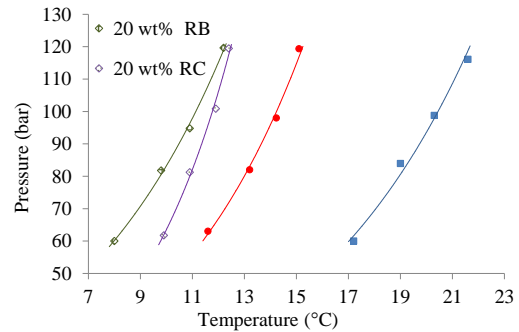
(d) Scenario C1



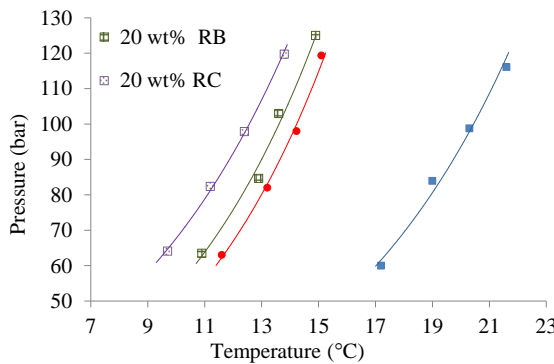
(e) Scenario C2



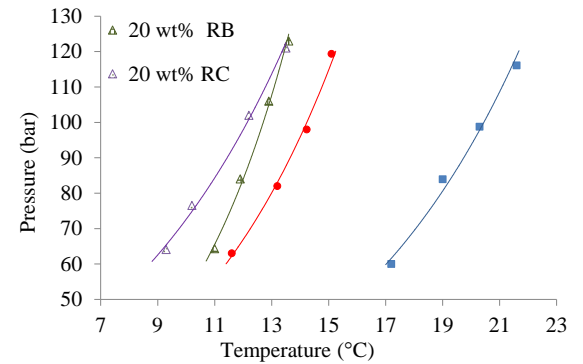
(f) Scenario E1



(g) Scenario E2



(h) Scenario F1



(i) Scenario F2

Figure 8-20. Experimental equilibrium points of natural gas hydrates in the presence of different Reboiler (RB) and Reclaimer (RC) MEG solutions for different scenarios (section 8.3.3); solid curves represent best fit; ● represent equilibrium conditions of 20 wt % fresh MEG; ■ represent equilibrium conditions of 100% deionized water.

The hydrate depression temperature of all samples collected from the reboiler outlet clearly showed a higher thermodynamic inhibition than fresh MEG (Table 8-5), i.e., it shifted more to the left side of the curve (lower temperature and higher pressure). Fresh MEG showed an average temperature depression of 6.13 °C. The highest average hydrate temperature depression was -9.26 oC for solution E2, while the

lowest measurement was $-6.78\text{ }^{\circ}\text{C}$ for solution F1 (a higher negative depression value corresponds to a better inhibition). This is mainly because of the synergistic hydrate inhibition effect of the MEG with the salt components present in the reboiler solutions (Mohammadi et al., 2009) (Figure 8-14), as a solution containing salts reduces the ability of gas hydrate formation (Chapoy,Mazloum, et al., 2012) and so works as a gas hydrate inhibitor (Mohammadi et al., 2009, Sloan et al., 2008b). Solution samples from the reclaimer outlet behaved differently to samples from the reboiler outlet. Some of the hydrate depression temperature values of the aqueous solutions collected from the reclaimer outlet show a higher depression temperature, compared to fresh MEG (scenarios E1, F2, E2, F1, and B1), while other samples show a lower depression temperature (scenarios A, C2, B2, and C1) (Table 8-6). The highest average hydrate depression temperature measured was $8.52\text{ }^{\circ}\text{C}$ for solution of scenario E1, while the lowest measurement was $2.83\text{ }^{\circ}\text{C}$ for solution of scenario C1. This difference in lower depression temperature is mainly because of the reclamation effect of removing more salts from the MEG solution (Figure 8-16). Additionally, as the reclaimer was operated at a high temperature of $160\text{ }^{\circ}\text{C}$, higher temperature can cause MEG degradation which would reduce the hydrate inhibition performance (AlHarooni et al., 2017, AlHarooni et al., 2015).

Table 8-5 Experimental hydrate depression temperature for natural gas with 20 wt % of various MEG solutions from the reboiler outlet, and the regression functions (sorted from poorest to highest inhibitor)^a

Reboiler solution scenario	Regression functions	ΔT_d °C	Pressure (bar)				Average ΔT_d
			120	100	80	60	
Fresh MEG	$P = 7.7189 e^{0.18T}$	°C	-6.73	-6.07	-5.6	-6.12	-6.13
F1	$P = 9.6097 e^{0.1721T}$	°C	-7.3	-6.87	-6.4	-6.55	-6.78
A	$P = 4.5446 e^{0.2387T}$	°C	-8.09	-7.4	-6.85	-6.2	-7.14
B1	$P = 17.067 e^{0.1333T}$	°C	-7.5	-7	-6.87	-7.8	-7.29
F2	$P = 4.2793 e^{0.2481T}$	°C	-8.42	-7.71	-7.03	-6.4	-7.39
E1	$P = 5.1143 e^{0.2469T}$	°C	-9.18	-8.29	-7.52	-7.42	-8.10
C1	$P = 5.4573 e^{0.2488T}$	°C	-9.52	-8.66	-7.97	-7.56	-8.43
B2	$P = 12.543 e^{0.1767T}$	°C	-8.98	-8.67	-8.35	-8.1	-8.53
C2	$P = 2.4954 e^{0.3237T}$	°C	-10.03	-8.92	-7.97	-7.44	-8.59
E2	$P = 16.427 e^{0.1623T}$	°C	-9.63	-9.23	-8.99	-9.2	-9.26

^a The regression function of 100 wt % deionized water found to be $P = 4.7313 e^{0.1492T}$, where P is pressure and T is temperature. A higher negative “ ΔT_d ” value corresponds to a higher dissociation temperature.

Table 8-6. Experimental hydrate depression temperature for natural gas with 20 wt % of various MEG solutions collected from the reclaimer outlet, and the fitted regression functions (sorted from poorest to highest inhibitor)^b

Reclaimer solution scenario	Regression functions	ΔT_d	Pressure (bar)				Average ΔT_d
			120	100	80	60	
C1	$P = 2.4489 e^{0.2134T}$ °C	-3.55	-3.4	-2.65	-1.7	-2.83	
B2	$P = 0.0176 e^{0.5444T}$ °C	-5.65	-4.57	-3.33	-2.1	-3.91	
C2	$P = 13.495 e^{0.1272T}$ °C	-4.82	-4.55	-4.55	-5.85	-4.94	
A	$P = 17.601 e^{0.1181T}$ °C	-5.65	-6	-5.93	-6.8	-6.10	
Fresh MEG	$P = 7.7189 e^{0.18T}$ °C	-6.73	-6.07	-5.6	-6.12	-6.13	
B1	$P = 10.196 e^{0.1604T}$ °C	-6.9	-6	-5.45	-6.4	-6.19	
F1	$P = 14.826 e^{0.1519T}$ °C	-8.08	-7.8	-7.68	-7.9	-7.87	
E2	$P = 4.8849 e^{0.2566T}$ °C	-9.47	-8.47	-7.87	-7.38	-8.30	
F2	$P = 16.314 e^{0.1493T}$ °C	-8.45	-8.33	-8.25	-8.25	-8.32	
E1	$P = 6.621 e^{0.2345T}$ °C	-9.58	-8.65	-8.33	-7.5	-8.52	

^b P is pressure and T is temperature. A higher negative “ ΔT_d ” value corresponds to a higher dissociation temperature.

8.5 Conclusions

This study established the interactions of regenerated and reclaimed MEG containing water, drilling mud, mineral salts, demulsifier, MDEA, and condensate on gas hydrate formation during the clean-up phase of a typical gas field. Understanding the kinetics of regenerated and reclaimed complex MEG solutions on hydrate phase equilibria forms the basis for improved system design, operations, and MEG dosage calculation. Also, the study investigated a highly complex process of six scenarios of MEG regeneration/reclamation. Understanding this process will help determine the optimum MEG plant operation for proper fluid separation, production, and

completion chemicals removal, mineral salts partition, and required MEG concentration, within a given industrial process, allowing appropriate control systems to be effectively managed.

The pretreatment section of the MEG pilot plant is designed to remove drilling mud, condensate, and low soluble/divalent salts. NaOH was injected to precipitate divalent cations in the solution. Rich MEG and condensate phases in the TPS remained cloudy, demonstrating that the drilling mud had no clear tendency to partition in either the condensate or the MEG phases. Adding a demulsifier leads to faster emulsion breakdown in the TPS, and a reduction in the drilling mud carry-over into the MPV. Heating the solution to 80 °C in the MPV helped to break down the emulsion. Rich MEG leaving the MPV was clear, indicating that most of the drilling mud stayed in the MPV and accumulated in the interface portion in the MPV, while a certain amount migrated to the RGT. The reclaimer operated in a semi-continuous mode at 160 °C to remove monovalent salts from the lean MEG.

Electrical conductivity (σ) measurement was used for evaluating salt concentrations in the MEG solution. Electrical conductivities at reclaimer slurry side showed the highest reading, representing high amount of precipitated salts (Figure 8-15). A pH measurement was used for evaluating acid concentrations in the MEG solution. pH values at the reclaimer condensed outlet and reboiler outlet were high, at an average of 9.2 and 11.3 respectively. The high pH can be explained by the transformation of bicarbonate ions (HCO_3^-) to hydroxide (OH^-) and carbonate (CO_3^{2-}) ions when the CO_2 boils off (Naaz et al., 2015). Generally, pH can be affected by acid gases picked up from the gas stream, the oxidation and thermal decomposition of glycol. To manage corrosion and scale risks, the pH levels throughout the plant must be carefully managed Emdadul (2012) recommended controlling the pH (after pretreatment phase) to values of 7.4-8.5 to prevent the corrosion/scale formation in the plant.

The effects of regenerated/reclaimed MEG solutions on the kinetics of gas hydrate inhibition were investigated. We reported the equilibrium conditions using the isochoric method of natural gas hydrate in the presence of 20 wt % of different MEG solutions for a pressure range of 65 to 125 bar (Figure 8-20 (a-i)).

A review was made of hydrate depression temperature, and the regression functions of the fitted data were reported (Table 8-5and Table 8-6). It is argued that the

principle possible reason for the higher temperature depression of tested solutions, as compared to fresh MEG, is the synergistic hydrate inhibition effect of the MEG with a salts component (Mohammadi et al., 2009). On the other hand, four samples from the reclaimer outlets show a lower depression temperature (less hydrate inhibition performance) than fresh MEG (Table 8-6). This is mainly because of salts removed from the MEG solution, and the presence of thermal degradation organic acids (AlHarooni et al., 2015). From a flow assurance point of view, although regenerated MEG shows a good hydrate inhibition performance, it is determined that this is because of the salts present in the solutions. However, this salt component may lead to other problems of scale build-up and corrosion if not addressed correctly.

In summary, this study has brought a new focus to the MEG regeneration and reclamation of complex solutions during the start-up and clean-up phases of the gas field, and the relationship of the final product with gas hydrate inhibition performance.

ABBREVIATIONS

- MEG: Mono Ethylene Glycol
- MDEA: Methyl Di-Ethanolamine
- FFCI: Film Forming Corrosion Inhibitor
- NG: Natural Gas
- PVT: Pressure Volume Temperature
- ICP-OES: Inductively Coupled Plasma Optical Emission Spectrometry
- IC: Ion Chromatography
- EOS: Equation Of State
- PPM: Part Per Million
- RTD: Resistance Temperature Detector.
- ppmv: Parts Per Million by Volume.
- TPS: Three Phase Separator
- RMH: Rich MEG Heater
- CT: Condensate Tank
- FB: Feed blender
- MPV: MEG Pre-treatment Vessel
- BT: Brine Tank
- RGT: Rich Glycol tank
- LGT: Lean Glycol Tank
- DC: Distillation Column
- RD: Reflux Drum
- CO: Reflux Condenser
- RB: Reboiler
- RC: Reclaimer
- PLC: Programmable Logic Control

Chapter 9 Conclusions and Recommendations

The first part of this chapter presents the overall conclusions from the studies reported in the previous chapters while the second part presents the recommendation for future work.

9.1 Conclusions

Gas hydrate formation will continue to be an area of major concern in flow assurance of natural gas production, transportation, and processing. Mono-ethylene glycol is widely used and preferred over methanol as a thermodynamic gas hydrate inhibitor, mainly in terms of relative safety and regeneration capability. During MEG regeneration, rich MEG with contaminants are purified by distillation and the reclamation process, where MEG undergoes thermal exposure through which its degradation may take place.

This thesis extensively evaluates, for the first time, the implications of thermally degraded and regenerated MEG and hydrate inhibition efficiency of natural gas hydrates with high methane content. Experimental studies using a PVT sapphire cell, autoclave and MEG regeneration pilot plant were conducted to assess the links between these two problems. This included several laboratory experiments to investigate the ability of thermally degraded and regenerated MEG to affect hydrate inhibition efficiency along pipelines. Based on the findings, hydrate equilibrium shifts were determined and a comprehensive MEG degradation scale was developed to assist in evaluating the degraded severity level. In addition, during this study, novel data was reported for the thermodynamic functions of MDEA and FFCI as gas hydrate inhibition. Another study was carried out to investigate gas hydrate problems and mitigation techniques applied at a gas lift system of an onshore field in the Sultanate of Oman. Finally, another set of experimental studies was conducted to evaluate the correlation of three hydrate prediction software and three MEG samples from three different suppliers with hydrate formation and dissociation curves. The study comprises six chapters, which are summarised below.

9.1.1 Investigation of gas hydrate problems and mitigation techniques applied in the gas-lift system at one of the oil fields in the Sultanate of Oman

- * Hydrate formation phase envelope for the field was developed, which shows that in the presence of water at 70 bar, gas hydrates will form at 19.04 °C.
- * Analysing and troubleshooting of wells/facility parameters showed that gas hydrate formation will not always cause a drop in production.
- * Four different thermodynamic hydrate inhibition and dissociating techniques were analysed.
 - A heating technique using electric heat tracing (EHT) provided good improvement. However, the heat did not prevent gas hydrate formation with high-temperature drops.
 - The pressure drop technique by decreasing 100 kPa from the line pressure was not enough to move the hydrate stability point.
 - Methanol injecting of 924 litres/day was used. Commingled with other thermodynamic techniques, this helped reduce the total field hydrate deferment from 26,159 bbl during winter 2013 to only 7336 bbl during winter 2017.

9.1.2 Evaluation of Different Hydrate Prediction Software and Impact of Different MEG Products on Gas Hydrate Formation and Inhibition

- * The hydrate formation points were predicted using three different software packages (P-R EOS): Pipesim, Multiflash and Hysys. The hydrate formation points were also compared with the experimental results. All software packages showed some deviation from the hydrate formation experimental results. The Pipesim and Multiflash results matched with the average temperature of the hydrate formation and hydrate dissociation points. However, the Hysys results matched the hydrate dissociation points.
- * New correlation regression functions were generated to predict hydrate formation for the three software.
- * Three MEG samples from three major suppliers were tested with respect to their hydrate inhibition performance. X-MEG showed the highest thermodynamic function with a hydrate formation temperature shift of -2.07 °C, followed by Z-MEG of -1.81 °C and Y-MEG of -1.71 °C.

9.1.3 Inhibition effects of thermally degraded MEG on hydrate formation for gas systems

- * We reported new hydrate full profile data of methane hydrate in the presence of pure and thermally exposed MEG solutions over a wide range of temperatures and pressures. This is a major contribution to current knowledge, as all known literature has not considered this research area.
- * The hydrate profile reveals that the temperature gap between the hydrate formation points and the hydrate dissociation points show a smaller gap at lower pressures and a higher gap at higher pressures.
- * The degradation products of MEG were identified as acetic, formic, and glycolic acids using IC and HPLC-MS analysis methods.
- * Hydrate inhibition performance tests of thermally exposed MEG to 165 °C for 4 and 48 hours shows that as MEG is exposed to higher duration, the hydrate formation temperature is also raised (0.33 and 0.72 °C respectively).
- * Hydrate inhibition performance test of thermally exposed MEG to 165, 180, and 200 °C for 48 hours shows that as MEG is exposed to higher temperatures, the hydrate formation temperature was also raised (0.72, 1.07 and 1.62 °C respectively).

9.1.4 Effects of Thermally Degraded Monoethylene Glycol with Methyl Diethanolamine and Film-Forming Corrosion Inhibitor on Gas Hydrate Kinetics

- * The MEG formulations with corrosion inhibitors (MDEA and FFCI) that were thermally exposed to 135-200 °C for 240 hours showed that thermal exposure degrades MEG and reduces the hydrate inhibition performance. The higher the exposure temperature, the higher the reduction in the inhibition performance.
- * Thermally degraded MEG with additives (MDEA and/or FFCI) inhibited methane hydrate formation more efficiently than pure thermally degraded MEG. Solution C (MEG/MDEA/FFCI) showed the best hydrate inhibition performance, because of the additional synergistic hydrate inhibition effects of both MDEA and FFCI, followed by solution A (MEG/MDEA) and solution B (MEG/FFCI).
- * The average hydrate depression temperature caused by MEG thermal degradation was around + 2 °C and showed a consistent hydrate profile.

- * For the first time, the thermodynamic functions test of pure MDEA and FFCI with methane gas hydrate were investigated and reported. We observed a directly proportional relationship between concentrations and hydrate inhibition performance. 25 wt% of MDEA and FFCI shows less hydrate depression temperature compared to 25 wt% MEG by 11% and 42%, respectively. FFCI showed anti-agglomeration effects as it delayed the time of full blockage by almost 40% compared to MDEA.
- * The metastable regions were narrower at lower pressures and broadened as the pressure was increased. The area covered by each metastable region was calculated. We found the area of the metastable region varied inversely with exposure temperature.
- * Hydrate profiles and regression functions for methane gas were generated.
- * In summary, this study provides a major contribution to current knowledge because all known literature has not considered thermally degraded MEG with MDEA/FFCI and thermodynamic function tests of pure DMEA and FFCI.

9.1.5 Analytical Techniques for Analysing Thermally Degraded Monoethylene Glycol with Methyl Diethanolamine and Film Formation Corrosion Inhibitor

- * This study provided an experimental methodology of six independent analytical techniques to evaluate the thermal degradation level of MEG solutions.
- * The pH measurement correlated well with the MEG thermal degradation levels, especially with the MEG+FFCI solution.
- * Electrical conductivity rose steadily with increasing thermal exposure temperatures of solutions containing MDEA. This is because of an increase in salt concentration generated by the reaction between MDEA and organic acids.
- * Solutions turned brownish as thermal degradation increased. Foam formation was observed on diluted MEG-MDEA solutions.
- * IC identified three degradation products (glycolic, acetic, and formic acids) while HPLC-MS detected only two (formic and acetic acids). High acetic acid concentrations were obtained for high exposure temperatures.
- * Thermally degraded MEG with corrosion inhibitors (MDEA and FFCI) significantly reduced the hydrate inhibition performance.

- * In summary, we conclude that exposing MEG solutions to higher temperatures (> 135 °C) leads to increased degradation levels, thus, reducing hydrate inhibition performance and increasing the risk of corrosion.
- * A novel MEG degradation scale was developed, classifying the degradation severity into five levels (0-4) using four analytical techniques. As the MEG solution approaches higher degradation, the hydrate and corrosion flow assurance strategies must be reviewed, with the option of replacing recycled MEG to enhance hydrate inhibition and prevent fouling and deposition of the process equipment.

9.1.6 Influence of Regenerated Mono-ethylene Glycol on Natural Gas Hydrate Formation

- * This study established the interactions of regenerated and reclaimed MEG containing water, drilling mud, mineral salts, demulsifier, MDEA, and condensate on gas hydrate formation.
- * Electrical conductivity (σ) at reclaimer slurry side showed the highest reading, representing a high amount of precipitated salts.
- * The pH values at the reclaimer condensed outlet and reboiler outlet were high, at an average of 9.2 and 11.3, respectively. The high pH can be explained by the transformation of bicarbonate ions (HCO_3^-) to hydroxide (OH^-) and carbonate (CO_3^{2-}) ions when the CO_2 boils off.
- * The possible principle reason for the higher hydrate temperature depression of tested solutions, as compared to fresh MEG, is the synergistic hydrate inhibition effect of the MEG with a salts component.
- * Reclaimer outlet solutions showed a lower hydrate depression temperature than fresh MEG. This is mainly because of salts removed from the MEG solution, and the presence of degradation products.
- * Although regenerated MEG showed a good hydrate inhibition performance, it was determined that this is because of the salts present in the solutions. However, these salts may lead to scale build-up and corrosion if not addressed correctly.
- * This study has brought a new focus to the relationship of the regenerated/reclaimed MEG and the gas hydrate inhibition performance.

9.2 Recommendations

Based on this thesis' results, the following research activities are recommended for future academic research.

- The reported hydrate phase boundary shifts of MDEA and FFCI are considered as newly reported data to the best of our knowledge; in that vein, further investigations should be conducted to test the thermodynamic functions of MDEA and FFCI with pure MEG. The findings will influence the calculation of the hydrate phase boundary and MEG injection rate for hydrate control.
- FFCI showed anti-agglomeration effects as it delayed the time of full blockage. A further study on the use of FFCI as anti-agglomerants is highly recommended for further investigation.
- **Effect of liquid condensate on gas hydrates conditions of natural gas with mono-ethylene glycol.**

The presence of condensate with MEG in pipelines can affect hydrate formation. This recommended research is to assist in the understanding of whether natural gas hydrate equilibrium points are affected by liquid condensate/MEG solutions. Several researchers have previously studied the solution characteristics of reservoir fluids/condensate and MEG. However, no research has been conducted, to the best of our knowledge, on the effects of this mixture on the equilibrium of natural gas hydrates. The primary experiment was conducted at 85 bar only for various MEG/condensate mixtures. Table 9-1 showed an equilibrium shift for the various MEG/condensate mixture. Further experiments should be conducted to obtain full equilibrium profile and the gas consumption values for the solution. The data obtained from this study will be employed in conjunction with simulation software to provide an understanding of the transported fluids under this specific condition. This will answer whether the formation of gas hydrates is sufficiently inhibited under the specific conditions.

Table 9-1 Experimental equilibrium condition of natural gas with various MEG/condensate mixture

Composition	Initial condition bar / °C	Experimental equilibrium condition bar / °C
100% condensate	85 / 20	No hydrate formed
5% Cond+ 95% DI Water (no MEG)	85 / 20	81.3 / 17
10% Cond+90% DI Water (no MEG)	85 / 20	80.66 / 16
15% Cond + 85% DI water (no MEG)	85 / 20	82.51 / 15.1
15% Cond + 5% MEG + 80% DI water	85 / 20	83.55 / 14.8
15% Cond +10% MEG + 75% DI water	85 / 20	80.69 / 13.7
15% Cond +15% MEG + 70% DI water	85 / 20	80.26 / 10.9
15% Cond +20% MEG+ 65% DI water	85 / 20	77.14 / 7.9

- Evaluating the memory effect and the isobaric and isochoric gas hydrate capture methodology for results generated using a PVT sapphire cell.

Many researchers have cited ‘memory’ effects in association with nucleation of clathrate hydrates. Some researchers appeal to this memory effect to explain the apparent reduction in induction time for hydrates formed repetitively from supercooled solutions. It is suggested that the ‘memory’ effect results from water obtained from melted hydrates possessing a “modified” structure that allows easier hydrate re-formation. A comprehensive experiment is recommended to study memory effect phenomenon under various conditions of:

- Isobaric and isochoric gas hydrate capture methodology.
- Heating the dissociated hydrate to various temperatures before retesting.
- Allowing various residence time for the dissociated hydrate before retesting.

- Applying different shear stresses for the dissociated hydrate before retesting.
- In the presence of hydrate promoters and nanoparticles (SiO_2).

Figure 9-1 shows primary experiment data illustrating the memory effect phenomena caused the irregularity hydrate formation pattern for solution dissociated from previous tests.

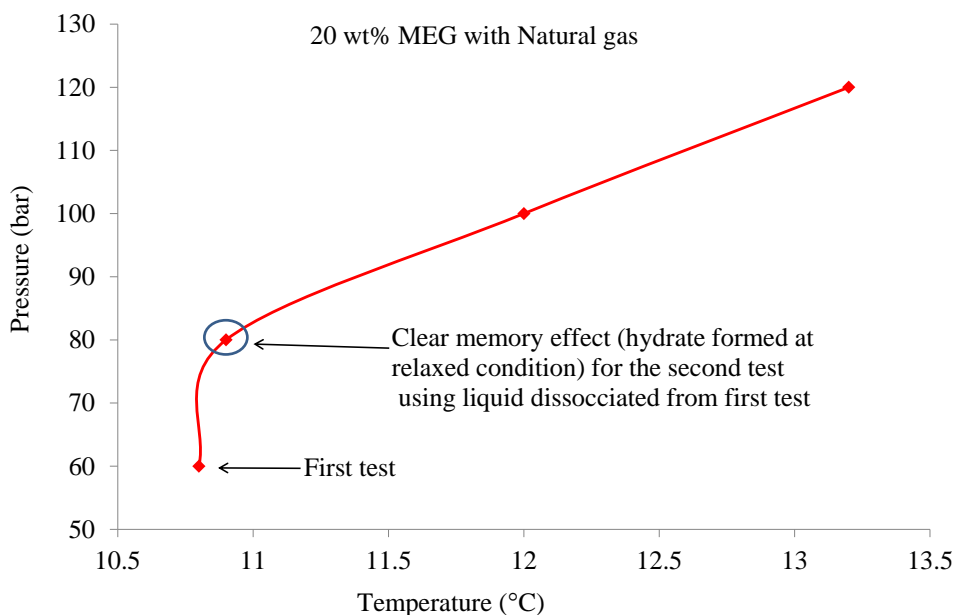


Figure 9-1 Memory effect experiment of 20 wt% MEG with natural gas.

A further study of the memory effect with different conditions can help with understanding quick hydrate reformation in pipelines after dissociation. On the other hand, this understanding can be utilised for the gas hydrate production industry as an effective method to promote gas hydrate nucleation.

- Empirical modelling of gas hydrate formation with thermally degraded MEG. Several theoretical predictive models have been used in software to predict hydrate equilibrium points. However, these models are not designed to accommodate MEG degradation variables. An empirical model should be developed, based merely on experimental results and incorporating the influences of degraded MEG variables on methane gas hydrate equilibrium points within a range of tested solutions.
- It is recommended that the image quality of the video camera used for recording gas hydrate formation is improved with advanced software for image processing. The advanced camera will improve macroscopic observation and enable

advanced analysis of the hydrate crystal morphology and agglomerant behaviour (Figure 9-2).

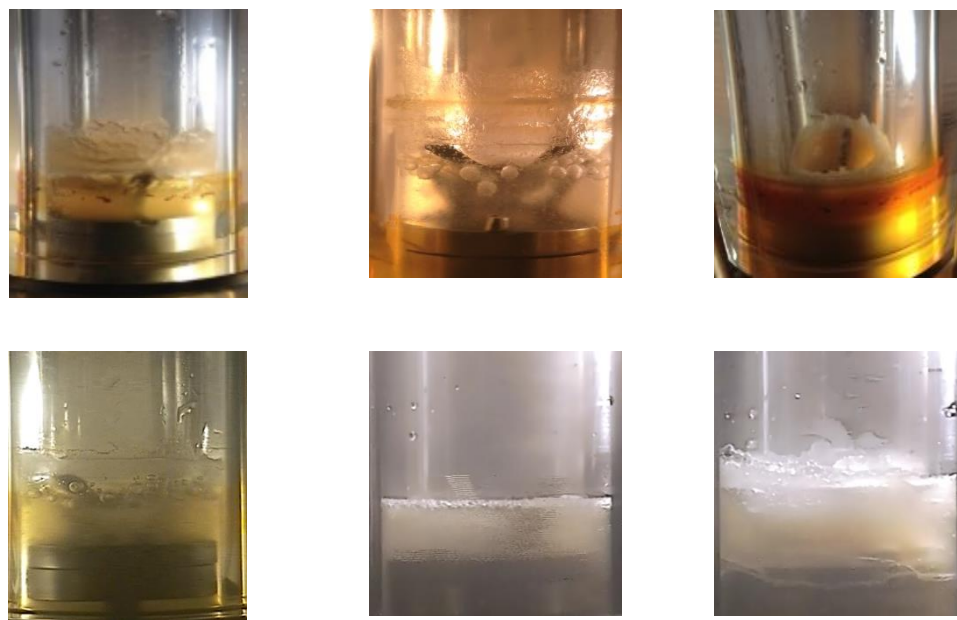


Figure 9-2 Various hydrate crystal morphology and agglomerants behaviour with current video recording facility.

APPENDIX A: Official Permissions and Copyrights

Sultanate of Oman
Ministry of Oil & Gas
Muscat

بِسْمِ اللّٰهِ الرَّحْمٰنِ الرَّحِيْمِ



سُلْطَانَةُ عُمَانٌ
مَسْقَطٌ
وزَارَةُ الْنَفْطِ وَالْغَازِ

MOG Ref: 7119/1/2621

Date: 19th April 2017.

Dr. Ali Al-Gheithy
Petroleum Engineering Functional Director
PDO

After Compliments,

Subject: REQUEST FOR RELEASE OF TECHNICAL MATERIAL

Title:

**Gas Hydrate Investigations of Natural Gas with High Methane Content
and Regenerated Mono-Ethylene Glycol**

Reference to your letter dated 4th of April 2017, on the above subject, please be advised that MOG has no objection for the release of data as illustrated in your letter PDO/UPD/April.17/02.

Best regards,


Saif Hamed Al-Salmani
Director General of Exploration
and Production of Oil & Gas .





Ref: PDO/UPD/April.17/02

4th April, 2017

Director General of Exploration
and Production of Oil & Gas
Ministry of Oil and Gas
P O Box 551, P.C. 100
Muscat
Sultanate of Oman

Attn: Mr. Saif bin Hamad Al-Salmani

After Compliments,

REQUEST FOR RELEASE OF TECHNICAL MATERIAL

Khalifa Mohamed Al-Harooni, a PDO staff member previously working with Operations North team, and currently a full-time student undergoing a PhD program at Curtin University in Australia. An essential component of the program is the submission of written thesis.

Khalifa's proposed thesis topic is:

**Gas Hydrates Investigations of Natural Gas with High Methane Content
and Regenerated Mono-Ethylene Glycol**

We hereby request your formal approval for the release of data as attached with this letter and let us have your clearance at your earliest convenience.

Thanking you in anticipation.

Yours faithfully,
For PETROLEUM DEVELOPMENT OMAN

Al-Gheithy 5 Apr 17
Dr. Ali Al-Gheithy
Petroleum Engineering Function Director
Tel: 2467-2898
Fax: 2467-4854

c.c: Khalifa Al-Harooni (ONO/15S)



Copyright
Clearance
Center

RightsLink®

[Home](#)
[Account
Info](#)
[Help](#)

Title:

Evaluation of Different Hydrate Prediction Software and Impact of Different MEG Products on Gas Hydrate Formation and Inhibition

Logged in as:
Khalifa Al Harooni
Curtin University
Account #:
3001157434

**Conference
Proceedings:**

Offshore Technology
Conference Asia

[LOGOUT](#)
Author:

K. M. AlHarooni, Curtin University; A. Barifcany, Curtin University; D. Pack, Curtin University et al

Publisher:

Society of Petroleum Engineers

Date:

2016

2016. Offshore Technology Conference

Order Completed

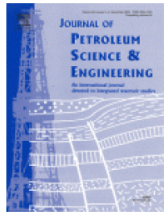
Thank you for your order.

This Agreement between Curtin University -- Khalifa Al Harooni ("You") and Society of Petroleum Engineers ("Society of Petroleum Engineers") consists of your license details and the terms and conditions provided by Society of Petroleum Engineers and Copyright Clearance Center.

Your confirmation email will contain your order number for future reference.

[Printable details.](#)

License Number	4138400539277
License date	Jun 29, 2017
Licensed Content Publisher	Society of Petroleum Engineers
Licensed Content Publication	SPE Proceedings
Licensed Content Title	Evaluation of Different Hydrate Prediction Software and Impact of Different MEG Products on Gas Hydrate Formation and Inhibition
Licensed Content Author	K. M. AlHarooni, Curtin University; A. Barifcany, Curtin University; D. Pack, Curtin University et al
Licensed Content Date	Jan 1, 2016
Type of Use	Thesis/Dissertation
Requestor type	author of the original work
SPE member	yes
SPE member number	4179464
Format	print and electronic
Portion	full article
Will you be translating?	no
Distribution	3
Order reference number	
Title of your thesis / dissertation	Gas Hydrates Investigations of Natural Gas with High Methane Content and Regenerated Mono-Ethylene Glycol
Expected completion date	Jun 2017
Estimated size (number of pages)	200
Requestor Location	Curtin University GPO Box U1987 Perth, Western Australia 6845 Australia Attn: Curtin University
Billing Type	Invoice
Billing address	Curtin University GPO Box U1987 Perth, Australia 6845 Attn: Curtin University
Total	0.00 USD



Title: Inhibition effects of thermally degraded MEG on hydrate formation for gas systems

Author: Khalifa Al Harooni,Ahmed Barifcani,David Pack,Rolf Gubner,Varun Ghodkay

Publication: Journal of Petroleum Science and Engineering

Publisher: Elsevier

Date: November 2015

Copyright © 2015 Elsevier B.V. All rights reserved.

Logged in as:
Khalifa Al Harooni
Curtin University

Account #:
3001157434

[LOGOUT](#)

Order Completed

Thank you for your order.

This Agreement between Curtin University -- Khalifa Al Harooni ("You") and Elsevier ("Elsevier") consists of your license details and the terms and conditions provided by Elsevier and Copyright Clearance Center.

Your confirmation email will contain your order number for future reference.

Printable details.

License Number	4119121095700
License date	May 30, 2017
Licensed Content	Elsevier
Publisher	
Licensed Content Publication	Journal of Petroleum Science and Engineering
Licensed Content Title	Inhibition effects of thermally degraded MEG on hydrate formation for gas systems
Licensed Content Author	Khalifa AlHarooni,Ahmed Barifcani,David Pack,Rolf Gubner,Varun Ghodkay
Licensed Content Date	Nov 1, 2015
Licensed Content Volume	135
Licensed Content Issue	n/a
Licensed Content Pages	10
Type of Use	reuse in a thesis/dissertation
Portion	full article
Format	both print and electronic
Are you the author of this Elsevier article?	Yes
Will you be translating?	No
Order reference number	
Title of your thesis/dissertation	Gas Hydrates Investigations of Natural Gas with High Methane Content and Regenerated Mono-Ethylene Glycol
Expected completion date	Jun 2017
Estimated size (number of pages)	200
Elsevier VAT number	GB 494 6272 12
Requestor Location	Curtin University GPO Box U1987
Total	Perth, Western Australia 6845 Australia Attn: Curtin University 0.00 USD

**Title:**

Effects of Thermally Degraded
 Monoethylene Glycol with Methyl
 Diethanolamine and Film-
 Forming Corrosion Inhibitor on
 Gas Hydrate Kinetics

Author:

Khalifa Al Harooni, David Pack,
 Stefan Iglaue, et al

Publication: Energy & Fuels**Publisher:** American Chemical Society**Date:** May 1, 2017

Copyright © 2017, American Chemical Society

 Logged in as:
 Khalifa Al Harooni
 Curtin University
[LOGOUT](#)**PERMISSION/LICENSE IS GRANTED FOR YOUR ORDER AT NO CHARGE**

This type of permission/license, instead of the standard Terms & Conditions, is sent to you because no fee is being charged for your order. Please note the following:

- Permission is granted for your request in both print and electronic formats, and translations.
- If figures and/or tables were requested, they may be adapted or used in part.
- Please print this page for your records and send a copy of it to your publisher/graduate school.
- Appropriate credit for the requested material should be given as follows: "Reprinted (adapted) with permission from (COMPLETE REFERENCE CITATION). Copyright (YEAR) American Chemical Society." Insert appropriate information in place of the capitalized words.
- One-time permission is granted only for the use specified in your request. No additional uses are granted (such as derivative works or other editions). For any other uses, please submit a new request.

**Title:**

Analytical Techniques for
 Analyzing Thermally Degraded
 Monoethylene Glycol with Methyl
 Diethanolamine and Film
 Formation Corrosion Inhibitor

Author:

Khalifa Al Harooni, David Pack,
 Stefan Iglaue, et al

Publication: Energy & Fuels**Publisher:** American Chemical Society**Date:** Dec 1, 2016

Copyright © 2016, American Chemical Society

 Logged in as:
 Khalifa Al Harooni
 Curtin University
[LOGOUT](#)**PERMISSION/LICENSE IS GRANTED FOR YOUR ORDER AT NO CHARGE**

This type of permission/license, instead of the standard Terms & Conditions, is sent to you because no fee is being charged for your order. Please note the following:

- Permission is granted for your request in both print and electronic formats, and translations.
- If figures and/or tables were requested, they may be adapted or used in part.
- Please print this page for your records and send a copy of it to your publisher/graduate school.
- Appropriate credit for the requested material should be given as follows: "Reprinted (adapted) with permission from (COMPLETE REFERENCE CITATION). Copyright (YEAR) American Chemical Society." Insert appropriate information in place of the capitalized words.
- One-time permission is granted only for the use specified in your request. No additional uses are granted (such as derivative works or other editions). For any other uses, please submit a new request.

Reference

- Aaron, Douglas, and Costas Tsouris. 2005. "Separation of CO₂ from flue gas: a review." *Separation Science and Technology* 40 (1-3):321-348.
- Abay, Hailu Kebede. 2011. "Kinetics of gas hydrate nucleation and growth." *University of Stavanger*.
- Abraham, W null. 1933. "The Functions of Mud Fluids Used in Rotary Drilling." 1st World Petroleum Congress.
- Achour, Mohsen, and Juri Kolts. 2015. "Corrosion Control by Inhibition Part I: Corrosion Control by Film Forming Inhibitors." CORROSION 2015. NACE International., Bartlesville, Oklahoma, USA, 2015/5/12.
- Act, Protection. 2000. Canadian Environmental Protection Act, 1999 Priority substances list state of the science report for Ethylene Glycol. Canada.
- Ahmad Syahrul, Mohamad. 2009. "Natural gas dehydration using triethylene glycol (TEG)." Universiti Malaysia Pahang.
- Akers, Thomas Jay. 2009. "Formation and Removal of Hydrates inside wellhead connectors." SPE Annual Technical Conference and Exhibition.
- Akpabio, Moses Gideon. 2012. "Hydrate Prevention in Subsea Natural Gas Production." Master, Department of Petroleum Engineering and Applied Geophysics, Norwegian University of Science and Technology.
- Akpabio, Moses Gideon. 2013. "Cold flow in long-distance subsea pipelines." Master, Department of Petroleum Engineering and Applied Geophysics, Norwegian University of Science and Technology.
- Al-Bimani, Atika Said, Samuel Armacanqui, Buthaina Al-Barwani, Said Al-Hajri, Iqbal Sipra, and Halima Al-Riyami. 2008. "Electrical Submersible Pumping System: Striving for Sustainable Run-Life Improvement in Oman Oil Fields." International Petroleum Technology Conference, Kuala Lumpur, Malaysia, 2008/1/1.
- Al-Khodhori, Shaikhan Mohammed. 2003. "Smart Well Technologies Implementation in PDO for Production & Reservoir Management & Control." Society of Petroleum Engineers, Bahrain, 2003/1/1.
- Al Dhafeeri, Mater A. 2007. "Identifying sources key to detailed troubleshooting of amine foaming." *Oil & Gas Journal*, 2007 Aug 27, 56-58,60,62,64,66-67.
- Al Salhi, M, A Al Maimani, and GH Mäkel. 2001. "A Switch from Verticals to Dual Lateral Producers Accelerate Oil Production and Reduces UTC for Natih Field." SPE Middle East Oil Show, Bahrain, 17/03/2001.
- AlHarooni, Khalifa, Ahmed Barifcani, David Pack, and Rolf Gubner. 2015. "Inhibition effects of thermally degraded MEG on hydrate formation for gas

systems.” *J. Pet. Sci. Eng.* 135 (0):608-617. doi: <http://dx.doi.org/10.1016/j.petrol.2015.10.001>.

AlHarooni, Khalifa Mohamed, David J Pack, Stefan Iglauer, Rolf Gubner, Varun Ghodkay, and Ahmed Barifcani. 2017. “The Effects of Thermally Degraded Mono Ethylene Glycol with Methyl Di-Ethanalamine and Film Formation Corrosion Inhibitor on Gas Hydrate Kinetics.” *Energy & Fuels*.

AlHarooni, Khalifa, David Pack, Stefan Iglauer, Rolf Gubner, Varun Ghodkay, and Ahmed Barifcani. 2016. “Analytical Techniques for Analyzing Thermally Degraded Monoethylene Glycol with Methyl Diethanolamine and Film Formation Corrosion Inhibitor.” *Energy & Fuels* 30 (12):10937-10949.

AlHarooni, KM, A Barifcani, D Pack, and S Iglauer. 2016. “Evaluation of Different Hydrate Prediction Software and Impact of Different MEG Products on Gas Hydrate Formation and Inhibition.” Offshore Technology Conference Asia, Kuala Lumpur, Malaysia, 22/03/2016.

Alhseinat, Emad, Priyabrata Pal, Mohammad Keewan, and Fawzi Banat. 2014. “Foaming study combined with physical characterization of aqueous MDEA gas sweetening solutions.” *Journal of Natural Gas Science and Engineering* 17:49-57.

Alink, B. A., Benjamin Outlaw, Vladimir Jovancicevic, Sunder Ramachandran, and Samuel Campbell. 1999. “Mechanism of CO₂ Corrosion Inhibition by Phosphate Esters.” NACE International., Houston, Texas 1999/1/1.

Aman, Zachary M, and Carolyn A Koh. 2016. “Interfacial phenomena in gas hydrate systems.” *Chemical Society Reviews* 45 (6):1678-1690.

Amani, Mahmood, Mohammed Al-Jubouri, and Arash Shadravan. 2012. “Comparative study of using oil-based mud versus water-based mud in HPHT fields.” *Advances in Petroleum Exploration and Development* 4 (2):18-27.

Ameta, RK, Man Singh, and RK Kale. 2013. “Synthesis, characterization, EDX, thermal, antioxidant, antibacterial, topographical, and gas adsorption studies of supramolecular tetraammoniumplatinato.” *J. Coord. Chem.* 66 (4):551-567.

Anklam, Mark R, J Dalton York, Luke Helmerich, and Abbas Firoozabadi. 2008. “Effects of antiagglomerants on the interactions between hydrate particles.” *AICHE journal* 54 (2):565-574.

Anne Marie K. Halvorsen, Tore R. Andersen, Erling N. Halvorsen, Gry P. Kojen, Jan Ivar Skar. 2007. “The Relationship Between Internal Corrosion Control Method, Scale Control And Meg Handling Of A Multiphase Carbon Steel Pipeline Carrying Wet Gas With CO₂ And Cetic Acid.” CORROSION 2007. NACE International.

Arjmandi, Mosayyeb, Bahman Tohidi, Ali Danesh, and Adrian C. Todd. 2005. “Is subcooling the right driving force for testing low-dosage hydrate inhibitors?”

- Arnold, Ken, and Maurice Stewart. 1999. *Surface Production Operations: design of gas handling systems and facilities*. 2nd edition. ed. Vol. 2. Houston, USA: Gulf Professional Publishing. Original edition, Gulf Publishing Company, Huston, TX.
- Atkins, Peter, and Julio De Paula. 2017. *Elements of physical chemistry*: Oxford University Press.
- Aylward, Gordon, and Tristan Findlay. 2008. *SI Chemical Data*. Vol. 6th edition. John Wiley & Sons Australia.
- Babu, DR, M Hosseinzadeh, A Ehsaninejad, R Babaei, MR Kashkooli, and H Akbary. 2015. "Carbonates precipitation in MEG loops—A comparative study of South Pars and Bass Strait gas fields." *Journal of Natural Gas Science and Engineering* 27:955-966.
- Báez, Luis A., and Paulette Clancy. 1994. "Existence of a density maximum in extended simple point charge water." *The Journal of Chemical Physics* 101 (11):9837-9840. doi: 10.1063/1.467949.
- Bahadori, A. 2009. "New model calculates solubility of light Alkanes in triethylene glycol." *Pet. Chem* 49 (2):171-179. doi: 10.1134/S0965544109020133.
- Bai, Yong, and Qiang Bai. 2005. *Subsea pipelines and risers*. Oxford, UK: Elsevier.
- Baraka-Lokmane, S, Ch Hurtevent, M Seiersten, E Flaten, M Farrell, O Bradshaw, S Hare, M Bonis, F Jacob, and N Carles. 2013. "Technical challenges and solutions in a closed loop MEG regeneration system for gas field offshore, UK." *WIT Transactions on Engineering Sciences* 79:511-522.
- Baraka-Lokmane, Salima, Christian Hurtevent, Jean-Luc Ohanessian, Guy Rousseau, Marion Elisabeth Seiersten, and Salim Deshmush. 2012. "Prediction of Mineral Scaling in a MEG Loop System of a Gas Production Offshore." SPE International Conference and Exhibition, Aberdeen, UK, 2012/3/30.
- Barmatov, Evgeny, Jill Geddes, Trevor Hughes, and Michaela Nagl. 2012. "Research On Corrosion Inhibitors For Acid Stimulation." 2012/1/1.
- Barmatov, Evgeny, Trevor Hughes, and Michaela Nagl. 2015. "Efficiency of film-forming corrosion inhibitors in strong hydrochloric acid under laminar and turbulent flow conditions." *Corrosion Science* 92:85-94. doi: <https://doi.org/10.1016/j.corsci.2014.11.038>.
- Becker, NC, KA Kozielski, ADJ Haymet, PG Hartley, and PW Wilson. 2008. "Nucleation of clathrates from supercooled THF/water mixtures shows that no memory effect exists." 6th International Conference on Gas Hydrates.
- Bergflødt, Linn, Lars Henrik Gjertsen, Johan Sjöblom, Harald Kallevik, and Gisle Øye. 2004. "Chemical influence on the formation, agglomeration, and natural

- transportability of gas hydrates. a multivariate component analysis.” *Journal of dispersion science and technology* 25 (3):355-365.
- Bhise, Vijay S. 1983. Process for preparing ethylene glycol. US Patents 4400559 issued August 23, 1983.
- Bikkina, Chaitanya, Narayanan Radhakrishnan, Sumit Jaiswal, Ryan Harrington, and Mark Charlesworth. 2012. “Development of MEG Regeneration Unit Compatible Corrosion Inhibitor for Wet Gas Systems.” SPE Asia Pacific Oil and Gas Conference and Exhibition, Perth, Australia, 2012/1/1.
- Bishnoi, P. Raj, and V. Natarajan. 1996. “Formation and decomposition of gas hydrates.” *Fluid Phase Equilib.* 117 (1–2):168-177. doi: [http://dx.doi.org/10.1016/0378-3812\(95\)02950-8](http://dx.doi.org/10.1016/0378-3812(95)02950-8).
- Bonyad, H., M. R. Mosayyebi, S. Mazloum, and B. Tohidi. 2011. “Field Evaluation Of A Hydrate Inhibition Monitoring System.” Offshore Mediterranean Conference and Exhibition, Ravenna, Italy, 2011/1/1.
- Boschee, Pam. 2012. “Gas Hydrate Control Using Monoethylene Glycol in the Gulf of Mexico.” *Oil and Gas Facilities* 1 (03):14-18.
- Boyd, PA, DL Whitfill, TS Carter, and JP Allamon. 1985. “New base oil used in low-toxicity oil muds.” *Journal of petroleum technology* 37 (01):137-142.
- Braun, Niklas O., Ulf Å Persson, and Hans T. Karlsson. 2001. “Densities and Viscosities of Mono(ethylene glycol) + 2-Amino-2-methyl-1-propanol + Water.” *J. Chem. Eng. Data* 46 (4):805-808. doi: 10.1021/je010004z.
- Brown, Paul W, Walter J Rossiter, and Kevin G Galuk. 1986. “A mass spectrometric investigation of the thermal oxidative reactivity of ethylene glycol.” *Solar energy materials* 13 (3):197-202.
- Broz, Stephen E. 1975. Process for preparing monoethylene glycol and ethylene oxide. U.S. Patent 3904656 issued September 9, 1975.
- Brustad, K. P. Loken, and J.G. Waalmann. 2005. “Hydrate Prevention using MEG instead of MeOH: Impact of experience from major Norwegian developments on technology selection for injection and recovery of MEG.” Offshore Technology Conference, Houston, TX, U.S.A, 2005/1/1.
- Buchanan, Piers, Alan K. Soper, Helen Thompson, Robin E. Westacott, Jefferson L. Creek, Greg Hobson, and Carolyn A. Koh. 2005. “Search for memory effects in methane hydrate: Structure of water before hydrate formation and after hydrate decomposition.” *The Journal of Chemical Physics* 123 (16). doi: 10.1063/1.2074927.
- Bylov, Martin, and Peter Rasmussen. 1997. “Experimental determination of refractive index of gas hydrates.” *Chemical Engineering Science* 52 (19):3295-3301. doi: 10.1016/S0009-2509(97)00144-9.

- Camargo, Ricardo, Marcelo Gonçalves, Claudio Barreto, Rafael Faraco, and Angela O Nieckele. 2011. "On The Safety Of Hydrate Remediation By One-Sided Depressurization." Proc. 7th Int. Conf. on Gas Hydrates.
- Cammann, Karl, Bernd Ross, Andreas Katerkamp, Jörg Reinbold, Bernd Gründig, and Reinhard Renneberg. 2000. "Chemical and Biochemical Sensors." In *Ullmann's Encyclopedia of Industrial Chemistry*. Wiley-VCH Verlag GmbH & Co. KGaA.
- Carroll, John. 2014. *Natural gas hydrates: a guide for engineers*: Gulf Professional Publishing.
- Carroll, John J. 2002. *Natural Gas Hydrates, A Guide for Engineers*: Elsevier Science & Technology Books.
- Cha, Minjun, Kyuchul Shin, Juneyoung Kim, Daejun Chang, Yutaek Seo, Huen Lee, and Seong-Pil Kang. 2013. "Thermodynamic and kinetic hydrate inhibition performance of aqueous ethylene glycol solutions for natural gas." *Chem. Eng. Sci.* 99:184-190. doi: <http://dx.doi.org/10.1016/j.ces.2013.05.060>.
- Chakma, A, and A Meisen. 1997. "Methyl-diethanolamine degradation—Mechanism and kinetics." *Can. J. Chem. Eng.* 75 (5):861-871.
- Chakma, Amitabha, and Axel Meisen. 1988. "Identification of methyl diethanolamine degradation products by gas chromatography and gas chromatography-mass spectrometry." *J. Chromatogr. A* 457:287-297. doi: [http://dx.doi.org/10.1016/S0021-9673\(01\)82076-8](http://dx.doi.org/10.1016/S0021-9673(01)82076-8).
- Chandra, Amitabh, Jatinder Rana, and Yingqin Li. 2001. "Separation, Identification, Quantification, and Method Validation of Anthocyanins in Botanical Supplement Raw Materials by HPLC and HPLC-MS." *J. Agric. Food. Chem.* 49 (8):3515-3521. doi: 10.1021/jf010389p.
- Chapoy, Antonin, Ross Anderson, Hooman Haghghi, Terry Edwards, and Bahman Tohidi. 2008. "Can n-Propanol Form Hydrate?" *Industrial & Engineering Chemistry Research* 47 (5):1689-1694. doi: 10.1021/ie071019e.
- Chapoy, Antonin, Saeid Mazloum, Rod Burgass, Hooman Haghghi, and Bahman Tohidi. 2012. "Clathrate hydrate equilibria in mixed monoethylene glycol and electrolyte aqueous solutions." *The Journal of Chemical Thermodynamics* 48:7-12. doi: <http://dx.doi.org/10.1016/j.jct.2011.12.031>.
- Chapoy, Antonin, and Bahman Tohidi. 2012. "Hydrates in High MEG Concentration Systems." 3rd International Gas Processing Symposium, Qatar, March.
- Chen, Jun, Ke-Le Yan, Meng-Lei Jia, Chang-Yu Sun, Yan-Qin Zhang, Si Si, Qing-Lan Ma, Lan-Ying Yang, Xiao-Qin Wang, and Guang-Jin Chen. 2013. "Memory effect test of methane hydrate in water+ diesel oil+ sorbitan monolaurate dispersed systems." *Energy & Fuels* 27 (12):7259-7266.
- Chen, Li Tao, Chang Yu Sun, Guang Jin Chen, Julian Y Zuo, and Heng Joo Ng. 2010. "Assessment of hydrate kinetic inhibitors with visual observations."

Choi, Y.-S., D. Duan, S. Nešić, F. Vitse, S. A. Bedell, and C. Worley. 2010. "Effect of Oxygen and Heat Stable Salts on the Corrosion of Carbon Steel in MDEA-Based CO₂ Capture Process." *Corrosion* 66 (12):125004-125004-10. doi: doi:10.5006/1.3524834.

Christiansen, Håkon Eidem. 2012. "Rate of Hydrate Inhibitor in Long Subsea Pipelines." Department of Petroleum Engineering and Applied Geophysics, Norwegian University of Science and Technology.

Christiansen, Richard L, and E Dendy Sloan. 1994. "Mechanisms and kinetics of hydrate formation." *Annals of the New York Academy of Sciences* 715 (1):283-305.

Cicek, Volkan, and Bayan Al-Numan. 2011. "Types of Corrosion Inhibitors." In *Corrosion Chemistry*, 43-45. John Wiley & Sons, Inc.

Clarke, Matthew A., and P. R. Bishnoi. 2005. "Determination of the intrinsic kinetics of CO gas hydrate formation using in situ particle size analysis." *Chemical Engineering Science* 60 (3):695-709. doi: <https://doi.org/10.1016/j.ces.2004.08.040>.

Clarke, Matthew A., and P. Raj Bishnoi. 2001a. "Measuring and modelling the rate of decomposition of gas hydrates formed from mixtures of methane and ethane." *Chemical Engineering Science* 56 (16):4715-4724. doi: [https://doi.org/10.1016/S0009-2509\(01\)00135-X](https://doi.org/10.1016/S0009-2509(01)00135-X).

Clarke, Matthew, and P Raj Bishnoi. 2001b. "Determination of the activation energy and intrinsic rate constant of methane gas hydrate decomposition." *The Canadian Journal of Chemical Engineering* 79 (1):143-147.

Clarke, Matthew, and P. R Bishnoi. 2000. "Determination of the intrinsic rate of ethane gas hydrate decomposition." *Chem. Eng. Sci* 55 (21):4869-4883. doi: [http://dx.doi.org/10.1016/S0009-2509\(00\)00137-8](http://dx.doi.org/10.1016/S0009-2509(00)00137-8).

Clifton, James R., Walter J. Rossiter Jr, and Paul W. Brown. 1985. "Degraded aqueous glycol solutions: pH values and the effects of common ions on suppressing pH decreases." *Sol. Energy Mater.* 12 (1):77-86. doi: [http://dx.doi.org/10.1016/0165-1633\(85\)90026-7](http://dx.doi.org/10.1016/0165-1633(85)90026-7).

Craig Dugan, John Gibbeson, Alex Perisa , Steve Fogarty, Mark McKenna, Mark Johnstone , Nathan Smith , John Kenez 2009. "MEG Regeneration Technical Meeting." Society of Petroleum Engineers, Port Campbell, Australia, 18/6/2009.

Cranford, P. J., D. C. Gordon Jr, K. Lee, S. L. Armsworthy, and G. H. Tremblay. 1999. "Chronic toxicity and physical disturbance effects of water- and oil-based drilling fluids and some major constituents on adult sea scallops (*Placopecten magellanicus*)."*Marine Environmental Research* 48 (3):225-256. doi: [https://doi.org/10.1016/S0141-1136\(99\)00043-4](https://doi.org/10.1016/S0141-1136(99)00043-4).

- Creek, J. L. 2012. "Efficient Hydrate Plug Prevention." *Energy & Fuels* 26 (7):4112-4116. doi: 10.1021/ef300280e.
- Cummings, Arthur L, Glen D Smith, and Dennis K Nelsen. 2007. "Advances in amine reclaiming—why there's no excuse to operate a dirty amine system." Laurance Reid Gas Conditioning Conference.
- Davarnejada, R., Jam. Azizia, and Jab. Azizib. 2014. "Prediction of Gas Hydrate Formation using HYSYS Software." *Int. J. Eng* 27:1328-1330. doi: 10.5829/idosi.ije.2014.27.09c.01.
- Davies, JM, JM Addy, RA Blackman, JR Blanchard, JE Ferbrache, DC Moore, HJ Somerville, A Whitehead, and T Wilkinson. 1984. "Environmental effects of the use of oil-based drilling muds in the North Sea." *Marine Pollution Bulletin* 15 (10):363-370.
- Davies, SR, MS Selim, ED Sloan, P Bollavaram, and DJ Peters. 2006. "Hydrate plug dissociation." *AIChE Journal* 52 (12):4016-4027.
- Davoudi, Mehdi, Yashar Heidari, Alireza Safadoost, and Saeed Samieirad. 2014. "Chemical injection policy for internal corrosion prevention of South Pars sea-pipeline: A case study." *J. Nat. Gas. Sci. Eng.* 21:592-599. doi: <http://dx.doi.org/10.1016/j.jngse.2014.09.017>.
- Davoudi, Mehdi, Ali Reza Safadoust, Seied Ali Akbar Mansoori, and Hamid Reza Mottaghi. 2014. "The impurities effect on thermal degradation and corrosivity of amine solution in South Pars gas sweetening plants." *J. Nat. Gas. Sci. Eng.* 19 (0):116-124. doi: <http://dx.doi.org/10.1016/j.jngse.2014.05.001>.
- De Rosa, Maria I. 1986. *Oxidative thermal degradation of PVC-derived, fiberglass, cotton, and jute brattices and other mine materials: a comparison of toxic gas and liquid concentrations and smoke-particle characterization*. Edited by C. D. Litton: Pittsburgh, Pa. (Cochrane Mill Rd., P.O. Box 18070, Pittsburgh 15236): U.S. Dept. of the Interior, Bureau of Mines.
- Del Villano, Luca, and Malcolm A Kelland. 2011. "An investigation into the laboratory method for the evaluation of the performance of kinetic hydrate inhibitors using superheated gas hydrates." *Chemical engineering science* 66 (9):1973-1985. doi: <http://dx.doi.org/10.1016/j.ces.2011.01.057>.
- Del Villano, Luca, Roald Kommedal, and Malcolm A Kelland. 2008. "Class of kinetic hydrate inhibitors with good biodegradability." *Energy & Fuels* 22 (5):3143-3149.
- Delgado, A. E., and Da-Wen Sun. 2001. "Heat and mass transfer models for predicting freezing processes – a review." *Journal of Food Engineering* 47 (3):157-174. doi: [https://doi.org/10.1016/S0260-8774\(00\)00112-6](https://doi.org/10.1016/S0260-8774(00)00112-6).
- Delli, Mohana L., and Jocelyn L. H. Grozic. 2014. "Experimental determination of permeability of porous media in the presence of gas hydrates." *J. Pet. Sci. Eng* 120:1-9. doi: <http://dx.doi.org/10.1016/j.petrol.2014.05.011>.

- Demirbas, Ayhan. 2010. "Methane hydrates as potential energy resource: Part 1–Importance, resource and recovery facilities." *Energy Conversion and Management* 51 (7):1547-1561.
- Diba, K. Dave, M. Guglielminetti, and S. Schiavo. 2003. "Glycol Reclaimer." Offshore Mediterranean Conference and Exhibition, Ravenna, 28-March-2003.
- Dickens, Gerald R, Charles K Paull, and Paul Wallace. 1997. "Direct measurement of in situ methane quantities in a large gas-hydrate reservoir." *Nature* 426.
- Ding, Ailin, Shuo Wang, Tina Pelemis, Carmelo Crisafio, Karen Kozielski, and Xia Lou. 2009. "Concentration Effect on the Inhibition Efficiency of Low Dose Hydrate Inhibitors." *Engineering Our Future: Are We up to the Challenge?: 27-30 September 2009, Burswood Entertainment Complex*:194.
- Ding, Ailin, Shuo Wang, Tina Pelemis, Carmelo Crisafio, and Xia Lou. 2010. "Specific critical concentrations of low dosage hydrate inhibitors in a THF–NaCl hydrate formation solution." *Asia-Pacific Journal of Chemical Engineering* 5 (4):577-584.
- Duchateau, Christophe, Jean-Louis Peytavy, Philippe Glénat, Tong-Eak Pou, Manuel Hidalgo, and Christophe Dicharry. 2009. "Laboratory Evaluation of Kinetic Hydrate Inhibitors: A Procedure for Enhancing the Repeatability of Test Results." *Energy & Fuels* 23 (2):962-966. doi: 10.1021/ef800710x.
- Dugstad, Arne, Liv Lunde, and S Nesic. 1994. "Control of internal corrosion in multi-phase oil and gas pipelines." Proceedings of the conference Prevention of Pipeline Corrosion, Gulf Publishing Co.
- Dugstad, Arne, and Marion Seiersten. 2004. "pH-stabilisation, a Reliable Method for Corrosion Control of Wet Gas Pipelines." SPE International Symposium on Oilfield Corrosion. Society of Petroleum Engineers, Aberdeen, UK, 2004/1/1.
- Dugstad, Arne, Marion Seiersten, and Rolf Nyborg. 2003. "Flow assurance of pH stabilized wet gas pipelines." CORROSION 2003. NACE International, 2003/1/1.
- Dwyer, Daryl F, and James M Tiedje. 1983. "Degradation of ethylene glycol and polyethylene glycols by methanogenic consortia." *Applied and environmental microbiology* 46 (1):185-190.
- Ebeltoft, Hege, Yousif Majeed, and Eirik Sørgård. 2001. "Hydrate Control During Deepwater Drilling: Overview and New Drilling-Fluids Formulations." *SPE Drilling & Completion*. doi: 10.2118/68207-PA.
- Elhady, Atef Abdallah. 2005. "Operating Experiences of DEG and MEG for Hydrate and Dew Point Control in Gas Production Offshore Mediterranean." International Petroleum Technology Conference, Doha, Qatar, 2005/1/1/.

- Emdadul, Haque Md. 2012. "Ethylene Glycol Regeneration Plan: A Systematic Approach to Troubleshoot the Common Problems." *J. Chem. Eng* 27 (1):21-26.
- Englezos, P, N Kalogerakis, PD Dholabhai, and PR Bishnoi. 1987a. "Kinetics of formation of methane and ethane gas hydrates." *Chemical Engineering Science* 42 (11):2647-2658. doi: [http://dx.doi.org/10.1016/0009-2509\(87\)87015-X](http://dx.doi.org/10.1016/0009-2509(87)87015-X).
- Englezos, P., N. Kalogerakis, P. D. Dholabhai, and P. R. Bishnoi. 1987b. "Kinetics of gas hydrate formation from mixtures of methane and ethane." *Chemical Engineering Science* 42 (11):2659-2666. doi: [http://dx.doi.org/10.1016/0009-2509\(87\)87016-1](http://dx.doi.org/10.1016/0009-2509(87)87016-1).
- Erstad, Kristin. 2009. "The influence of crude oil acids on natural inhibition of hydrate plugs."
- Eslamimanesh, Ali, Amir H. Mohammadi, Dominique Richon, Paramespri Naidoo, and Deresh Ramjugernath. 2012. "Application of gas hydrate formation in separation processes: A review of experimental studies." *The Journal of Chemical Thermodynamics* 46:62-71. doi: <http://dx.doi.org/10.1016/j.jct.2011.10.006>.
- Evans, WH, and EJ David. 1974. "Biodegradation of mono-, di-and triethylene glycols in river waters under controlled laboratory conditions." *Water Research* 8 (2):97-100.
- Ezrin, M., A. Zepke, J. Helwig, G. Lavigne, and M. Dudley. 2001. *Plastics failure due to oxidative degradation in processing and service*. Edited by M. Ezrin.
- Falenty, Andrzej, and Werner F Kuhs. 2009. "“Self-Preservation” of CO₂ Gas Hydrates-Surface Microstructure and Ice Perfection." *The Journal of Physical Chemistry B* 113 (49):15975-15988.
- Flaten, Ellen Marie. 2010. "The effect of MEG (mono ethyleneglycol) on the precipitation kinetics of calcium carbonate related to natural gas production from subsea wells." NTNU.
- Flaten, Ellen Marie, Marion Seiersten, and Jens-Petter Andreassen. 2009. "Polymorphism and morphology of calcium carbonate precipitated in mixed solvents of ethylene glycol and water." *Journal of Crystal Growth* 311 (13):3533-3538.
- Flaten, Ellen Marie, Marion Seiersten, and Jens-Petter Andreassen. 2010. "Growth of the calcium carbonate polymorph vaterite in mixtures of water and ethylene glycol at conditions of gas processing." *Journal of Crystal Growth* 312 (7):953-960.
- Flaten, Ellen Marie, Geir Watterud, Jens-Petter Andreassen, and Marion Elisabeth Seiersten. 2008. "Precipitation Of Iron And Calcium Carbonate In Pipelines At Varying Meg Contents." SPE International Oilfield Scale Conference, Aberdeen, UK,, 2008/5/29.

- Fonseca, José M. S., Ralf Dohrn, and Stephanie Peper. 2011. "High-pressure fluid-phase equilibria: Experimental methods and systems investigated (2005–2008)." *Fluid Phase Equilibria* 300 (1–2):1–69. doi: <http://dx.doi.org/10.1016/j.fluid.2010.09.017>.
- Fosfuri, Andrea. 2006. "The licensing dilemma: understanding the determinants of the rate of technology licensing." *Strategic Management Journal* 27 (12):1141–1158.
- Foster, Robert Dean, Thomas Arthur Maliszewski, Joseph Alton Sims Jr, and Glenn Alfred Taylor. 1978. Continuous process for producing alkylene glycols from alkylene carbonates. U.S. Patent 4,117,250, issued September 26, 1978.
- Franks, F, J Darlington, T Schenz, SF Mathias, L Slade, and H Levine. 1987. Antifreeze activity of Antarctic fish glycoprotein and a synthetic polymer. Nature Publishing Group.
- Fraser, Murray. 2013. "Tunable Diode Lasers- Measuring Water Content in Natural Gas Gathering Systems. ." <http://albertaanalytical.com/hello-world-2/>, 20/06/2013.
- Frostman, LM, and JL Przybylinski. 2001. "Successful applications of anti-agglomerant hydrate inhibitors." SPE International Symposium on Oilfield Chemistry.
- Frostman, LM, V Thieu, DL Crosby, and HH Downs. 2003. "Low-dosage hydrate inhibitors (LDHIs): reducing costs in existing systems and designing for the future." International Symposium on Oilfield Chemistry.
- Fu, SB, LM Cenegy, and CS Neff. 2001. "A summary of successful field applications of a kinetic hydrate inhibitor." SPE International Symposium on Oilfield Chemistry.
- Gabitto, Jorge F, and Costas Tsouris. 2010. "Physical properties of gas hydrates: A review." *Journal of Thermodynamics* 2010.
- Giavarini, Carlo, and Keith Hester. 2011. *Gas hydrates: Immense energy potential and environmental challenges*: Springer Science & Business Media.
- Gil, María I., Francisco A. Tomás-Barberán, Betty Hess-Pierce, Deirdre M. Holcroft, and Adel A. Kader. 2000. "Antioxidant Activity of Pomegranate Juice and Its Relationship with Phenolic Composition and Processing." *J. Agric. Food. Chem.* 48 (10):4581–4589. doi: 10.1021/jf000404a.
- Gizah, Fawaz Abd El-latif, Taher Abdel Raheem Ali, Mohammad Baydoon, Stephan Allenson, and Allan Scott. 2010. "Pioneer challenge Reduction of MEG consumption using KHI for hydrate control in a deepwater environment offshore Egypt." Offshore Technology Conference, Houston, Texas, USA, 2010/1/1/.
- Glenat, Philippe, Jean-Louis Peytavy, Nick Holland-Jones, and Martin Grainger. 2004. "South-Pars phases 2 and 3: The kinetic hydrate inhibitor (KHI)

- experience applied at field start-up.” Abu Dhabi International Conference and Exhibition, Abu Dhabi.
- Gomes, R, R Liteplo, and ME Meek. 2002. “Ethylene glycol: human health aspects.” *Concise international chemical assessment document*.
- Gonzalez, Juan Jose, Maria Elena Alfonso, and G. Pellegrino. 2000. “Corrosion of Carbon Steels in Monoethylene Glycol.” CORROSION 2000 NACE International, Houston, Texas, USA, 2000/1/1.
- Graham, Gordon M., and Craig Paul McMahon. 2002. “The Effect of Scale Inhibitor Performance Against Bulk (Homogeneous) and Surface (Heterogeneous) Scale Nucleation and Growth by the Addition of Film Forming Corrosion Inhibitors.” NACE International, 2002/1/1.
- Grigg, RB, and GL Lynes. 1992. “Oil-based drilling mud as a gas-hydrates inhibitor.” *SPE drilling engineering* 7 (01):32-38.
- Hagerup, Odd, and Stein Olsen. 2003. “Corrosion Control by pH Stabilizer, Materials and Corrosion Monitoring in 160 km Multiphase Offshore Pipeline.” NACE International, 2003/1/1.
- Haghghi, Hooman, Antonin Chapoy, Rod Burgess, and Bahman Tohidi. 2009. “Experimental and thermodynamic modelling of systems containing water and ethylene glycol: Application to flow assurance and gas processing.” *Fluid Phase Equilibria* 276 (1):24-30. doi: <http://dx.doi.org/10.1016/j.fluid.2008.10.006>.
- Hajilary, N, A Ehsani Nejad S Sheikhaei, and H Foroughipour. 2011. “Amine Gas Sweetening System Problems Arising from Amine Replacement and Solutions to Improve System Performance.” *J. Pet. Sci. Technol.* 1 (1):24-30.
- Halvorsen, Anne Marie K., and Tore R. Andersen. 2003. “PH Stabilization for Internal Corrosion Protection of Pipeline Carrying Wet Gas With CO₂ and Acetic Acid.” NACE International, 2003/1/1.
- Halvorsen, Erling Notto, Anne Marie Koren Halvorsen, Tore Roberg Andersen, Cecilia Bjørnstad, and Kristin Reiersolmen. 2009. “Qualification of Scale Inhibitors for Subsea Tiebacks With MEG Injection.” Society of Petroleum Engineers, The Woodlands, Texas, USA, 2009/1/.
- Halvorsen, Erling Notto, Anne Marie Koren Halvorsen, Kari Ramstad, Trine Tydal, and Cecilie Bjørnstad. 2006. “Scale Inhibitor Testing for Multiphase Pipelines in a Subsea to Shore Development with a closed MEG-loop system.” SPE International Oilfield Scale Symposium.
- Hammerschmidt, E. G. 1939. “Gas Hydrate Formations, A Further Study on Their Prevention and Elimination from Natural Gas Pipe Lines.” 15:30-34.
- Hammerschmidt, EG. 1934. “Formation of gas hydrates in natural gas transmission lines.” *Industrial & Engineering Chemistry* 26 (8):851-855.

- Han, Seongok, Chongyoup Kim, and Dongsook Kwon. 1997. "Thermal/oxidative degradation and stabilization of polyethylene glycol." *Polymer* 38 (2):317-323.
- Haritash, AK, and CP Kaushik. 2009. "Biodegradation aspects of polycyclic aromatic hydrocarbons (PAHs): a review." *Journal of hazardous materials* 169 (1):1-15.
- Haukalid, Kjetil, Kjetil Folgerø, Tanja Barth, and Stian Landmark Fjermestad. 2017. "Hydrate formation in water-in-crude oil emulsions studied by broad-band permittivity measurements." *Energy & Fuels*.
- He, Song, Deqing Liang, Dongliang Li, and Longlong Ma. 2011. "Experimental Investigation on the Dissociation Behavior of Methane Gas Hydrate in an Unconsolidated Sediment by Microwave Stimulation." *Energy & Fuels* 25 (1):33-41. doi: 10.1021/ef1011116.
- Hemmingsen, Pål V., Roderick Burgass, Karen Schou Pedersen, Keijo Kinnari, and Henrik Sørensen. 2011. "Hydrate temperature depression of MEG solutions at concentrations up to 60 wt%. Experimental data and simulation results." *Fluid Phase Equilib.* 307 (2):175-179. doi: <http://dx.doi.org/10.1016/j.fluid.2011.05.010>.
- Herath, Dinesh, Faisal Khan, Samith Rathnayaka, and M. A. Rahman. 2015. "Probabilistic estimation of hydrate formation." *J. Pet. Sci. Eng.* 135:32-38. doi: <http://dx.doi.org/10.1016/j.petrol.2015.08.007>.
- Herslund, Peter Jørgensen, Nagu Daraboina, Kaj Thomsen, Jens Abildskov, and Nicolas von Solms. 2014. "Measuring and modelling of the combined thermodynamic promoting effect of tetrahydrofuran and cyclopentane on carbon dioxide hydrates." *Fluid Phase Equilib.* 381:20-27. doi: <http://dx.doi.org/10.1016/j.fluid.2014.08.015>.
- Hess, Robert, Michael J Bartels, and Lynn H Pottenger. 2004. "Ethylene glycol: an estimate of tolerable levels of exposure based on a review of animal and human data." *Arch. Toxicol.* 78 (12):671-680.
- Hille, Bertil. 2001. *Ion channels of excitable membranes*. Third edition ed. Vol. 507: Sinauer Sunderland, MA, USA.
- Hinco. 2014. "TCA RTD Sensors." Hinco Instruments Pty Ltd, accessed 18/09/2014. <http://www.hinco.com.au/Brochures/page14-15-rtds.pdf>
- Holder, GD, DL Katz, and JH Hand. 1976. "Hydrate Formation in Subsurface Environments: GEOLOGIC NOTES." *AAPG Bulletin* 60 (6):981-988.
- Hong, Huifang. 2003. "Modeling of gas production from hydrates in porous media."
- Hoppe, Ron, Richard Lloyd Martin, Marek K. Pakulski, and Thane Douglas Schaffer. 2006. "Corrosion Mitigation With Gas Hydrate Inhibitors." Society of Petroleum Engineers, Calgary, Alberta, Canada, 2006/1/1/.

- Hossainpour, Reza. 2013. "Catalysts for Enhanced CO₂-CH₄ Exchange in Natural Gas Hydrates. An experimental feasibility study of exchange enhancement by use of chemical additives." University of Bergen.
- Huang, Chuanhui, Tongwen Xu, Yaping Zhang, Yanhong Xue, and Guangwen Chen. 2007. "Application of electrodialysis to the production of organic acids: State-of-the-art and recent developments." *J. Membrane. Sci.* 288 (1–2):1-12. doi: <http://dx.doi.org/10.1016/j.memsci.2006.11.026>.
- Huang, Lihua, P. Clayton Gough, and Michael R DeFelippis. 2009. "Characterization of Poly(ethylene glycol) and PEGylated Products by LC/MS with Postcolumn Addition of Amines." *Anal. Chem* 81 (2):567-577. doi: 10.1021/ac801711u.
- Huo, Z., E. Freer, M. Lamar, B. Sannigrahi, D. M. Knauss, and E. D. Sloan Jr. 2001. "Hydrate plug prevention by anti-agglomeration." *Chemical Engineering Science* 56 (17):4979-4991. doi: [http://dx.doi.org/10.1016/S0009-2509\(01\)00188-9](http://dx.doi.org/10.1016/S0009-2509(01)00188-9).
- Irmann-Jacobsen, Tine Bauck. 2012. "Flow Assurance—A System Perspective." *MEK4450 Offshore Technology Course, universitet i Oslo, Matematisk Institutt.*
- Jacobson, Liam C, and Valeria Molinero. 2010. "A Methane– water model for coarse-grained simulations of solutions and clathrate hydrates." *The Journal of Physical Chemistry B* 114 (21):7302-7311.
- Jager, M. D., and E. D. Sloan. 2001. "The effect of pressure on methane hydration in pure water and sodium chloride solutions." *Fluid Phase Equilib.* 185 (1–2):89-99. doi: [http://dx.doi.org/10.1016/S0378-3812\(01\)00459-9](http://dx.doi.org/10.1016/S0378-3812(01)00459-9).
- Jamaloei, B. Yadali, and K. Asghari. 2015. "The Joule-Thomson Effect in Petroleum Fields: II. CO₂ Sequestration, Wellbore Temperature Profiles, and Thermal Stresses and Wellbore Stability." *Energy Sources, Part A: Recovery, Utilization, and Environmental Effects* 37 (3):236-244. doi: 10.1080/15567036.2011.557701.
- Jamaluddin, A. K. M., N. Kalogerakis, and P. R. Bishnoi. 1991. "Hydrate plugging problems in undersea natural gas pipelines under shutdown conditions." *Journal of Petroleum Science and Engineering* 5 (4):323-335. doi: [http://dx.doi.org/10.1016/0920-4105\(91\)90051-N](http://dx.doi.org/10.1016/0920-4105(91)90051-N).
- Jensen, Lars, Kaj Thomsen, and Nicolas von Solms. 2008. "Propane hydrate nucleation: Experimental investigation and correlation." *Chem. Eng. Sci* 63 (12):3069-3080. doi: <http://dx.doi.org/10.1016/j.ces.2008.03.006>.
- Jensen, TB, KJ Harpole, and A Østhus. 2000. "EOR screening for Ekofisk." SPE European Petroleum Conference, Paris, France.
- Jeon, Yooil, Suyoul Park, Yutaek Seo, and Minsu Ko. 2014. "pH Measurement for Low Soluble Salts Monitoring in Monoethylene Glycol (MEG) Regeneration System." International Petroleum Technology Conference.

- Jin, Yusuke, Yoshihiro Konno, Jun Yoneda, Masato Kida, and Jiro Nagao. 2016. "In Situ Methane Hydrate Morphology Investigation: Natural Gas Hydrate-Bearing Sediment Recovered from the Eastern Nankai Trough Area." *Energy & Fuels* 30 (7):5547-5554. doi: 10.1021/acs.energyfuels.6b00762.
- Joachim, Sannes. 2013. "Hydrate plugs in subsea pipelines and non-invasive methodology for localization." University of Stavanger, Norway.
- Jonassen, Anette Hartveit. 2013. "Distribution of Hydrate Inhibitors in Processing of Gas-Condensate."
- Jones, T. J., E. L. Neustadter, and K. P. Whittingham. 1978. "Water-In-Crude Oil Emulsion Stability And Emulsion Destabilization By Chemical Demulsifiers." *Journal of Canadian Petroleum Technology* 17 (02). doi: 10.2118/78-02-08.
- Joosten, Michael W, Benjamin Tier, Marion Seiersten, and Christian Wintermark. 2007. "Materials Considerations for MEG (Mono Ethylene Glycol) Reclamation Systems." CORROSION 2007.
- Jordan, Myles Martin, Neil D. Feasey, and C. Johnston. 2005. "Inorganic Scale Control Within MEG/Methanol Treated Produced Fluids." 2005/1/1.
- Kadnar, Rainer, Martin Madera, and Ruth Schlifke. 2003. "Determination of inorganic corrosion inhibitors in heat transfer systems by ion chromatography." *J. Chromatogr. A* 997 (1-2):285-290. doi: [http://dx.doi.org/10.1016/S0021-9673\(03\)00630-7](http://dx.doi.org/10.1016/S0021-9673(03)00630-7).
- Kalka, Harald. 2017. "pH of Common Acids and Bases." accessed 25/05/2017. <http://www.aqion.de/site/191>.
- Kan, Amy, and Mason Tomson. 2011. "Scale Prediction for Oil and Gas Production." Society of Petroleum Engineers, 2012/6/1.
- Kashchiev, Dimo, and Abbas Firoozabadi. 2002. "Nucleation of gas hydrates." *J. Cryst. Growth* 243 (3-4):476-489. doi: [http://dx.doi.org/10.1016/S0022-0248\(02\)01576-2](http://dx.doi.org/10.1016/S0022-0248(02)01576-2).
- Kawabe, Kazuki. 2000. Method for producing monoethylene glycol. US Patents 6080897, issued June 27, 2000.
- Kawabe, Kazuki. 2010. "Development of highly selective process for mono-ethylene glycol production from ethylene oxide via ethylene carbonate using phosphonium salt catalyst." *Catalysis surveys from Asia* 14 (3-4):111-115.
- Kelland, Malcolm A. 2006. "History of the development of low dosage hydrate inhibitors." *Energy & Fuels* 20 (3):825-847.
- Kidnay, Arthur J, William R Parrish, and Daniel G McCartney. 2011. *Fundamentals of natural gas processing*. Vol. 218: CRC Press.

- Kim, H. C., P. R. Bishnoi, R. A. Heidemann, and S. S. H. Rizvi. 1987. "Kinetics of methane hydrate decomposition." *Chemical Engineering Science* 42 (7):1645-1653. doi: [http://dx.doi.org/10.1016/0009-2509\(87\)80169-0](http://dx.doi.org/10.1016/0009-2509(87)80169-0).
- Kim, Hyunho, Youngsub Lim, Yutaek Seo, and Minsu Ko. 2017. "Life cycle cost analysis of MEG regeneration process incorporating a modified slip stream concept." *Chemical Engineering Science* 166:181-192. doi: <https://doi.org/10.1016/j.ces.2017.03.045>.
- Kim, Jakyung, Kyuchul Shin, Juneyoung Kim, Daejun Chang, Yutaek Seo, and Kwang Pil Chang. 2014a. "Kinetic hydrate inhibition performance of MEG in under-inhibition system: reduction opportunities of MEG injection for offshore gas field developments." Offshore Technology Conference-Asia.
- Kim, Jakyung, Kyuchul Shin, Juneyoung Kim, Daejun Chang, Yutaek Seo, and Kwang Pil Chang. 2014b. "Kinetic Hydrate Inhibition Performance of MEG in Under-Inhibition System: Reduction Opportunities of MEG Injection for Offshore Gas Field Developments." Offshore Technology Conference, Kuala Lumpur, Malaysia, 2014/3/25.
- Kim, Juneyoung, Seong-yeob Lee, Jiheon Ryu, Youngkyun Seo, Suwon Seo, and Daejun Chang. 2017. "New MEG injection system with a seabed storage tank assisted by ship transportation." *Ocean Engineering* 140:50-56. doi: <https://doi.org/10.1016/j.oceaneng.2017.05.010>.
- King, Christopher Stephen, Brian Edward Messenger, Harihara V Nemmara, Z Frank Zheng, and ZHOU Shihui. 2015. Short contact, elevated temperature meg reclamation. Google Patents.
- Kjelstrup, Signe, and Dick Bedaux. 2001. *Elements of Thermodynamics for Engineers*: International Centre for Applied Thermodynamics.
- Koh, Carolyn A. 2002. "Towards a fundamental understanding of natural gas hydrates." *Chem. Soc. Rev* 31 (3):157-167.
- Koh, Carolyn A, and E Dendy Sloan. 2007. "Natural gas hydrates: Recent advances and challenges in energy and environmental applications." *AICHE journal* 53 (7):1636-1643.
- Koh, Carolyn, and Jefferson Creek. 2010. "Safety in Hydrate Plug Removal." *Natural Gas Hydrates in Flow Assurance* 37.
- Kohl, Arthur L, and Richard Nielsen. 1997. *Gas purification*. Fifth edition ed: Gulf Professional Publishing.
- Kokal, Sunil. 2002. "Crude Oil Emulsions: A State-Of-The-Art Review." Society of Petroleum Engineers, San Antonio, Texas, USA, 2002/10/2.
- Kokal, Sunil, and Martin Wingrove. 2000. "Emulsion Separation Index: From Laboratory to Field Case Studies." Society of Petroleum Engineers, Dallas, Texas, USA, 2000/1/1.

- Kondo, Wataru, Kaoru Ohtsuka, Ryo Ohmura, Satoshi Takeya, and Yasuhiko H. Mori. 2014. "Clathrate-hydrate formation from a hydrocarbon gas mixture: Compositional evolution of formed hydrate during an isobaric semi-batch hydrate-forming operation." *Appl. Energy* 113:864-871.
- Kvamme, Bjørn. 2000. "A Unified Nucleation Theory for the Kinetics of Hydrate Formation." *Annals of the New York Academy of Sciences* 912 (1):496-501. doi: 10.1111/j.1749-6632.2000.tb06804.x.
- Lam, Hon Loong, Jiří Jaromír Klemeš, Zdravko Kravanja, and Petar Sabev Varbanov. 2011. "Software tools overview: process integration, modelling and optimisation for energy saving and pollution reduction." *Asia-Pacific Journal of Chemical Engineering* 6 (5):696-712.
- Latta, T. M., A. A. Palejwala, S. K. Tipson, and N. P. Haigh. 2016. "Design Considerations for Mitigating the Impact of Contaminants in Rich MEG on Monoethylene Glycol Recovery Unit MRU Performance." Offshore Technology Conference, Kuala Lumpur, Malaysia, 2016/3/22/.
- Latta, Thomas Michael, Marion Elisabeth Seiersten, and Scott A. Bufton. 2013. "Flow Assurance Impacts on Lean/Rich MEG Circuit Chemistry and MEG Regenerator/Reclaimer Design." 2013/5/6.
- Laurier, L Schramm. 1992. "Emulsion fundamentals and applications in the petroleum industry." *Advances in Chem. Series* 99:231.
- Lederhos, J. P., J. P. Long, A. Sum, R. L. Christiansen, and E. D. Sloan. 1996. "Effective kinetic inhibitors for natural gas hydrates." *Chemical Engineering Science* 51 (8):1221-1229. doi: 10.1016/0009-2509(95)00370-3.
- Lee, Jeong Hwan, Young Soon Baek, and Won Mo Sung. 2005. "The Kinetics on Hydrate Formation in Pipelines." *Energy Sources* 27 (9):875-885. doi: 10.1080/00908310490479097.
- Lee, Jong Won, and Seong-Pil Kang. 2011. "Phase Equilibria of Natural Gas Hydrates in the Presence of Methanol, Ethylene Glycol, and NaCl Aqueous Solutions." *Ind. Eng. Chem. Res* 50 (14):8750-8755. doi: 10.1021/ie2001814.
- Lee, Ju Dong, and Peter Englezos. 2006. "Unusual kinetic inhibitor effects on gas hydrate formation." *Chem. Eng. Sci.* 61 (5):1368-1376. doi: <http://dx.doi.org/10.1016/j.ces.2005.08.009>.
- Lee, Ju Dong, Robin Susilo, and Peter Englezos. 2005. "Methane–ethane and methane–propane hydrate formation and decomposition on water droplets." *Chemical Engineering Science* 60 (15):4203-4212.
- Lee, Ju Dong, Huijie Wu, and Peter Englezos. 2007. "Cationic starches as gas hydrate kinetic inhibitors." *Chemical Engineering Science* 62 (23):6548-6555.

- Lehmann, M. N, A Lamm, H. M Nguyen, C. W Bowman, W. Y Mok, M Salasi, and R Gubner. 2014. "Corrosion Inhibitor and Oxygen Scavenger for use as MEG Additives in the Inhibition of Wet Gas Pipelines." Offshore Technology Conference Asia, Kuala Lumpur, 2014/3/25/.
- Lehmann, Marc N, Christopher William Bowman, Wai Yeung Mok, and Neil Jonathan Barr. 2016. Application of oxygen scavengers to glycol systems. US Patents 20140314620.
- Lekse, Jonathan, Charles E. Taylor, and Edward P. Ladner. 2007. "Effect of bubble size and density on methane conversion to hydrate." *J. Petrol. Sci. Eng.* 56 (1-3):97-100. doi: <http://dx.doi.org/10.1016/j.petrol.2005.08.007>.
- Link, Dirk D., Edward P. Ladner, Heather A. Elsen, and Charles E. Taylor. 2003. "Formation and dissociation studies for optimizing the uptake of methane by methane hydrates." *Fluid Phase Equilibria* 211 (1):1-10. doi: [https://doi.org/10.1016/S0378-3812\(03\)00153-5](https://doi.org/10.1016/S0378-3812(03)00153-5).
- Liu, Yucheng, Danni Wu, Mingyan Chen, Bo Zhang, Ju Chen, and Yuanzhi Liu. 2015. "Identification of Methyldiethanolamine Degradation Products and Their Influence on Foaming Properties during the Desulfurization Process for High-Sulfurous Natural Gas." *Ind. Eng. Chem. Res.* 54 (21):5836-5841. doi: 10.1021/ie504432d.
- Lonero, Andrew. 2008. "How Are Methane Hydrates Formed, Preserved, and Released." *Geology 340 Term Paper*:53-58.
- Long, J., and E. Sloan. 1996. "Hydrates in the ocean and evidence for the location of hydrate formation." *Journal of Thermophysical Properties and Thermophysics and Its Applications* 17 (1):1-13. doi: 10.1007/BF01448204.
- Loverude, Michael E, Christian H Kautz, and Paula RL Heron. 2002. "Student understanding of the first law of thermodynamics: Relating work to the adiabatic compression of an ideal gas." *American journal of physics* 70 (2):137-148.
- Lu, Zhengquan, and Nabil Sultan. 2008. "Empirical expressions for gas hydrate stability law, its volume fraction and mass-density at temperatures 273.15 K to 290.15 K." *Geochem. J* 42 (2):163-175. doi: 10.2343/geochemj.42.163.
- Luna-Ortiz, Eduardo, Matt Healey, Ross Anderson, and Eyvind Sørhaug. 2014. "Crystal Growth Inhibition Studies for the Qualification of a Kinetic Hydrate Inhibitor under Flowing and Shut-In Conditions." *Energy & Fuels* 28 (5):2902-2913. doi: 10.1021/ef402493x.
- Lunine, Jonathan I, and David J Stevenson. 1985. "Thermodynamics of clathrate hydrate at low and high pressures with application to the outer solar system." *Astrophys. J. Suppl. Ser.* 58:493-531.
- MacAdam, Jitka, and Simon A Parsons. 2004. "Calcium carbonate scale formation and control." *Reviews in Environmental Science and Biotechnology* 3 (2):159-169.

- Madera, M., W. Hoflinger, and R. Kadnar. 2003. "Ion chromatographic identification and quantification of glycol degradation products." *J. Chromatogr. A* 997 (1-2):279-284. doi: 10.1016/S0021-9673(03)00060-8.
- Maekawa, Tatsuo. 2001. "Equilibrium conditions for gas hydrates of methane and ethane mixtures in pure water and sodium chloride solution." *Geochem. J* 35 (1):59-66.
- Makogon, ІUriй Fedorovich. 1981. *Hydrates of natural gas*: PennWell Books Tulsa, Oklahoma.
- Makogon, ІUriй Fedorovich. 1997. *Hydrates of hydrocarbons*: Pennwell Books.
- Makogon, YF, TY Makogon, and SA Holditch. 2000. "Kinetics and mechanisms of gas hydrate formation and dissociation with inhibitors." *Annals of the New York Academy of Sciences* 912 (1):777-796.
- Makogon, Yu F. 1974. "Natural gas hydrates." *Moscow: Nedra* 285.
- Makogon, Yu F. 2015. "To the history of gas hydrates discovery." *Геология и полезные ископаемые мирового океана* (1 (39)).
- Makogon, Yuri F. 2010. "Natural gas hydrates – A promising source of energy." *Journal of Natural Gas Science and Engineering* 2 (1):49-59. doi: <http://dx.doi.org/10.1016/j.jngse.2009.12.004>.
- Malegaonkar, Mahendra B, Pankaj D Dholabhai, and P Raj Bishnoi. 1997. "Kinetics of carbon dioxide and methane hydrate formation." *The Canadian Journal of Chemical Engineering* 75 (6):1090-1099. doi: 10.1002/cjce.5450750612.
- Mao, Wendy L., Ho-kwang Mao, Alexander F. Goncharov, Viktor V. Struzhkin, Quanzhong Guo, Jingzhu Hu, Jinfu Shu, Russell J. Hemley, Maddury Somayazulu, and Yusheng Zhao. 2002. "Hydrogen Clusters in Clathrate Hydrate." *Science* 297 (5590):2247-2249. doi: 10.1126/science.1075394.
- Martín, Ángel, and Cor J Peters. 2009. "Hydrogen storage in sH clathrate hydrates: thermodynamic model." *The Journal of Physical Chemistry B* 113 (21):7558-7563.
- Masoudi, Rahim, Bahman Tohidi, Ali Danesh, Adrian C. Todd, Ross Anderson, Rod W. Burgass, and Jinhai Yang. 2005. "Measurement and prediction of gas hydrate and hydrated salt equilibria in aqueous ethylene glycol and electrolyte solutions." *Chemical Engineering Science* 60 (15):4213-4224. doi: <https://doi.org/10.1016/j.ces.2005.02.056>.
- McGinnis, B Dietrick, V Dean Adams, and E Joe Middlebrooks. 2000. "Degradation of ethylene glycol in photo Fenton systems." *Water Research* 34 (8):2346-2354.
- Mehta, AP, PB Hebert, ER Cadena, and JP Weatherman. 2002. "Fulfilling the promise of low dosage hydrate inhibitors: journey from academic curiosity to successful field implementation." Offshore Technology Conference.

- Melchers, RE. 2003. "Modeling of marine immersion corrosion for mild and low-alloy steels-part 1: phenomenological model." *Corros.* 59 (4):319-334.
- Menendez, C. M., J. Jardine, W. Y. Mok, S. Ramachandran, V. Jovancicevic, and A. Bhattacharya. 2014. "New Sour Gas Corrosion Inhibitor Compatible with Kinetic Hydrate Inhibitor." International Petroleum Technology Conference Doha, Qatar, 2014/1/19/.
- Miers, H. A., and F. Isaac. 1907. "The Spontaneous Crystallisation of Binary Mixtures. Experiments on Salol and Betol." Royal Society of London. Series A, Containing Papers of a Mathematical and Physical Character.
- Miresmaeili, S Omid H, Peyman Pourafshary, and Farhang Jalali Farahani. 2015. "A novel multi-objective estimation of distribution algorithm for solving gas lift allocation problem." *Journal of Natural Gas Science and Engineering* 23:272-280.
- Mohammadi, Amir H., and Dominique Richon. 2009. "Methane hydrate phase equilibrium in the presence of salt (NaCl, KCl, or CaCl₂) + ethylene glycol or salt (NaCl, KCl, or CaCl₂) + methanol aqueous solution: Experimental determination of dissociation condition." *The Journal of Chemical Thermodynamics* 41 (12):1374-1377. doi: <http://dx.doi.org/10.1016/j.jct.2009.06.012>.
- Mohebbi, V., A. Naderifar, R. M. Behbahani, and M. Moshfeghian. 2012. "Investigation of kinetics of methane hydrate formation during isobaric and isochoric processes in an agitated reactor." *Chem. Eng. Sci* 76 (0):58-65. doi: <http://dx.doi.org/10.1016/j.ces.2012.04.016>.
- Mokhatab, S, RJ Wilkens, and KJ Leontaritis. 2007. "A review of strategies for solving gas-hydrate problems in subsea pipelines." *Energy Sources, Part A* 29 (1):39-45.
- Mokhatab, Saeid, and William A Poe. 2012. *Handbook of natural gas transmission and processing*: Gulf Professional Publishing.
- Moloney, Jeremy, Wai Mok, and Chris Gamble. 2008. "Corrosion and Hydrate Control in Wet Sour Gas Transmission Systems." SPE Asia Pacific Oil and Gas Conference and Exhibition, Perth, Australia.
- Moloney, JJ, Wai Y Mok, and Chris G Gamble. 2009. "Compatible Corrosion and Kinetic Hydrate Inhibitors for Wet Sour Gas Transmission Lines." CORROSION 2009. NACE International.
- Montazaud, Thomas. 2011. "Precipitation of carbonates in the pretreatment process for regeneration of ethylene glycol." Department of Chemical Engineering, Norwegian University of Science and Technology, Digitala Vetenskapliga Arkivet (6427).
- Monticelli, C, G Brunoro, A Frignani, and F Zucchi. 1988. "Corrosion behaviour of the aluminium alloy AA 6351 in glycol/water solutions degraded at elevated

- temperature.” *Mater. Corros.* 39 (8):379-384. doi: 10.1002/maco.19880390805.
- Moon, C., P. C. Taylor, and P. M. Rodger. 2003a. “Clathrate nucleation and inhibition from a molecular perspective.” *Canadian Journal of Physics* 81 (1-2):451-457. doi: 10.1139/p03-035.
- Moon, Changman, Paul C. Taylor, and P. Mark Rodger. 2003b. “Molecular Dynamics Study of Gas Hydrate Formation.” *J. Am. Chem. Soc.* 125 (16):4706-4707. doi: 10.1021/ja028537v.
- Moon, Changman, Paul C. Taylor, and P. Mark Rodger. 2003c. “Molecular dynamics study of gas hydrate formation.” *Journal of the American Chemical Society* 125 (16):4706.
- Moore, Jennifer, Leonard Ver Vers, and Peter Conrad. 2009. “SS: Flow Assurance: Understanding Kinetic Hydrate Inhibitor and Corrosion Inhibitor Interactions.” Offshore Technology Conference, Houston, Texas, USA, 2009/1/1/.
- Mori, T., and Y. H. Mori. 1989. “Characterization of gas hydrate formation in direct-contact cool storage process.” *Int. J. Refrig.* 12 (5):259-265. doi: [http://dx.doi.org/10.1016/0140-7007\(89\)90091-1](http://dx.doi.org/10.1016/0140-7007(89)90091-1).
- Mostowfi, Farshid, and Heng-Joo Ng. 2014. Method and apparatus for characterizing clathrate hydrate formation conditions employing microfluidic device. U.S. Patent Application No. 15/038,324.
- Mrklas, Ole, Angus Chu, Stuart Lunn, and Laurence R Bentley. 2004. “Biodegradation of monoethanolamine, ethylene glycol and triethylene glycol in laboratory bioreactors.” *Water, Air, Soil Pollut.* 159 (1):249-263.
- Mullin, J. W. 2001. *Crystallization / J. W. Mullin.* 4th ed.. ed. Oxford: Oxford : Butterworth-Heinemann.
- Naaz, Asmaa, and Anshumali. 2015. “Seasonal Variation in Ph and Alkalinity of Groundwaters in Sidhi District, Central India.” *Current World Environment* 10 (3):1017-1021. doi: <http://dx.doi.org/10.12944/CWE.10.3.34>.
- Najafi, M. J., and V. Mohebbi. 2014. “Solubility measurement of carbon dioxide in water in the presence of gas hydrate.” *J. Nat. Gas. Sci. Eng.* 21:738-745. doi: <http://dx.doi.org/10.1016/j.jngse.2014.10.006>.
- Natarajan, V., P. R. Bishnoi, and N. Kalogerakis. 1994. “Induction phenomena in gas hydrate nucleation.” *Chem. Eng. Sci.* 49 (13):2075-2087. doi: [http://dx.doi.org/10.1016/0009-2509\(94\)E0026-M](http://dx.doi.org/10.1016/0009-2509(94)E0026-M).
- Nazzer, C. A., and J. Keogh. 2006. “Advances in Glycol Reclamation Technology.” Offshore Technology Conference, 2006/1/1/.
- Nengkoda, A, W. M. A Taha, A. S Al-Harthy, and H Reerink. 2009. “Gas Hydrate Problems in Desert of Sultanate of Oman, Experiences and Integrated

Inhibition Program.” Paper International Petroleum Technology Conference, Qatar.

Nielsen, RB, and RW Bucklin. 1983. “Gas processing developments. Why not use methanol for hydrate control.” *Hydrocarbon Process.;(United States)* 62 (4).

Nielsen, Robert P, and John H La Rochelle. 1977. Ethylene oxide process. U.S. Patent 4,012,425, issued March 15, 1977.

Niessen, W. M. A, and A. P Tinke. 1995. “Liquid chromatography-mass spectrometry General principles and instrumentation.” *J. Chromatogr. A* 703 (1-2):37-57. doi: [http://dx.doi.org/10.1016/0021-9673\(94\)01198-N](http://dx.doi.org/10.1016/0021-9673(94)01198-N).

Obanijesu, E. O, R Gubner, A Barifcany, V Pareek, and M. O Tade. 2014. “The influence of corrosion inhibitors on hydrate formation temperature along the subsea natural gas pipelines.” *J. Pet. Sci. Eng* 120 (0):239-252. doi: <http://dx.doi.org/10.1016/j.petrol.2014.05.025>.

Obanijesu, Emmanuel O, Ahmed Barifcany, Vishnu K Pareek, and Moses O Tade. 2014. “Experimental study on feasibility of H₂ and N₂ as hydrate inhibitors in natural gas pipelines.” *Journal of Chemical & Engineering Data* 59 (11):3756-3766.

Ogawa, Hiroyuki, Naotaka Imura, Tatsuya Miyoshi, Ryo Ohmura, and Yasuhiko H. Mori. 2009. “Thermodynamic Simulations of Isobaric Hydrate-Forming Operations for Natural Gas Storage.” *Energy & Fuels* 23 (2):849-856. doi: 10.1021/ef800799q.

Ohmura, R., T. Shigetomi, and Y. H. Mori. 2000. “Mechanical Properties of Water/Hydrate-Former Phase Boundaries and Phase-Separating Hydrate Films.” *Annals of the New York Academy of Sciences* 912 (1):958-966. doi: 10.1111/j.1749-6632.2000.tb06850.x.

Ohmura, Ryo, Mikio Ogawa, Kenji Yasuoka, and Yasuhiko H. Mori. 2003. “Statistical Study of Clathrate-Hydrate Nucleation in a Water/Hydrochlorofluorocarbon System: Search for the Nature of the “Memory Effect”.” *The Journal of Physical Chemistry B* 107 (22):5289-5293. doi: 10.1021/jp027094e.

Olabisi, Odutola Toyin, Sunday Ikiensikimama, and Dulu Appah. 2014. “Chemical Compromise: A Thermodynamic and Ionic Solution for Hydrate Control.” SPE Nigeria Annual International Conference and Exhibition.

Olsen, Stein. 2006. “Corrosion Control by Inhibition, Environmental Aspects, and pH Control: Part II: Corrosion Control by pH Stabilization.” CORROSION 2006. NACE International, Houston, Texas, 2006/1/1.

OSIsoft. 2017. "<http://www.osisoft.com/pi-system/>." OSIsoft, accessed 27/4/2017. <http://www.osisoft.com/pi-system/>.

P. M, Visakh editor, Yoshihiko editor Arao, and SpringerLink. 2015. *Thermal Degradation of Polymer Blends, Composites and Nanocomposites / edited by*

P. M. Visakh, Yoshihiko Arao: Cham : Springer International Publishing : Imprint: Springer.

- Pakulski, Marek K. 2007. "Accelerating Effect of Surfactants on Gas Hydrates Formation." SPE, Houston, Texas, U.S.A, 2007/1/1/.
- Parent, J. S., and P. R. Bishnoi. 1996. "Investigations into the nucleation behaviour of methane gas hydrates." *Chemical Engineering Communications* 144:51-64.
- Pauley, CR, Donald G Langston, and FC Betts. 1991. "Redesigned filters solve foaming, amine-loss problems at Louisiana gas plant." *Oil and Gas Journal;(USA)* 89 (5).
- Pedersen, Karen Schou, Peter L Christensen, and Jawad Azeem Shaikh. 2014. *Phase behavior of petroleum reservoir fluids*: CRC Press.
- Peng, Ding-Yu, and Donald B. Robinson. 1976. "A New Two-Constant Equation of State." *Ind. Eng. Chem. Fundam* 15 (1):59-64. doi: 10.1021/i160057a011.
- Peters, David, M Selim, and E Dendy Sloan. 2000. "Hydrate Dissociation in Pipelines by Two-Sided Depressurization: Experiment and Model." *Annals of the New York Academy of Sciences* 912 (1):304-313.
- Petroleum Development Oman, AlHadhrami, Marwa. 2016. Internal Note to File : Zauliyah Hydrates Formation Way Forward. Muscat, Mina Al Fahal: Petroleum Development Oman.
- Petroleum Development Oman, HMR Environmental Engineering Consultants. 2003. ENVIRONMENTAL ASSESSMENT OF BAHJA ASSET-2002 REVIEW AND UPDATE. Petroleum Development Oman: HMR Environmental Engineering Consultants.
- Pojtanabuntoeng, Thunyaluk, Mobin Salasi, and Rolf Gubner. 2014. "The Influence of Mono Ethylene Glycol (MEG) on CO₂ Corrosion of Carbon Steel at Elevated Temperatures (80 to 120 C)." CORROSION 2014. NACE International.
- Psarrou, Maria N., Leif O. Jøsang, Kristian Sandengen, and Terje Østvold. 2011. "Carbon Dioxide Solubility and Monoethylene Glycol (MEG) Degradation at MEG Reclaiming/Regeneration Conditions." *J. Chem. Eng. Data* 56:4720-4724.
- Qian, Zhi, Lian-Bin Xu, Zhen-Hu Li, Hua Li, and Kai Guo. 2010. "Selective Absorption of H₂S from a Gas Mixture with CO₂ by Aqueous N-Methyldiethanolamine in a Rotating Packed Bed." *Ind. Eng. Chem. Res.* 49 (13):6196-6203. doi: 10.1021/ie100678c.
- Radhakrishnan, Ravi, and Bernhardt L Trout. 2002. "A new approach for studying nucleation phenomena using molecular simulations: Application to CO₂ hydrate clathrates." *The Journal of chemical physics* 117 (4):1786-1796.

- Ranjbar, Khalil, and Arsalan Abasi. 2013. "Failure assessment of crude oil preheating tubes in mono ethylene glycol–water mixture solution." *Engineering Failure Analysis* 31:161-167.
- Rebsdat, Siegfried, and Dieter Mayer. 2000. "Ethylene glycol." *Ullmann's Encyclopedia of Industrial Chemistry*.
- Reddi, Ram Mohan, and Anurag K Srivastava. 2010. "Real time test bed development for power system operation, control and cyber security." North American Power Symposium (NAPS), 2010.
- Ribeiro, Cláudio P, and Paulo LC Lage. 2008. "Modelling of hydrate formation kinetics: State-of-the-art and future directions." *Chemical Engineering Science* 63 (8):2007-2034.
- Richardson, MC, and DT White-Stevens. 1986. "Santos' experience with field dehydration." Chemeca 86: The Fourteenth Australasian Chemical Engineering Conference; Chemical Engineering; Initiatives, Attitudes, Cycles.
- Riestenberg, David, Olivia West, Sangyong Lee, Scott McCallum, and Tommy J. Phelps. 2003. "Sediment surface effects on methane hydrate formation and dissociation." *Mar. Geol.* 198 (1-2):181-190. doi: [http://dx.doi.org/10.1016/S0025-3227\(03\)00100-2](http://dx.doi.org/10.1016/S0025-3227(03)00100-2).
- Ripmeester, John A, S Tse John, Christopher I Ratcliffe, and Brian M Powell. 1987. "A new clathrate hydrate structure." *Nature* 325 (6100):135-136.
- Robinson, DB. 1986. "Hydrate formation and inhibition in gas or gas condensate streams." *Journal of Canadian Petroleum Technology* 25 (04).
- Robson, John H, and E Keller II George. 1985. Process for the production of alkylene glycols. U.S. Patent 4,551,566, issued November 5, 1985.
- Rodger, Pm. 1990. "Stability of gas hydrates." *J. Phys. Chem.* 94 (15):6080-6089.
- Rodger, Pm. 2000. "Methane hydrate - Melting and memory." *Ann.NY Acad.Sci.* 912:474-482.
- Rojas, Yenny V, Chi M Phan, and Xia Lou. 2010. "Dynamic surface tension studies on poly (N-vinylcaprolactam/N-vinylpyrrolidone/N, N-dimethylaminoethyl methacrylate) at the air–liquid interface." *Colloids and Surfaces A: Physicochemical and Engineering Aspects* 355 (1):99-103.
- Rojey, Alexandre, and Claude Jaffret. 1997. *Natural gas: production, processing, transport*. Paris, France: Editions Technip.
- Rossiter, Jr, J Walter, Paul W Brown, and McClure Godette. 1983. "The determination of acidic degradation products in aqueous ethylene glycol and propylene glycol solutions using ion chromatography." *Sol. Energy Mater* 9 (3):267-279. doi: [http://dx.doi.org/10.1016/0165-1633\(83\)90049-7](http://dx.doi.org/10.1016/0165-1633(83)90049-7).

- Rossiter Jr, Walter J, McClure Godette, Paul W Brown, and Kevin G Galuk. 1985. "An investigation of the degradation of aqueous ethylene glycol and propylene glycol solutions using ion chromatography." *Sol. Energy Mater* 11 (5–6):455-467. doi: [http://dx.doi.org/10.1016/0165-1633\(85\)90016-4](http://dx.doi.org/10.1016/0165-1633(85)90016-4).
- Rovetto, Laura J., Timothy A. Strobel, Carolyn A. Koh, and E. Dendy Sloan Jr. 2006. "Is gas hydrate formation thermodynamically promoted by hydrophobic molecules?" *Fluid Phase Equilibria* 247 (1–2):84-89. doi: <http://dx.doi.org/10.1016/j.fluid.2006.06.018>.
- Rudenko, AI, AN Gershuni, and LV Kalabina. 1997. "Some characteristics of ethylene glycol as a heat-transfer agent for closed two-phase systems." *Journal of engineering physics and thermophysics* 70 (5):799-804.
- Sadeq, Dhifaf, Stefan Igglauer, Maxim Lebedev, Callum Smith, and Ahmed Barifcani. 2017. "Experimental determination of hydrate phase equilibrium for different gas mixtures containing methane, carbon dioxide and nitrogen with motor current measurements." *Journal of Natural Gas Science and Engineering* 38:59-73.
- Salasi, Mobin, Thunyaluk Pojtanabuntoeng, Sindee Wong, and Marc Lehmann. 2017. "Efficacy of Bisulfite Ions as an Oxygen Scavenger in Monoethylene Glycol (At Least 20 wt%)/Water Mixtures." *SPE Journal*.
- Sanchez, Francisco Javier, Matt Smith, Mahmoud Kindi, Don Alexander Gray, and Stephen Adetunji Aderele. 2011. "Drilling Efficiency Optimization (DEO) in Casing while Drilling (CwD) Operations in the Sultanate of Oman." Society of Petroleum Engineers, Muscat, Oman, 2011/1/1.
- Sandengen, Kristian, Baard Kaasa, and Terje Østvold. 2007. "pH Measurements in Monoethylene Glycol (MEG) + Water Solutions." *Ind. Eng. Chem. Res.* 46 (14):4734-4739. doi: 10.1021/ie061305a.
- Schicks, JM. 2010. "Natural Gas Hydrates." In *Handbook of Hydrocarbon and Lipid Microbiology*, 67-77. Springer.
- Schreiber, André, Jürgen Efer, and Werner Engewald. 2000. "Application of spectral libraries for high-performance liquid chromatography-atmospheric pressure ionisation mass spectrometry to the analysis of pesticide and explosive residues in environmental samples." *J. Chromatogr. A* 869:411-425. doi: 10.1016/S0021-9673(99)01271-6.
- Schroeter, JP, Riki Kobayashi, and MA Hildebrand. 1983. "Hydrate decomposition conditions in the system hydrogen sulfide-methane-propane." *Industrial & engineering chemistry fundamentals* 22 (4):361-364.
- Sefidroodi, Hamidreza, Eirin Abrahamsen, and Malcolm A. Kelland. 2013. "Investigation into the strength and source of the memory effect for cyclopentane hydrate." *Chemical engineering science* 87:133-140.

- Seiersten, Marion, and Arne Dugstad. 2015. "Measuring Alkalinity in Monoethylene Glycol (MEG) Solutions." 26th International Oil Field Chemistry Symposium, Geilo, Norway, 22-25 March-2015.
- Seo, Yutaek, and Seong-Pil Kang. 2012. "Inhibition of methane hydrate re-formation in offshore pipelines with a kinetic hydrate inhibitor." *J. Pet. Sci. Eng.* 88–89:61-66. doi: <http://dx.doi.org/10.1016/j.petrol.2011.11.001>.
- Servio, Phillip, and Peter Englezos. 2003. "Morphology of methane and carbon dioxide hydrates formed from water droplets." *AICHE journal* 49 (1):269-276.
- Shao, Weiming, Igor Boiko, and Ahmed Al-Durra. 2016. "Control-oriented modeling of gas-lift system and analysis of casing-heading instability." *Journal of Natural Gas Science and Engineering* 29:365-381.
- Shell Global Solutions, nd. 2009. "OMEGA and ethylene oxide/ethylene glycol technology." accessed 19/01/2017. <http://www.shell.com/business-customers/chemicals/factsheets-speeches-and-articles/factsheets/omega.html#vanity-aHR0cDovL3d3dy5zaGVsbC5jb20vZ2xvYmFsL3Byb2R1Y3RzLXNlcnZpY2VzL3NvbHV0aW9ucy1mb3ItYnVzaW5lc3Nlcy9jaGVtaWNhbHMvbWVkaWEtY2VudHJIL2ZhY3RzaGVldHMvb21lZ2EuaHRtbA>
- Shihab, Sufyan, Shaikhan Khadhuri, Salim Busaidy, and Solenn Rawnsley Bettembourg. 2011. "Real-time operations Portal (Nibras): another step En Route to a smart field management." SPE Middle East Oil and Gas Show and Conference.
- Shimadzu. 2014. "Automatic self-calibration electronic balance." <http://www.shimadzu.com/an/balance/toploading/qn50420000065rm-att/qn504200001bu8k.pdf>
- Sloan, E Dendy. 1998. "Gas hydrates: Review of physical/chemical properties." *Energy & Fuels* 12 (2):191-196.
- Sloan, E Dendy, Carolyn Ann Koh, and Amadeu Sum. 2010. *Natural gas hydrates in flow assurance*: Gulf Professional Publishing.
- Sloan, E. D., S. Subramanian, P. N. Matthews, J. P. Lederhos, and A. A. Khokhar. 1998. "Quantifying Hydrate Formation and Kinetic Inhibition." *Industrial & Engineering Chemistry Research* 37 (8):3124-3132. doi: 10.1021/ie970902h.
- Sloan, E. Dendy. 2003. "Fundamental principles and applications of natural gas hydrates." *Nature* 426 (6964):355-356.
- Sloan, E. Dendy. 2005. "A changing hydrate paradigm—from apprehension to avoidance to risk management." *Fluid Phase Equilib.* 228–229:67-74. doi: <http://dx.doi.org/10.1016/j.fluid.2004.08.009>
- Sloan, E. Dendy, Jr. 1991. "Natural Gas Hydrates." *Journal of Petroleum Technology*:1-414. doi: 10.2118/23562-PA.

- Sloan, E. Dendy, and Carolyn A. Koh. 2008a. *Clathrate hydrates of natural gases*. 3rd edition ed. Boca Raton, USA: CRC Press, Taylor and Francis Group.
- Sloan, E. Dendy, and Carolyn A. Koh. 2008b. *Clathrate Hydrates of Natural Gases*. Vol. chapter 8 Hydrates in Production, Processing, and Transportation: CRC Press Taylor & Francis Group, LLC.
- Smith, Brian C. 2011. *Fundamentals of Fourier Transform Infrared Spectroscopy*. 2nd edition ed. USA: Taylor and Francis Group, LLC.
- Smith, Callum, Ahmed Barifcani, and David Pack. 2016. "Helium substitution of natural gas hydrocarbons in the analysis of their hydrate." *Journal of Natural Gas Science and Engineering* 35:1293-1300.
- Son, K, and Charlie Wallace. 2000. "Reclamation/regeneration of glycols used for hydrate inhibition." *Deep Offshore Technology*.
- Sorensen, J. A., S. B. Hawthorne, J. R. Gallagher, and J. A. Harju. 1999. "Glycol Used for Natural Gas Dehydration: Evaluation of Subsurface Transport and Fate Issues." SPE/EPA Exploration and Production Environmental Conference Austin, Texas, 1999.
- Stewart, Maurice, and Ken Arnold. 2011. "Part 3 - Glycol Maintenance, Care, and Troubleshooting." In *Gas Dehydration Field Manual*, edited by Maurice Stewart and Ken Arnold, 169-237. Boston: Gulf Professional Publishing.
- Stillinger, Frank H. 1980. "Water revisited." *Science* 209 (4455):451-457.
- Strickler, Gary R, Von G Landon, Guo-shuh John Lee, and William J Rievert. 2000. Process and equipment for the production of ethylene glycols. U.S. Patent 6,137,015, issued October 24, 2000.
- Su, Zheng, George J. Moridis, Keni Zhang, and Nengyou Wu. 2012. "A huff-and-puff production of gas hydrate deposits in Shenhua area of South China Sea through a vertical well." *J. Pet. Sci. Eng.* 86–87:54-61. doi: <http://dx.doi.org/10.1016/j.petrol.2012.03.020>.
- Suess, Erwin, Gerhard Bohrmann, Jens Greinert, and Erwin Lausch. 1999. "Flammable ice." *Scientific American* 281 (5):76-83.
- Sum, Amadeu K, Carolyn A Koh, and E Dendy Sloan. 2009. "Clathrate hydrates: from laboratory science to engineering practice." *Industrial & Engineering Chemistry Research* 48 (16):7457-7465.
- Sum, Amadeu K., Robert C. Burruss, and E. Dendy Sloan. 1997. "Measurement of Clathrate Hydrates via Raman Spectroscopy." *J. Phys. Chem. B* 101 (38):7371-7377. doi: 10.1021/jp970768e.
- Swanson, T. A., M. Petrie, and T. R. Sifferman. 2005. "The Successful Use of Both Kinetic Hydrate and Paraffin Inhibitors Together in a Deepwater Pipeline with a High Water Cut in the Gulf of Mexico." Society of Petroleum Engineers, Houston, Texas, USA, 2005/1/1/.

- Sykes, Greg, and Mike Gunn. 2016. "Optimising MEG Chemistry When Producing Formation Water." Society of Petroleum Engineers, Perth, Australia, 2016/08/25.
- Takeya, Satoshi, Akira Hori, Takeo Hondoh, and Tsutomu Uchida. 2000. "Freezing-Memory Effect of Water on Nucleation of CO₂ Hydrate Crystals." *Journal of Physical Chemistry B* 104 (17):4164-4168.
- Talatori, Shiva, and Tanja Barth. 2011. "Rate of hydrate formation in crude oil/gas/water emulsions with different water cuts." *J. Pet. Sci. Eng.* 80 (1):32-40. doi: <http://dx.doi.org/10.1016/j.petrol.2011.10.010>.
- Tariq, Mohammad, Mert Atilhan, Majeda Khraisheh, Enas Othman, Marcelo Castier, Gregorio García, Santiago Aparicio, and Bahman Tohidi. 2016. "Experimental and DFT Approach on the Determination of Natural Gas Hydrate Equilibrium with the Use of Excess N₂ and Choline Chloride Ionic Liquid as an Inhibitor." *Energy & Fuels* 30 (4):2821-2832. doi: 10.1021/acs.energyfuels.6b00117.
- Tavasoli, Hamed, Farzaneh Feyzi, Mohammad Reza Dehghani, and Farzad Alavi. 2011. "Prediction of gas hydrate formation condition in the presence of thermodynamic inhibitors with the Elliott–Suresh–Donohue Equation of State." *J. Pet. Sci. Eng.* 77 (1):93-103. doi: <http://dx.doi.org/10.1016/j.petrol.2011.02.002>.
- Taylor, Craig J., Kelly T. Miller, Carolyn A. Koh, and E. Dendy Sloan Jr. 2007. "Macroscopic investigation of hydrate film growth at the hydrocarbon/water interface." *Chem. Eng. Sci.* 62 (23):6524-6533. doi: <http://dx.doi.org/10.1016/j.ces.2007.07.038>.
- Taylor, Ross, and Rajamani Krishna. 1993. *Multicomponent mass transfer*. Vol. 2: John Wiley & Sons.
- Teixeira, A. M., J. L. Medeiros, and O. Q. F. Araújo. 2015. "Offshore Monoethylene Glycol Recovery Units: The Importance of Choice of MEG State in the Reference Environment for Effective Exergy Analysis." Offshore Technology Conference, Rio de Janeiro, Brazil, 2015/10/27/.
- Teixeira, Alexandre Mendonça, Lara de Oliveira Arinelli, José Luiz de Medeiros, and F Araújo Ofélia de Queiroz. 2016. "Exergy Analysis of Monoethylene glycol recovery processes for hydrate inhibition in offshore natural gas fields." *Journal of Natural Gas Science and Engineering* 35:798-813.
- Timmis, Kenneth N, T McGenity, JR Van Der Meer, and V De Lorenzo. 2010. *Handbook of hydrocarbon and lipid microbiology*: Springer Berlin/Heidelberg.
- Timothy S. Collett, Arthur H. Johnson, Camelia C. Knapp, and Ray Boswell. 2009. *Natural gas hydrates-Energy resource potential and associated geologic hazards*. Vol. 89, AAPG AAPG.

- Toews, Karen L, Robert M Shroll, Chien M Wai, and Neil G Smart. 1995. "pH-defining equilibrium between water and supercritical CO₂. Influence on SFE of organics and metal chelates." *Analytical Chemistry* 67 (22):4040-4043.
- Tohidi, B., R. W. Burgass, A. Danesh, K. K. ØStergaard, and A. C. Todd. 2000. "Improving the Accuracy of Gas Hydrate Dissociation Point Measurements." *Annals of the New York Academy of Sciences* 912 (1):924-931. doi: 10.1111/j.1749-6632.2000.tb06846.x.
- Tohidi, Bahman, Ross Anderson, M. Ben Clennell, Rod W. Burgass, and Ali B Biderkab. 2001. "Visual observation of gas-hydrate formation and dissociation in synthetic porous media by means of glass micromodels." *Geology* 29:867-870. doi: 10.1130/0091-7613(2001)029<0867:VOOGHF>2.0.CO;2
- Uchida, T, IY Ikeda, Ryo Ohmura, and S Tsuda. 2007. "Effects of additives on formation rates of CO₂ hydrate films."
- Uchida, T., T. Ebinuma, and H. Narita. 2000. "Observations of CO 2-hydrate decomposition and reformation processes." *Journal of Crystal Growth* 217 (1):189-200. doi: 10.1016/S0022-0248(00)00470-X.
- Unisim, Honeywell. 2017. "Honeywell Unisim Design." accessed 02/05/2017. <https://www.honeywellprocess.com/en-US/Pages/search-results.aspx?k=unisim%20design>.
- van den Berg, Frans G., Cristopher Weiss, Jaap van Dijk, Robert Tulalian, Martins Amos, Said Alharthy, and Mayowa Awobadejo. 2016. "Collaborative Working - Harvesting Value and Evolving with New Technologies." Society of Petroleum Engineers, 2016/9/6/.
- Van der Waals, JH, and JC Platteeuw. 2007. "Clathrate solutions." *Advances in Chemical Physics, Volume 2*:1-57.
- van Hal, Jaap W., John S. Ledford, and Xiankuan Zhang. 2007. "Investigation of three types of catalysts for the hydration of ethylene oxide (EO) to monoethylene glycol (MEG)." *Catalysis Today* 123 (1-4):310-315. doi: <https://doi.org/10.1016/j.cattod.2007.02.015>.
- Van Kruchten, Eugene Marie Godfried Andre. 1999. Process for the preparation of alkylene glycols. U.S. Patent 5,874,653, issued February 23, 1999.
- Van Son, K., and Wallace, C. 2000. "Reclamation/Regeneration of Glycols Used for Hydrate Inhibition." Deep Offshore Technology 2000.
- Vanus, Jan, Radek Martinek, Petr Bilik, Jan Zidek, and Jaroslav Machac. 2015. "Energy management strategies in intelligent office building using PI system." Proceedings of the 8th International Scientific Symposium on Electrical Power Engineering, ELEKTROENERGETIKA.

- Verykios, Xenopiion E, Fred P Stein, and Robert W Coughlin. 1980. "Oxidation of ethylene over silver: Adsorption, kinetics, catalyst." *Catalysis Reviews—Science and Engmeering* 22 (2):197-234.
- Vijayamohan, Prithvi, Ahmad Afif Abdul Majid, P Chaudhari, E. Dendy Sloan, Amadeu K Sum, Carolyn A Koh, Emmanuel Dellecase, and Michael Volk. 2014. "Hydrate Modeling & Flow Loop Experiments for Water Continuous & Partially Dispersed Systems." Offshore Technology Conference, Houston, Texas, USA, 2014.
- Von Stackelberg, M. 1949. "Feste gashydrate." *Naturwissenschaften* 36:327-333.
- Vysniauskas, A., and P. R. Bishnoi. 1983. "A kinetic study of methane hydrate formation." *Chemical Engineering Science* 38 (7):1061-1072. doi: 10.1016/0009-2509(83)80027-X.
- Wang, F, K Cassidy, and B Lum. 1993. Incineration alternatives for combustible waste ultraviolet/hydrogen peroxide process. Annual report, FY 1992. Lawrence Livermore National Lab., CA (United States).
- Weisz, Paul B., and Pa. Media. 1962. Catalytic production of ethylene glycol. U.S. Patent 3,028,434, issued April 3, 1962.
- Wilson, PW, and ADJ Haymet. 2010. "Hydrate formation and re-formation in nucleating THF/water mixtures show no evidence to support a "memory" effect." *Chemical engineering journal* 161 (1):146-150.
- Windmeier, Christoph, and Lothar R Oellrich. 2014a. "Visual observation of the methane hydrate formation and dissociation process." *Chem. Eng. Sci* 109:75-81. doi: <http://dx.doi.org/10.1016/j.ces.2014.01.018>.
- Windmeier, Christoph, and Lothar R. Oellrich. 2014b. "Experimental Methane Hydrate Dissociation Conditions in Aqueous Solutions of Lithium Salts." *J. Chem. Eng. Data* 59 (2):516-518. doi: 10.1021/je4010036.
- Worthington, Paul F. 2010. "Petrophysical evaluation of gas-hydrate formations." *Petroleum Geoscience* 16 (1):53-66. doi: 10.1144/1354-079309-018.
- Wu, Ming, Shumiao Wang, and Hongbo Liu. 2007. "A Study on Inhibitors for the Prevention of Hydrate Formation in Gas Transmission Pipeline." *Journal of Natural Gas Chemistry* 16 (1):81-85. doi: [http://dx.doi.org/10.1016/S1003-9953\(07\)60031-0](http://dx.doi.org/10.1016/S1003-9953(07)60031-0).
- Wu, Qiang, and Baoyong Zhang. 2010. "Memory effect on the pressure-temperature condition and induction time of gas hydrate nucleation." *Journal of Natural Gas Chemistry* 19 (4):446-451.
- Wu, Reuben, Karen A Kozielski, Patrick G Hartley, Eric F May, John Boxall, and Nobuo Maeda. 2013. "Probability distributions of gas hydrate formation." *AIChE J.* 59 (7):2640-2646.

- Wurts, William A, and Robert M Durborow. 1992. "Interactions of pH, carbon dioxide, alkalinity and hardness in fish ponds."
- Xiao, JJ, George Shoup, Greg Hatton, and Veet Kruka. 1998. "Predicting hydrate plug movement during subsea flowline depressurization operations." Offshore Technology Conference.
- Xu, Wenyue, and Carolyn Ruppel. 1999. "Predicting the occurrence, distribution, and evolution of methane gas hydrate in porous marine sediments." *J. Geophys. Res-Sol. Ea.* 104 (B3):5081-5095. doi: 10.1029/1998JB900092.
- Yanicki, G, and MA Trebble. 2006. "Experimental measurements of foaming tendencies in aqueous gas sweetening solutions containing MDEA over a temperature range of 297–358 K and a pressure range of 101–500 kPa." *Chem. Eng. Commun.* 193 (10):1151-1163.
- Yasuoka, K., and S. Murakoshi. 2000. "Molecular dynamics simulation of dissociation process for methane hydrate." *Ann.NY Acad.Sci.* 912:678-684.
- Yong, A., and E. O. Obanijesu. 2015. "Influence of natural gas production chemicals on scale production in MEG regeneration systems." *Chem. Eng. Sci.* 130:172-182. doi: <http://dx.doi.org/10.1016/j.ces.2015.03.037>.
- Yousif, M. H. 1994. "The Kinetics of Hydrate Formation." Society of Petroleum Engineers, New Orleans, LA, USA, 1994/1/1/.
- Zaboon, Sami, Adam Soames, Varun Ghodkay, Rolf Gubner, and Ahmed Barifcani. 2017. "Recovery of Mono-Ethylene glycol distillation and the impact of dissolved salts simulating field data." *Journal of Natural Gas Science and Engineering*.
- Zang, Xiaoya, and Deqing Liang. 2017. "Phase Equilibrium Data for Semiclathrate Hydrate of Synthesized Binary CO₂/CH₄ Gas Mixture in Tetra-n-butylammonium Bromide Aqueous Solution." *Journal of Chemical & Engineering Data*. doi: 10.1021/acs.jced.6b00876.
- Zerpa, Luis E, Jean-Louis Salager, Carolyn A Koh, E Dendy Sloan, and Amadeu K Sum. 2010. "Surface chemistry and gas hydrates in flow assurance." *Ind. Eng. Chem. Res.* 50 (1):188-197.
- Zheng, Liangfu, James Landon, Naser S. Matin, Gerald A. Thomas, and Kunlei Liu. 2016. "Corrosion mitigation via a pH stabilization method in monoethanolamine-based solutions for post-combustion CO₂ capture." *Corros. Sci.* doi: <http://dx.doi.org/10.1016/j.corsci.2016.02.013>.

Every reasonable effort has been made to acknowledge the owners of copyright material. I would be pleased to hear from any copyright owner who has been omitted or incorrectly acknowledged.